Utilising transmission electron microscopy to better understand viral replication cycles: the characterisation of cytoplasmic replication in Tula virus, rotavirus and herpesvirus

Benjamin Mark Chadwick

Submitted in accordance with the requirements for the degree of Doctor of Philosophy

The University of Leeds

Faculty of Biological Sciences

School of Molecular and Cellular Biology

July 2022

The candidate confirms that the work submitted is his own, except where work which has formed part of jointly-authored publications has been included. The contribution of the candidate and the other authors to this work has been explicitly indicated below. The candidate confirms that appropriate credit has been given within the thesis where reference has been made to the work of others. Chapter three forms work published in Cells: Katherine A Davies, Benjamin Chadwick, Roger Hewson, Juan Fontana, Jamel Mankouri, John N Barr “The RNA Replication Site of Tula Orthohantavirus Resides within a Remodelled Golgi Network” 2020. Figure 2 was completed by the candidate, which forms Chapter three, figure 3.10, 3.11, and 3.13.

Acknowledgements

I would like to thank my supervisor Dr Juan Fontana for always being available with advise and support and for putting up with me for five years. I would have undoubtedly quit a number of times without your encouragement.

I would also like to thank my co-supervisors Professor Adrian Whitehouse and Dr Paolo Actis for offering me their expertise and resources.

Additionally I would like to thank my lab group, especially Lorelai Vennard and Ollie Antoniak who were particularly welcoming at the start when I first moved to Leeds and did not know anyone. A special shoutout to Sammy Hover, who demonstrated how the importance of having a postdoc in the lab, and for always answering my questions and being an all-round fount of knowledge. I would also like to thank Ellie Todd for being super supportive as I finished my thesis.

I would like to thank the Leeds electron microscopy facility for always offering their expertise and for also being friendly. In particular I would like to thank Martin Fuller who taught me how to process and image cells through transmission electron microscopy.

Moreover, I would like offer my gratitude to the Whitehouse lab for teaching me their western blot tips and tricks and for always offering me reagents and stocks. Specifically I would like to thanks James Murphy and Holli Carden for always answering my constant stream of questions.

A big thanks goes out to all of my friends who have been my support network throughout the entirety of my PhD. Especially, Charlotte, India, Toni, Kyra, and Kat who were always there for me, whether with food, drink, a couch, or a pep talk for my several breakdowns. I would also like to thank my old housemates Maia, Baz, Alice, and Clair for helping make Leeds my home for the last five years.

Finally, I would like to thank my family for always supporting me throughout the last 26 years, and especially my parents for putting up with me for this recent difficult year.

Abstract

Viruses are intracellular parasites that can subvert host cellular systems to enable the production of progeny viruses, which are then able to infect more cells. Transmission electron microscopy is one the main ways in which viral replication within cells can be directly visualised in a way that reveals ultrastructural details. Throughout this project I have utilised transmission electron microscopy to elucidate aspects of viral replication cycles within the cytoplasm of infected cells.

In chapter three I investigated the effects of Tula virus infection on cellular architecture in collaboration with Katherine Davies. Tula virus belongs to the hantavirus genus along with several other hantaviruses which are responsible for zoonotic illness in humans. From our investigation it was found that Tula virus forms large filamentous structures within the cytoplasm of infected cells that increase in size as infection progresses. These filamentous structures have been observed in New World hantavirus infected cells before, but this is the first time that the filaments have been identified in an Old World hantavirus. Furthermore, it was found that Tula virus infection results in the enlargement of the cell endoplasmic reticulum, potentially through inducing endoplasmic reticulum stress.

In chapter four I explored the role of liquid-liquid phase separation in rotavirus viroplasm formation. Rotaviruses are the most common cause of diarrhoeal disease in children, and they form viral factories within infected cells known as viroplasms. I found that when rotavirus infected cells were treated with an inhibitor of liquid-liquid phase separation, viroplasms reduced in size. This indicated that liquid-liquid phase separation is an important aspect of rotavirus viroplasm development.

Finally, in chapter five I examined the role of the host guanine nucleotide exchange factor DOCK5 on herpesvirus cellular egress. Herpesviruses are known for causing life-long infections in humans in over half the global population. I found that the gammaherpesvirus Kaposi’s sarcoma associated herpesvirus causes endoplasmic reticulum remodelling in infected cells, potentially in a manner similar to herpes simplex virus 1. I also found that evidence that DOCK5 is located within the nucleus of fibroblast and lymphocytes, despite the literature describing it as a cytoplasmic protein.

The experiments above demonstrate how transmission electron microscopy can be utilised to better understand viral replication cycles.

Table of contents

List of Tables

List of Figures

Abbreviations

(-): Negative-sense

(+): Positive-sense

3': 3 prime

5': 5 prime

ANDV: Andes Virus (*herpesvirus*)

ASFV: African swine fever virus

CD-M6PR: Cation-dependant mannose-6-phosphate receptors

CHOL: Choclo virus (*hantavirus*)

CLEM: Correlative light electron microscopy

CPE: Cytopathic Effect

cRNA: Complementary RNA strand (*Hantavirus*)

DLP: Double-layered particle (*rotavirus*)

DMEM: Dulbecco's modified Eagle's medium

DOBV: Dobrava-Belgrade virus (*hantavirus*)

Dp_{inf}: Days post infection

ds: Double-stranded

E: Early (*herpesvirus*)

EBV: Epstein-Barr virus (*herpesvirus*)

ELISA: enzyme-linked immunosorbent assay

EM: Electron Microscopy

EP: Early penetration (*rotavirus*)

ER: Endoplasmic reticulum

ERGIC: ER-Golgi intermediate compartment

ET: Electron tomography

FBS: Foetal bovine serum

FIB: Focused ion beam

FM: Fluorescence microscopy

GEF: Guanine nucleotide exchange factor

HCMV: Human cytomegalovirus (*herpesvirus*)

HPS: Hantavirus pulmonary syndrome (*hantavirus*)

HCV: Hepatitis C Virus

HD: 1,6-hexanediol (*rotavirus*)

HFF1: Human foreskin fibroblasts 1

HFRS: Haemorrhagic fever with renal syndrome

Hp_{ind}: Hours post induction

Hp_{inf}: Hours post infection

HS: Heparan sulphate

HSV1: Herpes simplex virus 1 (*herpesvirus*)

HSV2: Herpes simplex viruses 2 (*herpesvirus*)

HTNV: Hantaan virus (*hantavirus*)

ICTV: International committee on taxonomy of viruses

IE: Immediate-early (*herpesvirus*)

JC: John Cunningham

KS: Kaposi's sarcoma (*herpesvirus*)

L: Late (*herpesvirus*)

LANA: Latency-associated nuclear antigen (*herpesvirus*)

LAT: Latency-associated transcript (*herpesvirus*)

LB: Lamellar body

LLPS: Liquid-liquid phase separation

LP: Late penetration (*rotavirus*)

MCD: Multicentric Castle-man's disease (*herpesvirus*)

MCP: Major capsid protein

miRNA: MicroRNAs

MOI: Multiplicity of infection

N: Nucleoprotein (*respiratory syncytial virus)*

N-protein: Nucleocapsid protein (*SARS-CoV-2*)

NaB: Sodium butyrate

NaOH: Sodium hydroxide

NCR: Non-coding region

NEC: Nuclear egress complex (*herpesvirus*)

NPC: Nuclear pore complex

NSP: Non-structural protein (*Rotavirus*)

NSs: Non-structural (*hantavirus*)

NW: New World

ORFs: Open reading frames

OW: Old World

P: phosphoprotein polymerase cofactor (*respiratory syncytial virus*)

P-bodies: Processing bodies

p/s: Penicillin and streptomycin

PABP: Poly(A) binding protein

PB: Phosphate buffer

PBS: Phosphate buffered saline

PCR: Polymerase chain reaction

PEL: Primary effusion lymphoma (*herpesvirus*)

PERK: PKR-like ER kinase

pORFs: Open reading frame products (*herpesvirus*)

pU$_L$: Long unique sequence protein (*herpesvirus*)

pU$_S$: Short unique sequence protein (*herpesvirus*)

PUUV: Puumala virus (*hantavirus*)

RdRp: RNA-dependent RNA polymerase

RER: Rough endoplasmic reticulum

RPMI: Roswell Park memorial institute

RSV: Respiratory syncytial virus

RT: Reverse transcription

S1P: Site-1 protease

SA: Sialic acid

SCP: Small capsid protein

SEM: Scanning electron microscopy

SEOV: Seoul virus (*hantavirus*)

SNV: Sin Nombre virus (*hantavirus*)

SOX: Shutoff and exonuclease (*herpesvirus*)

ss: Single-stranded

ssTEM: Serial sectioning TEM

TEM: Transmission electron microscopy

TLP: Triple-layered particle

TPA: 12-O-tetradecanoyl-phorbol-13-acetate

TREx: TREx BCBL1-Rta

TULV: Tula virus (*hantavirus*)

UPR: Unfolded protein response

VHS: Virion host shutoff (*herpesvirus*)

VP: Viral protein (*Rotavirus*)

VPA: Valproic acid

vRNA: Viral RNA

VZV: Varicella zoster virus (*herpesvirus*)

WT: Wild type

ZIKV: Zika virus

Chapter 1 : Utilising transmission electron microscopy to better understand viral replication cycle

1.1 Introduction

Viruses are obligate intracellular parasites that convert host cells into viral production factories. They can infect all known forms of life, ranging from prokaryotic archaea and bacteria all the way to complex multicellular eukaryotes and even other viruses (Koonin et al., 2015, Mougari et al., 2019). Viruses employ a variety of strategies to infect their host, although most enveloped viruses employ viral glycoproteins to attach to specific host receptors to gain entry (Dimitrov, 2004). Once a virus has entered a cell, it immediately begins subverting anti-viral host responses in addition to co-opting the cellular metabolism. Eukaryotic viruses often seize control by manipulating host organelles and remodelling cellular membranes to form viral factories which act as a centralised base for protein production and genome replication (Fernández de Castro et al., 2020). Although the specific details vary per virus (e.g. viral factory structure, components, location, *etc.*), they are unified by the outcome; viral propagation. After the viral components have been produced they must be assembled into functional virions. Virions often contain a genome, protein capsid, and sometimes a lipid outer membrane (Prasad and Schmid, 2012). After assembly, the fully formed virus is released from the cell in a number of different ways, ranging from explosive lysis to gradual budding. Entire viral replication cycles are extremely complex and variable (Jones et al., 2020). Replication cycle variations can even exist between the same virus that infects different cells (e.g. herpes simplex virus 1 [HSV1] can infect both neuronal and epithelial cells (Schelhaas et al., 2003)). A greater understanding of viral cellular processes is crucial for understanding how these viruses work and subsequently how they can be inhibited. One way to study virus replication inside a cell is to employ transmission electron microscopy (TEM), which provides atomic to molecular understanding of the cell.

1.2 Transmission electron microscopy

TEM utilises a high-voltage electron beam which is focused through magnetic lenses to image samples. The biological sample (e.g. tissues or cells) are embedded within plastic and are sliced into ultra-thin sections, allowing the electron beam to transit through (Graham and Orenstein, 2007, Winey et al., 2014). Due to the low electron density of biological samples, heavy metal stains are used to saturate the membranes, proteins, and genomic material within the sample (Watson, 1958). The

heavy metal stains obstruct the electron beam as it passes through the sample in proportion to their relative electron density. The electron beam is then captured on a fluorescent screen which can be seen in real-time. The magnetic lenses can be used to focus the view, which can then be imaged on a digital camera as an electron micrograph (Graham and Orenstein, 2007, Winey et al., 2014).

Due to the extremely small nature of viruses and the resolving power of electron microscopes, TEM remains one of the main techniques of directly visualising viruses within infected cells. This is in part due to the difficulty in using light microscopy to image viral ultrastructure in detail (Cheng and Walz, 2009, Romero-Brey and Bartenschlager, 2015). Whilst biochemical tests such as polymerase chain reaction (PCR) and enzyme-linked immunosorbent assay (ELISA) provide quicker and often simpler diagnostic results, EM is considered as a gold-standard in the identification of novel emerging viruses and as such is often used in combination with other biochemical tests in diagnostics (Romero-Brey and Bartenschlager, 2015, Hazelton and Gelderblom, 2003, Dittmayer et al., 2020). For example, EM has been useful in the recent pandemic severe acute respiratory syndrome coronavirus 2 (SARS-CoV-2) (Udugama et al., 2020, Kim et al., 2020). In addition to viral classification and diagnostics, EM has been key to the visualisation of viral structures and the elucidation of viral life cycles, which is the main focus of this thesis (Romero-Brey and Bartenschlager, 2015, Cheng and Walz, 2009, Hesketh et al., 2018, Punch et al., 2018, Davies et al., 2020, Liu et al., 2019).

1.3 Sample preparation for TEM

For biological samples to be imaged via TEM, they need to be able to withstand the harsh environment within the microscope, which operates in a vacuum and bombards the sample with harsh ionising radiation. Therefore, samples need to be prepared in a way which minimises damage, and preserves their biological ultrastructure (Figure 1.1). For example, hard and dry materials which contain heavy metals are less likely to be damaged by radiation and will provide good image contrast. Consequently, organic materials which are neither hard, dry, nor possess heavy metals will need to be processed in a way which prepares them for TEM (Franken et al., 2020). As TEM has been used to image biological samples for decades, there are numerous preparation methods, with the specific approach being optimised for the sample in question (Graham and Orenstein, 2007). I will briefly go over the main steps in TEM sample preparation below.

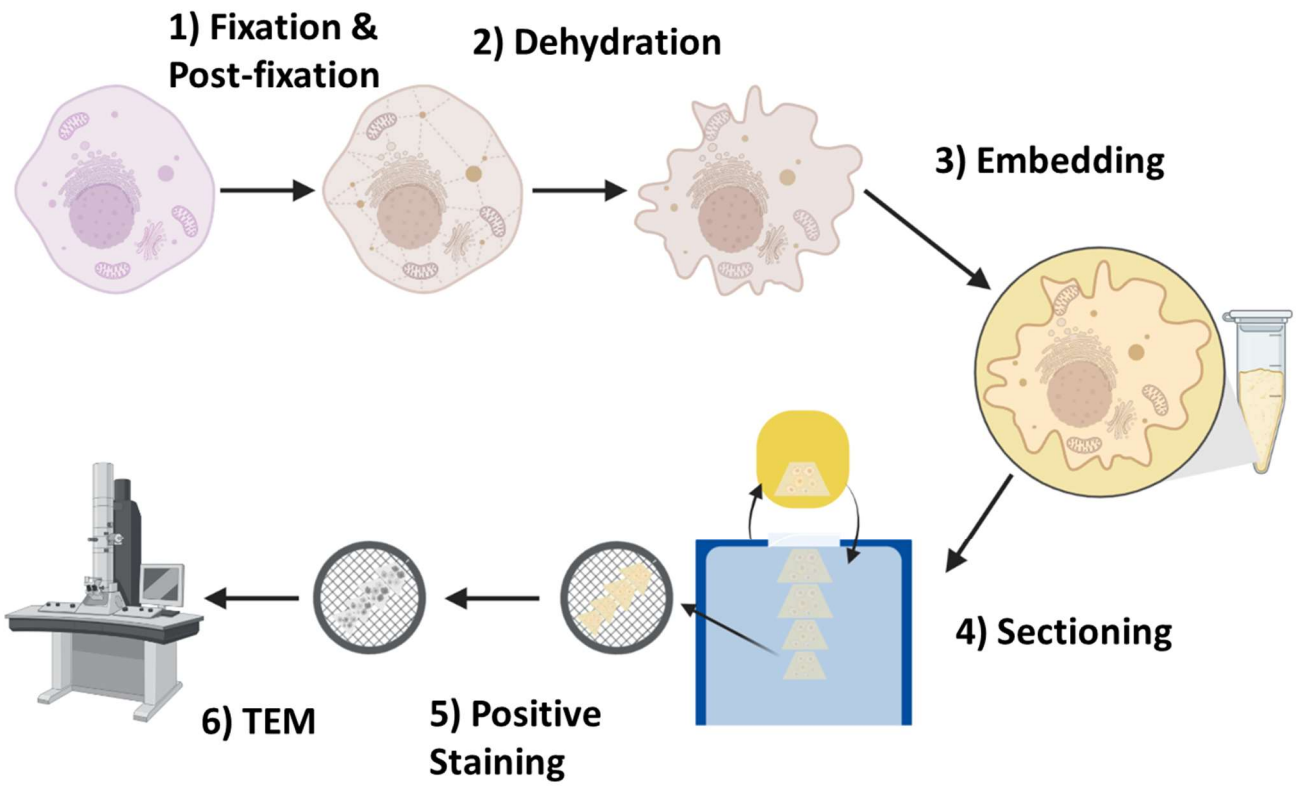

Figure 1.1: A simplified overview of the sample preparation for TEM.

Starting with fixation (1), cells are fixed in a number of different fixing agents (e.g. glutaraldehyde) to freeze metabolism and preserve the sample. Following fixation, cells undergo an additional post-fixation staining step with heavy metals (e.g. osmium tetroxide or uranyl acetate). Next, cells are dehydrated (2) with an ascending ethanol series to remove water from the sample. After dehydration, cells are embedded (3) within an epoxy resin which solidifies the sample. Once the cells are embedded, they can be sectioned (4) with an ultra-microtome to generate ultra-thin sections which are placed on an electron microscopy grid. Post sectioning, the cells are positively stained (5) in uranyl acetate and lead citrate. Finally, stained cells are imaged by transmission electron microscopy (TEM) (6). Figure was made using BioRender.

1.3.1 Fixation

The first step in the preservation of biological samples is fixation. Fixation stops metabolism in the tissues or cells and aims to preserve subject in life-like conditions (Wisse et al., 2010a). The most common method of fixation is through chemicals such as formaldehyde, glutaraldehyde or paraformaldehyde. These chemicals create cross-links between molecules within the sample, stabilising and preserving structural details (Romero-Brey and Bartenschlager, 2015). The fixatives used should be matched to the physiological conditions of the sample as much as possible, and so should be isothermic to avoid temperature shock, and also isotonic

to avoid unwanted fluid movement (Wisse et al., 2010a). Once fixed, samples undergo post-fixation staining with heavy metals such as uranyl acetate or osmium tetroxide. Osmium tetroxide is useful for staining lipids, encouraging the retention of lipids and also acts as a protein fixative (Nielson and Griffith, 1979, Stoeckenius and Mahr, 1965).

A newer and perhaps better method of preserving samples is cryo-fixation. Cryo-fixation involves freezing tissue or cells instantly at extremely low temperatures using liquid nitrogen. Frequently, the sample is actually frozen in liquid ethane or a mixture of ethane and propane which is cooled by the liquid nitrogen. The quick speed of the freezing produces glass-like vitreous ice, and prevents the formation of crystalline ice (Studer et al., 2008). Not only does crystalline ice damage the sample as it expands, but it also interacts with the electron beam, obscuring the sample (Dubochet et al., 1988, Studer et al., 2008). Cryo-fixation is limited to thin samples (~<10 μm), as the increased thickness slows freezing at the centre of the sample, resulting in crystalline ice formation. This can be mitigated by high-pressure freezing, which allows cryo-fixation of thicker samples (up to ~300 μm) (Franken et al., 2020, Vanhecke et al., 2008). Interestingly, chemical and cryo-fixation can be combined together (Romero-Brey and Bartenschlager, 2015). This technique is frequently used when working on extremely hazardous pathogens, where access to cryo-fixation equipment is often not available (Sherman et al., 2013). Therefore, the pathogenic samples are first chemically fixed, allowing for their removal from the secure laboratory as they are chemically inactivated and no longer pathogenic. The samples are then cryo-fixed, resulting in a double-fixation which has been shown to result in better subcellular structure preservation than chemical fixation alone (Romero-Brey and Bartenschlager, 2015, Sosinsky et al., 2008, Romero-Brey et al., 2012c).

1.3.2 Dehydration

The next step in sample preparation is the removal of water from the tissues or cells (Graham and Orenstein, 2007). The dehydration of the sample is necessary for two reasons. Firstly, water in a vacuum (e.g. inside an electron microscope) will spontaneously evaporate, resulting in severely damaged cells. Secondly, the resin that the sample is later embedded within is hydrophobic. Sample dehydration is achieved through submerging cells within a series of ascending alcohol concentrations (e.g. 40 %, 60 %, 80%, and 100%) (Stadtländer, 2005, Graham and Orenstein, 2007). This increasing concentration results in a gentler removal of water from the sample, reducing the formation of artefacts. Although shrinkage along with

protein and lipid extraction can occur from ethanol dehydration. Next, the sample is submerged in propylene oxide which acts as a transitional solvent as it is miscible with the plastics used for embedding (Stadtländer, 2005).

1.3.3 Embedding

Once dehydrated, the samples can be embedded. The process of embedding involves the infiltration of epoxy resin into the cells and tissues, which are then polymerised to form a hard plastic that can be sectioned (Winey et al., 2014). A variety of different resins are applicable for use in TEM, with epoxy resins being the easiest to section and stain. The large degree of structural preservation achieved with epoxy resin allows for high resolution imaging (Romero-Brey and Bartenschlager, 2015). Cells that have been cryo-fixed can also be embedded in resin through a process known as freeze-substitution. Freeze-substitution replaces the ice with a solvent (such as acetone) containing a fixative and contrasting agent. The sample is then infiltrated with an acrylic resin as mentioned above and polymerised (Hawes, 2015, Bykov et al., 2016). Freeze-substitution also allows for the preservation of (part of) the sample's epitopes, allowing for immunogold labelling.

1.3.4 Sectioning and Staining

Due to the inability of the electron beam to transit through an entire resin embedded cell, the sample must be sectioned before being imaged. To generate sections that are thin enough to be imaged, a glass or diamond knife must be used along with a ultramicrotome (Winey et al., 2014). Ultrathin sections in TEM are often between 60-80 nm in thickness, and will float on top of the water-filled boat that surrounds the knife, allowing for easy collection onto the TEM grid (Winey et al., 2014). As the TEM sample grid is small (~3 mm), sections must also be small to be loaded onto it (usually <1 mm). Once collected, sections will need to be further contrasted with heavy metal in post-section staining. The post-section staining of samples is frequently carried out first with uranyl acetate, and then with lead citrate (Reynolds, 1963, Winey et al., 2014). The contrasting of tissues and cells with uranyl acetate often occurs through positive staining, as opposed to the negative staining used for

-particle analysis. In positive staining, the uranyl acetate is allowed to penetrate deep within the sample, staining the internal cell structures (Tokuyasu, 1978). In negative staining, the stain forms an electron dense shadow around the particle of interest with the particle within appearing lighter (Scarff et al., 2018). Positive staining involves submerging the sample grid within uranyl acetate for longer, and is followed with lead citrate staining. Once the newly stained grids have dried, they are ready to be imaged using a transmission electron microscope.

1.4 TEM techniques

TEM can be combined with additional techniques to generate more information. TEM alone generates two-dimensional, grey-scale micrographs, which can offer limited insights into complex 3D biological processes. Therefore conventional TEM has been augmented overt-time to generate 3D reconstructions, and to identify specific components. Below I describe some TEM approaches, and illustrate their potential to image viral life cycles with selected examples.

1.4.1 Serial Section TEM

There are several ways of generating 3D *in situ* images through TEM, which offer greater information on 3D biological structures. One of the earlier techniques used was serial sectioning TEM (ssTEM) (Schauflinger et al., 2013b). ssTEM is a process in which a sequential length of ultrathin (<100 nm thick) sections are created, imaged through TEM, and then stacked together computationally to form a 3D image (Harris et al., 2006, Schauflinger et al., 2013b). The technique only requires the essential equipment for TEM, and can be combined with other techniques such as immunogold labelling (Schauflinger et al., 2013b). The method is however limited by the technical difficulty in obtaining a continuous sequence of sections, which can lead to missing sections and image alignment issues. As a result of how labour intensive and technically difficult ssTEM is, other methods of 3D EM have been developed (Jin et al., 2018, Harris et al., 2006, Romero-Brey and Bartenschlager, 2015, Denk and Horstmann, 2004). Despite this, ssTEM remains a fundamental technique that requires relatively inexpensive equipment and can result in high quality images (Fontana et al., 2008, Roingeard et al., 2008). For example, ssTEM was used by Schauflinger et al. (2013a) to better understand secondary

envelopment in human cytomegalovirus (HCMV). The researchers created 3D-reconstructions of the stages of HCMV budding into host membranes at the viral assembly complex, revealing ultrastructural details of HCMV morphogenesis (Schauflinger et al., 2013a).

1.4.2 Electron tomography

One of the more popular techniques for generating 3D models is electron tomography (ET). ET generates 3D volumes (known as a tomogram) of target objects and has been used to visualise cellular structures (e.g. organelles, membranes, filaments *etc.*) by taking several images of a 3D structure over a range of orientations (Scott et al., 2012, McIntosh et al., 2005). As such, ET can be used to visualise virus-cell interactions to a resolution of 5 to 10 nm (Ishikawa, 2016, Diebolder et al., 2012). ET circumvents the section alignment issues mentioned above through the use of thicker sections. Due to the increase in section thickness (200-400 nm) there are more structures contained within each section, resulting in a greater amount of information being available per section. However, although sections do not need to be aligned, ET projections do. Recently, ET projection alignment have been automated making it less work-intensive than the manual alignment of sections (Mastronarde and Held, 2017). Consequently, most of the time ET does not rely on multiple sections to generate tomograms. However, ET can still run into the same issue as ssTEM. Structures that are larger than 1 µm (e.g. mitochondria, viroplasms, *etc.*) do not fit within this ET range. Serial section ET can be used to mitigate this, but it runs into the same issues as serial sectioning (Jin et al., 2018, Denk and Horstmann, 2004, Koning et al., 2018). For example, ET was used by Gui et al. (2016) to better understand membrane fusion in influenza virus. Through cryo-ET, they were able to create 3D reconstructions of four distinct membrane intermediate structures that lead to fusion events in influenza entry, by mixing influenza virus and liposomes in vitro at low pH.

1.4.3 Correlative Light Electron Microscopy

Correlative light-electron microscopy (CLEM) combines the resolving power of TEM, with the ability of fluorescence microscopy (FM) to localise specific structures. The process involves preparing cells for TEM, in a way that preserves fluorescent tags or their epitopes. That way, cells can be fluorescently imaged prior to TEM, to identify

the structure or regions of interest. Then the cells are imaged through TEM, the orientation is matched with the fluorescent images, and the same regions of interest can be imaged with molecular detail (de Boer et al., 2015, Cortese et al., 2009, Santarella-Mellwig et al., 2018b). Samples can be prepared for TEM already fluorescently tagged, or the labelling can occur post embedding. Regardless, the usual TEM preparation is normally specifically determined by the research question (Bykov et al., 2016). For example, embedding samples within epoxy resin denatures proteins resulting in the loss of epitopes, rendering immunolocalisation experiments invalid (Begemann and Galic, 2016, Bykov et al., 2016). A solution to this is cryo-fixation which removes the need for resin embedding when the sample is imaged through cryo-TEM. Samples can also undergo freeze-substitution, as long as certain resins are used. For example, methacrylate-based resins preserve some protein structure allowing for antibody localisation (de Boer et al., 2015, Bykov et al., 2016). Probes have even been developed for CLEM which are visible during both FM and TEM. For example, Quantum dots appear as colourful fluorescent probes by FM, and as black dots through TEM (Killingsworth and Bobryshev, 2016). CLEM has been employed in a number of studies to better understand virus-cell interactions. For example, CLEM was used by Wang et al. (2017) to better understand virological synapses in HIV T-cells. Virological synapses are structures that form at points of contact between infected and non-infected cells, facilitating viral transmission (Chen et al., 2007). Through CLEM, researchers were able to identify distinct concentrates of viral proteins within endocytic and nonendocytic vesicles inside of previously non-infected target cells (Wang et al., 2017).

1.5 Aims

TEM is a powerful tool for the imaging of viral replication cycles in infected cells at the cellular and molecular level. The research displayed in this introduction helps to demonstrate how TEM can be used alone or in combination with other techniques to elucidate the details of viral replication. In this thesis I will be utilising TEM to better understand cytoplasmic replication in Tula virus, rotavirus, and herpesvirus.

Chapter 2 :
Materials and Methods

2.1 Materials

2.1.1 Chemicals and reagents

All chemicals and reagents were purchased from Thermo Fisher Scientific, Sigma-Aldrich, New England Biolabs, or TAAB Laboratories unless otherwise stated. Solutions were sterilised by autoclaving, or filtering with a 0.22 µm filter prior to use.

2.1.2 Mammalian cell lines

A list of the cell lines used during this project are below (Table 2.1).

Table 2.1: Mammalian cell lines used in project

Cell line	Growth Medium	Source	Supplier
Vero E6	Dulbecco's modified Eagle's medium (DMEM) supplemented with 10% fetal bovine serum (FBS) and 1 % penicillin and streptomycin (p/s)	African green monkey kidney	Dr. John Barr (University of Leeds)
MA104	DMEM supplemented with 10% FBS and 50 µg/ml gentamicin	African green monkey kidney	Dr. Alex Borodavka (University of Cambridge)
MA-NSP5-EGFP	DMEM supplemented with 10% FBS, 50 µg/ml gentamicin, and 1 mg/ml Geneticin	African green monkey kidney	Dr. Alex Borodavka (University of Cambridge)
TREx BCBL1-Rta	Gibco Roswell Park Memorial Institute (RPMI) 1640 supplemented with 10% FBS, 1 % p/s, and 100 µg/mL hygromycin B	Human B lymphoblast	Prof. Adrian Whitehouse (University of Leeds)
HFF1	DMEM supplemented with 10% FBS and 1 % p/s	Human Foreskin fibroblasts	Prof. Adrian Whitehouse (University of Leeds)

2.1.3 Viral strains

A list of the viruses used during this project are below (Table 2.2).

Table 2.2: Virus strains used in this project

Virus	Virus Strain	Origin	Background
Tula virus	Moravia/5302v/95	Dr. John Barr (University of Leeds)	Isolated from infected vole lung sample in Moravia (Vapalahti et al., 1996).
Rotavirus	Simian rotavirus strain SA-11	Dr. Alex Borodavka (University of Cambridge)	Isolated from rhesus macaques and is globally one of the most widely used reference strains. (Westerman et al., 2006)
Kaposi's sarcoma associated herpes virus	BCBL1 KSHV strain	Prof. Adrian Whitehouse (University of Leeds)	Cells containing the latent KSHV genome were isolated from a body cavity-based lymphoma biopsy (Komanduri et al., 1996).
Herpes simplex virus 1	SC16	Prof. Adrian Whitehouse (University of Leeds)	A highly neuroinvasive wildtype strain of HSV1 and is one of the most frequently used HSV1 strains in research (Cavallero et al., 2014).

2.1.4 Antibodies

A list of the antibodies used during this project are below (Table 2.3).

Table 2.3: Antibodies used in this project

Target	Species	Dilution	Type	Catalogue #	Supplier
GAPDH	Mouse	1 in 2500	Polyclonal	sc-47724	Santa Cruz Biotechnology
Lamin B1	Rabbit	1 in 1000	Polyclonal	ab65986	abcam
DOCK5	Rabbit	1 in 1000	Polyclonal	A304-988A-M	Thermo Fisher Scientific
pORF57 (KSHV)	Rabbit	1 in 5000	Polyclonal	600-401-A94	Thermo Fisher Scientific
pORF62 (KSHV)	Mouse	1 in 1000	Monoclonal	MA5-14770	Thermo Fisher Scientific
pU_L19 (HSV1)	Mouse	1 in 1000	Monoclonal	ab6508	abcam
Anti-Mouse	Goat	1 in 5000	Horseradish peroxidase secondary antibody	L3032	Generon
Anti-Rabbit	Goat	1 in 3000	Horseradish peroxidase secondary antibody	#7074	Cell Signalling Technologies

2.1.5 miRIDIAN microRNA hairpin inhibitor

The miRIDIAN microRNA hairpin inhibitor used in this project was hsa-miR-365a-3p, catalogue number: IH: 300666-05-0002.

2.1.6 Buffer recipes

A list of the buffers and their recipes used in in this project are below (Table 2.4)

Table 2.4: Buffers and their recipes used in this project

Buffer	Recipe	Use
0.1 M Phosphate buffer (pH 7.2)	0.1 M sodium phosphate dibasic stock	Transmission electron microscopy
	0.1 M sodium phosphate monobasic stock	
	Add monobasic solution to the dibasic solution until the pH is 7.2	
RIPA Cell lysis buffer	150 mM sodium chloride	Cell lysis
	50 mM Tris-hydrochloride (pH 8)	
	1 % NP-40 (v/v)	
	0.1 % sodium dodecyl sulfate (w/v)	
	dH2O	
2 x loading buffer	100 mM Tris-hydrochloride (pH 6.8)	Western blot
	4 % sodium dodecyl sulfate (w/v)	
	10 % glycerol (v/v)	
	0.2 % bromophenol blue (w/v)	
	dH2O	
10 x transfer buffer	0.25 M Tris	Western blot
	0.885 M glycine	
	dH2O	
Semi-dry transfer buffer	1 x transfer buffer (v/v)	Western blot
	20 % methanol (v/v)	
	dH_2O	
10 x Tris-buffered saline	0.25 M Tris	Western blot
	1.37 M NaCl	
	Adjust pH to 7.5 with HCl	
Tris-buffered saline	10 x Tris-buffered saline	Western blot
	dilute 1:9 in dH_2O	

2.2 Mammalian cell culture and viruses

2.2.1 Mammalian cell maintenance and storage

2.2.1.1 Routine cell maintenance

All cells were grown in their relevant media according to according to table 2.1, at 37°C with 5% CO_2 in a humidified incubator. Cells were split every two to three days when they reached ~80 % confluency. Adherent cell lines were detached with 3 mL trypsin-EDTA (0.25 % [w/v]) for 5 to 10 minutes before being resuspended in 7 mL of complete relevant media to deactivate the trypsin.

For long term storage, confluent cells were preserved in their respective media with 5 % dimethyl sulfoxide and stored at -80°C.

2.2.1.2 Assessing cell viability

Cell viability was assessed through the use of the EVE™ automatic cell counter (NanoEntek). Cells were first mixed 1:1 with trypan blue (0.4 %), and then 10 µl of mixture was loaded onto each of the two EVE™ Cell counting slide chambers. The counting slide was then inserted into the automatic counter and manually focused. Once correctly focused, the cells were counted.

For TREx BCBL1-Rta (TREx) cells, the parameters used were as follows- Sensitivity: 5, minimum cell size: 7, maximum cell size: 60, circularity: 80.

2.2.1.3 Hexanediol treatment

For the rotavirus experiments in chapter 4, MA104 and MA-NSP5-EGFP cells had 1,6-hexanediol (HD) added to cell culture media (4 % [v/v]) for ~30 seconds and then the treated media was replaced with fresh serum-free media and the cells prepared for TEM.

2.2.1.4 Transfection

The hsa-miR-365a-3p miRIDIAN microRNA hairpin inhibitor was inserted into cellular nuclei via nucleofection. Firstly, 8 x 10^6 cells were pelleted at 4500 rpm for 6 minutes and the suspension was removed. The cell pellet was then suspended in 100 µl of room-temperature InGenio® electroporation solution. Next, the miRIDIAN microRNA hairpin inhibitor was added to the cell solution at a final concentration of 100 nM. The cell solution was then gently mixed and added into a 0.2 cm InGenio® cuvette. The cuvette was then added into the Amaxa nucleofector I and the T-01 program was used to transfect the cells. Afterwards, 300 µl of relevant antibiotic free growth medium was added and the cells were left at room temperature for 10 minutes. The cells were then diluted in 10 ml of complete growth media and left to recover for 24 hours under normal growing conditions, at which point viral induction or infection could occur.

2.2.2 TULV primary infection

Vero E6 cells were infected with Tula virus (TULV) when at ~90 % confluency. Prior to inoculation, cells were washed three times in phosphate buffered saline (PBS). Then TULV was diluted to a multiplicity of infection (MOI) of 0.1 in serum free DMEM and then added to media-free cells. Inoculated cells were then incubated at 37 °C with gentle rocking for 90 minutes to allow for virus adsorption. Once adsorbed, complete DMEM with 2 % FBS was added and the cells were incubated until the relevant time point.

2.2.3 TULV stock propagation

Originally stocks of TULV were generated by Katherine Davies, with the MOI being calculated via plaque assay as described in (Davies et al., 2019).

2.2.4 Rotavirus primary infection

MA104 or MA-NSP5-EGFP cells were infected with rotavirus when confluent. Prior to inoculation, cells were washed three times in PBS, and the rotavirus virions were treated with trypsin (final concentration of 10 µg/ml) for 1 hour in a 37°C water bath to cleave the outer viral attachment protein. Following activation, rotavirus was diluted to a MOI of 1 in serum free DMEM and then added to media-free cells. Inoculated cells were then incubated at 37 °C with gentle rocking for 1 hour. Following adsorption, viral media was removed and the cells were washed with serum free DMEM. Complete DMEM was then added to the cells, which were then incubated for the relevant times.

2.2.5 KSHV lytic induction

TREx cells are PEL B-cell lines that are latently infected with KSHV and have been modified to possess a doxycycline inducible promoter for Rta, the lytic activator of KSHV (Nakamura et al., 2003). KSHV lytic activation was stimulated at ~80 % confluency specifically with either the addition of 0.2, 1.0, or 2.0 µg/ml doxycycline, or were non-specifically activated with addition of 20 ng/ml 12-O-tetradecanoyl-phorbol-13-acetate (TPA), 0.3 mM sodium butyrate (NaB), both TPA and NaB (20 ng/ml and 0.3 mM, respectively), or valproic acid (VPA) at either 0.6 or 1.2 mM. The inducing agent was added directly to the cells which were suspended in fresh complete RPMI media and thoroughly mixed.

2.2.6 HSV1 primary infection

Prior to infection, confluent human foreskin fibroblasts (HFF1) cells were washed twice with PBS and the media was removed. HSV1 stock was diluted to an MOI of 4 in serum free media and added to the washed, media-free HFF1 cells. The cells were then incubated with gentle shaking for 2 hours at 37°C. The virus media was removed and the cells were washed with PBS. Finally, 3 ml of complete media was added and the cells were incubated for the relevant times.

2.2.7 HSV1 stock propagation

To create new stocks of HSV1, confluent HFF1 cells in a 75cm^2 Corning™ Cell Culture Treated Flasks had their media removed and were washed twice with PBS. HSV1 stock was then diluted in 3 ml of serum free culture media to a MOI of 0.01 and then added to the cells. Cells were then incubated for 2 hours at 37 °C with gentle shaking. The virus was then replaced with 3 ml of complete DMEM media and incubated for 3 to 4 days at 37 °C until the cells were showing 100 % cytopathic effect (CPE). At this point the cell suspension was removed from the flask and added to 3 ml of autoclaved milk (9 % [w/v] non-fat milk powder in dH_2O). The cell-milk mixture was then centrifuged at 2000 g for 5 minutes at 4 °C, and the supernatant was collected (pellet contains cell-debris). Viral supernatant was then stored at -80 °C.

2.2.8 HSV1 plaque assay

Initially, 2.0 x 10^5 HFF1 cells were counted manually with a haemocytometer and then seeded into each well of a 12-well plate one day before the assay, resulting in ~90 % confluency on the day. Next, a serial dilution of the unknown concentrations of HSV1 stock was created in serum free media, and the cells were washed in PBS twice. 200 µl of each HSV1 dilution was added to each of the designated wells in triplicate. The inoculated cells were then incubated for 2 hours with gentle mixing at 37 °C. After incubation, ~1.5 ml of overlay (a 1:1 ratio of DMEM media with 20% FBS added to 2.4 % [w/v] low-viscosity Avicel® in water) was gently added to each of the wells, and the cells were incubated for ~3 days (until plaques appear). After ~3 days, cells were fixed in 1.5 ml 10 % (v/v) formaldehyde for 15 minutes. After 15 minutes, the formaldehyde-overlay mixture was removed and the cells were gently washed with PBS. Finally, 500 µl of 1 % crystal violet ([v/v] in 20% [v/v] ethanol) was added to each of the wells for 15 minutes with gentle rocking. After 15 minutes the crystal violet was washed off with water and the wells were left to dry. Once dry, the plaques were counted, and the pfu/ml calculated (n × 5 × d = PFU/ml [where n equals the number of plaques counted and d equals the dilution]).

2.3 Transmission electron microscopy

2.3.1 Sample fixation

Suspension cells were pelleted at 14000 rpm for 2 minutes and the supernatant was removed. Cells were then fixed in 1 ml of 2.5 % glutaraldehyde ([v/v] in 0.1 M phosphate buffer [PB]) and incubated at room temperature for 2.5 hours.

For adherent cells, media was replaced with serum free media and equal amounts of 5 % glutaraldehyde ([v/v] in 0.1 M PB) was added and the cells were incubated for two hours at room temperature. After incubation, cells were scraped from the flask and transferred to an Eppendorf.

2.3.2 Sample post-fixing, dehydration and embedding

Post fixation, cells were pelleted at 14000 rpm for 2 minutes, to remove the glutaraldehyde. The fixed cells were then washed twice in 0.1 M PB for 30 minutes. Next, the cells were then post-fixed in 1% osmium tetroxide ([w/v] in 0.1 M PB) for 1 hour on ice. Then, the post-fixed cells were washed four times in 0.1 M PB on ice. Subsequently, the post-fixed cells were dehydrated using ascending ethanol concentrations (40%, 60%, 80% and 2 x 100%) for 20 minutes each, and then twice in propylene oxide for 20 minutes each to remove any ethanol (all of these dehydration and propylene oxide steps were on ice). Afterwards, the dehydrated cells were carefully mixed with a 1:1 mixture of propylene oxide and araldite epoxy resin. The araldite epoxy resin was composed of a mixture of araldite CY212 (27 g), DDSA (23 g), and DMP 30 (1 g) which was mixed thoroughly through a vortex and then centrifuged at max speed for 15 minutes to remove bubbles *****. The cells and propylene oxide-resin mixture were placed on a rotator overnight to allow for resin infiltration. The sample was centrifuged and the mixture was then removed, pure araldite was added and the sample was placed on the rotator for 8 hours, four-times****** (over two-days). At this point, the araldite was replaced with a fresh amount of pure resin and the embedded cells were polymerised at 60 °C for 24 hours.

2.3.3 Sectioning, positive staining and TEM

Embedded cells were then sectioned in the ultra-thin range (80 to 100 nm) using a Reichert-Jung Ultracut E ultramicrotome and a diamond knife. Ultra-thin sections were then placed upon formvar coated, copper grids and stained with uranyl acetate and lead citrate according to (Reynolds, 1981). Briefly, sectioned cells were stained in 8% saturated uranyl acetate ([W/V] with ultrapure water) for 1 hour. Stained grids were then washed in dH_2O for 5 minutes (five times). Afterwards, the sections were stained with filtered* lead citrate for 10 minutes in a petri dish with sodium hydroxide (NaOH) pellets. The lead citrate-stained grids were then washed in 0.02 M NaOH for 1 minute (three times), and in dH_2O for 1 minute (five times). KSHV prepared samples were then imaged using a JEOL 1400 electron microscope at 120 kV, whereas TULV and rotavirus samples were imaged using a FEI Tecnai T12 electron microscope at 120 kV.

2.4 Biochemical techniques

2.4.1 Cell lysis

2.4.1.1 Whole cell lysis

Cells were washed in PBS and ice-cold RIPA lysis buffer was added to the cells (200 µl for a 6-well plate, or 100 µl for a 12-well plate), swirling to ensure full coverage. The cells were then placed on an orbital shaker at a gentle speed for 15 minutes (still on ice). Adherent cells were then scraped off, and the lysate was collected (suspension cell lysate was directly collected). Lysate was then centrifuged at maximum speed for 10 minutes to pellet cell debris. Finally, supernatant was collected and stored at -20 °C for up to six months.

2.4.1.2 Subcellular fractionation

For adherent cells media was removed, PBS was added, and cells were then scraped. Suspension, or scraped adherent cells were then centrifuged at 1700 rpm for 7 minutes, and the supernatant was discarded. Cells were then lysed in 600 µl of 1 % Triton X-100 ([v/v] with PBS) and left on ice for 10 minutes. After 10 minutes,

250 µl of the total volume was removed and left on ice, that was the whole cell fraction. The remaining 350 µl was then centrifuged at 720 x g for 5 minutes at 4 °C. The supernatant was then removed and kept on ice, that was the cytoplasmic fraction. The cytoplasmic supernatant was the purified by centrifugation at 720 x g for 5 minutes at 4 °C, with the top ¾ of the supernatant being carefully collected *.

The remaining pellet nuclei (nuclear fraction) was then washed in PBS to remove any cytoplasm-containing supernatant and centrifuged at 720 x g for 5 minutes at 4 °C. The nuclear pellet was then lysed in 100 µl PBS with 1 % Triton X-100 ([v/v] with PBS). Afterwards, protein samples were frozen at -20 °C for up to six months.

2.4.1.3 Determination of protein concentration

Protein concentration of whole cell and subcellular lysates were assessed via Pierce™ BCA Protein Assay Kit using the set protocol (Thermo Fisher Scientific).

2.4.2 SDS-PAGE

Prior to SDS-PAGE, protein supernatants were supplemented at a 1:1 ratio with 2x SDS loading buffer and 50 mM dithiothreitol and were subsequently incubated at 95 °C for 5 minutes. The lysates were then allowed to cool to room temperature, and then loaded into SDS-polyacrylamide gels (see Table 2.5 for gel recipe) for ~50 minutes at 180 V in 1 x Tris/Glycine/sodium dodecyl sulfate electrophoresis buffer (diluted in dH_2O) (Bio-Rad Laboratories).

Table 2.5: SDS-PAGE gel recipe for one gel

Reagents	6 % resolving gel	8 % resolving gel	10 % resolving gel	Stacking Gel
1.5 M Tris-hydrochloride (pH 8.8)	2.5 ml	2.5 ml	2.5 ml	-
1.5 M Tris-hydrochloride (pH 6.9)	-	-	-	0.125 ml
dH_2O	5.3 ml	4.6 ml	4 ml	1.495 ml
30 % acrylamide	2 ml	2.7 ml	3.3 ml	0.33 ml
10 % sodium dodecyl sulfate	0.1 ml	0.1 ml	0.1 ml	0.02 ml
10 % ammonium persulfate	0.1 ml	0.1 ml	0.1 ml	0.02 ml
tetramethylethylenediamine	0.032 ml	0.024 ml	0.016 ml	0.01 ml

2.4.3 Western blot

Separated protein samples were then then transferred from gels onto nitrocellulose membranes through semi-dry transfer. Transfer occurred using the BIO-RAD Trans-blot® Turbo™ on the standard SD setting (25 V, 1.0 A, for 30 minutes) submerged within semi-dry transfer buffer. Transfer efficiency was assessed through Ponceau S staining solution (Thermo Fisher Scientific) which was later removed and reused, with the membrane being washed three times with dH_2O. The membranes were then blocked overnight with tris-buffered saline with 0.1% tween (v/v) and 5% dried skimmed-milk powder (w/v) at 4 °C. Proteins were then labelled with relevant primary antibodies in 5 % milk for one hour at room temperature. Membranes were then washed three times for 5 minutes each in tris-buffered saline with 0.1% tween (v/v). Proteins were then incubated with the relevant horseradish peroxidase tagged secondary antibody for one hour at room temperature. Next, membranes were then washed three times for 5 minutes in tris-buffered saline with 0.1% tween (v/v). Finally, Horseradish peroxidase labelling was then detected with the EZ-ECL

enhanced chemiluminescence kit (Biological Industries) and imaged through the Syngene™ G:Box XX9 gel imaging system.

2.5 Data presentation, analysis and bioinformatic analysis

Statistical tests were carried out on Microsoft Excel and TEM micrograph analysis was carried out on Image J (Schneider et al., 2012). Images were prepared for publication using Microsoft PowerPoint.

Bioinformatic analysis was carried out using amino acid sequences from UniProt (see table 2.6) (The UniProt, 2021). Protein hydrophobic regions were predicted using Kyte and Doolittle (1982), Abraham and Leo (1987), and Bull and Breese (1974) tests of hydropathy which were accessed on the Swiss-Prot ExPASy ProtScale Server (Gasteiger et al., 2005). Next, protein structure predictions were generated using AlphaFold (Jumper et al., 2021, Varadi et al., 2021). Finally, the lipid-droplet promoting propensity was assessed using FuzDrop and disordered regions of the proteins in question were assessed using flDPnn (Hatos et al., 2022, Hu et al., 2021).

Table 2.6: List of the proteins used in the bioinformatic analysis and their UniProt accession codes.

Virus	Protein	UniProt Accession	Citation
Rotavirus A	NSP2	A2T3N6	Kanai et al., 2017
Rotavirus A	NSP5	A2T3Q9	Jiang et al., 2006
Rotavirus A	NSP2	4G0J	Hu et al., 2012a
Rotavirus B	NSP2	Q86197	Jiang et al., 2005
Rotavirus B	NSP5	P18571	Chen et al.,1990
Rotavirus C	NSP2	Q9PY93	Taraporewala et al., 2006
Rotavirus C	NSP5	Q00682	Lambden et al., 1992
Rotavirus D	NSP2	E2EBU6	Trojnar et al., 2010
Rotavirus D	NSP5	E2EBV0	Trojnar et al., 2010
Rotavirus F	NSP5	M4H296	Kindler et al., 2013
Rotavirus G	NSP2	U3QY07	Phan et al., 2013
Rotavirus G	NSP5	U3R085	Phan et al., 2013
Rotavirus A	VP4	A0A0D5CDS5	Delogu et al., 2015
SARS-CoV-2	N-protein	P0DTC9	Bessa et al,. 2022

Chapter 3 : Tula virus forms a filament network during cell infection

3.1 Tula virus introduction

Hantaviruses are enveloped viruses that are found globally in a variety of rodent and insectivore hosts. Hantaviruses are zoonotic, with transmission occurring primarily via the aerosolised excreta (saliva, faeces, urine) of infected rodents (Vapalahti et al., 2003). This group of viruses are endemic to several regions globally and are separated into two groups based on geography and pathobiology: New World (NW) hantaviruses and Old World (OW) hantaviruses (Engdahl et al., 2021). Hantaviral disease can be severe, with two different clinical manifestations resulting from whether infection was with a NW or and OW hantavirus. Hantaviruses represent an emerging public health threat with ~150,000 to 200,000 people each year affected (Munir et al., 2021, Verner-Carlsson et al., 2015).Hantaviruses have a tripartite single-stranded (ss) negative-sense (-) RNA genome that encodes only four viral proteins. Viral replication occurs within the cytoplasm of infected cells where they transcribe and translate their viral RNA (vRNA) before assembly and egress (Mir et al., 2008). TULV is an OW hantavirus found throughout Eurasia in common voles (*Microtus arvalis*) and is rarely responsible for pathogenicity in humans (Hofmann et al., 2021).

3.1.1 Hantavirus Taxonomy

Hantavirus is a familiar name for the genus *Orthohantavirus*. These are RNA viruses that belong to the *Hantaviridae* family within the *Bunyavirales* order (Laenen et al., 2019). There are 36 unique hantaviruses in the *Orthohantavirus* genus recognised by the International Committee on Taxonomy of Viruses (ICTV) (Table 3.1) (Munir et al., 2021, Mull et al., 2020, Abudurexiti et al., 2019, Laenen et al., 2019).

Table 3.1: A list of the main pathogenic hantaviruses responsible for causing haemorrhagic fever with renal syndrome (HFRS) and hantavirus pulmonary syndrome (HPS) (Laenen et al., 2019).

	Hantavirus Species	Virus Abbreviation	Reservoir Host		Continent	Disease
Old World Hantavirus	*Dobrava-Belgrade orthohantavirus*	DOBV	*Apodemus flavicollis*	Mouse	Europe	HFRS
	Puumala orthohantavirus	PUUV	*Myodes glareolus*	Vole	Europe	HFRS
			Myodes rufocanus	Vole	Europe	HFRS
	Tula orthohantavirus	TULV	*Microtus arvalis*	Vole	Europe	HFRS
			Microtus rossiaemeridionalis	Vole	Europe	HFRS
	Hantaan orthohantavirus	HTNV	*Apodemus agrarius*	Mouse	Asia	HFRS
	Seoul orthohantavirus	SEOV	*Rattus norvegivus*	Rat	Asia	HFRS
New World Hantavirus	*Bayou orthohantavirus*	BAYV	*Oryzomys palustris*	Rat	N. America	HPS
	Black Creek Canal orthohantavirus	BCCV	*Sigmodon hispidus*	Rat	N. America	HPS
	Prospect Hill orthohantavirus	PHV	*Microtus pennsylvanicus*	Vole	N. America	HPS
	Sin Nombre orthohantavirus	SNV	*Peromyscus maniculatus*	Mouse	N. America	HPS
	Andes orthohantavirus	ANDV	*Oligoryzomys longicaudatus*	Rat	S. America	HPS
	Choclo orthohantavirus	CHOV	*Oligoryzomys fulvescens*	Rat	S. America	HPS
	El Moro Canyon orthohantavirus	ELMCV	*Reithrodontomys megalotis*	Mouse	S. America	HPS
	Laguna Negra orthohantavirus	LANV	*Calomys laucha*	Mouse	S. America	HPS

3.1.2 Hantavirus Disease

3.1.2.1 Clinical Characteristics

Hantavirus infection can result in one of two diseases: haemorrhagic fever with renal syndrome (HFRS), or hantavirus pulmonary syndrome (HPS). Both HFRS and HPS target the pulmonary, cardiac, nervous, and hormonal systems resulting in acute disease with the potential for long-term damage (no chronic disease cases have been detected) (Krüger et al., 2011). HFRS and HPS share several clinical characteristics and are consequently considered to share a root pathogenesis, resulting in similar initial symptoms. Differences in hantavirus disease results from the targeting of different vascular systems. HPS targets the pulmonary capillaries, with HFRS targeting the renal medullar capillaries (Hjelle and Torres-Pérez, 2010, Avšič-Županc et al., 2019).

3.1.2.1.1 HFRS

The severity of HFRS is extremely variable, with disease outcome ranging from asymptomatic to lethal. Complications in HFRS cases can result in haemorrhaging, oedema, and shock (Vaheri et al., 2013, Munir et al., 2021). Fatality in HFRS occurs in 1 % to 15 % of cases (Engdahl et al., 2021). The main hantaviruses responsible for HFRS are Puumala virus (PUUV), Hantaan virus (HTNV), Seoul virus (SEOV), and Dobrava-Belgrade virus (DOBV) (Munir et al., 2021). Nephropathia epidemica is a milder form of HFRS caused by PUUV and is characterised by anaemia, thrombocytopenia, haematuria, and proteinuria with a fatality rate of up to 0.4% (Mustonen et al., 2013).

3.1.2.1.2 HPS

When compared to HFRS, HPS is the more severe illness and has a case fatality rate of 30-50 % depending on virus strain (Avšič-Županc et al., 2019, Enria et al., 2001). HPS is often characterised by pulmonary oedema and cardiogenic shock resulting in rapid respiratory failure and is consequently considered a severe disease (Bellomo et al., 2021). Sin Nombre virus (SNV), Andes virus (ANDV), and Choclo virus (CHOV), are responsible for causing the deadlier forms of HPS (Munir et al., 2021).

3.1.2.2 Hantavirus Pathology

Hantavirus symptoms arise from the direct targeting of the cellular endothelium of various organs (e.g. kidneys or lungs) and the immune response (e.g. macrophages) (Mustonen et al., 2013, Avšič-Županc et al., 2019). Both diseases are characterised by thrombocytopenia, and increased vascular and microvascular bed permeability (Hjelle and Torres-Pérez, 2010). The infection of endothelial cells in alveolar or glomerular capillary beds by NW and OW hantaviruses respectively results in HPS or HFRS (Mackow and Gavrilovskaya, 2009). Compared to other RNA viruses, hantavirus replication is slow, with viraemia taking 5-10 days after infection to occur (Mackow and Gavrilovskaya, 2009).

Post inhalation, it is unknown how hantaviruses traffic to their target replication sites. Currently it has been predicted that immature dendritic cells are involved with hantavirus distribution. Dendritic cells transit through the lymphatic system, interact with endothelial cells, and express β3-integrin receptors (a known hantavirus target receptor) (Schönrich and Raftery, 2019). The infection of dendrites, macrophages, and lymphatic cells can also lead to immune system activation (Jonsson et al., 2010, Avšič-Županc et al., 2019). The antiviral immune response can be involved in disease prognosis. The inflammatory cytokines interleukin-10 and tumour necrosis factor-α were found to be significantly higher in patients with severe cases of HFRS (Saksida et al., 2011). Furthermore, higher levels of hantavirus-activated CD8+ T cells and the over abundant cytokine production by macrophages have been found in severe cases of HPS (Kilpatrick et al., 2004). Haemorrhagic viruses commonly prevent infected dendritic cell from maturing. However, in acute hantavirus infection dendritic maturation is triggered, resulting in a robust T cell reaction (Kilpatrick et al., 2004). The pathogenesis of hantavirus disease involves a complicated interplay between endothelial cell barrier failure, immunopathology, and platelet dysfunction which when combined together can lead to patient death (Avšič-Županc et al., 2019).

3.1.2.3 TULV Infection

TULV rarely causes clinical hantaviral disease in humans, with only four cases being confirmed to date, with no fatalities having been reported (Bourquain et al., 2019). Serological evidence of TULV infection has been further found in 4% of ~500 German forestry workers tested, and in one blood donor in the Czech Republic (Mertens et al., 2011, Vapalahti et al., 1996). Additionally, a population survey of

6,537 healthy individuals in Germany found serological evidence of TULV infection in 1 of the samples (Ulrich et al., 2004). However, there is often no differential distinction between HFRS caused by PUUV or TULV, with most being classed as the more commonly pathogenic PUUV. This is due to the close antigenic and genetic connection between PUUV and TULV, meaning that anti-TULV and anti-PUUV seroreactivites cannot be distinguished unless using a neutralisation assay (Hofmann et al., 2021). Consequently cases of TULV infections could be being diagnosed as PUUV, and therefore TULV infections would be underrepresented (Clement and Van Ranst, 2016, Bourquain et al., 2019). As a result of the few confirmed cases of TULV infection in humans, little is known about TULV pathogenicity in humans (Hofmann et al., 2021, Zelená et al., 2013).

3.1.2.4 Diagnosis, Treatment and Prevention

3.1.2.4.1 Diagnosis

Hantavirus diseases are diagnosed based upon clinical symptoms, epidemiological data (location, rodent exposure, *etc.*), and through laboratory tests. The first step in diagnosis is the recognition of hantavirus symptoms by the physician. However, due to the non-specific nature of these flu-like symptoms, diagnosis cannot be made at this point (Avšič-Županc et al., 2019, Mattar et al., 2015). A follow up laboratory diagnosis will be often be performed using either serology or reverse transcription (RT)-PCR (Mattar et al., 2015). Serological analysis is the most frequently used method of hantavirus diagnosis, which detects antibodies against hantavirus Gn, Gc, and nucleocapsid proteins (NPs) (Maes et al., 2004, Figueiredo et al., 2008). ELISA is the most commonly used serological test which can be used to detect anti-hantavirus IgM (early infection) or IgG (retrospective studies) (Maes et al., 2004). The RT-PCR uses primers specific to the S and M hantavirus genome segments (Moreli et al., 2004, Mattar et al., 2015).

3.1.2.4.2 Treatment

To date, there are no FDA approved therapeutic agents for hantaviral infections, although there are ongoing trials for a number of vaccines (Engdahl et al., 2021, Avšič-Županc et al., 2019). Ribavirin has shown some success in treating HFRS in Chinese clinical studies. Mortality rate was significantly reduced if ribavirin was administered within the first five days of symptom onset (Huggins et al., 1991). This was supported by a more recent report on the admission of ribavirin for HFRS in Korea (Rusnak et al., 2009). Unfortunately, studies investigating the use of ribavirin

for HPS have been less successful, with no significant reduction in mortality found (Moreli et al., 2014). The majority of treatment for hantavirus disease is supportive, with severe cases being handled by intensive care units. Furthermore, human monoclonal antibodies isolated from ANDV survivors have been shown to have therapeutic applications when tested on animal models (Engdahl et al., 2021).

3.1.2.4.3 Prevention

Most preventative measures rely on reducing the incidence of hantavirus host-human interactions. The main risk factor in hantavirus disease incidence is cleaning houses or sheds, living in forested areas, and careers in farming, forestry, and the military (Abu Sin et al., 2007, Van Loock et al., 1999). Subsequently, preventative measures primarily focus on rodent control, removing rodent food sources, and destroying rodent habitat (Avšič-Županc et al., 2019). Besides the use of basic preventative measures, vaccines would need to be employed to reduce viral spread. Inactivated hantavirus vaccines have currently been used with success in China and Korea but are not approved for use in the US or Europe. Currently, a mixture of inactivated, virus-like particle, recombinant protein, and DNA based vaccines are being tested, with the USA conducting several clinical trials on the latter (Liu et al., 2020, Dheerasekara et al., 2020).

3.1.3 Hantavirus Epidemiology

3.1.3.1 Transmission

Hantaviruses are zoonotic, and so disease outbreaks in humans occur when human-host interactions occur. Hantaviruses are primarily transmitted to humans via the inhalation of aerosolised rodent excreta. Hantavirus transmission from rodent bites is rare (Kruger et al., 2015). However, person-to-person transmission has been documented several times for ANDV in Argentina and Chile, where large social gatherings or prolonged contact increased the likelihood of transmission (Martínez et al., 2020, Alonso et al., 2020, Martinez et al., 2005). One factor that affects transmission is hantavirus stability. Hantavirus virions can be infectious for long periods of time, depending upon factors such as humidity and temperature (Kruger et al., 2015). For example, HTNV virions are still infective for up to 9 days at 37 °C, and 96 days at 4 °C (Hardestam et al., 2007). PUUV and TULV virions are infective at room temperature for up to 5-11 days, and up to 18 days at 4 °C (Kallio et al., 2006). Hantavirus stability increases the window of opportunity for infection over

prolonged periods of time and allows for indirect transmission of disease (Kallio et al., 2006).

3.1.3.2 Animal Hosts

All hantaviruses possess reservoir hosts which determine their geographical spread, with each hantavirus being associated with at least one reservoir species. These hosts are mammalian, with rodents and insectivores (moles, shrews, and bats) acting as a source of hantavirus (Vaheri et al., 2013, Meyer and Schmaljohn, 2000). Hantaviruses typically do not cause disease in its hosts, however hantavirus infection has been implicated with the decreased survival of rodent hosts in PUUV and SNV (Luis et al., 2012, Kallio et al., 2007). Hantavirus persistence in animal hosts has been linked to the differences in immune response to the infection between animals and humans. When compared to humans, rodents have lower levels of inflammation and antiviral responses which is mediated by both host and virus (Easterbrook and Klein, 2008).

3.1.3.3 Geographical Distribution

Hantaviruses can be split into two groups, NW and OW. NW hantaviruses are endemic in North and South America, with OW hantaviruses mainly being found in Europe and Asia (Engdahl et al., 2021). Due to each hantavirus having a specific relationship with one or more reservoir hosts, host location acts as the primary factor in the geographic distribution of hantaviruses (Dearing and Dizney, 2010). In Europe, the most prevalent causes of hantavirus disease are PUUV, causing 98 % of reported cases (ECDC, 2021). In addition to PUUV, the DOBV hantavirus also causes hantavirus illness in Europe, although to a lesser degree (Schilling et al., 2007). Typically north-western Europe is dominated by PUUV, with DOBV being present in the south-east of the continent (Kruger et al., 2015). Thankfully PUUV infections cause a relatively mild form of HFRS (nephropathia epidemica) with fatalities being rare (Vaheri et al., 2021).

In the last decade, SEOV has been identified as causing human infection in Europe (and the USA) (Cuperus et al., 2021, Kerins et al., 2018, Reynes et al., 2015). SEOV is primarily found in Asia, however cases have been found in the UK, France, and the Netherlands where transmission occurred from feeder or pet rats (Swanink et al., 2018, Reynes et al., 2017, Jameson et al., 2013, Kruger et al., 2015). Additionally, antibodies and SEOV RNA has been found in wild brown rats in several European

countries leading to concerns that SEOV will become an emergent disease (Cuperus et al., 2021). The primary hantaviruses causing HFRS in Asia are HTNV and SEOV, with there being 40,000 to 60,000 cases in humans annually (99 % of these are within China) (Wang et al., 2022, Kruger et al., 2015). The majority of severe HFRS cases in Asia arise from HTNV which has a mortality rate of up to 15 %, with SEOV causing a moderate form of the disease (1 % to 2 % mortality rate) (Wang et al., 2022).

There are to date, 30 different hantavirus strains that have been identified in North and South America since 1993 (Figueiredo et al., 2014, Kruger et al., 2015). In total, there have been 5243 confirmed hantaviral disease cases in South America (1993-2016), and 807 confirmed cases between in North America (1993-2020) (WHO, 2017, CDC, 2022). The most prevalent NW hantaviruses responsible for causing disease are SNV and ANDV which are primarily found in North and South America respectively (Matheus et al., 2006, Vergote et al., 2017, Engdahl et al., 2021). In North America there are six other hantaviruses besides SNV, with only Bayou virus, Black Creek Canal virus, and Prospect Hill virus (PHV) being identified as pathogenic to humans. Whilst in South America there are six more species of hantavirus besides ANDV, with Laguna Negra, CHOL, and El Moro Canyon viruses being pathogenic to humans (Bellomo et al., 2021, Mull et al., 2020). The Araraquara strain of ANDV has been identified as responsible for the most virulent HPS, with a mortality rate of 50 % (Kruger et al., 2015, Mull et al., 2020).

3.1.3.4 Hantavirus Emergence

The repeated identification of novel pathogenic hantaviruses has resulted in the genus being classified in the group of emerging viruses (Kruger et al., 2015). Changes in case numbers are dependent upon location, with cases in Europe (especially Germany) showing a clear increase in hantavirus disease (beyond that explained by better diagnostics) (Krüger et al., 2013). Even China, where cases were decreasing between 1990s and 2009 (due to their rodent control measures and HFRS vaccination program), has been experiencing an increase in cases since 2011 (He et al., 2013, Wang et al., 2021a). As the spread of hantavirus is facilitated by its mammalian reservoirs, changes in host populations can affect the spread of hantaviral disease. SEOV is of current concern, with several reported cases of SEOV being found circulating in host animals of the USA and several European countries. Furthermore, the PUUV reservoir host (bank vole) is ubiquitous in the UK and so is a prime candidate for PUUV emergence (Bennett et al., 2010). Additionally,

bank vole populations and subsequent hantavirus epidemics in humans have been correlated with high summer temperatures. In 2020, Europe had its hottest year since instrumental records began, with temperatures predicted to continue rising by 1.2 °C to 8.5°C by 2071 to 2100 (dependent upon the SSP scenario) (EEA, 2021). Consequently, temperature increase could result in a significant bank vole population increase, increasing the risk of PUUV to human health in Europe (Reusken and Heyman, 2013).

3.1.4 Hantavirus Structure

Hantavirus virions are spherical or elongated enveloped particles with a diameter range of 110-170 nm (Figure 3.1, A). Interestingly, there is a large degree of variability between the morphology of different hantavirus virions, with tubular, irregular and round particle classifications being identified (figure 3.1, B-D). For example, 80% of the Black Creek Canal hantavirus virions were tubular, compared to SNV virions which were mainly irregular in shape (Parvate et al., 2019). The viral genome is trisegmented, with each of the three RNA segments enclosed within a helical nucleocapsid protein (NP) oligomer (Hepojoki et al., 2012, Huiskonen et al., 2010, Arragain et al., 2019). The pleomorphic lipid envelope is studded with the viral glycoprotein spike which consists of Gn and Gc and extends ~10 nm outwards from the viral membrane. Each glycoprotein spike is made up of tetrameric Gc-Gn heterodimers ([Gn/Gc]4) with a fourfold symmetry. These tetrameric glycoprotein spikes are square-shaped and form ordered patches on the viral envelope due to their interactions with neighbouring spikes. The glycoprotein spike possesses a Gn central region surrounded by the Gc which controls the lateral bonds with adjacent spikes (Huiskonen et al., 2010). The x-ray structure of Gc reveals three β-sheet rich domains (I-III) that are typical of several viral (e.g. alphaviruses and flavivirus) class-II fusion proteins (Serris et al., 2020). Class-II fusion proteins are dimeric structures that form homotrimers during fusion to allow for membrane penetration (they possess a roughly hairpin structure) (Kielian and Rey, 2006). In the case of hantaviruses, the Gc protein is responsible for forming the post fusion trimer in the hairpin confirmation (Serris et al., 2020).

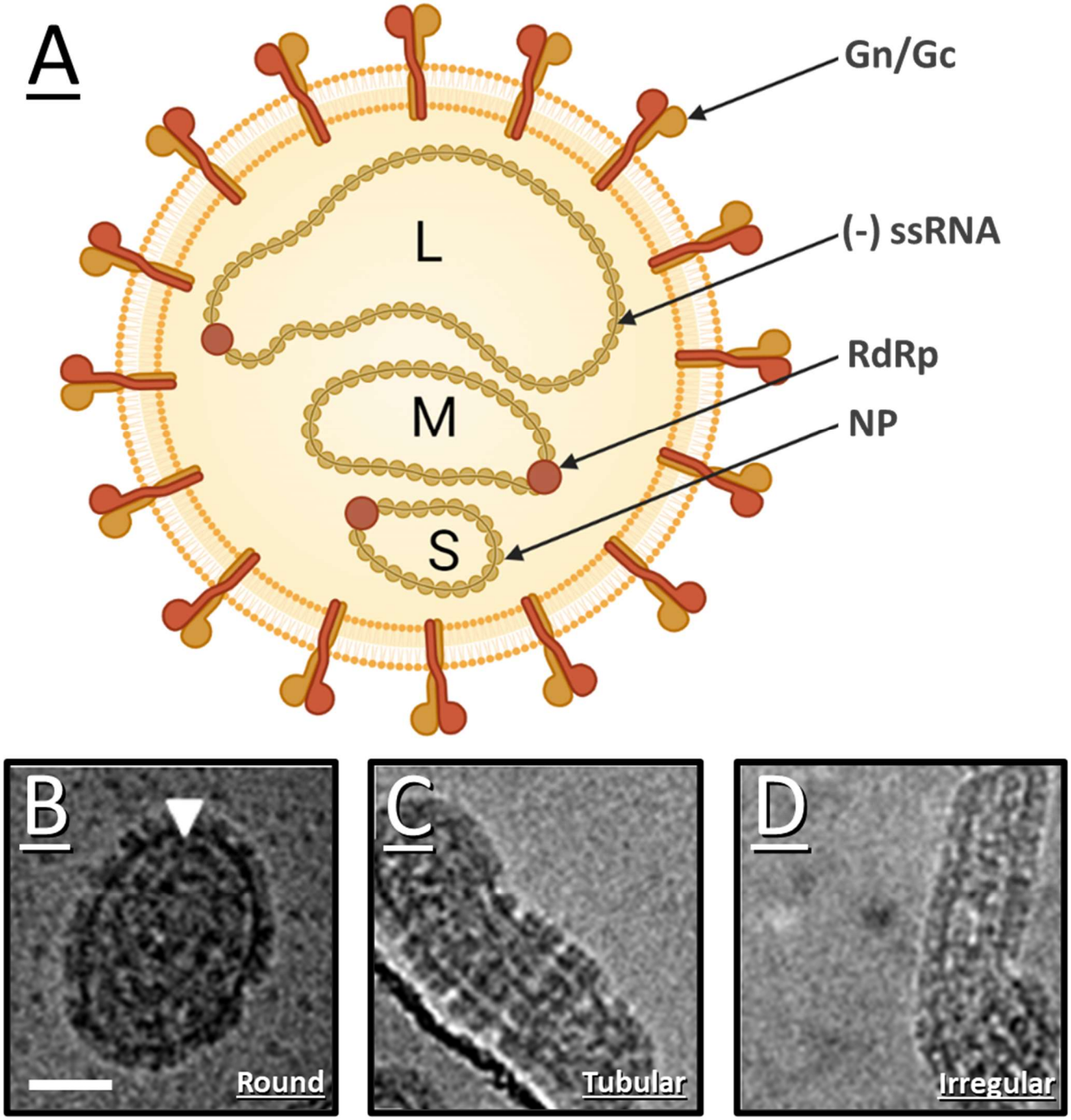

Figure 3.1: A schematic representation of the hantavirus virion.

(A) A schematic of a hantavirus virion cross-section. The outer envelope is studded with tetrameric glycoprotein spikes (Gn and Gc). The tripartite negative sense RNA genome has the small (S), medium (M), and large (L) segments coiled around the trimeric nucleocapsid protein (NP) chain. Each genomic segment has a bound RNA dependent RNA polymerase. Created with BioRender, based on figure 1a by Vaheri et al. (2013), and figure 2 by D'Souza and Patel (2020). (B-D) Cryo-EM images of HTNV particles representing the three classes of hantavirus virion morphology. Scale bar represents 50 nm. Images adapted from figure 1, from Parvate et al. (2019).

3.1.5 Hantavirus Genome

Hantaviruses are (-)ssRNA viruses with a trisegmented genome that consists of small (S), medium (M), and large (L) segments (Figure 3.2) (Hjelle and Torres-Pérez, 2010, Vaheri et al., 2013). The S segment (1.8-2.1 kb) encodes the NP, the M-segment (3.7-3.8 kb) encodes the glycoprotein precursor (GPC), and the L-segment (6.5-6.6 kb) encodes the RNA-dependent RNA polymerase (RdRp [also known as L protein]) (Rothenberger et al., 2016). Additionally, several hantaviruses (e.g. TULV, PUUV, and ANDV *etc.*) have another, non-structural (NSs) protein encoded by their S segment and is transcribed via leaky scanning. The NSs protein in hantaviruses and other *Bunyavirales* is nonessential for viral replication, but aids in viral infection by acting as an interferon antagonist. The NSs protein is a weak interferon inhibitor in TULV and PUUV, which increases survival in interferon-competent cells (Jääskeläinen et al., 2007, van Knippenberg et al., 2013, D'Souza and Patel, 2020, Jääskeläinen et al., 2008, Vera-Otarola et al., 2020). Each of the three bunyavirus segments consists of an open reading frame (ORF), with a non-coding region (NCR) at the 5 prime (5') and 3 prime (3') ends. These terminal NCRs form a panhandle structure, typical of bunyaviruses, which forms due to the binding of complimentary nucleotide sequences in the NCR (and potentially are involved in RdRp binding) (Meier et al., 2021). This panhandle acts as an essential viral promoter for viral transcription and replication (Vaheri et al., 2013b).

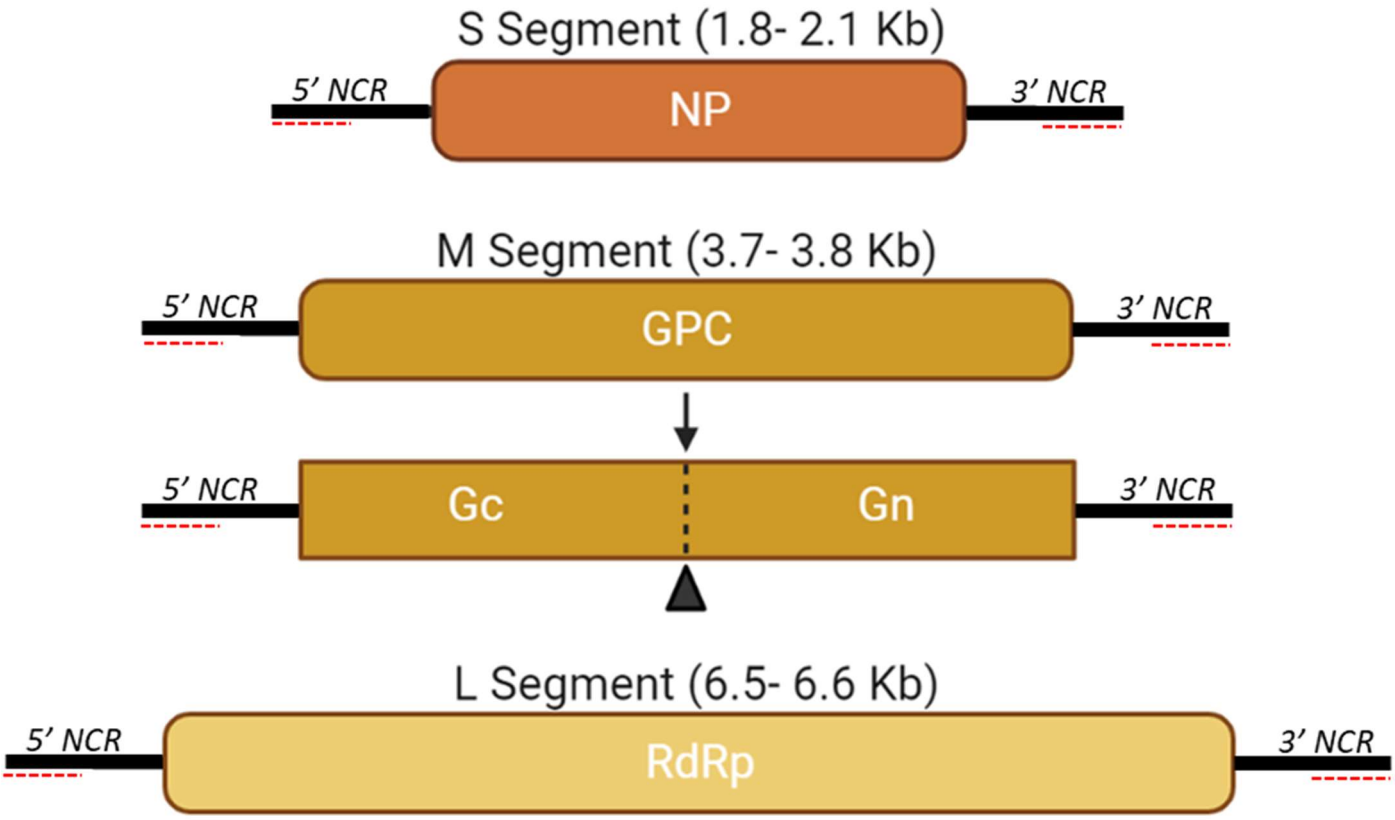

Figure 3.2: A simplified representation of the hantavirus tripartite genome.

The small (S) genome segment encodes for the nucleocapsid protein (NP), the medium (M) genome segment encodes the glycoprotein precursor (GPC) (which is later cleaved to form the glycoproteins Gn and Gc), and the large (L) genome segment which encodes the RNA dependent RNA polymerase (RdRp). Each genome segment has a terminal 5' and 3' non-coding region (NCR) which contain complimentary nucleotide sequences (red dashed line) allowing for the binding and formation of the characteristic panhandle structure. This figure was created with BioRender.

3.1.6 Hantavirus Replication Cycle

3.1.6.1 Attachment

The first stage in most viral replication cycles is attachment (Figure 3.3). Several cellular surface proteins are associated with hantavirus entry, with integrins being suggested as the main entry receptor (Mackow and Gavrilovskaya, 2009). Integrins are transmembrane proteins found on the cell surface that are essential in cellular migration and adhesion. Integrins are heterodimers consisting of an α and β chain, with there being at least 18 α and 8 β chains in humans forming 24 different heterodimers (Takada et al., 2007). Different hantaviruses have been found to use different cellular integrins. The integrin αVβ1 is used by Sangassou virus, the integrin

αVβ3 is used by PUUV, SEOV, HTNV, and SNV, whereas TULV and PHV use the α5β1 integrin (Gavrilovskaya et al., 1998, Mou et al., 2006, Klempa et al., 2012, Matthys et al., 2011). Other cell receptors have been implicated in hantavirus entry, with the complement receptor gC1qR/p32, decay-accelerating factor CD55, and protocadherin-1 being identified (Jangra et al., 2018, Mittler et al., 2019, Krautkrämer and Zeier, 2008, Choi et al., 2008). Furthermore, a loss-of-function genetic screen of host cells revealed that cell membrane cholesterol levels determine HTNV and ANDV cell entry (Kleinfelter et al., 2015). Interestingly research into pathogenic and non-pathogenic hantaviruses has indicated that different integrins are utilised between the two groups. The most prevalent pathogenic hantaviruses have been found to use αVβ3 with non-pathogenic hantaviruses using α5β1 (Raymond et al., 2005, Matthys et al., 2011). B3 receptors are responsible for regulating the fluid barrier on endothelial cells and platelets, which is interrupted in hantavirus disease (Matthys et al., 2011). Therefore it likely that their ability to target β3 integrins for attachment also allows pathogenic hantaviruses to interrupt barrier functions.

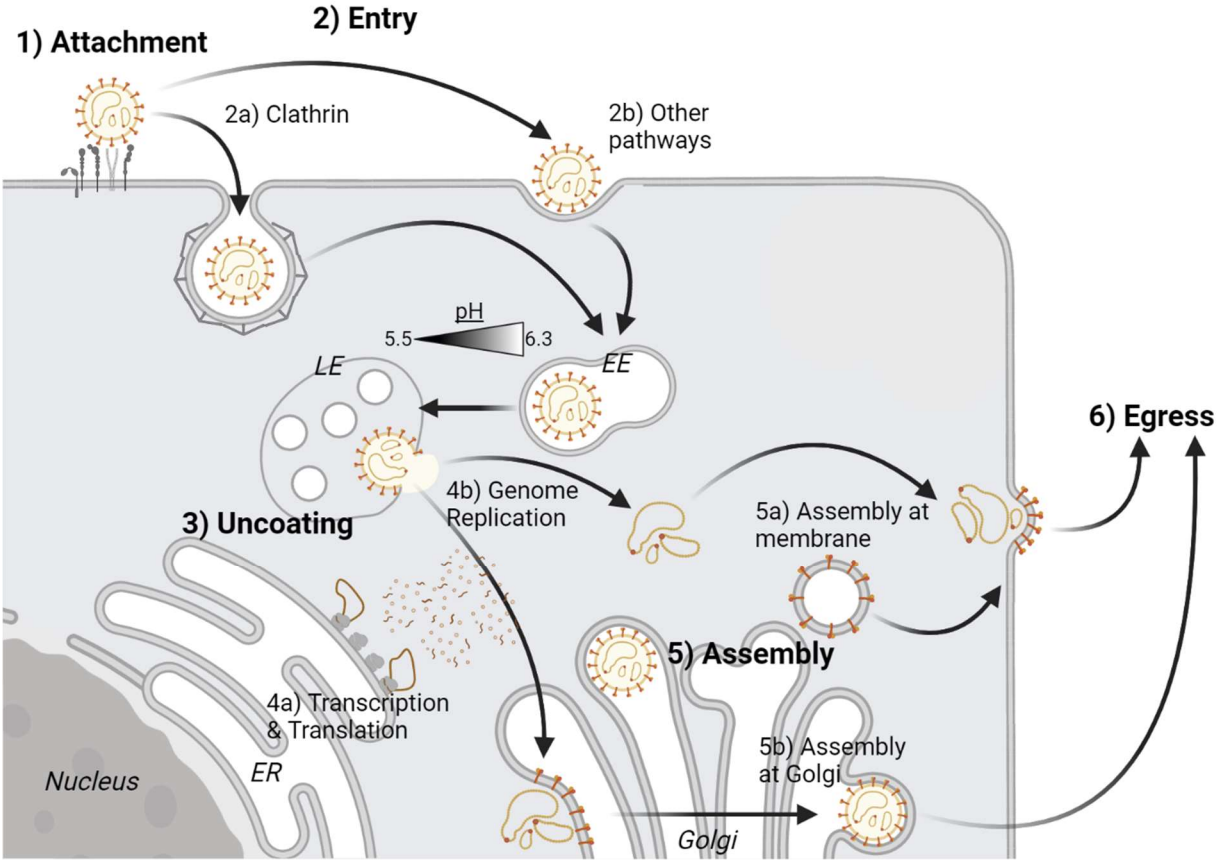

Figure 3.3: A schematic representation of the Hantavirus replication cycle.

Hantaviruses are known to use several cellular receptors during attachment (1). The primary receptors associated with hantavirus binding are integrins, although complement receptor gC1qR/p32, decay-accelerating factor CD55, and protocadherin-1 have also been identified. Once the virion has attached it will enter the cell (2) either via clathrin-mediated endocytosis (2a) or by other means (2b), such as macropinocytosis depending upon hantavirus strain. Viral particles are then internalized via the endocytic pathway, progressing from the early endosome (EE) to the late endosomes (LE) where the low pH triggers viral uncoating (3) and release into the cytoplasm. Once the viral RNA has been released into the cytoplasm, genomic transcription, transcription (4a), and replication can occur (4b). Depending on the specific hantavirus, viral glycoproteins accumulate within Golgi and either transit to the plasma membrane for assembly (5a), or stay in the Golgi and assemble there (5b). Virions that assemble at the Golgi will then traffic through the Golgi until they reach the plasma membrane for egress (6). This figure was created with BioRender and is based upon figure 2 by Cifuentes-Muñoz et al. (2014), figure 2 by Mittler et al. (2019), and figure 2 by Vaheri et al. (2013).

3.1.6.2 Entry

Once the hantavirus particle has attached onto the target cell surface, the virion will enter the cell. Hantaviruses enter cells through several different mechanisms depending upon the hantavirus, cell type, and experimental conditions (Mittler et al., 2019). For example, the OW hantavirus HTNV enters via clathrin-mediated endocytosis (Jin et al., 2002). Whereas the entry mechanism is more complicated for NW hantavirus ANDV (Mittler et al., 2019). For example, it has been found that ANDV entry is dynaminindependent (Ramanathan et al., 2008). Dynamin is an essential component of clathrin-mediated endocytosis as it separates emerging vesicles from the cellular membrane (Cheng et al., 2021). Further research found that ANDV entry requires host factors involved in dynamin-independent macropinocytosis (e.g. cholesterol and the Rho GTPase Rac1) (Torriani et al., 2019). Conversely, in a screen of 140 membrane trafficking genes, it was found that ANDV entry is dependent upon the genes encoding the clathrin heavy chain, dynamin, and AP2 (another component clathrin-mediated endocytosis) (Chiang et al., 2016). These studies indicate that hantavirus entry is complicated, and perhaps utilises clathrin-mediated endocytosis in addition to an unknown clathrin-independent, macropinocytosis-like mechanism (Chiang et al., 2016).

3.1.6.3 Uncoating

Post-entry, hantavirus virions traffic through early endosomes and eventually reach late endosomes and lysosomal compartments. As the endosome matures, the pH decreases. At a pH of 6.3 to 5.5 (dependent upon the individual hantavirus), a conformational change in the hantavirus glycoprotein Gn/Gc interface is triggered (Mittler et al., 2019, Kleinfelter et al., 2015). The change in glycoprotein structure allows the Gc fusion loop to insert itself into the endosomal membrane, facilitating endosomal and viral membrane fusion (Meier et al., 2021). Across all hantaviruses, membrane fusion has been found to be dependent upon host cell membrane cholesterol levels. Kleinfelter et al. (2015)found that the CRISPR disruption of the site-1 protease (S1P) gene resulted in reduced OW and NW hantavirus infection (Kleinfelter et al., 2015). S1P is a membrane-bound transcription factor involved in cholesterol homeostasis (Danyukova et al., 2022). Kleinfelter et al. (2015) proposed that the reduction of cholesterol through S1P inhibition prevents the hantavirus glycoprotein-facilitated fusion of viral and cellular membranes. Interestingly, they also

found that ANDV may specifically target cholesterol rich islands in host endosomal membranes during fusion. In ANDV membrane fusion, a pH of 5.5 is required, indicating that membrane fusion occurs in late endosomes. A liposome fusion assay further revealed that ANDV GP-lead fusion requires a higher host membrane concentration of cholesterol than is available in late endosomes. Therefore, for fusion to occur in the late endosome, ANDV must be able to target cholesterol-rich domains of endosomal membranes (Kleinfelter et al., 2015).

Membrane fusion results in the release of the hantavirus virion genome into the cytoplasm where it is transported to sites of viral replication and transcription (Ramanathan et al., 2007, Ramanathan et al., 2008). The details of viral uncoating and viral transport are currently unknown and require further investigation (Mittler et al., 2019). Nevertheless, Ramanathan et al. (2007) reported that the HTNV NP is likely trafficked via the microtubule network, with the disruption of the microtubule network resulting in lower levels of intracellular vRNA.

3.1.6.4 Transcription, replication, and translation

3.1.6.4.1 RdRp Binding

The transcription and replication of the bunyavirus RNA genome is carried out by the viral RdRp through different mechanisms. Genome replication results in the formation of an identical (-) RNA strand, whilst transcription forms capped mRNAs (Figure 3.4) (Olschewski et al., 2020). As mentioned earlier, each of the three hantavirus RNA segments are flanked by complimentary NCRs that form panhandle structures. The panhandles on each segment end are believed to facilitate genome replication in bunyaviruses by binding to the viral RdRp (Meier et al., 2021). The binding of viral ribonucleoproteins to the RdRp forms the functional unit of genome transcription and replication. Cheng et al. (2014)found that the NP has a RdRp binding domain on its N-terminus, with the RdRp similarly having an NP binding domain on its C-terminus (Cheng et al., 2014). Although it is unknown how RdRp binds to the encapsidated vRNA, it likely involves RdRp-NP binding. The current model suggests that the RdRp-NP binding brings RdRp into the vicinity of the vRNA, this locally disrupts the NP oligomer bound to the RNA, allowing for RdRp reading of the RNA (Meier et al., 2021, Arragain et al., 2019).

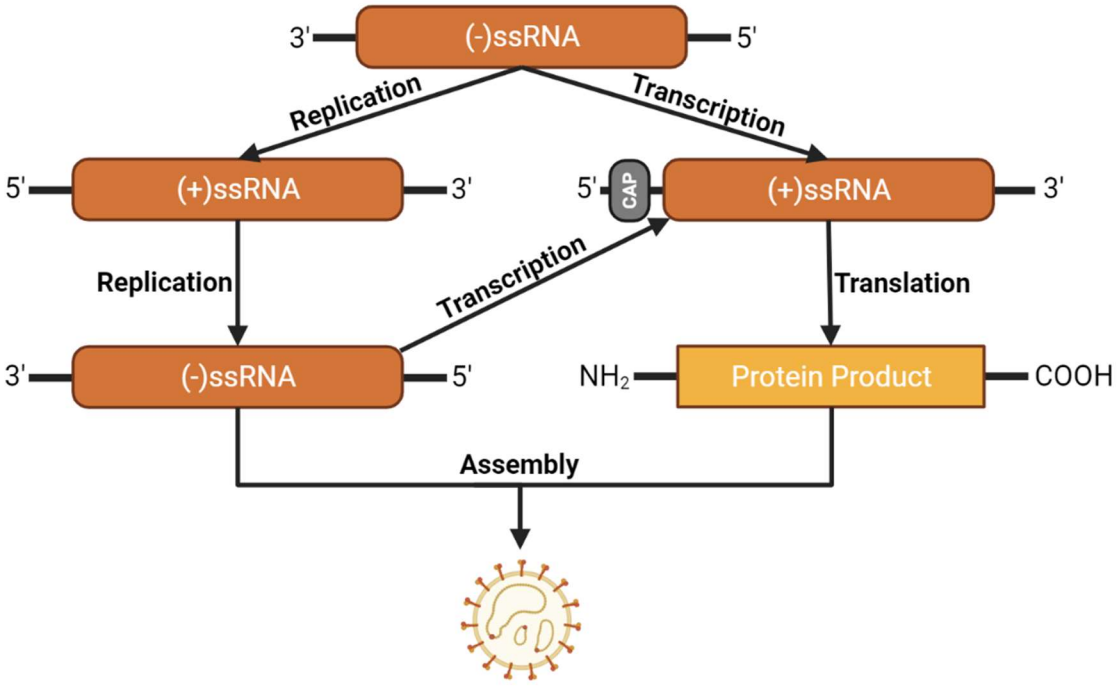

Figure 3.4: An overview of genome transcription, translation and replication for hantaviruses

Upon entry into the cell, hantavirus replicates its negative-sense (-), single-stranded (ss) RNA genome by producing a complimentary positive-sense (+) template which is used for producing more (-)ssRNA viral genomes. The (-)ssRNA is transcribed to produce (+) mRNA transcripts which are translated to produce viral proteins. Viral proteins and viral (-)ssRNA genomes combine to form progeny virions. This figure was created with BioRender and is based upon figure 1 by Jonsson and Schmaljohn (2001).

3.1.6.4.2 Transcription

In transcription, hantavirus mRNA transcripts are produced via prime-and-realign combined with an additional cap-snatching mechanism (Figure 3.5). The cap-snatching mechanism is not unique to hantaviruses, and is found in other segmented (-) RNA viruses. The process involves the ‘snatching’ of host mRNA 5’ caps which are then used to prime vRNA for the transcription of mRNA (Garcin et al., 1995, Meier et al., 2021). To remove these caps an endonuclease is needed, and for hantaviruses the endonuclease is located within the N-terminus of the RdRp (Fernández-García et al., 2016). In prime and realign transcription the host-derived 5’ cap is used as a primer (Figure 1.1.5). The snatched cap binds to the cytosine of the vRNA AUC start codon with its terminal guanine residue (Amroun et al., 2017, Kearse and Wilusz, 2017). After this priming step, elongation of the cap occurs along the vRNA for a few nucleotides. At this point the RdRp realigns the 5’ cap back three nucleotides so that the guanine residue is overhanging and no longer bound to the

vRNA. The cap remains attached to the heterogenous, viral mRNA (Amroun et al., 2017). The S segment mRNA is translated to form the NP (and occasionally NSs). The M segment mRNA is translated to form GPC on ER-bound ribosomes which is cleaved into Gn and Gc. And finally the L segment mRNA is translated to form the RdRp (Muyangwa et al., 2015).

The host mRNA targets of hantavirus cap-snatching process are currently unknown, however it has been proposed that caps are taken from non-coding RNA in processing bodies (P-bodies). P-bodies are non-membrane bound compartments in the cytoplasm of cells which are responsible for RNA storage (for later translation), or degradation (Meier et al., 2021, Mir et al., 2008). Mir et al. (2008) found that not only do SNV hantavirus NPs concentrate within P bodies through confocal microscopy, but they are also capable of binding and protecting the 5’ cap of cellular mRNAs. P-bodies therefore act as a store of NP-bound 5’ cap ends for subsequent viral mRNA synthesis by the RdRp. This is supported by the finding that PUUV NP was found to co-localise with P-bodies in infected cells imaged through immunofluorescence microscopy (Welke et al., 2022).

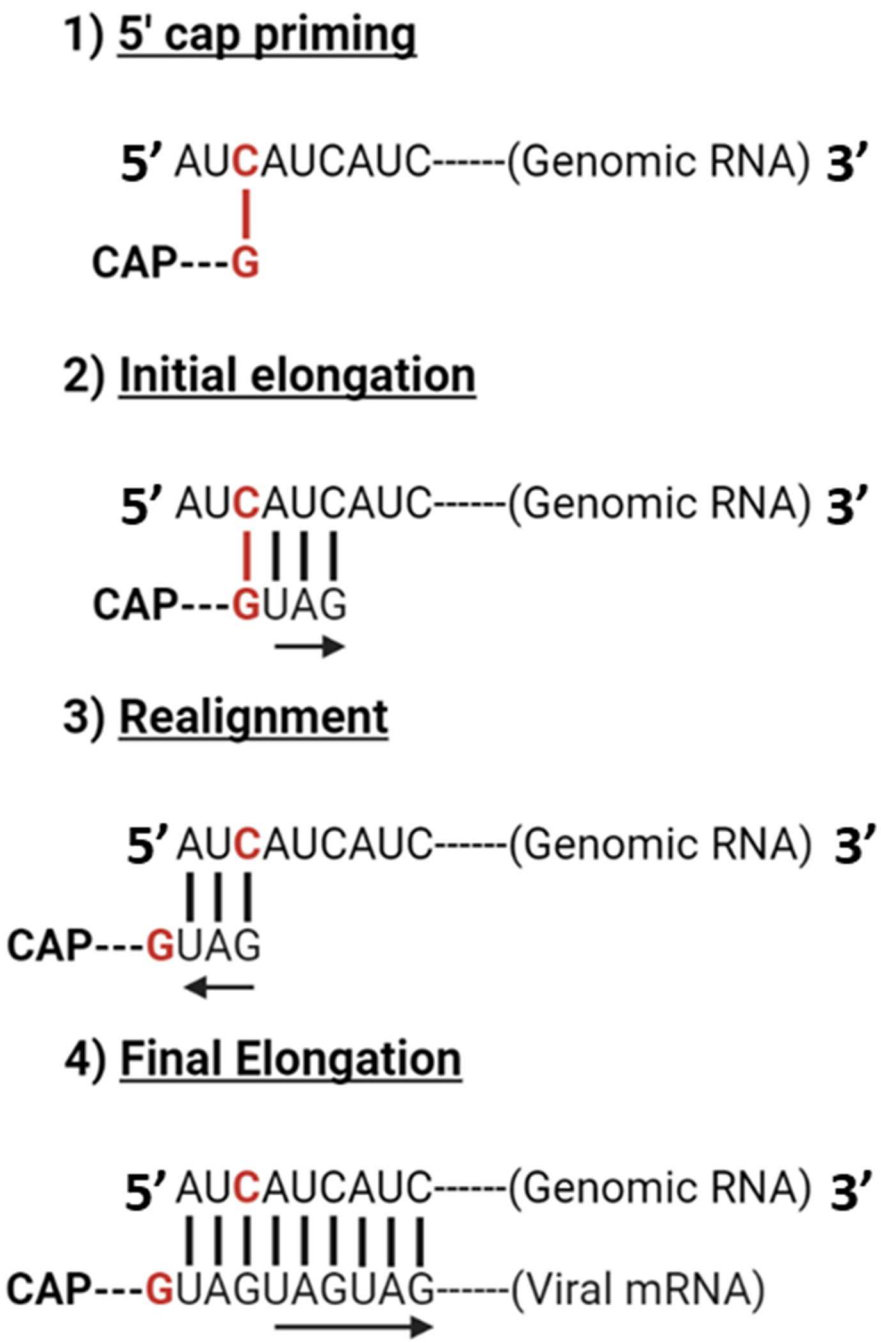

Figure 3.5: A simplified depiction of viral genome transcription via the prime and realign mechanism and cap snatching.

Hantavirus transcription occurs within the cytoplasm of infected cells and is facilitated by the RNA dependent RNA polymerase. Initially the appropriated host mRNA 5' cap is used to prime the viral genomic RNA by the binding of its guanine residue to the vRNA cytosine. Next, the viral mRNA is elongated by three nucleotides. After this the strand is realigned, pushing the 5' cap backwards off of the genomic RNA. Once the mRNA has been realigned, it will be elongated, forming the full length of mRNA. This figure was created with BioRender and is based upon figure 1, A by Muyangwa et al. (2015) and figure 9, A by Amroun et al. (2017).

3.1.6.4.3 Translation

Once the viral mRNAs have been produced with the host cell 5' caps, viral translation can occur. For HTNV it has been suggested that the NP can facilitate the preferential expression of viral mRNA by mimicking the function of the eukaryotic initiation factor 4F complex (eIF4F) (Meier et al., 2021, Mir and Panganiban, 2008). Furthermore, it has been suggested that the HTNV NP is able to disrupt the host eIF4F, inhibiting host mRNA translation whilst promoting viral translation. The HTNV NP does this with its C-terminal lobe, which shares a structural similarity with the host tumour suppressor protein- programmed cell death 4 (Olal and Daumke, 2016, Meier et al., 2021). By simultaneously inhibiting and imitating the host eIF4F, HTNV NP facilitates the preferential translation of viral mRNA over host mRNA.

The specific site of hantavirus genome replication and transcription within the cytoplasm is currently unknown (Meier et al., 2021). However, it was found by Ramanathan et al. (2007) through confocal microscopy that the HTNV NP forms perinuclear structures which colocalise with the endoplasmic reticulum (ER)-Golgi intermediate compartment (ERGIC) markers, but not the ER or Golgi. The ERGIC is a membranous complex that acts as an independent interface between the Golgi and ER with its own unique protein composition and structure (Appenzeller-Herzog and Hauri, 2006). As OW hantaviruses are known to bud through the Golgi prior to egress, it suggests that the HTNV NP traffics to the remodelled ERGIC, before the Golgi (Jäntti et al., 1997, Pattabiraman et al., 2020). Once within the Golgi complex, the HTNV virion (and associated NP) quickly egresses and does not accumulate within the Golgi (Ramanathan et al., 2007).

3.1.6.4.4 Genome Replication

Genome replication begins with the formation of a positive-sense (+) complementary RNA strand (cRNA) via a prime-and-realign mechanism (Figure 3.6) (Olschewski et al., 2020). In prime and realign replication, the guanine of GTP binds to cytosine of the AUC start codon (Kearse and Wilusz, 2017, Amroun et al., 2017). After this priming step elongation of the cap occurs along the vRNA for a few nucleotides. At this point the RdRp realigns the GTP cap back three nucleotides so that the guanine residue is overhanging and no longer bound to the vRNA. After the realignment, the RdRp elongates the cRNA until it reaches the termination signal. Finally the GTP is cleaved and removed, forming the new antigenomic cRNA. This is the process for both genomic and antigenomic RNA synthesis (Amroun et al., 2017). The cRNA acts as a template for the production of the viral (-) RNA genome. In Bunyaviruses, both

the (-) RNA genome and (+) cRNA are always found bound to the viral NP, which is not the case for the viral mRNA (Meier et al., 2021, Hacker et al., 1989).

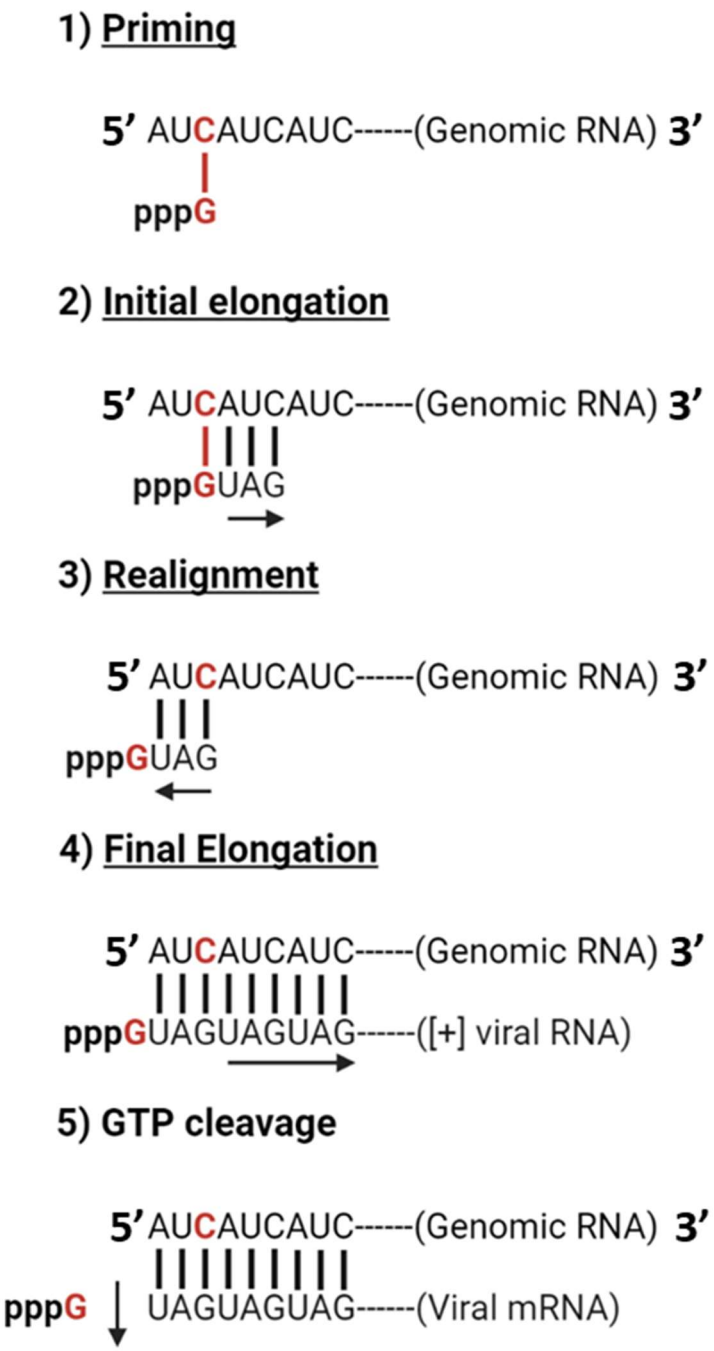

Figure 3.6: A simplified depiction of viral genome replication via the prime and realign mechanism.

Hantavirus RNA genome replication occurs within the cytoplasm of infected cells and is facilitated by the RNA dependent RNA polymerase. First, the genomic RNA is primed at the 5' end with GTP. Next the copy RNA (cRNA) strand is elongated with three new nucleotides. After this, the strand is realigned, pushing the GTP backwards off of the genomic RNA. Next the final elongation of the cRNA occurs resulting in the formation of a full positive sense RNA strand. Finally the GTP is cleaved and removed. The cRNA acts as a future template for future vRNA production. This figure was created with BioRender and was based upon figure 1, B by Muyangwa et al. (2015) and figure 9, B by Amroun et al. (2017).

3.1.6.5 Assembly

3.1.6.5.1 Ribonucleoprotein Formation

After the vRNA genome has been replicated, it must be encapsidated with the NP. The NP has a two-lobed structure, bisected by an RNA binding groove and has two arms on the N and C-terminals (Figure 3.7). These arms allow for the oligomerisation of the NP in a helical fashion around the vRNA (Olal and Daumke, 2016, Guo et al., 2016, Arragain et al., 2019). Firstly, the NP trimerises before binding to the NCR of genomic segments (Mir and Panganiban, 2004). The NP binds to the viral genomic RNA in different ways dependent upon the hantavirus in question (Meier et al., 2021). In HTNV, the NP was found bind to the ss 5' NCR in RNA competition experiments (Severson et al., 2001). Whereas in SNV, the NP was found to bind to the double-stranded (ds) region of the 5' and 3' panhandle in the NCRs and not the ss region in filter binding assays (Mir and Panganiban, 2004).

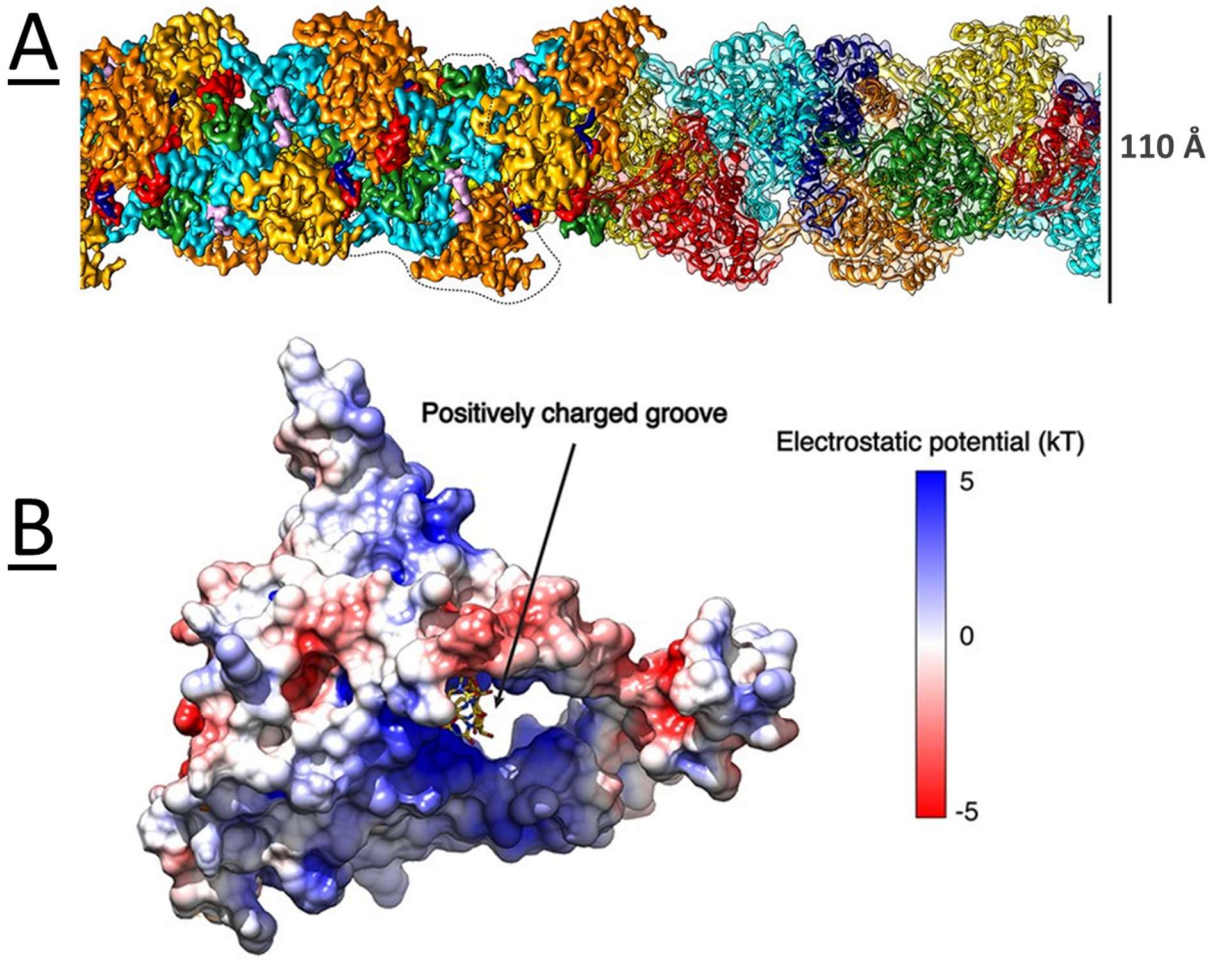

Figure 3.7: HTNV NP and RNA structure.

(A) Helical arrangement of HTNV NP filament, each colour corresponds to a different NP monomer. (B) The HTNV NP monomer with RNA shown within the positively charged groove. The 3D-structure is mapped with the electrostatic surface representation. Figure adapted from figure 1 A and C Arragain et al. (2019).

3.1.6.5.2 Glycoprotein Maturation

GPC undergoes maturation when it is cleaved by the cellular signal peptidase complex as it enters the ER. This cleavage happens at signal sequence situated between Gc and Gn regions the GPC, resulting in the formation of the two glycoproteins (Löber et al., 2001). Once cleaved, the two glycoproteins transit from the ER to the Golgi, forming heterodimers which further combine to form tetrameric spikes (Serris et al., 2020). In PUUV, the translocation of Gn into the Golgi from the ER is highly reliant upon Gc due to its cytoplasmic tail (the cytoplasmic tail in Gn provides stability), with its removal preventing Golgi localisation (Sperber et al., 2019). Furthermore, the Gc:Gc interactions between neighbouring spike glycoproteins are predicted to facilitate the necessary membrane curvature needed for viral entry into the Golgi. This was suggested due to the interruption of the Gc:Gc interaction by mutations in the contact residues between Gc:Gc resulting in inhibited virion production (Bignon et al., 2019). Once bound to the Golgi membrane, the cytoplasmic tails of the Gn and Gc spike complex bind to both the RNA, and the NP of the ribonucleoprotein genome segments, allowing for the formation of the hantavirus virion. (Hepojoki et al., 2010, Strandin et al., 2011). The glycoprotein-NP binding was proven by Hepojoki et al. (2010) who co-immunoprecipitated both glycoprotein and NP bound together. Whereas, Strandin et al. (2011) revealed that Gn cytoplasmic tail can non-specifically bind to RNA through cross-linking and co-immunoprecipitation.

3.1.6.6 Egress

The details of hantavirus egress are largely unknown. However it has been suggested that OW hantavirus virions assemble at the Golgi and are then released by exocytosis, whereas NW hantaviruses are assembled and released directly at the plasma membrane (Meier et al., 2021, Ravkov et al., 1997, Goldsmith et al., 1995). However, the situation is not quite so clear cut (Meier et al., 2021). In the original study, suspected virions were identified within the Golgi of SNV infected cells when imaged through EM. Another study found SNV virions within the perinuclear region, indicating intracellular assembly (Goldsmith et al., 1995, Zaki et al., 1995). Furthermore, recent EM imaging of cryo-preserved cells infected with the OW hantavirus HTNV found extracellular virions in the vicinity of membrane projections, indicative of direct viral budding at the plasma membrane (Parvate et al., 2020, Meier et al., 2021).

3.1.7 Chapter Aims

To date, little is known regarding the hantavirus cellular replication cycle, especially in regards to the location of genome replication. This is particularly relevant for the TULV hantavirus which has not been as well studied when compared to other more pathogenic hantaviruses (e.g. SNV and PUUV). The aim of this chapter was to investigate the cellular ultrastructure of cells infected with hantavirus via TEM. Cells were imaged at early, peak and persistent time points to see how the virus induced changes develop over the course of infection. The TEM images would then be compared with immunofluorescence images taken of similarly infected cells in collaboration with Katherine Davies of the John Barr laboratory. The results from this collaboration are the subject of this chapter and were published (Davies et al., 2020). All of the TEM micrographs were taken by me, whereas Katherine Davies worked on the immunofluorescence images. The combination of TEM with immunofluorescence combines the higher resolving power of EM with protein localisation of immunofluorescence. This allowed us to elucidate structural details of TULV replication in addition to investigating the viral and cellular components involved.

3.2 Tula virus results

3.2.1 TULV infected cells show no sign of viral modification at 36 hp_{inf}

Little is known about the hantavirus replication cycle, especially the sites of viral replication and assembly. Even less is known about TULV replication cycle when compared to the other hantaviruses. An improved understanding of the cellular mechanisms of TULV replication could aid in the development of novel antivirals for both TULV and other hantaviruses. To determine whether TULV modifies cellular ultrastructure, TEM was used to visualise TULV infected cells at 36 hour post infection (hp_{inf}), 7 days post infection (dp_{inf}) and 30 dp_{inf} to represent early, peak and persistent stages of TULV replication. Vero E6 cells were infected with TULV at an MOI 0.1 and incubated for their respective time points. Next the cells were fixed, embedded in resin, sectioned, stained, and finally imaged via electron microscopy (EM).

Resin was initially mixed slowly by hand to prevent the bubble formation observed in previous practice attempts. This lead to the accidental failure to adequately mix the resin and the loss of samples. Consequently, I changed the protocol for all of the micrographs below to allow for the thorough mixing via vortexing and subsequent bubble removal through centrifugation. Originally, resin was left to infiltrate into samples over one day, however the time was extended for the TULV samples. This improved the infiltration and reduced the number of bubbles seen in sections. Additionally, prepared aliquots of lead citrate were originally not filtered prior to use. However, lead citrate precipitation occasionally appeared on imaged sections, so I started to filter aliquots prior to use for TULV experiments. This reduced but did not eliminate completely the appearance of lead citrate precipitation.

The mock infected 36 hp_{inf} cells possessed intact organelles (e.g. mitochondria and rough endoplasmic reticulum [RER]) and nuclear and cytoplasmic membranes (Figure 3.8). Similarly, TULV 36 hp_{inf} cells were indistinguishable from mock infected cells, with no observable signs of viral infection (e.g. virions, viral factories or disrupted cellular membranes/organelles) (Figure 3.9).

Particles were frequently spotted in the cytoplasm of 36 hp_{inf} infected (Figure 3.9, B '>'). Particles were characterised as small vesicles with protein studded electron dense membranes which resembled viral particles. However, later these particles were also identified within the cytoplasm of mock infected cells. Due to their presence in the mock infected cells, it was concluded that the particles were likely to

be clathrin-coated vesicles which had been misidentified. Clathrin-coated vesicles have a similar appearance to that of TULV virions due to their protein studded-vesicular morphology. As a result, there were no signs of viral infection in 36 hp_{inf} TULV infected cells when imaged via TEM.

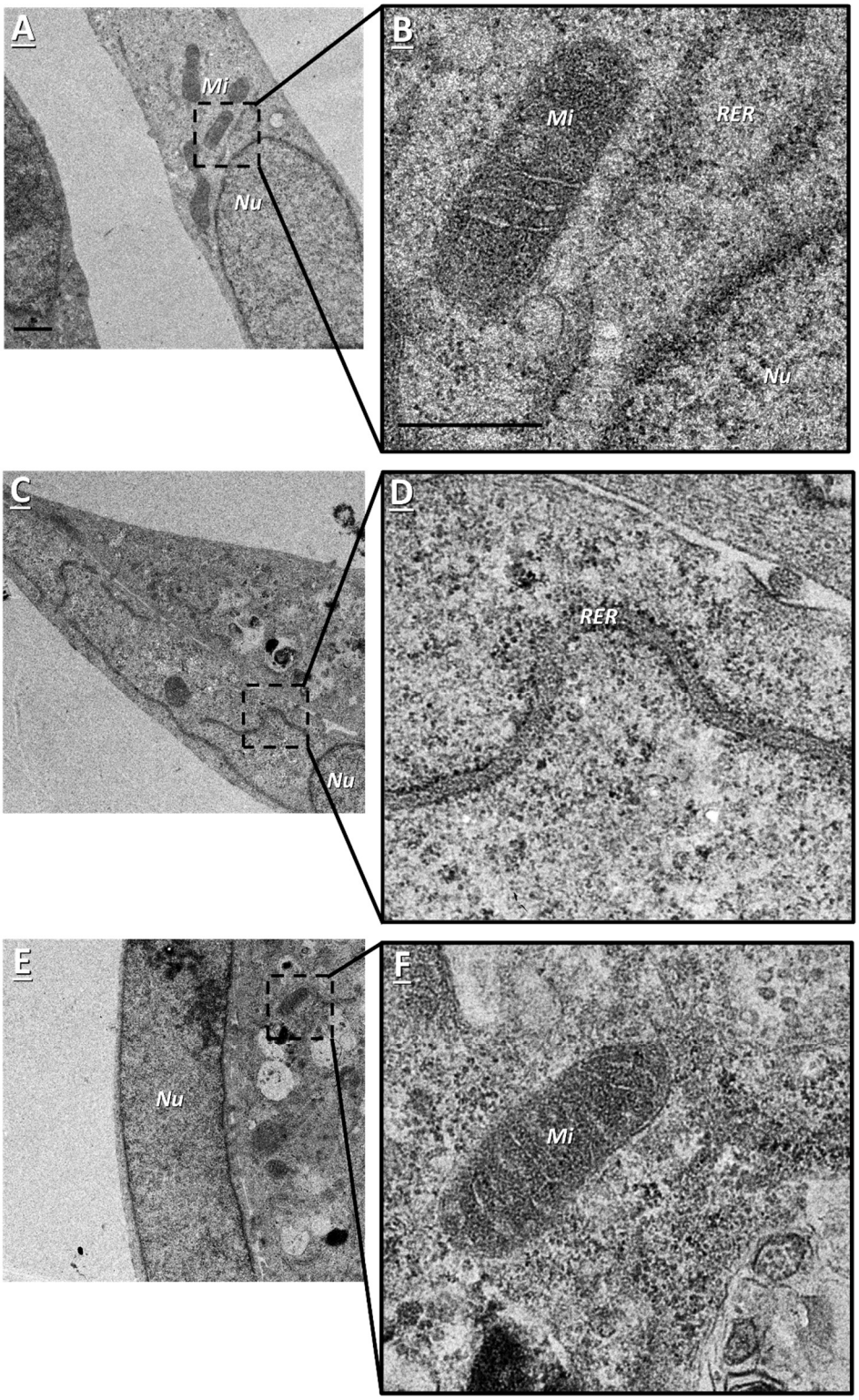

Figure 3.8: TULV mock infected cells - 36 hp_{inf}.

Non-infected Vero E6 cells were mock infected and incubated for 36 hours. Following incubation, cells were processed for TEM. Micrographs A-B, C-D, and E-F are three different cells, with higher magnification images being shown sequentially on the right. The nucleus (*Nu*), mitochondria (*Mi*), and rough endoplasmic reticulum (*RER*) are labelled accordingly. Scale bars for the two lower magnifications represent 1 µM with the highest magnification scale bar representing 500 nm.

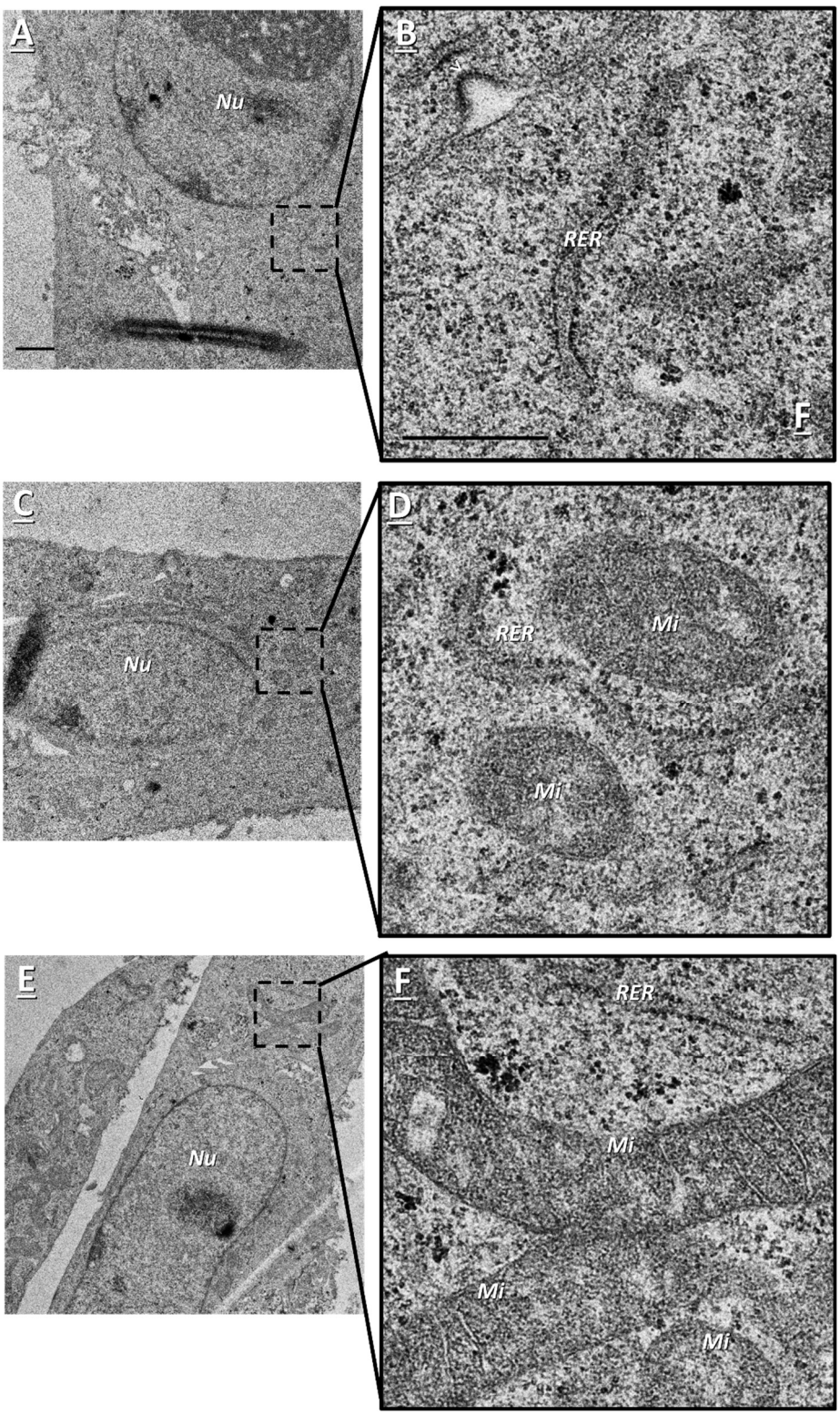

Figure 3.9: 36hp$_{inf}$ TULV infected cells.

Vero E6 cells were infected with TULV and incubated for 36 hours. Following incubation, cells were processed for TEM. Micrographs A-B, C-D, and E-F are three different cells, with higher magnification images being shown sequentially on the right. The nucleus (*Nu*), mitochondria (*Mi*), rough endoplasmic reticulum (*RER*), and virus-like particles (>) are labelled accordingly. Scale bars for the two lower magnifications represent 1 µM with the highest magnification scale bar representing 500 nm.

3.2.2 7 dp_{inf} TULV infected cells have cytoplasmic filamentous structures and enlarged RER

After characterising cells infected for 36 hp_{inf}, I moved onto the mid-infection time point to see if there are any signs of TULV infections present at 7 dp_{inf}. At 7dp_{inf} differences began to appear between the mock infected (Figure 3.10) and infected cells (Figure 3.11). 7 dp_{inf} mock infected cells were again characterised by normal cell ultrastructure which was indistinguishable from the mock 36 hp_{inf} conditions (Figure 3.8). Although infected 7 dp_{inf} cells also possessed normal cell architecture, filamentous structures and enlarged RER were also present.

Filamentous structures appeared in large diffuse clusters in the cytoplasm of infected cells, with only one filamentous cluster seen per cell (Figure 3.11, A to B). Each filamentous cluster consisted of smaller bundles of varying width and length. Although individual filament bundles were characterised by tightly packed parallel fibres, neighbouring filamentous bundles had a variety of orientations. Some of the filament bundles were parallel to neighbouring bundles, with others running perpendicular.

In addition to filamentous structures, there were also signs of RER enlargement in infected cells when compared to the mock infected (Figure 3.10, D vs. Figure 3.11, D). There also seemed to be greater branching of the RER tubule network.

There were still no confirmed TULV virions found intra or extracellularly in the 7 dp_{inf} conditions. Due to TULV virions having a similar appearance to cellular vesicles, often TEM micrographs of TULV virions in the literature are extracellular, with the virus being imaged next to the cellular membrane. Despite this, no extracellular virions were identified when imaging these spaces. Consequently, 7 dp_{inf} TULV infected cells show signs of viral infection characterised by filamentous structures and enlarged RER, with particles being found in both mock and infected conditions.

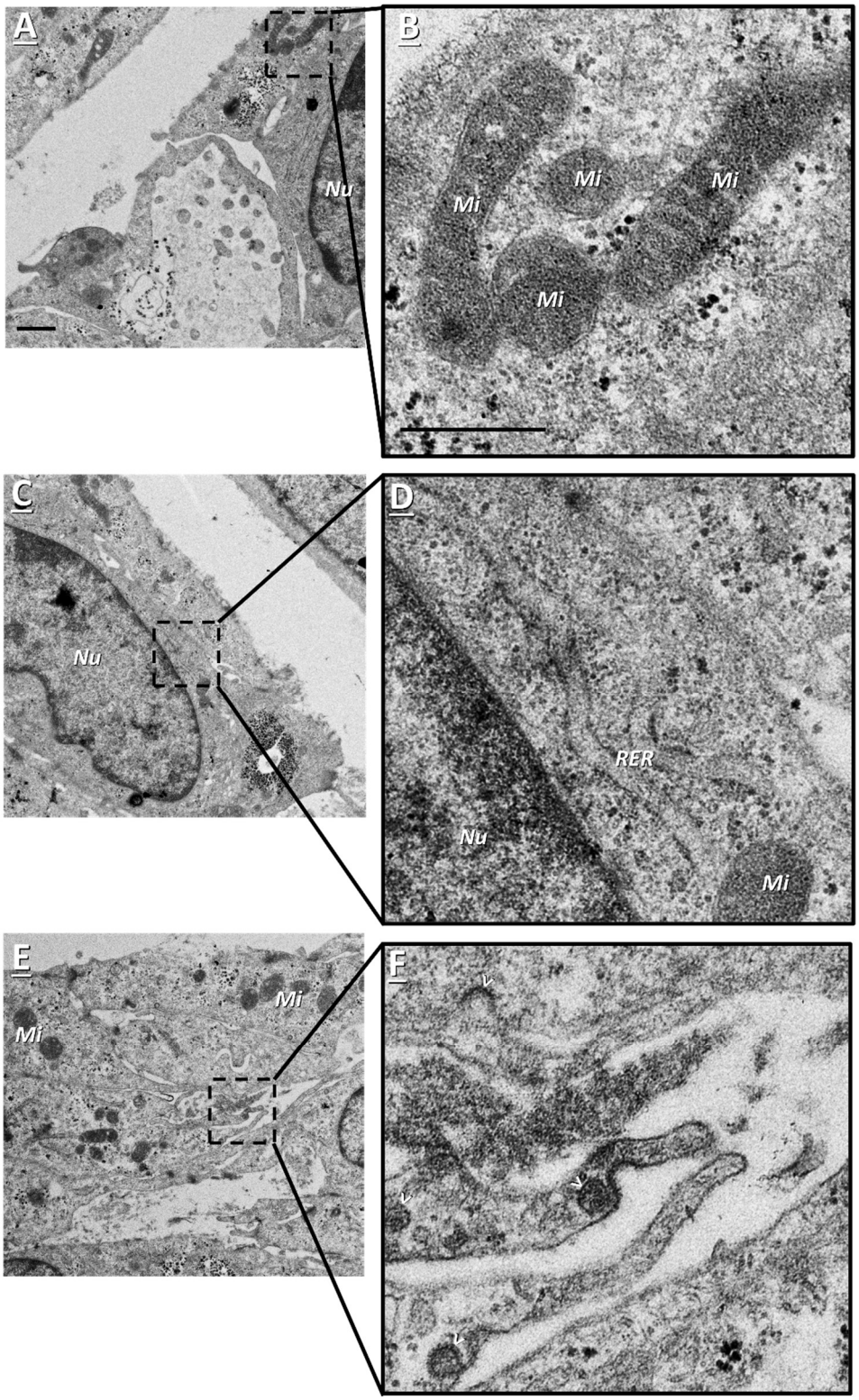

Figure 3.10: TULV mock infected cells - 7 dp_{inf}.

Vero E6 cells were mock infected and incubated for 7 days. Following incubation, cells were processed for TEM. Micrographs A-B, C-D, and E-F are three different cells, with higher magnification images being shown sequentially on the right. The nucleus (*Nu*), mitochondria (*Mi*), rough endoplasmic reticulum (*RER*), and particles (>) are labelled accordingly. Scale bars for the two lower magnifications represent 1 µM with the highest magnification scale bar representing 500 nm.

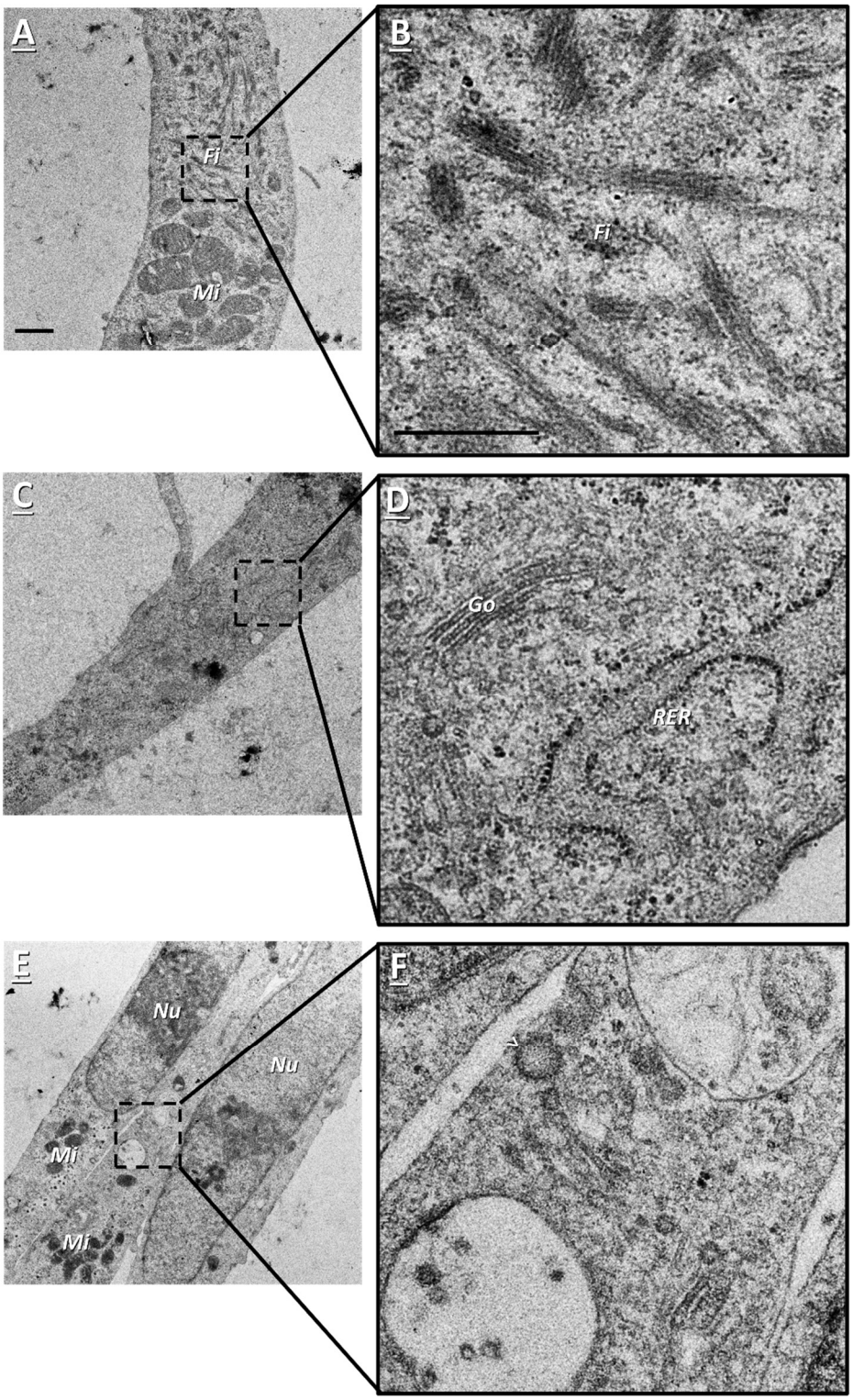

Figure 3.11: 7dp$_{inf}$ TULV infected cells

Vero E6 cells were infected with TULV and incubated for 7 days. Following incubation, cells were processed for TEM. Micrographs A-B, C-D, and E-F are three different cells, with higher magnification images being shown sequentially on the right. The nucleus (*Nu*), mitochondria (*Mi*), rough endoplasmic reticulum (*RER*), filaments *(Fi),* Golgi (*Go*) and particles (>) are labelled accordingly. Scale bars for the two lower magnifications represent 1 µM with the highest magnification scale bar representing 500 nm.

3.2.3 30 dp_{inf} TULV infected cells have larger filamentous structures than 7 dp_{inf} and enlarged RER.

To assess the effect of TULV on cell ultrastructure during persistent infection, TULV-infected cells were imaged at 30 dp_{inf}. At this time point there were signs of cell death in both the mock infected (Figure 3.12) and TULV infected cells (Figure 3.13). Cell death was characterised by a loss of both cellular and nuclear membrane integrity resulting in low cytoplasmic density and occasional loss of nuclear chromatin. 30 dp_{inf} mock infected cells were difficult to image due to the poor membrane integrity in living cells. This can be seen in figure 3.12 where membranes appear indistinct, with low contrast between organelles and the cytoplasm. Despite 30 dp_{inf} infected cells also showing signs of cell death, they were in better condition than that of the 30 dp_{inf} mock infected cells when imaged through TEM. This was corroborated by a colleague when qualitatively viewing both conditions via light microscopy in cell culture- there were more living cells in the infected condition at 30 dp_{inf} than the mock infected. Additionally, in both conditions, cells had large structures resembling phagosomes which contained debris- potentially the remains of apoptotic cells (Figure 3.13, C and E).

There are two ways that cells can die: There is primary necrosis (unregulated cell death) which occurs when severe damage to a cell causes immediate cell membrane breakdown. Or there is apoptosis (regulated cell death) which is slower and planned, allowing for cell contents to be released within vesicles (Sachet et al., 2017). In apoptosis cell contents can be cleared by nearby phagocytic cells (mainly macrophages). If the apoptotic cell is not cleared by phagocytosis, the cell progresses into late apoptosis which is characterised by a loss of cell integrity (secondary necrosis) (Wyllie et al., 1980, Silva, 2010). The phagocytosis of apoptotic cell remains allows for most efficient recycling of cellular material and is therefore desirable by the organism. However, secondary necrosis can occur when the rate of apoptosis is greater than the phagocytic capability of the neighbouring cells (i.e. there is too much cell death) (Garg et al., 2016). Vero E6 cells are epithelial cells which despite not being not being macrophages are still capable of phagocytosis (Monks et al., 2005). When the cells died from starvation or viral infection at 30 dp_{inf}, they were phagocytosed resulting in the phagosomes seen in the micrographs. There are dead cells in the micrographs that were not phagocytosed, which is likely due to there being too many apoptotic cells resulting in secondary necrosis. Interestingly, there did seem to be more healthy cells in the TULV infected condition

compared to mock infected. However, as I was focusing on imaging living cells with intact cellular membranes I cannot validate this claim.

The filamentous clusters seen earlier in the 7 dp_{inf} TULV infected cells (Figure 3.11, B) were also present in the 30 dpi_{nf} TULV cells. 30 dp_{inf} filaments were again arranged in individual bundles of parallel fibres which were clustered into large diffuse sites within the cytoplasm. Typically, the filament clusters were situated in the middle of the cell or in the perinuclear region. Again, there were no confirmed virions imaged. In summary, during persistent stages of infection, TULV may form large filamentous structures and could further enlarge the RER, with no difference seen in particles between mock and infected cells.

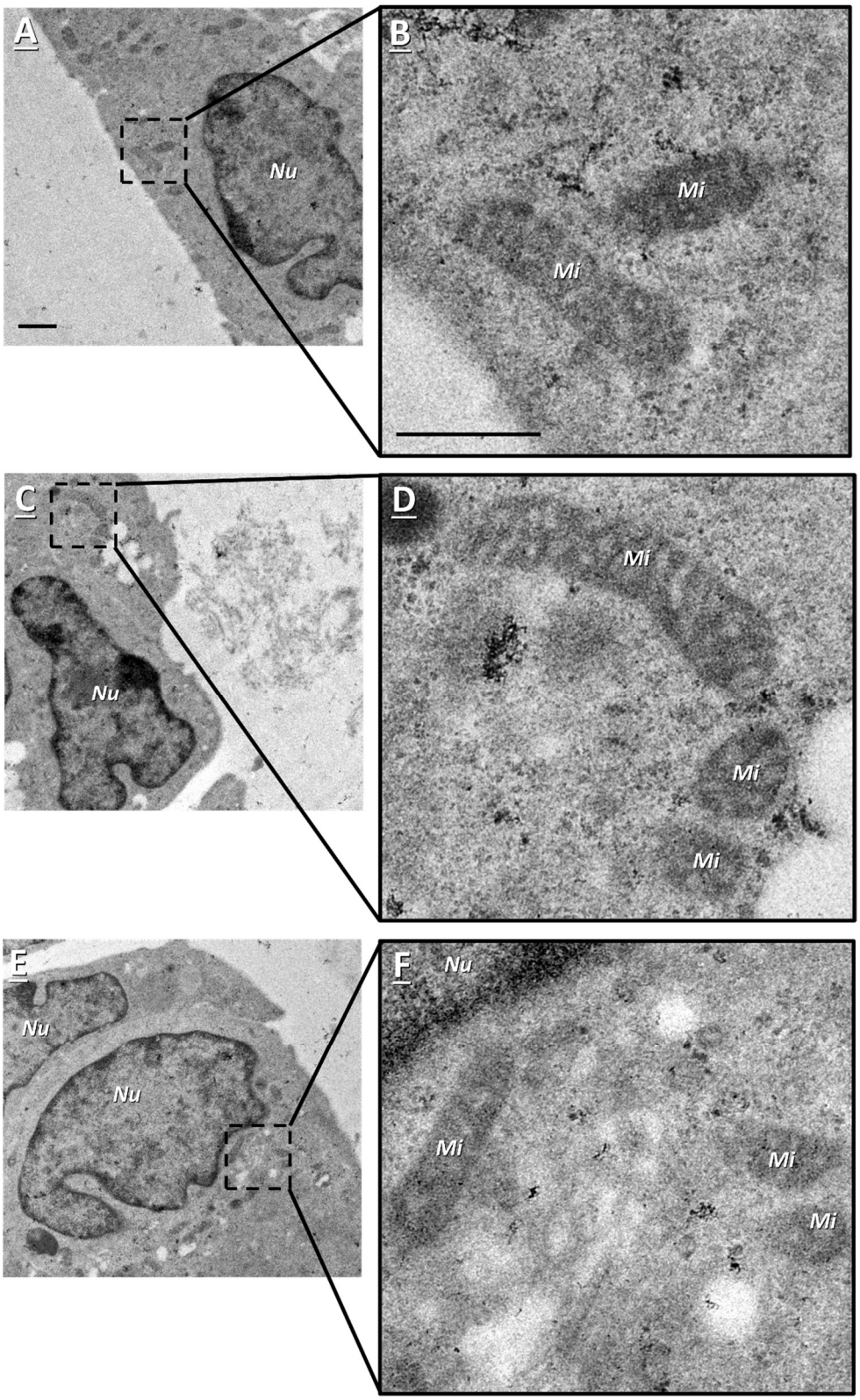

Figure 3.12: TULV mock infected cells - 30dp$_{inf}$

Vero E6 cells were mock infected and incubated for 30 days. Following incubation, cells were processed for TEM. Micrographs A-B, C-D, and E-F are three different cells, with higher magnification images being shown sequentially on the right. The nucleus (*Nu*), and mitochondria (*Mi*) are labelled accordingly. Scale bars for the two lower magnifications represent 1 µM with the highest magnification scale bar representing 500 nm.

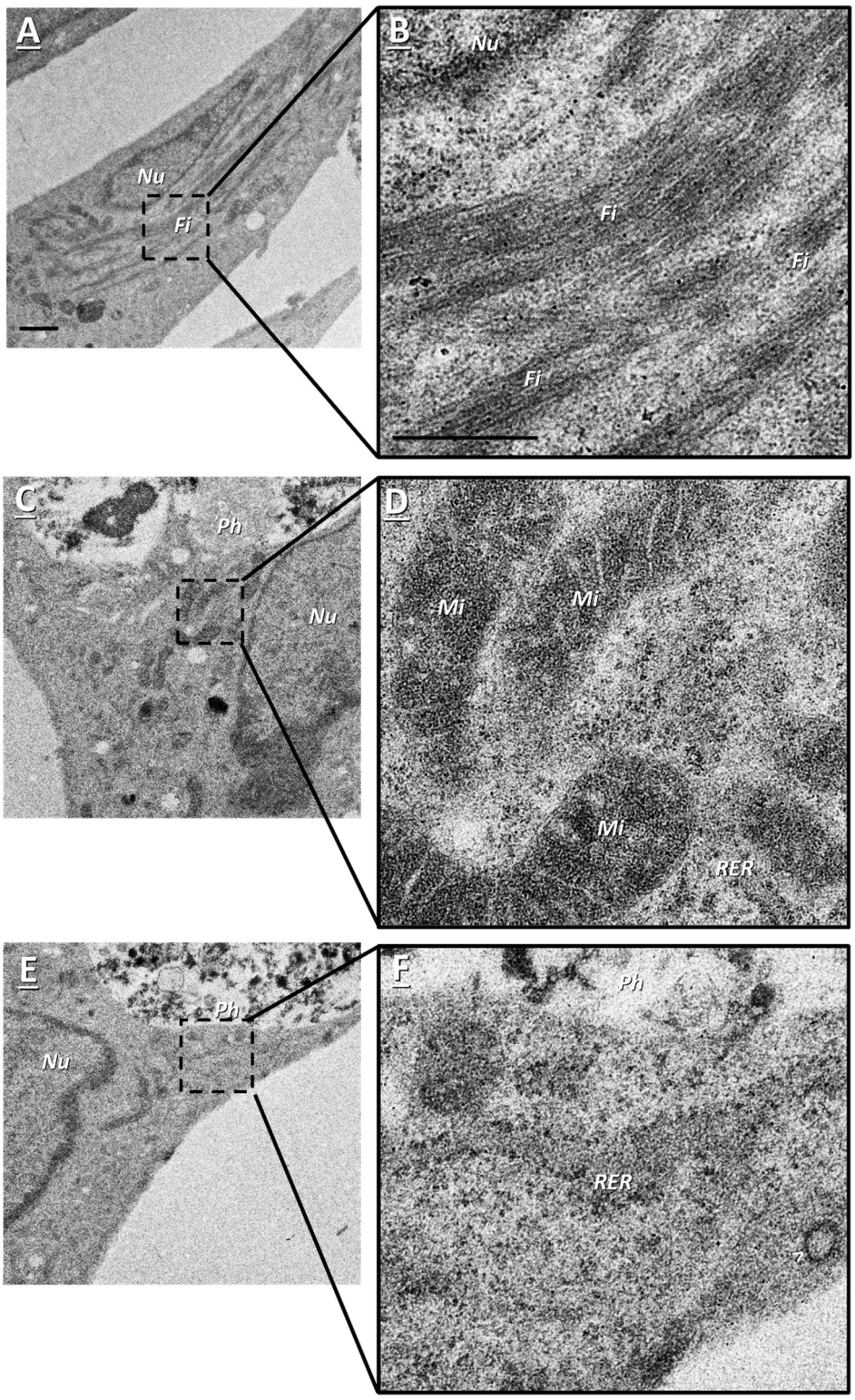

Figure 3.13: 30dp$_{inf}$ TULV infected cells

Vero E6 cells were infected with TULV and incubated for 30 days. Following incubation, cells were processed for TEM. Micrographs A-B, C-D, and E-F are three different cells, with higher magnification images being shown sequentially on the right. The nucleus (*Nu*), mitochondria (*Mi*), rough endoplasmic reticulum (*RER*), filaments *(Fi),* phagosomes (*Ph*) and particles (>) are labelled accordingly. Scale bars for the two lower magnifications represent 1 µM with the highest magnification scale bar representing 500 nm.

3.2.4 Filamentous bundles increase in length from peak to persistent TULV infection

The filamentous structures imaged during TULV infection were only seen in infected cells. Therefore, I decided to investigate this novel observation as a potential hallmark of TULV infection. Filaments were observed in the cytoplasm of 4% of the 224 7 dp_{inf} cells imaged, and 5% of the 92 30 dp_{inf} infected cells (Figure 3.14, D). There was a variety of filamentous bundles sizes which can be seen by the large error bars of figure 3.14, A-C. Within the imaged sections, the average 2D-width of the filament bundles at 7 dp_{inf} was 77 +/- 42 nm (j) with 30 dp_{inf} having filament bundles having a larger width of 113 +/- 50 nm. An independent samples t-Test of log(10) transformed data indicated that the filament bundles in 30 dp_{inf} cells were statistically wider, $t(613) = 1.96$, $p = < 0.001$ (two-tailed). The length of the filamentous bundles was similarly varied with the 7 dp_{inf} filament bundles having an average length of 258 +/- 151 nm, and the 30 dp_{inf} filament bundles having a larger average length of 394 +/- 279 nm. An independent samples t-Test of log(10) transformed data indicated that the filament bundles in 30 dp_{inf} cells were statistically longer, $t(613) = 1.96$, $p = < 0.001$ (two-tailed).

At 7 dp_{inf}, each filament cluster had on average 42 +/- 39 filament bundles, with 30 dp_{inf} filament clusters having on average 55 +/- 49 filament bundles per cell (Figure 3.14, E). A Mann-Whitney U test indicated that this was not statistically significant, $U(N_{7dpinf} = 8 , N_{30dpinf} = 5) = 18$, $p = > 0.05$ (two-tailed). All of the filamentous structures counted above were found in living cells, as a number of filamentous bundles at 30dp_{inf} were found in the debris of apoptotic cells that had been phagocytosed by living cells (Figure 3.14, F-H). Filaments in phagocytic compartments were not counted due to extracellular material being difficult to identify. In conclusion, the filamentous bundles on average grew larger from 7 dp_{inf} to 30 dp_{inf}, with the percentage of cells with filaments, and the average number of filament bundles per filament cluster staying constant between time-points.

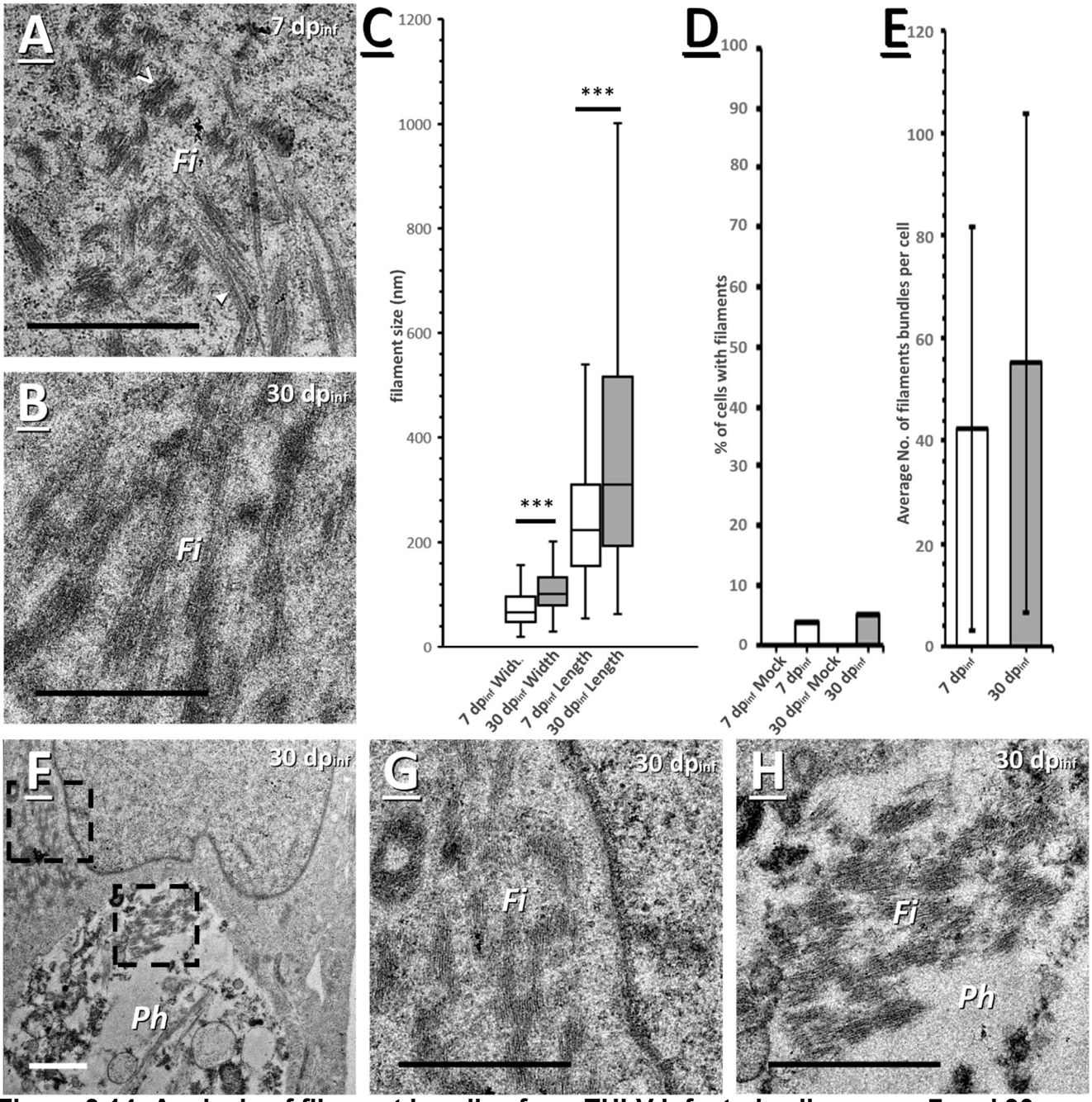

Figure 3.14: Analysis of filament bundles from TULV infected cells across 7 and 30 dp_{inf}

Vero E6 cells were infected with TULV and incubated for 7 or 30 days. Following incubation, cells were processed for TEM. (A-B) cytoplasmic filamentous bundles from cells infected at 7 dp_{inf} and 30 dp_{inf} respectively. (A) Filament bundles at 7 dp_{inf}, shorter bundles are highlighted with a '>', and longer bundles are highlighted by an arrowhead. (B) Filament bundles at 30 dp_{inf}. (C) length and width of filament bundles were measured for both time points and are shown as a box plot. Error bars represent standard deviation and significance bars represent a p-value of < 0.001 (D) percentage of living cells that contain filament bundles at 7 and 30 dp_{inf}. (E) average number of filament bundles found in each cell that is filament positive; error bars represent standard deviation. (F-H) images of a 30 dp_{inf} cell that has filamentous bundles, with (F) showing the low magnification image, (G) showing the higher magnification of filaments within the cytoplasm, and (H) showing the higher magnification image of the filaments within a phagosome. Filaments *(Fi*) and phagosomes (*Ph*) are labelled accordingly. Scale bars represent 1 µM.

3.2.5 Enlarged RER further confirms successful TULV infection

One of the easiest ways to confirm successful viral infection is to identify viral structures such as capsids, virions, or viral factories. However as mentioned above, TULV virions are difficult to identify due to their ambiguous morphology, making it easy to confuse them with normal cellular vesicles. Despite TULV virions being difficult to identify, suspected particles were selected and compared between infected and mock infected conditions. Figure 3.15 below shows a set of these particles from all conditions. Particles were characterised by having a single-layered membrane, an electron-dense core, and a studded exterior. Although most of the particles were indistinguishable between infected and mock infected conditions, the particles from Figure 3.15, I is visually different from other particles as it has a darker core. Interestingly, this particles has a second outer membrane, which indicates that this is potentially a TULV virion that has undergone entry within an endosome. With only one potential TULV virion being identified, there needs to be more evidence of successful infection identified.

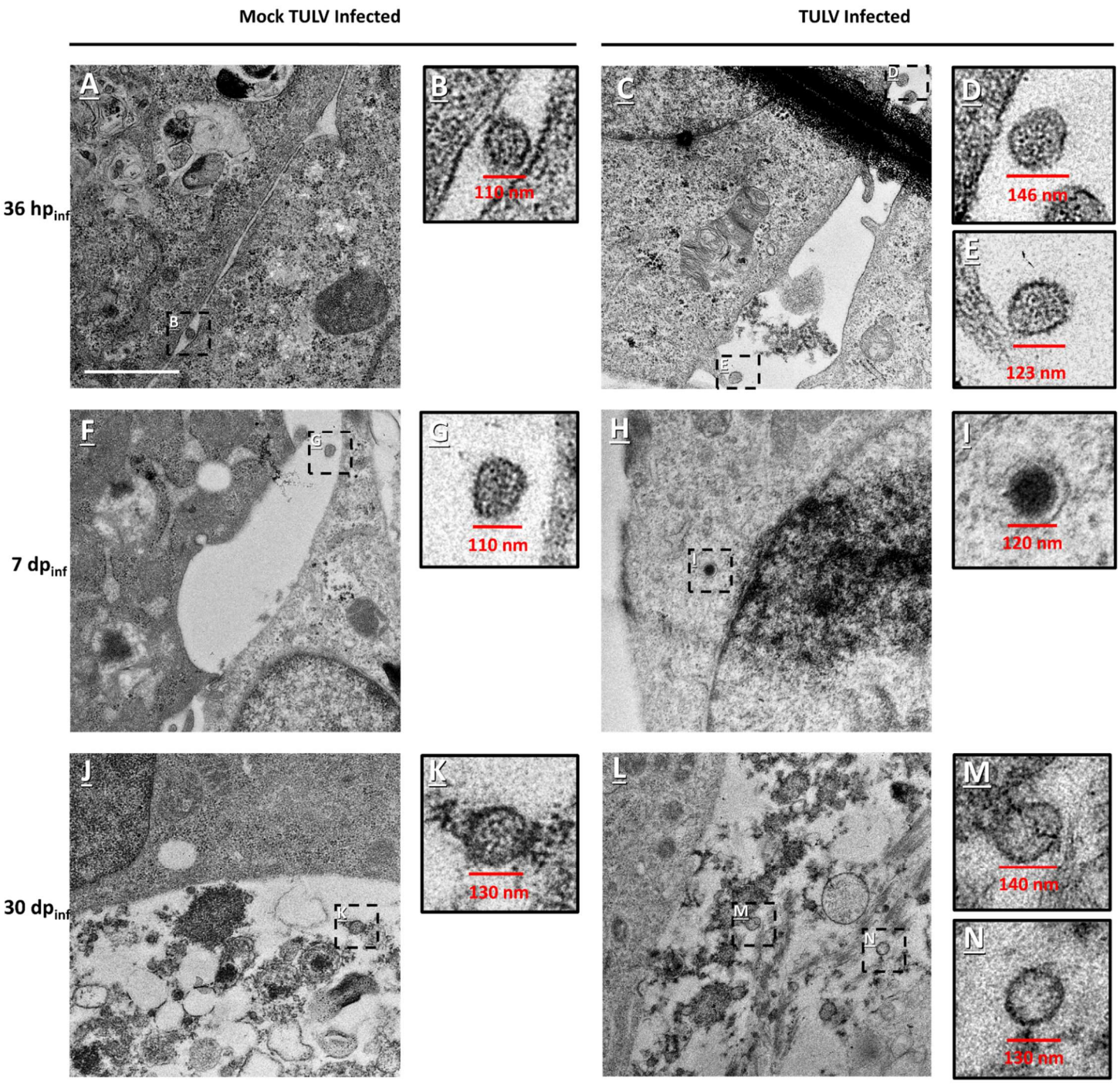

Figure 3.15: Collection of particles from across all TULV infected and mock conditions

Vero E6 cells were infected with TULV or mock infected and incubated for 36 hours, 7 days, or 30 days. Following incubation, cells were processed for TEM. Extracellular and intracellular particles were then identified in all time points with representative examples being displayed above. Scale bar for the lower magnifications represents 1 μM.

The Golgi apparatus is frequently modified by viruses during cellular infection. Certain hantaviruses have been found to assemble at the Golgi, and NP has identified within membrane-bound structures around the Golgi (Meier et al., 2021, Ramanathan et al., 2007). Work from Davies et al. (2020) found TULV induced changes to the Golgi complex structure. Consequently, the Golgi were inspected next for any noticeable changes in morphology in TULV infected cells (Figure 3.16). Of the 224 cells imaged, only 26 Golgi could only be identified in 7 dp_{inf} TULV infected cells, and 10 in the 97 7 dp_{inf} mock infected cells. However, there were no identifiable differences in Golgi morphology between TULV infected and mock infected conditions, with Golgi being characterised by a typical morphology of stacked tubes of cisternae surrounded by vesicles. TULV viral infection therefore could not be confirmed from the remodelling of Golgi structure imaged by TEM. This difference in results is likely due to the different techniques used. The immunofluorescence work from Davies et al. (2020) used the Golgi marker- receptor binding cancer antigen expressed on SiSo cells to identify Golgi within the cell. However for my TEM investigation no Golgi markers were used. Consequently, I could only identify Golgi based upon their structural characteristics (e.g. stacked, sac-like cisternae). Therefore, I could only identify “standard-looking Golgi”; and as a consequence, any Golgi that had been distorted beyond the characteristic appearance would not be identified. This creates a selection bias where only wildtype-like Golgi are identified.

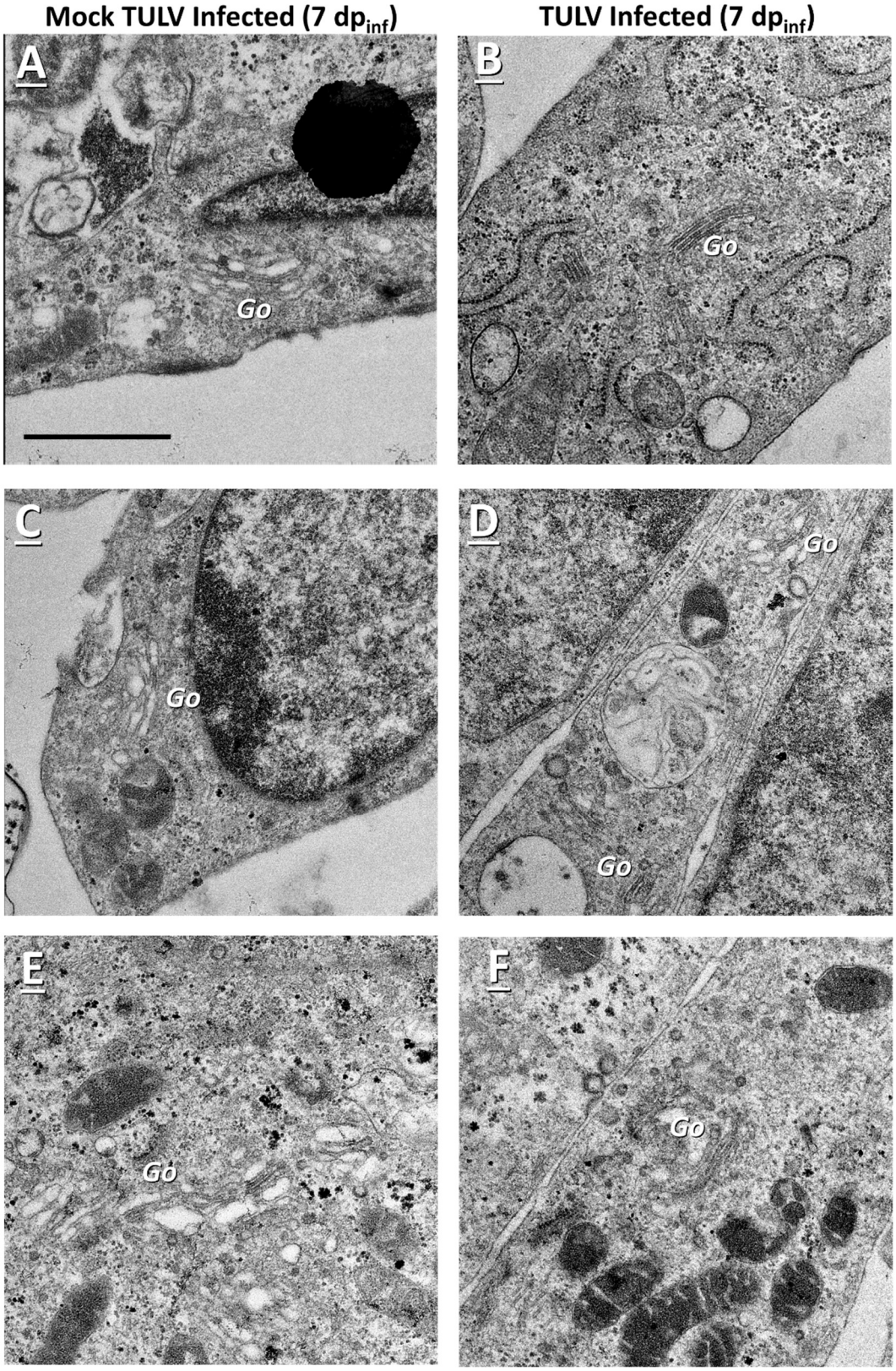

Figure 3.16: Comparison of Golgi between mock and 7 dp_{inf} TULV infected cells

Vero E6 cells were infected with TULV or mock infected and incubated for 7 days. Following incubation, cells were processed for TEM. Golgi (*Go*) were identified and compared from different time point, with representative examples being displayed above. Scale bar represents 1 μM.

When imaging the different TULV conditions, a large number of suspected lamellar bodies (LBs) were identified in both mock and TULV infected cells. Previous work from Sanz-Sánchez and Risco (2013) found evidence LB manipulation in Bunyamwera virus infected cells, the prototypical virus of the *Bunyavirales* order. Suspected LBs were found in all of the conditions (Figure 3.17), except the 30 dp_{inf} mock infected where none were found due to issues with the membrane integrity. LBs are easily identifiable due to their unique multilamellar structure (Figure 3.17), although there were no identifiable changes in LB morphology identified across any of the conditions in which LBs were found. There were also no differences observed between LB to cell ratios between conditions. Therefore, the results suggest that TULV infection does not lead to any noticeable changes in LB morphology or frequency.

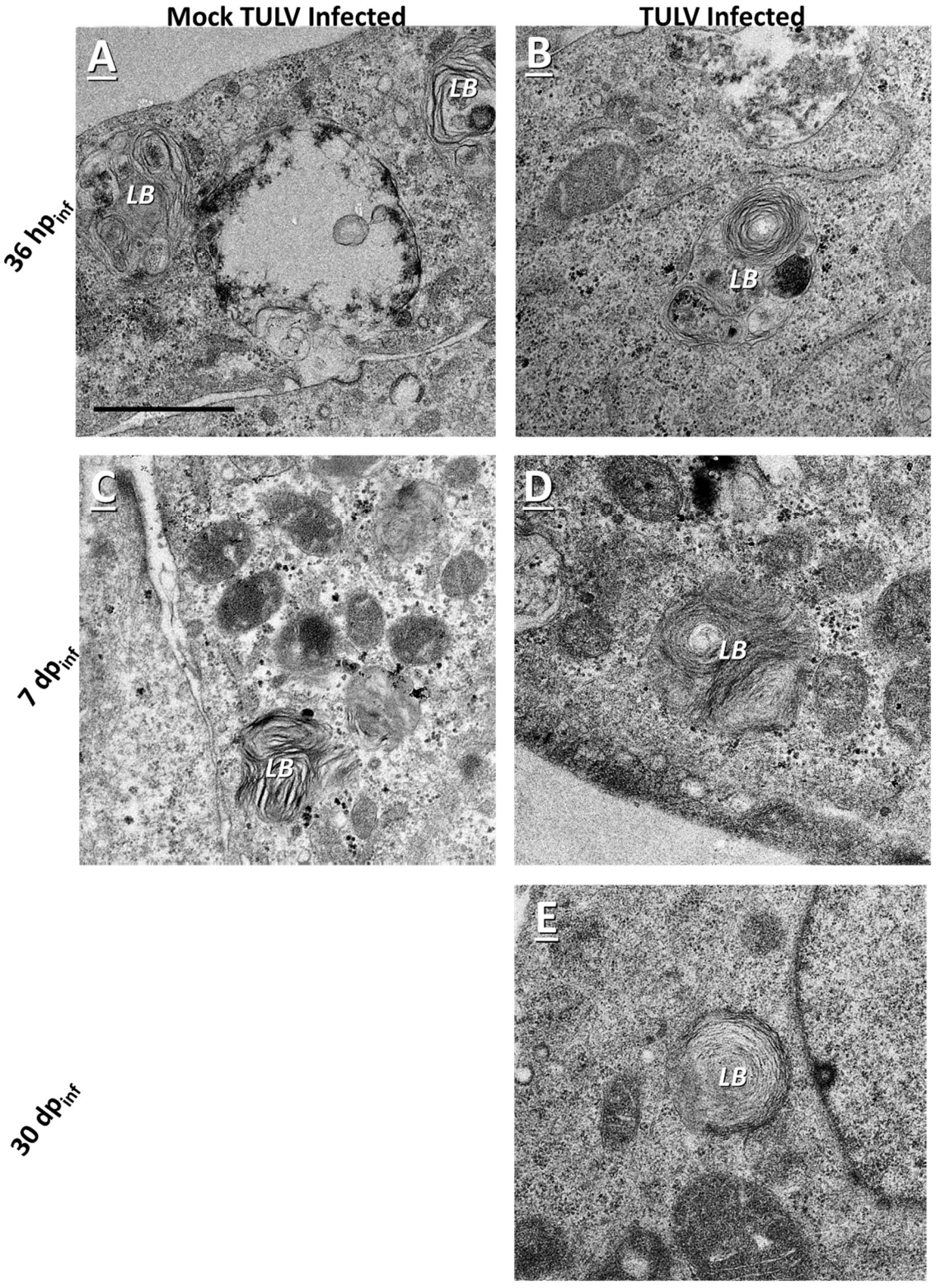

Figure 3.17: Comparison of lamellar bodies in mock and TULV infected cells at different time points

Vero E6 cells were infected with TULV or mock infected and incubated for 36 hours, 7 days, or 30 days. Following incubation, cells were processed for TEM. (A-E) Lamellar bodies (LBs) were identified and compared from different time points, with representative examples being displayed above. No LBs could be found in the mock infected cells at 30 dp_{inf}. Scale bar represents 1 μM. (F) The LB to cell ratio of all conditions.

Hantaviruses are known to utilise the RER as part of their cellular replication, and TULV has been found to trigger ER stress in Vero E6 cells (Li et al., 2005). Thus, the RER were analysed for any signs of TULV alteration (Figure 3.18). RER were observed in abundance across the majority of conditions (1104 across all conditions). There were clear signs of RER enlargement in TULV infected cells from 7 dp_{inf} onwards, with 55 % of 338 7 dp_{inf} RER imaged showing signs of enlargement vs 17 % of the 367 RER in the 7 dp_{inf} mock infected cells. At 30 dp_{inf}, 48 % of the 160 RER imaged were enlarged. Unfortunately, due to poor cellular viability at 30 dp_{inf} mock infected, only 16 RER were identified, making the findings not highly representative at this time point. In addition to RER enlargement, there was evidence of RER tubule fusion in TULV infected 7 and 30 dpi_{nf} cells (Figure 3.18, D and F). The fusion of the RER resulted in a branched phenotype characterised by increased lumen area. In conclusion, TULV infection may result in an increase in RER size and tubule fusion when compared to the mock infected control, therefore it could be used as a confirmation of successful TULV infection, in addition to the presence of filamentous bundles.

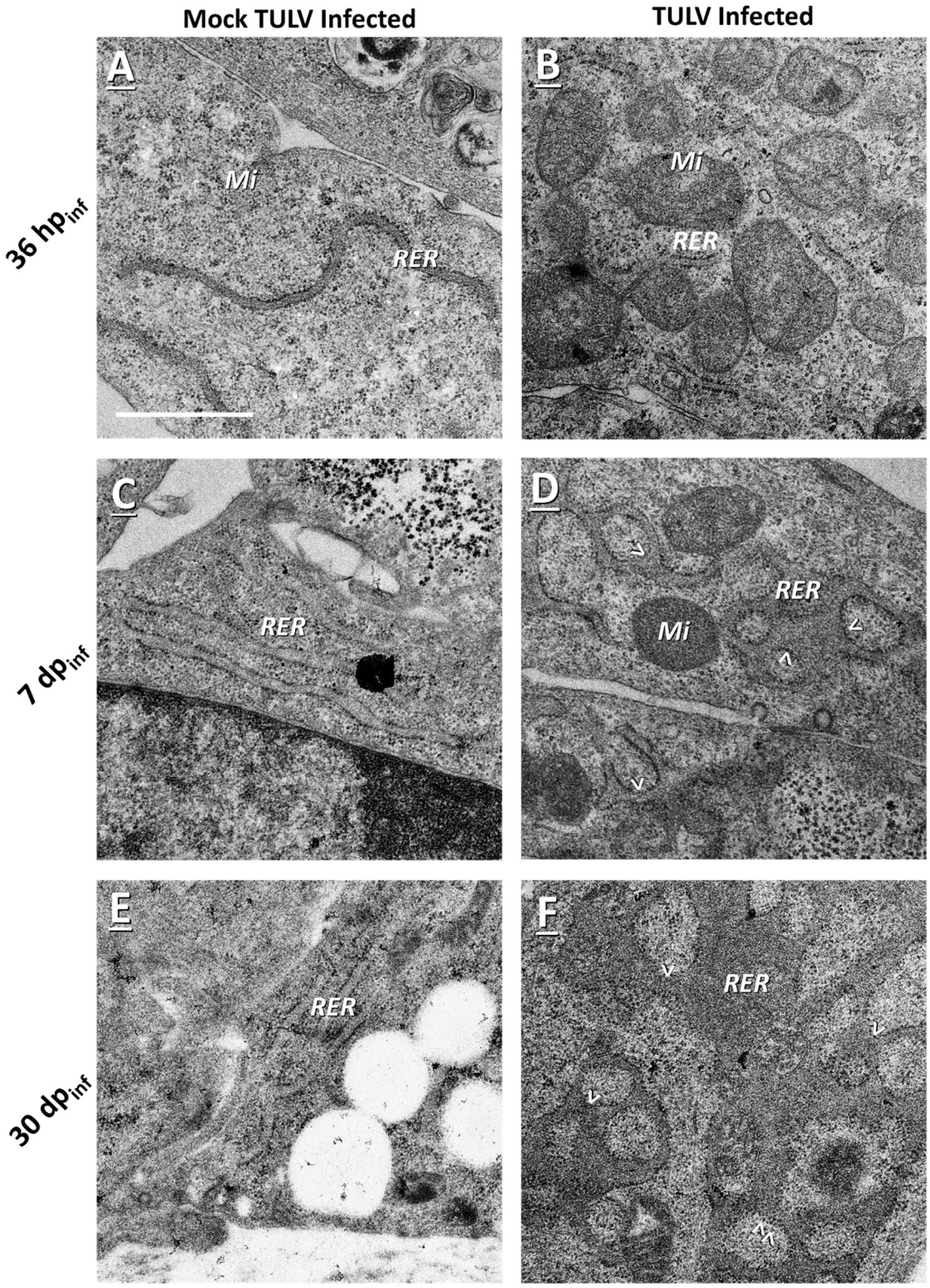

Figure 3.18: Comparison of RER between mock and TULV infected cells at different time points

Vero E6 cells were infected with TULV or mock infected and incubated for 36 hours, 7 days, or 30 days. Following incubation, cells were processed for TEM. The mitochondria (Mi), RER, and RER tubule fusion (>) are labelled accordingly. RER were identified and compared at different time points, with representative examples being displayed above. Scale bar represents 1 μM.

3.3 Tula virus discussion

The aim of this chapter was to investigate the cellular ultrastructure of cells infected with hantavirus via TEM. This project was carried out in collaboration with Katherine Davies who carried out the immunofluorescence experiments. Cells were imaged at early, peak and persistent time points to ascertain how Tula virus induces change over the course of infection. It was found that filamentous structures form in TULV infected cells at peak and persistent time points, with structures significantly increasing in length and width as infection progresses. Furthermore, evidence of ER enlargement was also identified in peak and persistent time points.

3.3.1 TULV Filamentous Structures

3.3.1.1 TULV filamentous structures are a key aspect of the hantavirus replication cycle

One of the most striking findings from the imaging of Vero E6 cells infected with TULV is the presence of the large filamentous structures in the cytoplasm of infected cells at peak and persistent stages. The first stage in investigating these structures was to identify whether the filaments were unique to TULV, or found in other hantaviruses (Figure 3.19). The first evidence of filaments mentioned in relation to hantavirus infection focused on investigating the ultrastructure of Vero E6 cells infected with SNV through TEM (Figure 3.19, A) (Goldsmith et al., 1995). The authors identified large (~1 μm) filamentous inclusions within the cytoplasm of infected cells, which contained multiple filaments in a parallel arrangement. These structures bear a striking resemblance to the filamentous bundles I identified in TULV infected cells. Furthermore, the size and morphology of the filamentous bundles shown matched the filaments seen in persistent TULV infected cells (30 dp_{inf}). Although the paper does not mention at which time point post infection that they imaged the cells. The identification of filaments in SNV infected cells was supported by another paper in the same year which found similar structures in SNV infected capillary endothelial cells from lung tissue sections (Zaki et al., 1995) (Figure 3.19, B). Finally, a more recent report from Pizarro et al. (2019) found filamentous “masses” when using TEM on lung samples from fatal cases of ANDV HPS (Figure 3.1, C). The 2 μm long masses were located within the cytoplasm of

alveolar epithelial cells and macrophages. Again, the structures were similar in appearance to the filamentous structures seen in TULV infected cells. The identification of these filamentous structures within TULV infected cells represents the first OW hantavirus to be identified in the literature that produces these structures. Furthermore, the presence of these filamentous structures in several different cell types (e.g. macrophages, endothelial, and epithelial), in both *in vitro* and *in vivo*, and also across NW (SNV and ANDV) and OW (TULV) hantaviruses indicates that these structures might be involved in key hantavirus processes.

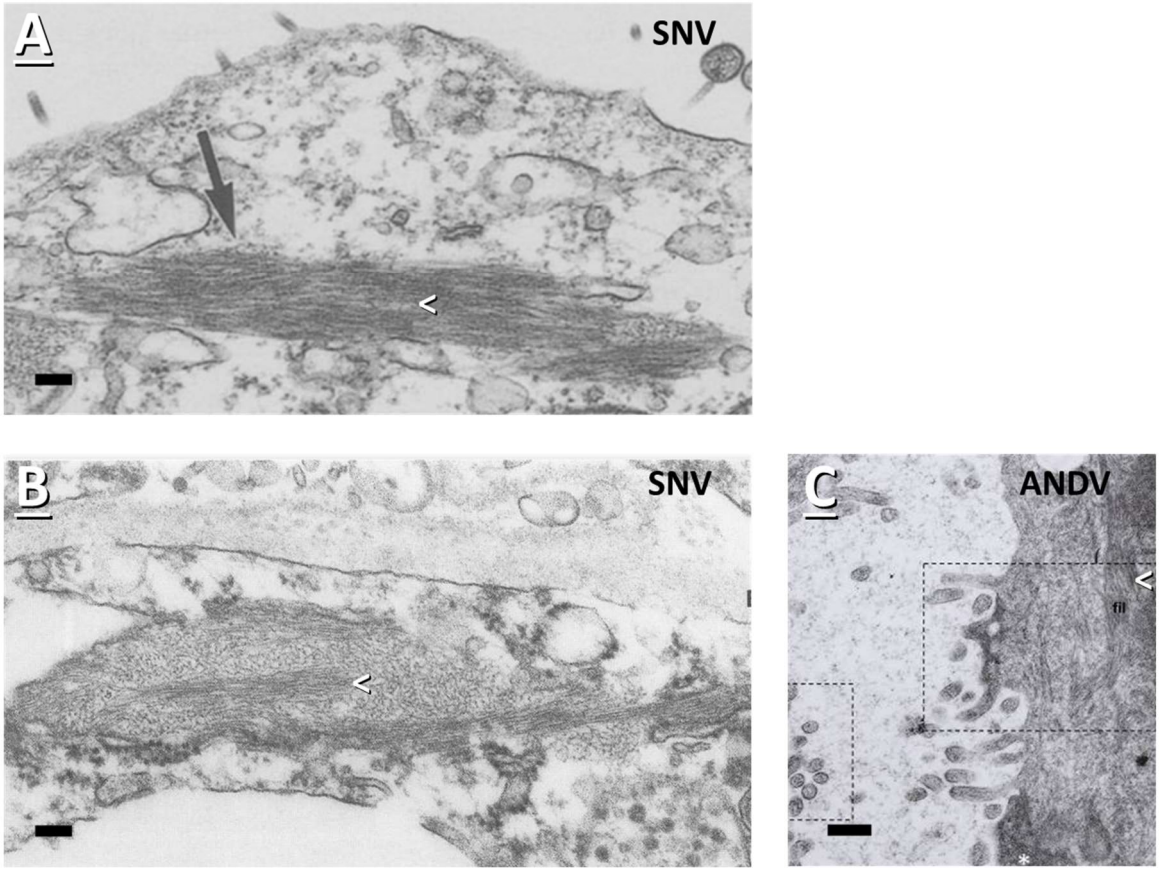

Figure 3.19: Collection of hantavirus filamentous structures from the literature.

(A) TEM micrograph of Vero E6 cells infected with Sin Nombre hantavirus (SNV). Filament bundles highlighted with a '<'. Figure adapted from Figure 6, B by Goldsmith et al. (1995). Scale bar represents 100 nm. (B) TEM micrograph of capillary endothelial cells from lung tissue sections infected with SNV. Filament bundles highlighted with a '<'. Figure adapted from Figure 13, A by Zaki et al. (1995). Scale bar represents 100 nm. (C) TEM micrograph of lung cells from lung tissue sections infected with Andes hantavirus (ANDV). Filament bundles highlighted with a '<'. Figure adapted from Figure 4, B by Pizarro et al. (2019). Scale bar represents 175 nm.

3.3.1.2 TULV filamentous structures act as a site of vRNA replication and transcription

Although previous work has identified filamentous structures in both SNV and ANDV, none of the papers investigated the composition or function of the structures. As mentioned earlier, the TEM work on TULV was carried out in conjunction with Katherine Davies of the John Barr group. I carried out the TEM work which can be seen above, whereas Katherine Davies worked on the immunofluorescence work. One of Katherine's figures can be seen below, showing stained filamentous NP structures imaged by confocal microscopy (Figure 3.20). Katherine utilised confocal, immunofluorescence and fluorescent in-situ hybridisation (FISH) to identify which components localise to the filamentous structures (Davies et al., 2020). She found through immunofluorescence that the filamentous structures contain NP. Furthermore, that the filamentous structures co-localise with a Golgi marker, the stress granule marker TIA-1, and vimentin. Additionally, the FISH analysis showed that both vRNA and mRNA localise with the filaments (Davies et al., 2020).

The presence of vRNA, mRNA, and the stress granule protein TIA-1 within the filamentous structures indicate that this might be the site of TULV genome replication and transcription (Davies et al., 2020). As mentioned in the introduction, hantavirus transcription is dependent upon host mRNA cap-snatching. For cap-snatching to occur, there must be a readily available source of mRNAs. Work from Mir et al. (2008) found that SNV NP accumulated in cellular P bodies which act as a source of mRNA and subsequently, 5' caps. Stress granules are structures composed of mRNA and protein and therefore could act as a source 5' caps for TULV (Wheeler et al., 2016).

Stress granules are involved in promoting cellular survival during periods of stress by acting as an organisation centre for mRNA. Untranslated mRNAs can either be stored within the stress granules, transported to the p-bodies for degradation, or transported to the polysomes for expression (Campos-Melo et al., 2021, Anderson and Kedersha, 2008). Stress granule formation is initiated by either the phosphorylation eIF2α during cell stress or by eIF4A (Mazroui et al., 2006, Low et al., 2005). Either eIF2α or eIF4A trigger stress granule formation through the release of mRNA from the polyribosomes. The mRNA then acts as a scaffold for RNA-binding proteins, initiating stress granule formation (Bounedjah et al., 2014). Stress granules consist of two regions: the highly concentrated core region and the relatively less concentrated and dynamic shell region. The two zones are predicted to carry out different functions, but these are currently unknown (Bounedjah et al.,

2014, Protter and Parker, 2016). TIA-1 is one of the RNA-binding proteins found in stress granules and regulates assembly (Gilks et al., 2004).

The association between the stress granule marker TIA-1 at the filamentous NP structures in addition to viral mRNA, indicates that this could be the site of TULV transcription. Furthermore, the grouping of NP, vRNA and viral mRNA suggest that viral genome replication and transcription may occur at the same location: the filamentous structures (Davies et al., 2020). The role of TIA-1 and stress granules in TULV transcription could be further investigated. Through the use of siRNA, TIA-1 expression could be knocked-down to investigate the effect on TULV transcription. Successful TIA-1 down-regulation could be assessed through western blot analysis, and TULV virion production could be quantified through qPCR. If the suppression of TIA-1 results in a decrease in TULV viral production, it would further indicate that the stress granules play a role in TULV infection.

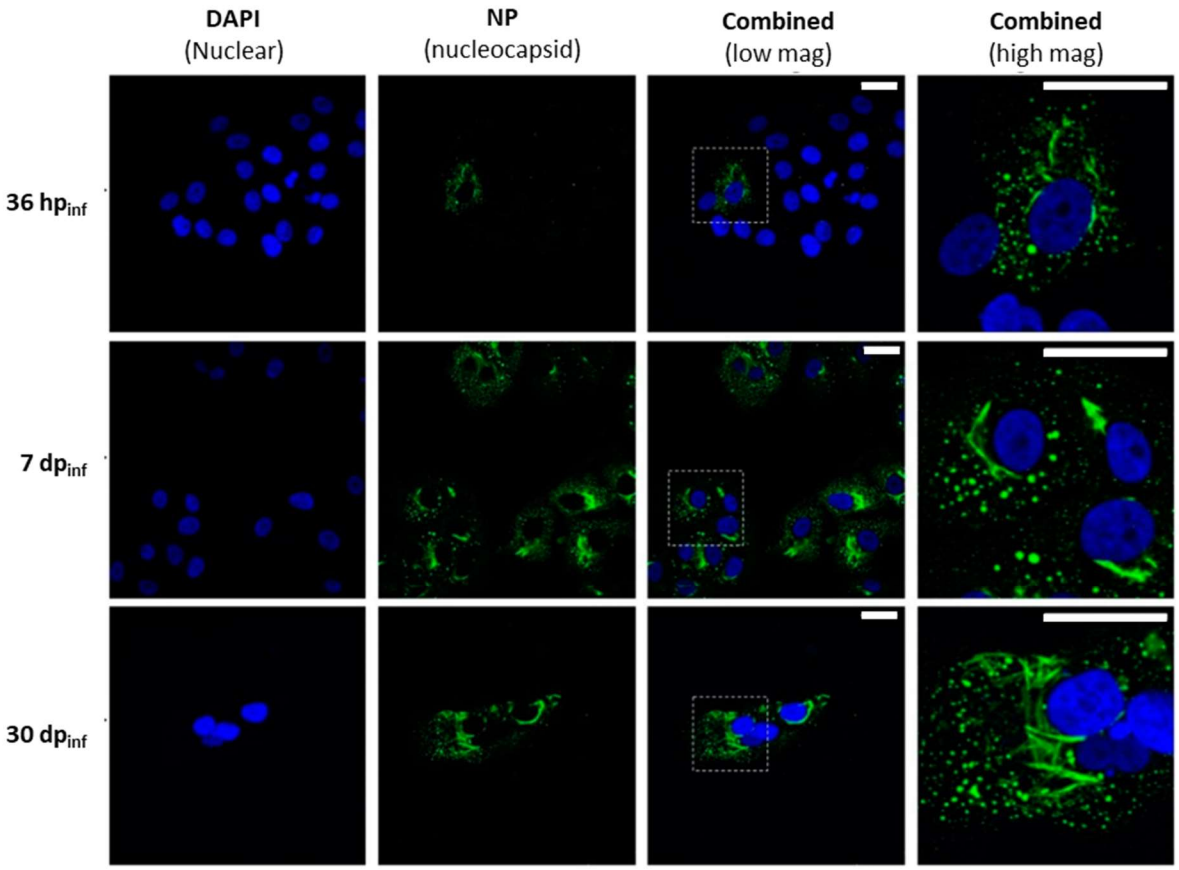

Figure 3.20: Filamentous NP stained structures in TULV infected cells.

Confocal images showing filamentous nucleocapsid (NP) structures in tula virus (TULV) infected cells at early (36 hp_{inf}), peak (7 dp_{inf}), and persistent infection (30 dp_{inf}) stages. Vero E6 cells were infected at a multiplicity of infection of 0.1, and images were taken at the relevant time point. Nuclei were stained with DAPI (blue), and the TULV NPs were stained with NP antisera (green). Scale bars represent 30 µm. Images were taken by Katherine Davies, adapted from figure 1, A (Davies et al., 2020).

3.3.1.3 TULV NP forms the filamentous structures

It is particularly interesting that the Golgi marker is also associated with the filamentous bundles. As mentioned in the introduction, hantavirus glycoproteins are frequently associated with the Golgi; for example, in PUUV the glycoproteins Gn and Gc are found enriched within the Golgi (Sperber et al., 2019). However, the TEM images of the filamentous structures do not seem to possess any membranes. This indicates that TULV infection might result in the relocation of Golgi-associated proteins to the filamentous structures, rather than replicating within the Golgi.

The next question that needs answering is what the filamentous structures are assembled from. Research from Davies et al. (2020) found significant localisation of NP and vRNA with the filamentous structures. Recent cryo-EM imaging of the HTNV NP allowed for the creation a high-resolution structure of the helical arrangement of the NP (Arragain et al., 2019). The 3.3 Å resolution structure revealed a continuous helical oligomer chain with a positively charged groove that allows for vRNA binding, although no RNA was present. The cryo-EM micrographs revealed long fibrils similar to those seen in TULV filamentous structures. Admittedly, the HTNV NP fibrils were only ~100-300nm, although the addition of vRNA to the NP fibrils might improve stability. Additionally, it is difficult to ascertain the length of individual filaments in the TULV filamentous bundles due to the uneven overlapping of the filaments. This is further supported by Welke et al. (2022) who investigated PUUV NP intracellular dynamics. They found when rodent cell lines were transfected with a fluorescently tagged PUUV NP, the NP formed small punctate clusters which developed into larger fibrillar aggregates as the infection progressed. This indicates that even without vRNA (or any other viral components), that the NP is capable of forming these larger filamentous structures. All of this evidence suggests that NP might be responsible for forming the filamentous structures in TULV infected cells.

To further investigate the correlation of the filamentous structures with the Golgi markers, I would repeat the immunofluorescence work using several different Golgi markers. This would help identify whether it is a singular Golgi protein that is associating with the filamentous structures, or several. There are a number of Golgi markers which can be used, such as syntaxin B which is involved in the trafficking of intracellular vesicles, and Beta1,4-galactosyltransferase 6 which is an internal Golgi membrane marker (Bock et al., 1997, Zhang et al., 2013, Teasdale et al., 1992). For the imaging of several different Golgi markers (in different cells), it would be practical to use immunofluorescence microscopy with different antibodies for the different markers. If all of the different markers associate with the filamentous structures in

TULV infected cells, it would suggest that the Golgi is being restructured, as opposed to the relocation of one individual Golgi protein.

Additionally, as a further confirmation that the filamentous structures contain TULV NP, CLEM could be utilised to image infected cells. Antibodies can be used to immuno-label specific structures in CLEM, a technique known as immuno-CLEM (Oorschot et al., 2021). However, the sample has to be prepared in a way that preserves protein antigenicity. Once such technique is the Tokuyasu cryo-preparation which enhances the fluorescent labelling of probes and preserves antigenicity (Griffiths et al., 2015). Probing for TULV NP would further confirm that the filamentous structures seen through TEM are indeed the same structures identified by the TULV NP immunofluorescence work carried out by Katherine Davies (Figure 3.20).

3.3.1.4 Host Vimentin forms cages around TULV NP filaments

Davies et al. (2020) also found that vimentin associates with the TULV filament bundles at 7 dp_{inf} and 30 dp_{inf}. Vimentin is a Type III intermediate filament which has a tripartite structure consisting of a core α-helical shaft with a carboxy-terminal tail and amino-terminal head. The main function of vimentin is to maintain optimum protein levels within the cell (i.e., proteostasis). When protein levels are too high or proteins have been misfolded, they are trafficked to the centrosome. Vimentin then surrounds the centrosome and trafficked proteins, forming a structure known as an aggresome. The aggresome acts to store the unwanted proteins for later degradation (Johnston et al., 1998; Morrow and Moore, 2020). Whilst vimentin is not essential for aggresome formation, several studies have suggested that it acts as a scaffolding for the individual components (e.g. proteosomes) needed for the establishment of proteostasis (Morrow and Moore, 2020; Morrow et al., 2020). It was found by Pattabiraman et al. (2020) through comparative interactome analysis and immunofluorescence microscopy that vimentin directly associated with protein aggregates, misfolded proteins, and RNA binding proteins during stress, forming a cage structure around them. Curiously, they also found that vimentin interacts with stress granule components and enables stress granule formation. The researchers suggest that rather than vimentin forming around the aggregated protein at the juxtanuclear region, that protein traffics to the vimentin (Pattabiraman et al., 2020).

Several viruses are known to manipulate vimentin over the course of their replication cycle. African swine fever virus (ASFV) rearranges vimentin to form cages around its

viral factories via the phosphorylation of vimentin (Stefanovic et al., 2005). However it is unknown whether this vimentin modulation is directed by ASFV to aid in viral replication by forming an assembly site or by acting as a scaffold for viral proteins; or whether it is directed a cell-mediated antiviral response to sequester viral proteins into an aggresome (Stefanovic et al., 2005). Additionally, Turkki et al. (2020) investigated the role of vimentin in the replication of enterovirus group B viruses. The researchers found that the transfection of cells with foreign dsRNA did not trigger the formation of vimentin cages. However, when they blocked viral protein expression they found that vimentin cages did not form, indicating that the creation of vimentin cages is caused by viral protein expression, not viral RNA. (Turkki et al., 2020). Vimentin has been further linked with hepatitis C (HCV) virus, vaccinia virus, cowpea mosaic virus, Japanese encephalitis virus, rabies virus, and Epstein-Barr virus (EBV) to name a few (Ghosh et al., 2011, Risco et al., 2002, Plummer et al., 2012, Das et al., 2011, Wang et al., 2011, Meckes et al., 2013).

Therefore, it might be that TULV infection results in the formation of similar vimentin cage structures to those formed by ASFV. Intriguingly, this is not the first time that vimentin has been associated with hantavirus infection. Ramanathan et al. (2007) found that NP was linked with vimentin in HTNV infected Vero E6 cells at 5 dp_{inf}. Vimentin formed cage like structures around condensed regions of NP when imaged through immunofluorescence. They hypothesised that the restructuring of vimentin could improve HTNV replication and transcription by providing a ‘scaffold’ or favourable environment. The formation of vimentin cages in the periphery around NP is similar to the observation that vimentin was adjacent to TULV NP at 30 dpi in TULV infected cells (Davies et al., 2020). Furthermore, Welke et al. (2022) (who was mentioned earlier in regards to NP) found that when cells were transfected with PUUV NP, the filamentous NP structures had significant co-localisation with vimentin. This lead them to conclude that contact with NP and vimentin occurred in the absence of other viral components. The interaction of vimentin and NP in HTNV and PUUV further reinforces the hypothesis that vimentin is involved in OW hantavirus replication.

A future area of research would be to investigate the cause of vimentin potentially forming cages around the TULV NP filaments. At the moment, it is unknown whether the process a natural cell response to the presence of foreign protein, or if it is intentionally triggered by TULV infection. One possible way to examine this would be to transfect cells with different proteins. For example, one condition could be transfected to allow the expression of the TULV NP protein. Another condition could be transfected with a foreign protein, and the final condition could see the cell line transfected with a normal cell protein (a negative control). Cells would then be

imaged through CLEM to identify whether the vimentin response is the same for all three conditions, or whether it is different in TULV NP transfected cells. If the vimentin response is unique to NP expression, it indicates that TULV might be triggering or influencing the vimentin response. The use of CLEM will provide detailed structural information from the EM, which can then be combined with the identification of structures by the fluorescence microscopy. Additionally, vimentin could be inhibited to identify if there is any impact on TULV viral infection. There are a number of compounds which inhibit vimentin, such as ajoene which triggers vimentin intermediate filament break down, Fluvastatin which activates the proteolysis of vimentin via caspase-3, and silibinin which represses vimentin expression (Strouhalova et al., 2020). Successful vimentin disruption could then be confirmed through a combination of western blot and immunofluorescence, with TULV virion production quantified through qPCR analysis. If TULV virion production decreases in vimentin inhibited cells, it could indicate that it plays a role in successful virus production.

3.3.2 TULV induces ER enlargement by triggering the ER stress response

The other cell ultrastructure change observed during TULV infection was the enlargement and increased branching of the RER. The ER is a large, membranous organelle with a highly dynamic structure that has several roles (e.g. protein synthesis, folding, transport *etc.*). It has several domains which vary in structure and function, with the two main domains being the nuclear envelope and the peripheral regions of the ER (Baumann and Walz, 2001, Schwarz and Blower, 2016). The peripheral ER was originally believed to mainly consist of tubules and sheets. However, this view has been challenged by super resolution imaging which found that the peripheral ER contains a dense cluster of highly dynamic tubules (Nixon-Abell et al., 2016). The ER can change its shape due to a group of membrane-associated proteins and cytosol-based factors which can be split into different groups. There are the proteins that alter ER membrane curvature and tubule formation, such as the deleted in polyposis locus 1 protein and the reticulons (Voeltz et al., 2006). There are also the GTPase atlastins which generate ER tubule branching (Hu et al., 2009). Overall, the ER is a highly dynamic structure that is capable of rapidly changing its shape depending upon changing cellular environment.

The ER can be become enlarged as a direct response to physiological stress. Factors such as ER Ca^{2+} exhaustion, hypoxia, viral infection, and ER-Golgi transport failure can all lead to the accumulation of unfolded, or misfolded proteins, which can trigger the ER stress response (Lin et al., 2008, Schuck et al., 2009). ER stress triggers the unfolded protein response (UPR) which includes three separate protein sensors that aim to resolve ER stress (Mateus et al., 2018). For example, the UPR can increase ER protein-folding capacity alongside boosting the degradation of misfolded proteins (Lin et al., 2008). Another UPR mechanism to alleviate ER stress is the increase of lipid biosynthesis to expand the size of the ER. It is currently unknown if the expansion of the ER reduces ER stress by providing more space for misfolded proteins, or if it has a more direct role (Schuck et al., 2009, Short, 2009). If the ER stress continues, cell death can be activated through stimulation of pro-apoptotic proteins such as CHOP (Zinszner et al., 1998).

During viral infection, viruses often exploit the ER to mass produce proteins in addition to exploiting the ER membrane for envelopment. Consequently, viruses often trigger ER stress (Jheng et al., 2014). For example, Zika virus (ZIKV) is able to exploit the fluidic nature of the ER to enhance viral replication by triggering the UPR. During ZIKV infection, the ER lumen dilates and forms viral structures such as convoluted membranes, vesicle packets, zippered-ER, and viroplasm-like constructions which facilitate vRNA replication (Mohd et al., 2020, Rossignol et al., 2017, Cortese et al., 2017). ZIKV is able to induce these changes by directly manipulating the host reticulon 3.1A, which induces ER membrane curvature. ER curvature allows for the formation of vesicle packets which act as sites of vRNA synthesis (Rossignol et al., 2017, Aktepe et al., 2017). This demonstrates how ZIKV is able to control the host response to protein misfolding to aid in its replication cycle.

The swelling of the ER due to induced ER stress is also a prominent aspect of the hantavirus replication cycle. Recent research found that the HTNV infection of a monocyte cell line resulted in significantly higher levels of several ER-stress related proteins (e.g. PKR-like ER kinase [PERK]). However, they did not observe any signs of apoptosis in infected cells and CHOP mRNA levels were not elevated, indicating that HTNV can activate the UPR without triggering cellular apoptosis (Li et al., 2021). The recent EM investigation of HTNV infected Vero E6 cells by Parvate et al. (2020) found signs of swollen ER at 7 dp_{inf}, with the researchers stating that ER enlargement was a hallmark sign of HTNV infection. HTNV is not the only hantavirus which has been found to induce ER stress. TULV infection was also found to trigger ER stress in Vero E6 cells. Researchers found that TULV infection increased the expression of the ER-located chaperone Grp78/BiP which is involved in the ER stress response. They proposed that this was due to the misfolding of TULV

glycoproteins triggering the UPR (Shi and Elliott, 2004, Li et al., 2005). The above findings show that ER stress triggered by hantavirus infection can lead to ER-enlargement. Therefore, I propose that TULV enlargement of the ER seen in the TEM micrographs might be caused by the triggering of the UPR, likely due to the misfolding of TULV glycoproteins in the ER.

However, this model does not answer whether the ER enlargement is just a cellular response to protein misfolding, or whether TULV manipulates the process to aid in viral replication. Further investigation will be needed to answer this question. A better structural understanding of the ER enlargement could help to answer whether there is any benefit for the virus in restructuring of the ER (e.g. as seen in ZIKV). A technique that could be used to investigate this is focused ion beam (FIB) scanning electron microscopy (SEM). FIB SEM involves using a laser to 'slice' off layers of cell whilst imaging each top layer via scanning EM (SEM). This allows for the imaging of a larger region of a cell, rather than imaging a singular ~100 nm section. Consequently, more 3D information is gained allowing for the recreation of a larger structure. FIB-SEM has been used to visualise the details of herpesvirus nuclear egress, revealing the mechanics of envelopment and de-envelopment (Villinger et al., 2015).

3.3.3 Proposed Model of TULV replication site formation and ER enlargement

All of the evidence has led me to suggest a speculative model on the formation of the TULV replication site. Upon TULV infection of the cell and subsequent protein expression, NP proteins are produced within the cytoplasm. Upon the accumulation of TULV NP into the cytoplasm, it independently forms into filaments. This is supported by Welke et al. (2022) who found that PUUV NPs formed into filaments when cells were transfected with just NP. Next, the concentrated aggregates of NP filaments triggers the cells proteostasis response, causing either vimentin to relocate to the NP filaments, or the NP to relocate to the vimentin (Morrow et al., 2020; Pattabiraman et al., 2020). This process might be similar to how protein production in enterovirus group B virus infection triggers the formation of vimentin cages (as mentioned earlier) (Turkki et al., 2020). Next, the vimentin forms a cage-like structure around the NP filaments, as shown in HTNV, PUUV, and Katherine Davies' findings (Ramanathan et al., 2007; Welke et al., 2022; Davies et al., 2020). This cage-like structure could then act as a scaffolding for the components needed for vRNA replication and transcription e.g. stress granules (Pattabiraman et al., 2020;

Ramanathan et al., 2007). The stress granules act a source of 5’ mRNA caps for TULV transcription resulting in increased viral protein production, as suggested by Davies et al. (2020). The increased production of viral mRNA allows for upregulated expression of viral proteins. The translation of M segment mRNA and post-translational cleavage results in the formation of the glycoproteins Gn and Gc (Löber et al., 2001). In late infection, the overexpression of Gn and Gc might result in the misfolding and the triggering the UPR within the ER, resulting in the expansion of the ER (Li et al., 2005, Shi and Elliott, 2004).

Clearly the TULV replication system is complex, and this speculative model requires further work to determine its validity; but it provides a number of hypotheses that can be tested experimentally. Additionally, there are still several questions that need answering. For example, does vimentin form around the NP filaments, or does the NP filaments form adjacent to vimentin? This could be investigated by disabling vimentin (e.g. with acrylamide, β′-iminodipropionitrile, or okadaic acid), and then transfecting the cells with NP and determining if the NP forms the same structure in the same location. Furthermore, what is the structural layout of the TULV replication site? ET could be used to further elucidate the structural details of the TULV filamentous structure. ET has been used to study several viral replication compartments *in situ*. For example, ET has been used to image the replication sites of flock house nodavirus, SARS-CoV-2 and reovirus to name a few (Ertel et al., 2017; Klein et al., 2020; Tenorio et al., 2018). In any case, the hypothesis above of TULV replication site formation provides a framework for future work.

Chapter 4 :
Treatment of rotavirus infected cells with an aliphatic alcohol decreases viroplasm size due to the disruption of liquid-liquid phase separation

4.1 Rotavirus Introduction

Rotaviruses are non-enveloped, segmented dsRNA viruses that cause severe gastroenteritis and are responsible for the majority of paediatric diarrhoeal deaths worldwide. In 2016 rotavirus-based diarrhoea was responsible for 128,500 deaths in children under five (Burnett et al., 2020, Crawford et al., 2017, Troeger et al., 2018). Although rotavirus infections occur globally, they have a greater impact in low-income countries which bear the highest percentage of infant mortalities (Tate et al., 2016). Rotaviruses are transmitted via the faecal-oral route, with the majority of disease spread occurring directly between infected individuals (Kraay et al., 2018). When ingested, rotavirus virions transit through the digestive tract until they reach the small intestine where they target mature enterocytes and enteroendocrine cells (Amimo et al., 2021). They use their outer capsid proteins to attach to and enter the target host cells. Once inside they transit through endocytic pathway before exiting and forming viroplasms within the cytoplasm. The viroplasms act as viral factories for genome replication and capsid assembly. Once assembled, the progeny virions transit through the ER and egress at the plasma membrane, ready to infect other neighbouring cells (Patra et al., 2021).

4.1.1 Rotavirus Taxonomy

Rotaviruses belong to the *Rotavirus* genus, one of 15 within the *Reoviridae* family of viruses (Desselberger, 2014). There are nine different rotavirus species which are currently accepted by the ICTV named A to D, and F to J (also known as rotavirus groups) which are classified from genomic sequence and antigenic differences in VP6 (Johne et al., 2022, ICTV, 2021, Matthijnssens et al., 2012). However, two more groups have been proposed (K and L) from rotaviruses isolated from shrews (Johne et al., 2022, Johne et al., 2019). The rotavirus A group is of particular interest as it is responsible for the majority of infections in children (Parashar et al., 2013).

4.1.2 Rotavirus Disease

4.1.2.1 Clinical Characteristics

Rotavirus infection can cause severe, acute gastroenteritis and is especially prevalent in children, with rotavirus species A in particular being responsible for the majority of paediatric infections (Parashar et al., 2013). The onset of rotavirus disease is typically associated with vomiting and fever, with watery, non-bloody diarrhoea following over the next day or two. Within three to seven days the remaining gastrointestinal symptoms should be over (Parashar et al., 2013). Other less frequent symptoms can include signs of central nervous system disease, presenting as encephalitis and benign convulsions (Dickey et al., 2009). Although rotavirus infection can lead to severe diarrhoea, it can also cause asymptomatic or mild gastroenteritis. Disease symptoms and severity can be dependent upon patient age, with children younger than one month being frequently asymptomatic as a result of protection from the maternal antibodies gained from breast milk or the placenta (Haffejee, 1991, Haffejee et al., 1990). Symptomatic cases typically start in children older than three months, with the peak incidence occurring in children between 4 and 23 months of age (Raúl Velázquez et al., 1993, Crawford et al., 2017). Reinfection with rotavirus is a frequent occurrence with immunity not protecting against reinfection. However, subsequent infections are associated with less severe symptoms (Bishop et al., 1983). As a result, adults who are infected with rotavirus can either be asymptomatic, or present mild symptoms such as nausea, headaches, malaise, diarrhoea, fever, and abdominal cramps. Individuals who are elderly, travellers, or immunocompromised are at risk of more severe or even chronic illness (Anderson and Weber, 2004).

4.1.2.2 Rotavirus Pathology

The first step in rotavirus pathogenesis is the navigation of the host digestive tract to reach target cells. The digestive system is a hostile environment to transit, encompassing mechanical, mucosal, enzymatic, antibody, and acidic stressors which all aim to inhibit and destroy invading pathogens (Santaolalla et al., 2011, Coates et al., 2019, Smith, 2003). To combat this, rotaviruses have a triple layered capsid which provides stability and helps to prevent inactivation when on route to the small intestine. The outermost capsid layer is particularly stiff and resistant to stress,

providing protection whilst the particle travels through the digestive tract (Jiménez-Zaragoza et al., 2018). In addition to their outermost capsid, research has found that rotaviruses egress from cells within extracellular vesicles. These vesicles contain clusters of rotavirus, and are shed in the stool of infected animals. The vesicles aid in rotavirus infection of cells by delivering a large number of infectious virions to the cell surface, and by also shielding the viruses from the digestive system (Santiana et al., 2018). Rotaviruses attach to and replicate primarily within mature enterocytes and enteroendocrine cells within the small intestine (Lundgren and Svensson, 2001, Amimo et al., 2021). Viral attachment and subsequent entry is facilitated by the outer capsid viral proteins VP4 and VP7. The rotavirus VP4 spike protein is proteolytically cleaved by trypsin-like proteases of the gastrointestinal tract, allowing it to attach to host cells through its V8* and V5* domains (Li et al., 2017).

Once rotavirus has entered the cell and begun viral replication, it starts inducing rotavirus gastroenteritis. This is achieved by several known mechanisms. The first way that rotavirus triggers diarrhoea is by directly damaging the intestinal border (Crawford et al., 2017). Rotavirus damages the intestinal wall by infecting and killing enterocytes located there, resulting in the injury and loss of microvilli and villi. Additionally, infected enterocytes show signs of stress, losing their brush border enzymes and possess swollen ER and mitochondria (Omatola and Olaniran, 2022). The damage to the intestinal lining prevents the absorption of electrolytes, fluid, and nutrients. This in turn changes the osmotic balance within the intestine, resulting in the movement of water into the intestinal lumen and subsequent diarrhoea. The severity of diarrhoea can be further increased via crypt cell hyperplasia, where an increase in the secretory cells leads to further fluid loss (Colbère-Garapin et al., 2007). Another way in which rotavirus can trigger diarrhoea is through the rotavirus enterotoxin NSP4. The NSP4 protein in rotavirus infected cells acts as a viroporin (viral ion channel) in the ER, transporting ER Ca^{2+} into the cytosol (Hyser et al., 2010, Tian et al., 1995). Increases in intracellular Ca^{2+} concentration triggers the Ca^{2+} activated chloride channels which pump Cl^- ions into the intestinal lumen (Omatola and Olaniran, 2022, Chang-Graham et al., 2019, Das et al., 2018). The movement of Cl^- ions into the intestinal lumen further disrupts the osmotic balance, drawing more water into the lumen and contributing to the watery diarrhoea (Das et al., 2018). The increase is intracellular Ca^{2+} concentrations by NSP4 can additionally enhance diarrhoea through the activity of serotonin. Serotonin is secreted by enteroendocrine cells as a response to elevated Ca^{2+} levels, activating the enteric nervous system (Hagbom et al., 2011). The activation of the enteric nervous system enhances intestinal motility which is associated with the onset of diarrhoea (Bialowas et al., 2016).

4.1.2.3 Diagnosis, Treatment, and Prevention

4.1.2.3.1 Diagnosis

Rotavirus-based disease is indistinguishable from other pathogenic diarrhoeal diseases (e.g. enteric adenovirus, norovirus, *Escherichia coli*, *etc.*). However, certain factors such as seasonality can be used to differentiate between rotavirus and other pathogens. For example, if a child shows signs of diarrhoeal illness during winter in a non-equatorial region, it will likely be due to rotavirus or norovirus infection (Crawford et al., 2017). For a more objective diagnosis, a laboratory test can be requested by the physician. An ELISA test can detect rotavirus within faecal samples, and RT-PCR can be used to pick up viral genomic material for vaccine or epidemiological studies. RT-PCR analysis has a higher degree of sensitivity when compared to ELISA testing and can be used to genotype viral isolates (Parashar et al., 2013). Moreover, the concentration of vRNA being shed directly corresponds to the severity of rotavirus disease in children (Kang et al., 2004).

4.1.2.3.2 Treatment

Dehydration as a result of rotavirus-associated diarrhoeal disease is severe and can be life threatening (especially in young children) (Carlson et al., 1978). Consequently, treatment of rotavirus-based illness focuses on rehydrating patients orally or intravenously (Parashar et al., 2013). Fluid replacement is achieved through the use of oral rehydration solution which is a mix of water, glucose, and salt. The glucose and sodium is absorbed by the small intestine via sodium-glucose linked transporters, and the water follows the sodium (King et al., 2003). Besides rehydration, other areas of treatment can include electrolyte and dietary management, anti-emetics, probiotics, antiviral, and antisecretory drugs (Crawford et al., 2017).

4.1.2.3.3 Prevention

Vaccination is the best way to prevent the severe gastroenteritis caused by rotavirus infection (Velasquez et al., 2018). Two live attenuated oral vaccines against rotavirus have been licenced since 2006, Rotarix (by GlaxoSmithKline) and RotaTeq (by Merck) (Tate et al., 2012, Burnett et al., 2020, Clark et al., 2019). In 2009, the World Health Organisation advised that a live oral rotavirus vaccine should be incorporated into the routine infant immunisation programmes of all countries (WHO, 2007). Since then, over a one hundred countries have introduced rotavirus vaccinations into their immunisation programs (Burnett et al., 2020). The use of the rotavirus vaccine has

resulted in a 40 % decrease in child (younger than 5) hospital admissions for rotavirus disease, and global annual deaths have decreased by 25 % (Tate et al., 2016, Burnett et al., 2017, Aliabadi et al., 2019). Prior to the introduction of vaccines, rotavirus-related gastroenteritis was responsible for 453,000 deaths in children under five in 2008. Of the 453,000 deaths, over 50 % occurred in just five countries (Pakistan, India, Nigeria, Ethiopia, and the Democratic Republic of Congo) (Tate et al., 2012). Despite the vaccination program dramatically reducing the annual number of deaths, the reduction in mortality rate was lower than expected (Burnett et al., 2020). This is due to effectiveness of rotavirus vaccination being sub-optimal in low-income countries (Velasquez et al., 2018). It was found that the vaccines were more effective in countries with low-child mortality, and less effective in countries with higher rates (Clark et al., 2019). The reason for this difference in vaccine efficacy is unknown, however possible factors could include seasonality, microbiome, and maternal antibodies. It was found that administering additional vaccine doses and adjusting vaccine schedules slightly improved immunogenicity, but it might not be cost-effective for low-income countries (Velasquez et al., 2018).

4.1.3 Rotavirus Epidemiology

4.1.3.1 Transmission

The main transmission route of rotavirus infection is via the faecal-oral route from person-to-person, or through contact with contaminated water. This occurs primarily due to the large concentration of rotavirus found within with the stools of individuals suffering from rotaviral diarrhoea (Kraay et al., 2018). Elevated viral shedding combined with the low infectious dose increases the transmission of the disease (Ward et al., 1986). Typically, transmission in households and through fomites is considered to be a greater source of spread when compared to the indirect transmission from contaminated water (Kraay et al., 2018, Dennehy, 2000). However, waterborne transmission is likely to be more of a factor in populations that have slow-moving or standing water sources, and may play a role in initiating outbreaks which are sustained by direct transmission (Kraay et al., 2018).Additionally, hospital and care settings fomites can play a significant role in rotavirus transmission (Butz et al., 1993, Ganime et al., 2016). Rotavirus transmission through fomites can be particularly problematic due to its perseverance, as the virus is able to survive on fomites for over two months (Boone and Gerba,

2007). Furthermore, there have even been reports of animal to human transmission in group A rotaviruses, and animals may act as a source genetic diversification for human rotaviruses via reassortment (Martella et al., 2010, Midgley et al., 2012).

4.1.3.2 Geographical Distribution

Although rotavirus disease is found globally, it has a large impact on low to middle income countries. Of the rotavirus fatalities in 2013, more than 90 % occurred in 72 low-income to low-middle-income countries, with 56 % of deaths occurring in the sub-Saharan region. The country with the largest number of estimated rotavirus deaths was India, accounting for over one fifth of rotavirus deaths in 2013 (Tate et al., 2016). Besides sub-Saharan Africa, the Eastern Mediterranean region is also an area in which rotavirus disease is prevalent. The Eastern Mediterranean region contains a diverse mixture of low and high income countries and is of interest in relation to rotavirus mortality rates. Additionally, lower-income countries such as Pakistan, Afghanistan, Sudan, Somalia and Yemen have a higher rotavirus mortality rate when compared to their higher income neighbours (Khoury et al., 2011, Badur et al., 2019). Furthermore, seven countries in the Middle East region (Egypt, Lebanon, Syria, Tunisia, Somalia, Iran and Oman) have not utilised the rotavirus vaccine in their vaccination programs, with three of them having no available rotavirus vaccines (Iran, Syria, and Somalia) (Badur et al., 2019). In conclusion, although rotavirus disease is found globally, low to middle-low income countries bear the brunt of the disease burden. Better disease surveillance in countries with vaccination programs, and the introduction of rotavirus vaccination programs in countries without them are needed to help mitigate the disease impact (Badur et al., 2019).

4.1.4 Rotavirus Structure

Rotavirus virions consist of a complex, icosahedral triple-layered protein capsid that encompasses a dsRNA genome which is comprised of 11 separate segments (Figure 4.1, A, C and D). The rotavirus capsid is ~80-100 nm in diameter, possesses no outer lipid envelope and is studded with protein projections (Matthijnssens et al., 2010, Long and McDonald, 2017, Boudreaux et al., 2015). The wheel-like appearance of the rotavirus capsid forms the basis of its naming, with the Latin word for wheel being '*rota*' (Crawford et al., 2017). The outermost layer is constructed out of VP7 which is studded with 60 VP4 spike trimers. The VP4 spike possesses the

VP8* and VP5* domains which are involved in cell attachment and entry (Figure 4.1, B).The next layer contains VP6, and the final core layer comprising of a thin VP2 shell (Settembre et al., 2011, Li et al., 2009, Boudreaux et al., 2015). Within the capsid, the vRNA genome is encased alongside VP1 (viral RdRp) and VP3 (vRNA capping enzyme) (Boudreaux et al., 2015). The VP2 shell is bound to VP1 and VP3 which together, form a heterodimer located beneath each of the five-fold VP2 vertices (Prasad et al., 1996, Estrozi et al., 2013).

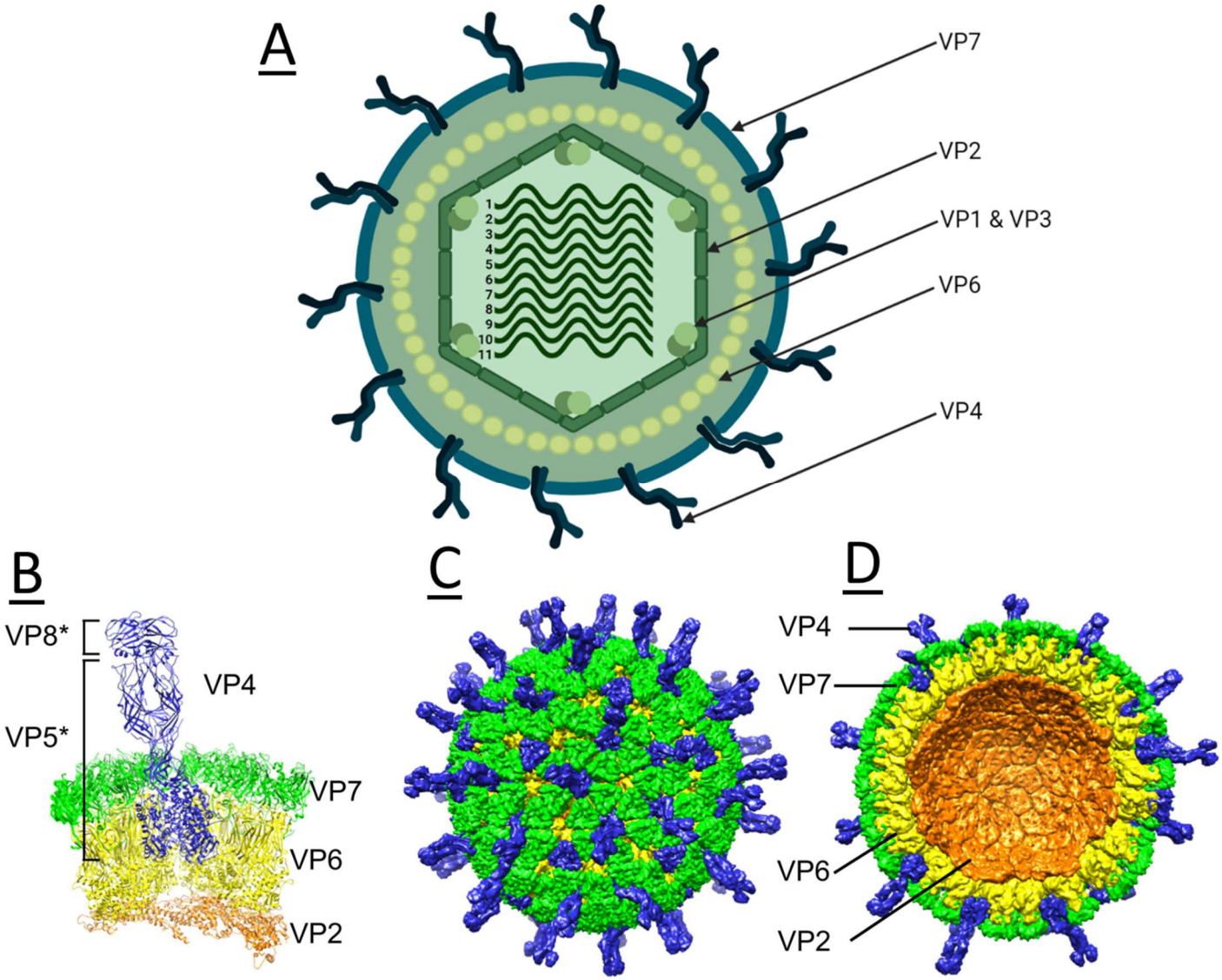

Figure 4.1: A schematic representation of the rotavirus virion.

(A) A cross-section of the rotavirus triple-layered capsid, consisting of an outer capsid shell of VP7, studded with the VP4 spike protein. The middle capsid layer consists of VP6, and the final innermost layer is comprised of VP2. The dsRNA genome found in the center has eleven segments. This figure was created with BioRender and is based upon figure 1, a by Crawford et al. (2017). (B-D) a cryo-EM structure of the rotavirus capsid, showing a close up of the VP4 spike protein (B), an outer view of the whole capsid (C), and a cross-section of the inside of a capsid (D). Figure adapted from figure 1, Eren et al. (2016).

4.1.5 Rotavirus Genome

Rotaviruses have a dsRNA segmented genome that consists of ~18,500 bp (Desselberger, 2014). The rotavirus dsRNA genome consists of 11 separate segments that encodes 12 proteins (Figure 4.2). The 12 proteins are split into 6 non-structural proteins (NSP1 to NSP6), and six structural viral proteins (VP1 to VP4, VP6, and VP7 (Crawford et al., 2017). In rotavirus A strains, VP1 to VP4 are encoded by the RNA segments 1, 2, 3, and 4, respectively. VP6 and VP7 are encoded by segments 6 and 9. Segments 5, 7, 8, and 10 encode for NSP1, NSP2, NSP3, and NSP4, respectively. All of the genes encode for one protein, except for segment 11 which encodes for two (NSP5 and NSP6).

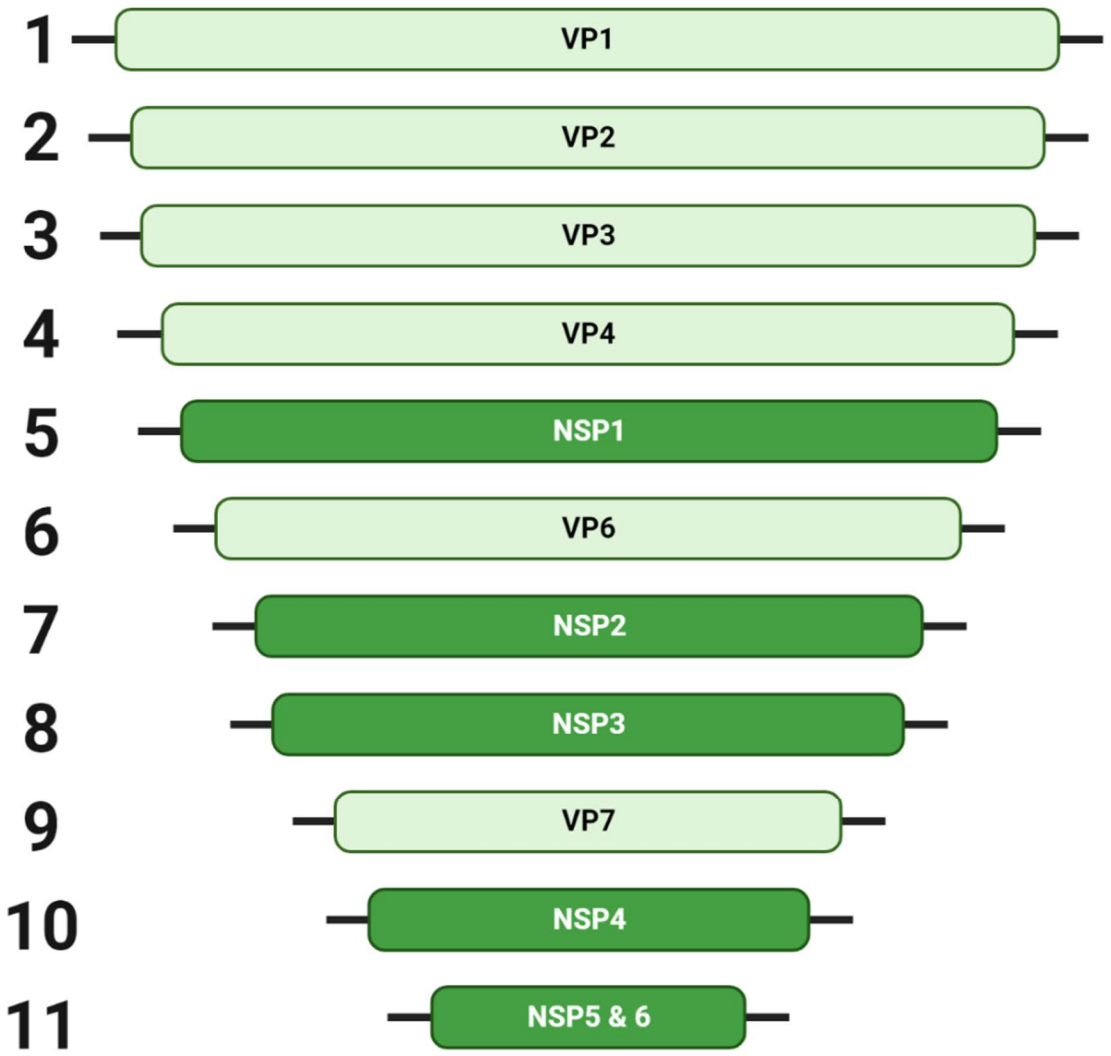

Figure 4.2: A simplified representation of the rotavirus A segmented, double-stranded RNA genome.

The rotavirus A genome consists of eleven separate RNA segments which encode 6 non-structural proteins (NSP) 1 – 6, and six structural proteins (VP) 1 - 4, and 6 – 7. Each segment encodes for one protein, except for segment 11 which encodes for two. This figure was created using BioRender and is based upon figure 1 by Desselberger (2014).

4.1.6 Rotavirus Replication Cycle

The rotavirus replication cycle starts with the attachment of rotavirus to small intestinal epithelial and enteroendocrine cells (Figure 4.3). Rotavirus facilitates attachment and entry with VP7 and VP4 by binding to several host cell receptors, triggering endocytic entry (Sun et al., 2021). Once internalised, rotavirus passes

through the endosomal system before uncoating into the cell cytoplasm, shedding its outermost capsid layer in the process (Patra et al., 2021). Once within the cellular cytoplasm, rotaviruses form a viroplasm with NSP2 and NSP5 which act as sites of combined viral genome replication and capsid assembly (Papa et al., 2021). A double-layered particle (DLP) is produced within the viroplasm containing the 11 segmented dsRNA genome. This DLP exits the viroplasm and buds into the ER membrane, which is studded with NSP4, acquiring a temporary outer membrane (Crawford et al., 2019). NSP4 facilitates the acquirement of the final capsid layer consisting of VP4 and VP7 which encompasses the DLP, forming a triple-layered particle (TLP) (Martínez et al., 2022). The TLP then exits the ER, and egresses from the cell lytically or non-lytically (Doyle and Wang, 2019, Santiana et al., 2018).

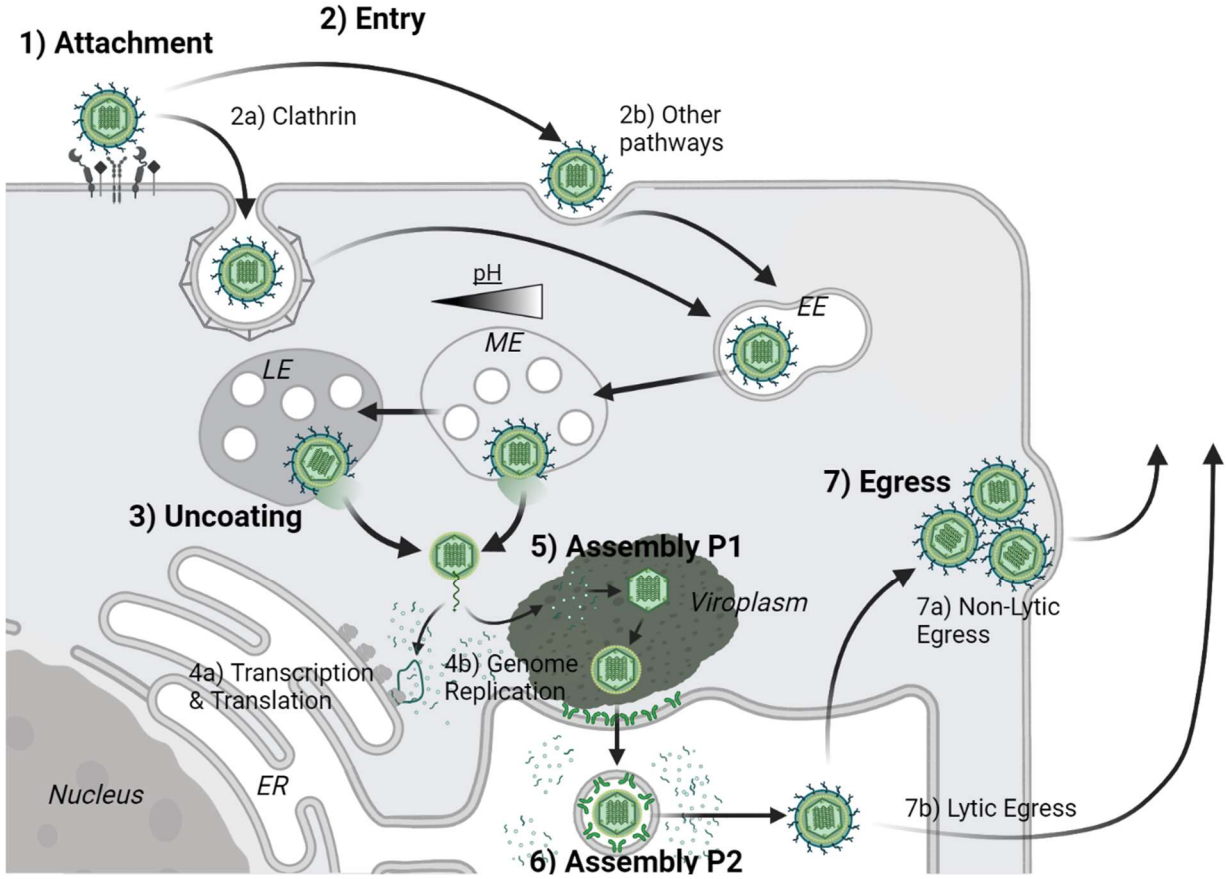

Figure 4.3: A schematic representation of the rotavirus replication cycle.

Rotaviruses employ several receptors to attach onto host cells (1). Once attached, rotavirus then interacts with co-receptors to facilitate entry via endocytosis (2). The endocytic entry can be clathrin-dependent (2a) or clathrin-independent (2b), depending upon the rotavirus strain. The rotavirus virion is then internalized within an endosome where early penetration rotaviruses strains exit the early endosomes (EE) independently of pH, whereas late penetration rotavirus strains exit the mature endosome (ME) or late endosomes (LE) in a pH dependent manner. The uncoating resuls in the loss of the outermost capsid layer as the now double-layered particle (DLP) enters the cytoplasm (3). The rotavirus genome is then transcribed to form positive stranded viral mRNA within the DLP (4a). The viral mRNA strand then leaves the DLP to be translated by host ribosomes (4a), or travels to the viroplasm to form the viral double-stranded RNA genome (4b). The viroplasm is a viral membraneless factory formed in the cytoplasm of infected cells, which acts the site of viral genome replication and viral capsid assembly. Viral capsid assembly within the viroplasm (5) occurs at the same time as viral genome replication, resulting in the formation of a DLP around the newly formed viral genome. The newly formed DLP then exits the viroplasm and enters the endoplasmic reticulum (ER). The DLP buds into the ER membrane which is coated with the non-structural protein (NSP) 4, forming a temporary NSP4 studded envelope around the DLP. NSP4 aids in the assembly of the outer capsid layer (6). In the process of forming the triple-layered particle (TLP), the ER-derived envelope and NSP4 is removed. Finally, the TLP exits from the host cell via either lysis (7a), or non-lytically via an extracellular vesicle (7b). This figure was created BioRender and is based upon figure 1 by Patra et al. (2021), figure 4 by Crawford et al. (2017) and figure 1 by Arias et al. (2015).

4.1.6.1 Attachment

The attachment of rotavirus to small intestinal enteroendocrine and mature enterocytes is facilitated by the rotavirus outer capsid proteins VP4 and VP7 (Venkataram et al., 2014). The rotavirus spike protein VP4 is proteolytically cleaved by trypsin-like proteases within the gastrointestinal tract into its VP8* and VP5* domains (Arias et al., 2015). The VP8* domain of VP4 is involved in cell attachment, whereas the VP5* and the outermost capsid protein VP7 enable entry (Arias et al., 2015). Several host factors such as histo-blood group antigens, sialic acids (SAs), heat shock cognate protein (hsc70), and integrins have all been associated with rotavirus attachment and entry (Arias et al., 2015, Guerrero et al., 2000). Additionally, different rotavirus strains have different required entry receptors, although the subject is complex (Guerrero et al., 2000).

4.1.6.2 Entry

After rotavirus particles have attached to the cell surface glycans, they then bind to co-receptors for the post-attachment stage (Venkataram et al., 2014). At this stage, the virus is believed to target integrins (e.g. α2β1, αXβ2, and αVβ3) and hsc70 to initiate entry (Lopez and Arias, 2006, Patra et al., 2021). There is some rotavirus-strain based variance in the entry process. For example, out of the four rotavirus strains tested all of them required hsc70 to enter cells, with only particular strains needing integrins (Gutiérrez et al., 2010). Other cell surface molecules that have been implicated in rotavirus cell entry are the tight junction proteins JAM-A, occludin, and ZO-1 (Torres-Flores et al., 2015). Gangliosides have also been implicated in rotavirus entry as well as attachment. Four different representative rotavirus strains were tested against cells with inhibited ganglioside synthesis, with a decrease in rotavirus infection seen in all four strains. Of note, the inhibition of ganglioside synthesis had no effect on rotavirus attachment (Martínez et al., 2013). Presently, it is unknown whether all of these cell surface molecules are involved in rotavirus entry in a sequential manner or individually, with more research needed to confirm the specific mechanisms and chronology (Arias et al., 2015, Patra et al., 2021).

Once rotavirus has attached to the cell surface and triggered the relevant co-receptors, it enters the cell via endocytosis (Arias et al., 2015). Again, rotavirus strain variation affects cell entry, with different rotavirus strains utilising different endocytic pathways (Gutiérrez et al., 2010). Most of the tested rotavirus strains have been

found to enter cells via clathrin-mediated endocytosis, with other rotavirus strains (e.g. simian) using a caveolin and clathrin independent endocytosis mechanism (Silva-Ayala et al., 2013). Cell surface receptor tropism in rotaviruses does not define the endocytic pathway used, with clathrin-mediated endocytosis being used by both sialidase-sensitive and resistant strains of rotavirus (Arias et al., 2015, Silva-Ayala et al., 2013). Instead, the endocytic pathway used is dependent on VP4, with a single amino acid substitution in the VP8* domain of VP4 switching the endocytic entry route (Díaz-Salinas et al., 2014). Despite the different endocytic entry mechanisms, all rotaviruses end up in early endosomes as they enter the cell (Patra et al., 2021). The entry of rotavirus via early endosomes was confirmed due to the dependency of rotavirus infection on endosomal machinery (Rab5, EEA1, and ESCRT) (Silva-Ayala et al., 2013, Díaz-Salinas et al., 2014, Wolf et al., 2012).

4.1.6.3 Uncoating

Once the rotavirus virion has trafficked to the mature endosome, there is another rotavirus strain-based divergence. Certain rotavirus strains exit the endosomal system at the mature endosome (early penetration [EP]), whereas other strains progress into the late endosome (late penetration [LP]). Whether the rotavirus virion exits the endosomal system in the mature, or late endosome is dependent upon interactions with Rab7 (Silva-Ayala et al., 2013, Díaz-Salinas et al., 2014, Arias et al., 2015). Rab7 is a Rab GTPase that is responsible for the maturation of endosomes into late endosomes (Elbaz-Alon et al., 2020). Therefore, if a rotavirus strain is reliant upon Rab7 for its successful infection, it suggests that it traffics into the late endosome before releasing into the cytoplasm. Of the LP rotaviruses that travel to the late endosomes, further host factors are involved in their infectivity. Host GTPase Rab9a, cation-dependant mannose-6-phosphate receptors (CD-M6PR), and the cysteine cathepsins B, L, and S are all implicated in the majority of LE rotavirus infectivity (Díaz-Salinas et al., 2014). The CD-M6PR is responsible for trafficking lysosomal enzymes (such as cysteine cathepsins) from the Golgi to the endosome, and the Rab9a GTPase recycles CD-M6PR back to the Golgi (Bohnsack et al., 2009, Nottingham et al., 2012). The cysteine cathepsins are proteases that are active in low pH environments (such as the late endosome) (Turk et al., 2012). It was hypothesised by Arias et al. (2015) that rotavirus needs the cysteine cathepsin proteases to cleave the outer capsid. This releases the DLP into the cytoplasm in a manner similar to what other viruses use the cysteine cathepsins for.

4.1.6.4 Genome Transcription, Translation, and Replication

4.1.6.4.1 Transcription

Rotavirus transcription is initiated by the VP1 RdRp within the DLP, which produces (+) ssRNA from each of the eleven vRNA genome segments. To achieve this, first VP1 must separate the dsRNA genome through the helicase activity of the RdRp N-terminal, which recognises the cap-binding site of the 5' (+) RNA strand (Ding et al., 2019). Next, the RdRp binds to the separated (-) RNA strand mediated by interactions with its ssRNA recognition site and uses it as a template for viral transcription. The newly synthesised (+)RNA is then separated from the (-)RNA template through the helicase activity of the RdRp C-terminal 'bracelet' region (Ding et al., 2019). The template (-)ssRNA strand undergoes a U-turn back into the capsid where it reanneals with the original (+) ssRNA strand (Lawton et al., 2000, Long and McDonald, 2017, Ding et al., 2019). For viral mRNA translation and genome replication to occur, the mRNA strands must first leave the DLP via aqueous pores found at each of the capsids five-fold vertices (Lawton et al., 1997). The binding of VP1 RdRp next to these aqueous pores allows the (+) ssRNA transcript to immediately leave the capsid post transcription (Ding et al., 2019). The final stage of rotavirus transcription is the 5' capping of the mRNA transcript by the VP3 RNA capping enzyme. It was originally believed that VP3 was located in the VP2 capsid interior alongside VP1 (Estrozi et al., 2013). However, recent findings from Ding et al. (2019) indicate that the VP3 capping enzyme is located outside the cap, near the aqueous pore. It was found that it takes 15 minutes for rotavirus transcription to occur post infection (Salgado et al., 2017). Once the (+) ssRNA strand has exited the DLP, it then travels to either ribosomes for translation, or the viroplasm for genome replication by the VP1 RdRp (McDonald et al., 2016, Papa et al., 2021).

4.1.6.4.2 Translation

Rotavirus can hijack host translation machinery so efficiently, that by the end of infection most of the proteins being produced are viral (López et al., 2016). Rotavirus is able to take over host translation through several mechanisms. Firstly, viral mRNA is not polyadenylated like host mRNA and instead possesses a 5' cap which is produced by the VP3 capping enzyme (Boudreaux et al., 2015). Rotavirus mRNA also has a 3' consensus sequence consisting of four nucleotides (GACC) which is conserved on eleven viral genes (Poncet et al., 1994). The consensus sequence acts as a translational enhancer that is recognised by rotavirus NSP3. NSP3 then competes with the host poly(A) binding protein (PABP) for eIF4G binding (Gratia et

al., 2015). Normally in non-infected cells, host mRNA translation is facilitated by PABP which binds to mRNA 3' polyadenylated tails and eIF4E which binds to the mRNA 5' cap. The mRNA, PABP, and eIF4E complex are joined together through the scaffold protein eIF4G to form a circularised mRNA. The complex then recruits the necessary components for translation (e.g. 40S ribosomal subunit) (Hao et al., 2020). NSP3 is able to outcompete PABP for eIF4G as it has a higher affinity for the host eIF4G than PABP (Deo et al., 2002). NSP3 is additionally able to sequester PABP in the host nucleus by interacting with the host Rotavirus X protein associated with NSP3, further reducing host translation (Harb et al., 2008). Therefore, NSP3 preferentially promotes viral translation over host translation (López et al., 2016).

4.1.6.4.3 Viroplasms

Viroplasms are discrete cytoplasmic aggregates which are ~0.1- 5 μm in diameter and possess no membranes. Viroplasms act as viral factories, responsible for concentrating the elements needed for dsRNA replication and capsid assembly (Eichwald et al., 2004, Papa et al., 2021). The rotavirus viroplasm is formed from the interaction between NSP2 and NSP5. Viroplasm assembly dynamics have been studied by fluorescently tagging NSP2 and NSP5. The experiment showed that as the infection progresses, the number of viroplasms initially increases and then begins to decrease. Alongside the number of viroplasms decreasing, the area of the individual viroplasms increases, implying that the viroplasms are combining together and aggregating (Eichwald et al., 2004). Studies into NSP2 showed that it forms a large octamer which act as a RNA chaperone, and can destabilise RNA helixes, implicating its role in vRNA replication (Papa et al., 2021, Bravo et al., 2018, Taraporewala and Patton, 2001). However, less is known about the function of NSP5, although the inhibition of NSP2 or NSP5 does inhibit viroplasm formation (Papa et al., 2019a).

In addition to interacting with viral components, viroplasms also interact with cellular elements such as lipid droplets, microtubules, stress granules and P bodies (Papa et al., 2021). Lipid droplets are storage organelles involved in energy homeostasis, and their inhibition or upregulation has been found to decrease or increase the number and size of viroplasms, respectively (Olzmann and Carvalho, 2019, Cheung et al., 2010, Gaunt et al., 2013). Furthermore, rotavirus has been found to remodel host stress granules and P bodies, removing selected proteins that inhibit rotavirus replication whilst sequestering the remodelled P body and stress granule structures within the viroplasm for viral replication (Dhillon and Rao, 2018). Finally, rotavirus infection has been found to depolymerise the host microtubule network through NSP2, storing the resulting tubulin granules within the viroplasm (Martin et al., 2010).

4.1.6.4.4 Genome Replication

Within the viroplasm, the VP1 RdRp interacts with the VP2 core capsid protein, and the (+) ssRNA strand to form the rotavirus replication complex. The rotavirus replication complex produces a (-)RNA strand, which anneals to the (+) ssRNA, forming the rotavirus dsRNA genome (Boudreaux et al., 2015, Trask et al., 2012, Papa et al., 2021, Ding et al., 2019). The resulting dsRNA rotavirus genome is then ejected out of the VP1 RdRp, into the proto-capsid (Ding et al., 2019). Currently, the process of sorting and packaging the eleven dsRNA genomic segments into the capsid is not clearly understood. However, recent findings indicate that sequence-specific RNA-RNA interactions between the NCRs at the 3' or 5' ends of the (+) ssRNA segments are involved. Fajardo et al. (2017) found that the rotavirus genome segments S9-S11 interacted with each other, and when connections between S10 and S11 were inhibited with oligoribonucleotides, viral synthesis was inhibited. Additionally, the interruption of S10 and S11 interactions did not interfere with protein synthesis, implying that the inhibition of viral replication was due to the disruption of genome segment sorting and packaging. The RNA-RNA interactions are assisted by viral chaperones such as NSP2. NSP2 manages RNA-RNA interactions by facilitating sequence specific RNA binding. It also blocks non-specific interactions between the different rotavirus genome segments and aids in genome packaging (Bravo et al., 2021, Papa et al., 2021). Once NSP2 has assisted in rotavirus genome assortment, it is removed from the precursor capsid (Borodavka et al., 2017). In each of the proto-capsids, eleven VP1 RdRps produce each of the eleven vRNA genome strands in synchrony (Gallegos and Patton, 1989, Long and McDonald, 2017).

4.1.6.5 Assembly

As mentioned above, rotavirus capsids are assembled in tandem with the viral genome within the viroplasm. As the viral genome is replicated, the viral capsid is assembled around and encases the new genomic vRNA, starting with the VP2 core protein (Long and McDonald, 2017, Trask et al., 2012). By isolating the vRNA genome inside of the proto-capsid, it is predicted that rotavirus prevents the host antiviral detection system from activating (Boudreaux et al., 2015). The intermediate capsids that form within the viroplasms are difficult to image by EM due to the electron-dense nature of viroplasms, and light microscopy lacks the resolving power (Boudreaux et al., 2015). However, through biochemical techniques precursor capsids can be separated from the viroplasm. Isolated precursor capsids were found to contain VP1-VP3, VP6, and NSP2 (Hu et al., 2012b). Also, these precursor

capsids have a variety of sizes and shapes. There were smaller ~30-40 nm diameter capsids with smooth borders, and larger ~50-70 nm diameter capsids with rough borders. These findings lead to a suggested chronology of rotavirus capsid formation, with the smaller, smooth capsids forming the larger, rough capsids, which then go on to form DLPs (Long and McDonald, 2017, Gallegos and Patton, 1989).

As the vRNA genome is replicated, the precursor capsid expands to form the DLP with the addition of the intermediate capsid protein VP6, and the removal of NSP2. The DLP then exits the viroplasm, budding into the nearby ER where NSP4 is added (Trask et al., 2012, Crawford et al., 2019). NSP4 is bound to the ER membrane, and so encompasses the now, temporarily enveloped DLP as it enters the ER. This occurs through the interaction of the NSP4 C-terminal cytoplasmic tail with the intermediate capsid protein VP6, triggering ER-budding (Taylor et al., 1996). NSP4 is required for the addition of the outer-capsid proteins VP4 and VP7 which forms the TLP once the temporary DLP envelope is removed by a currently unknown mechanism (Crawford et al., 2019, Martínez et al., 2022).

4.1.6.6 Egress

Originally, rotaviruses were classed as a purely lytic viruses, lysing and killing cells as they escape (Musalem and Espejo, 1985). However, research found that rotaviruses in polarised cells egress from the apical cell surface prior to cell lysis (Cevallos et al., 2016, Ciarlet et al., 2001). The apical egress of viruses is typically associated with the localised dissemination of the virus to neighbouring cells, with basolateral egress associated with systemic infection (Cevallos et al., 2016). This fits with rotavirus infection, which normally causes localised infection in the small intestine. However, rotavirus has been found to spread to other locations (e.g. serum, cerebrospinal fluid, liver, kidney, *etc.*) (Blutt and Conner, 2007, Medici et al., 2011). The systemic spread of rotavirus is not currently understood, however extracellular vesicles have been suggested as a potential mechanism for the spread of rotavirus to different locations (Iša et al., 2020).

Extracellular vesicles are a heterogenous group of lipid structures that are released into the extracellular space by cells. Santiana et al. (2018) found clusters of rotavirus capsids within extracellular vesicles that were released non-lytically from *in vitro* cultured cells, and were also found *in vivo* in animal stools. The rotavirus-packed vesicles have been implicated in rotavirus spread as they are able to survive faecal-oral transmission, delivering high MOI packages to host cells. Furthermore, Iša et al. (2020) found that rotavirus infection of cultured cells causes a large increase in

extracellular vesicle release. These viral vesicles were protected from neutralising antibodies and were able to enter cells without the protease cleavage of VP4.

4.1.7 Chapter Aims

Currently, how viroplasms remain separated from the host cytoplasm is not known. Viroplasms do not possess an outer-membrane and so it is predicted that they remain separate from the cytoplasm through liquid-liquid phase separation (LLPS) as was identified in other viral structures (Guseva et al., 2020, Alenquer et al., 2019, Heinrich et al., 2018). To test this hypothesis, I treated cells infected with rotavirus with the aliphatic alcohol HD at a late time point (12 hp_{inf}). Cells were then processed and imaged through TEM to identify any changes in viroplasm structure or number. HD is known to disrupt the electrostatic interactions that occur in LLPS interfaces (Geiger et al., 2021). Therefore, if viroplasms form through LLPS, HD treatment should disrupt them. The work was carried out in collaboration with Alexander Borodavka (currently at the University of Cambridge).

4.2 Rotavirus Results

4.2.1 The aliphatic alcohol HD has no observed effect on uninfected cells

Rotavirus viroplasms are an amalgamation of viral proteins and RNA concentrated in discrete locations within the cytoplasm. Despite not being membrane-bound, viroplasms exist as a distinguishable entity to the cellular cytoplasm around it. It is predicted that this parting from the cytosol is based on LLPS. HD is an aliphatic alcohol that interrupts LLPS bonds like a detergent interrupts water-oil separation (Geiger et al., 2021). Therefore, if viroplasms are indeed subject to LLPS, treatment with HD should alter the viroplasms within infected cells. To ascertain whether HD has any effect on rotavirus viroplasms, TEM was used to image rotavirus infected cells that had been treated with HD. The late infection time point of 12 hp_{inf} was selected so that larger viroplasms could be observed and potentially interrupted with HD. The idea being that the difference between untreated and HD treated conditions would be greater during late infection when the viroplasms were larger, and their subsequent disruption through HD more prominent.

Mock infected cells (Figure 4.4, A-B) acted as a negative control to be used as a comparison for virally infected cells. Mock infected cells were characterised by healthy cell ultrastructure with intact cellular membranes and normal organelle appearance. There were no visible signs of viral infection or any other anomalous result. Similarly, HD treated mock infected cells were also used as a negative control to confirm that HD treatment alone had no visible effect on cellular ultrastructure (Figure 4.4, C-D). Treated cells were exposed to 4 % (v/v) HD ~30 seconds prior to fixation and TEM sample preparation. During TEM embedding, resin was initially mixed slowly by hand to prevent bubble formation in previous attempts. This lead to the accidental failure to adequately mix the resin and the loss of samples. Consequently, I changed the protocol for all of the micrographs below to allow for thorough mixing via vortexing and subsequent bubble removal via centrifugation. Originally resin was left to infiltrate into samples over one day, however the time was extended for rotavirus samples. This improved the infiltration and reduced the number of bubbles seen in sections (e.g. inside capsids). Finally, prepared aliquots of lead citrate were formally not filtered prior to use. However, lead citrate precipitation occasionally appeared on imaged sections, so I started to filter aliquots prior to use for TULV experiments. This reduced but did not eliminate completely the appearance of lead citrate precipitation. The imaged HD treated mock infected cells

possessed normal cell architecture indistinguishable from the mock infected cells above.

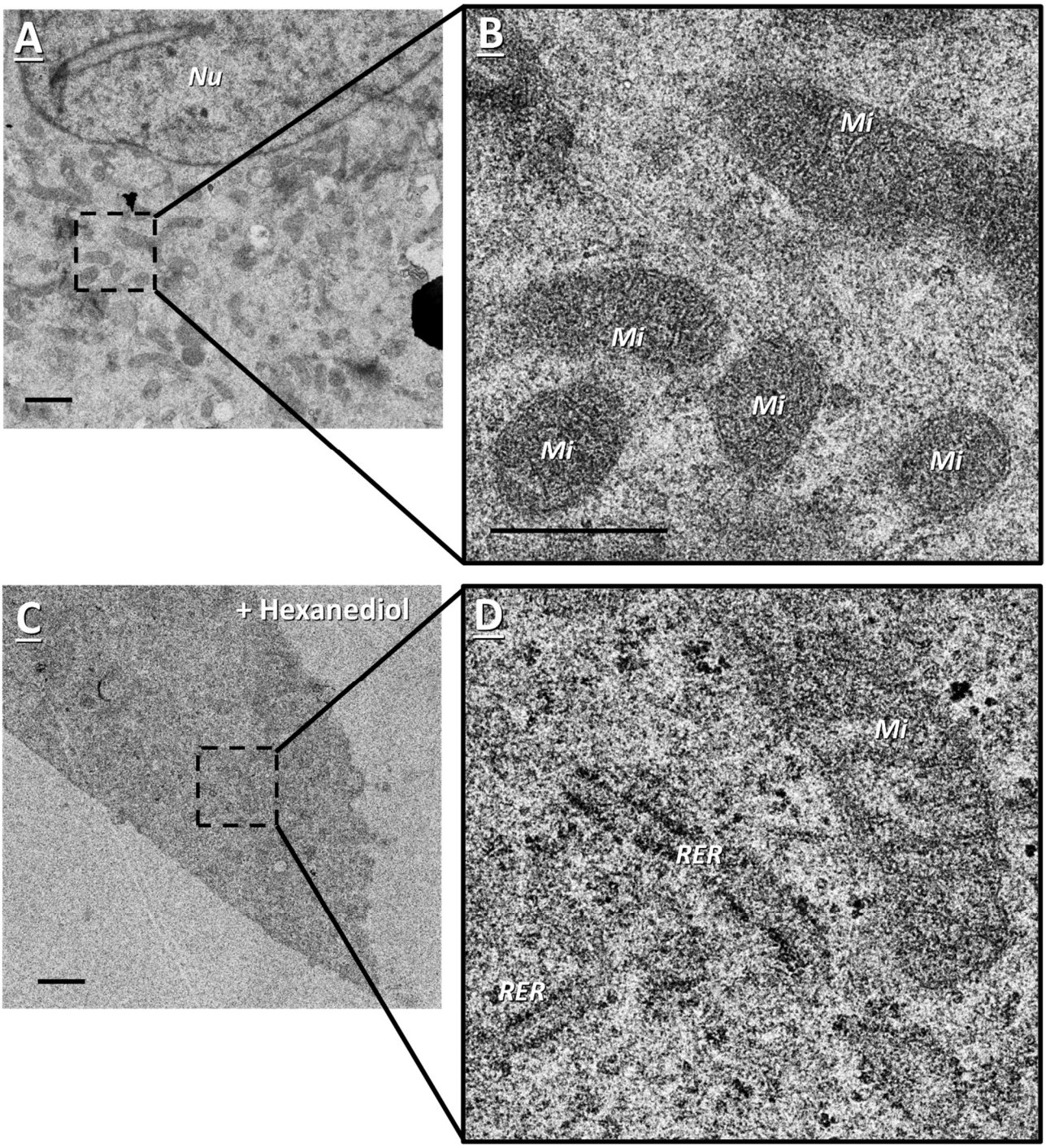

Figure 4.4: Rotavirus mock infected cells and HD treated, mock infected cells.

MA104 cells were mock infected with rotavirus and incubated for 12 hp_{inf} (A-B), a separate group of mock infected cells were then treated with 4 % (v/v) hexanediol (HD) for ~ 30 seconds (C-D). Following incubation, cells were processed for TEM. Micrographs A-B and C-D are two different cells, with higher magnification images being shown sequentially on the right. The nucleus (*Nu*), mitochondria (*Mi*), and rough endoplasmic reticulum (*RER*) are labelled accordingly. Scale bars for the two lower magnifications represent 1 µM. The highest magnification scale bar represents 500 nm.

4.2.2 Rotavirus kills all WT MA104 cells at 12 hp_{inf}

To investigate the effect of HD on rotavirus viroplasms I first needed to identify viroplasms in untreated, infected cells. MA104 cells were infected with rotavirus at an MOI of 1 and incubated until 12 hp_{inf}. The time point of 12 hp_{inf} was selected as a time point due to viroplasms being larger at late infection (12 hp_{inf}) (Eichwald et al., 2012). Therefore, increasing the chances of identifying viroplasms. At 12 hp_{inf}, wild type (WT) MA104 cells infected with rotavirus showed signs of extreme CPE (Figure 2.2.3). Of the 34 cells imaged, all of the cells were dead and showed signs of viral infection. Cell death was confirmed by damaged cellular and nuclear membranes which resulted in low cytoplasmic density and loss of nuclear chromatin. Cell damage was so severe that the majority of the cytoplasmic contents were lost. Often only the nucleus remained, with broken membrane vesicles clinging to or adjacent to the nuclear membrane. Of note, clusters of numerous rotavirus capsids could be seen in fragmented membranous vesicles around nuclei (Figure 4.5, A-D) or alone (Figure 4.5, E-F). The rotavirus capsids have a central, electron-dense punctum, which corresponds to the vRNA core, and an outer ring, corresponding to the capsid coat. Two different sizes of viral capsid can be seen in figure 4.5, B and D. The larger of the two has an outer membrane derived from the RER, whereas the smaller capsids will either be DLP or TLP depending on whether they are in the cytoplasm or RER (respectively) (Trask et al., 2012). The fact that the rotavirus capsids are clustered in a vesicular membrane and the presence of membrane-bound capsids, indicates that these capsids are within the RER, the final stages of the rotavirus life cycle. In conclusion, 12 hp_{inf} is too late to image cells with viroplasms due to the rotavirus induced CPE.

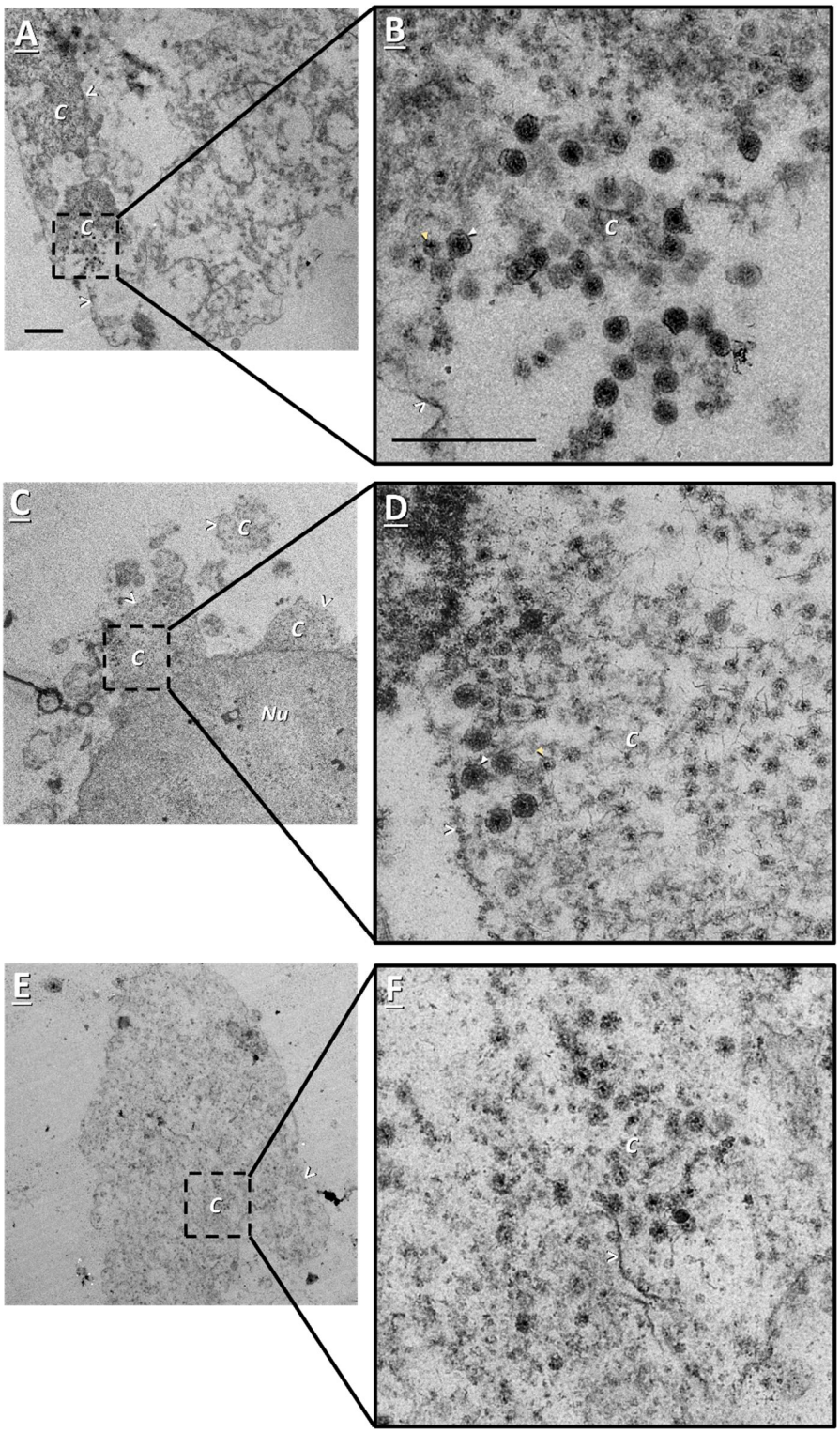

Figure 4.5: 12 hp_{inf} rotavirus infected WT cells result in cell death.

WT MA104 cells were infected with rotavirus and incubated for 12 hp_{inf}. Following incubation, cells were processed for TEM. Micrographs A-B, C-D, and E-F are the remains of three different cells, with higher magnification images being shown sequentially on the right. The nucleus (*Nu*), rotavirus capsids (*C*), RER membranes (>), membrane-bound capsids (white arrowhead), and DLPs/TLPs (yellow arrowhead) are labelled accordingly. Scale bars for the two lower magnifications represent 1 µM. The highest magnification scale bar represents 500 nm.

Next, to investigate the effect of HD treatment on rotavirus viroplasms, MA104 cells were infected with rotavirus, and then treated with HD for ~30 seconds at 12 hp_{inf} prior to fixation for TEM. Despite there being no living WT cells infected with rotavirus at 12 hp_{inf} (Figure 4.5), living cells were present in the HD treated condition (Figure 4.6). Of the 32 HD treated cells imaged, 50 % of the cells were alive. All of the viable cells showed signs of CPE, such as poor membrane integrity and irregular cytoplasmic density. Within the cytoplasm of the living cells viewed, viruses and viroplasms can be seen. The majority of viruses appeared in membrane bound clusters as described above (Figure 4.5), often with large electron dense viroplasms found adjacent. The viroplasms had a round, granular appearance with a round or lobed surface. Unfortunately, due to there being no viroplasms identified in WT cells infected with rotavirus at 12 hp_{inf}, comparisons cannot be made regarding viroplasm morphology in treated and untreated cells.

The discrepancy in cell death seen between untreated and HD treated cells at 12 hp_{inf} is unexpected. Although the HD treated cells were clearly close to death (e.g. poor membrane integrity), the cells were still more intact when compared to the untreated cells. The most obvious cause of the difference in cell death rate is HD treatment. However, this is unlikely as the cells were treated with HD immediately prior to fixation and processing for cellular TEM. It is improbable that the HD disruption of viroplasm and rotavirus replication explains the lower death rate as the cells would likely have been dead from viral infection prior to treatment. The next possible cause of the difference in cell death is due to the TEM sample processing. Artifacts are a common issue in TEM and there are several steps when processing cells that can create cellular artifacts (Ayache et al., 2010, Varga et al., 2020). However, the first step in TEM cell processing is fixation which stops cell metabolism, fixes organelles and stabilises cell material for later processing (Wisse et al., 2010b). If the fixation was successful, it would prevent cells from deteriorating after this. Although I cannot rule out suboptimal fixation (e.g. from poor fixative infiltration), both conditions were processed for the TEM in parallel, so any artifacts that occurred to one would likely appear in the other. Finally, there is the possibility that issues occurred during viral infection, where a possible inconsistency in MOI or viral incubation time could result in higher levels of cell death in the untreated condition (López et al., 2011). Although I cannot pinpoint the exact cause of the difference in cell viability between HD treated and untreated cells, it is likely down to human error.

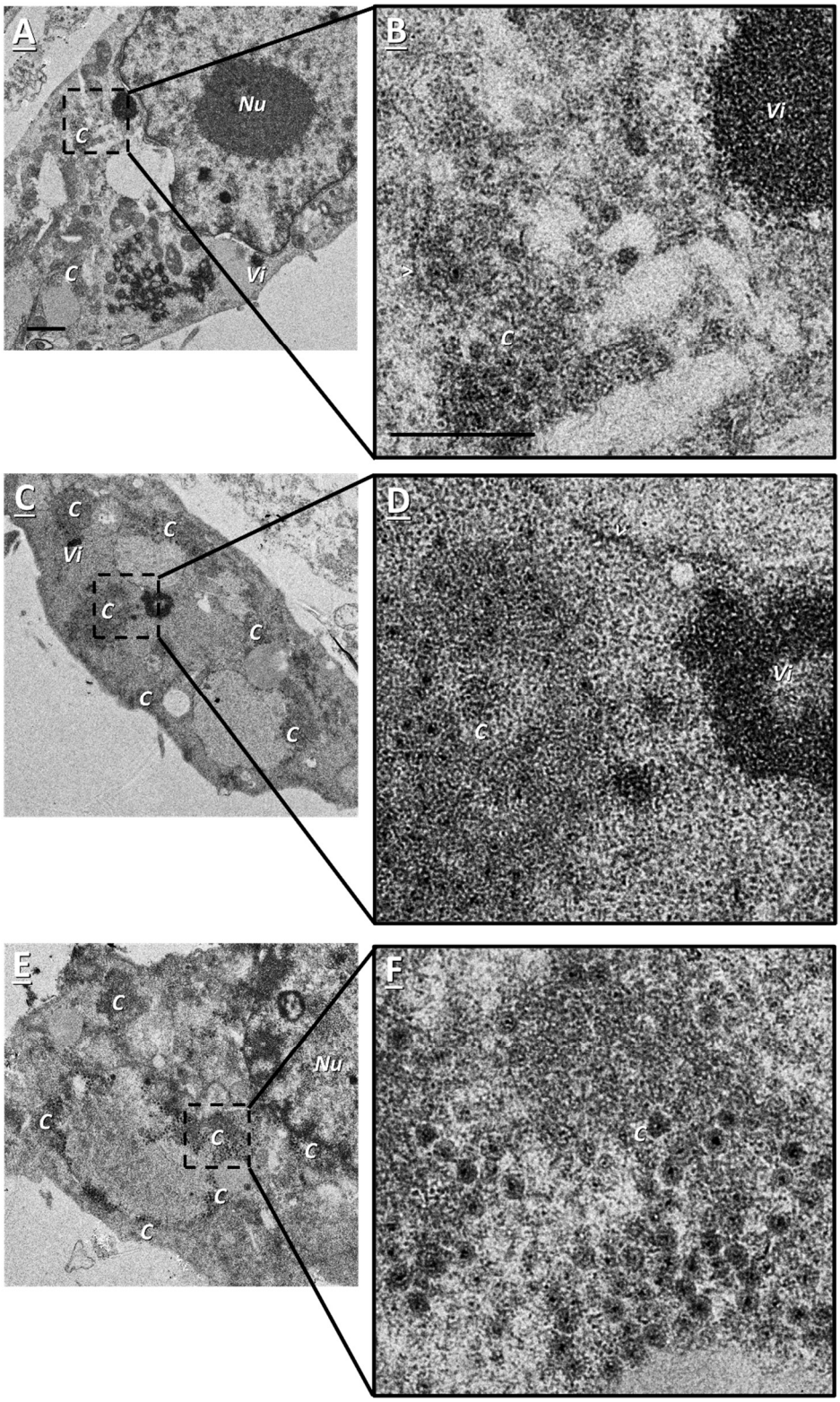

Figure 4.6: 12 hp_{inf} rotavirus infected WT cells treated with HD

WT MA104 cells were infected with rotavirus, incubated for 12 hp_{inf} and then treated with 4 % (v/v) hexanediol (HD) for ~30 seconds. Following incubation, cells were processed for TEM. Micrographs A-B, C-D, and E-F are three different cells, with higher magnification images being shown sequentially on the right. The nucleus (*Nu*), viroplasms (*Vi*), rotavirus capsids (*C*), and RER membranes (>) are labelled accordingly. Scale bars for the two lower magnifications represent 1 µM. The highest magnification scale bar represents 500 nm.

4.2.3 Rotavirus is less cytopathic when infecting MA-NSP5-EGFP cells than WT MA104 cells at 12 hp_{inf}

To assess the effect that HD has on rotavirus viroplasms I would need to be able to image viroplasms from both treated and untreated cell lines. Untreated WT cells infected with rotavirus and imaged at 12 hp_{inf} were all dead (Figure 4.5), therefore the experiment would have to be modified to incorporate this. Adding GFP-tags to viral proteins can reduce viral infectivity and can allow for the tracking of viroplasm formation via live FM (Zheng and Kielian, 2013, Costantini and Snapp, 2015, Geiger et al., 2021). Our collaborator possessed an MA104 cell line that expressed GFP-tagged NSP5 (MA-NSP5-EGFP). The GFP-tagged NSP5 remains evenly distributed in the cytoplasm of noninfected cells but localises to the viroplasm in rotavirus infected cells (Papa et al., 2019a, Eichwald et al., 2004). The MA-NSP5-EGFP cells when infected with rotavirus were observed to have slower viral life cycles when compared to the WT MA104 cells infected with rotavirus (Eichwald et al., 2004, Papa et al., 2019a).

As the MA-NSP5-EGFP cells were a new cell line, new negative controls were created. Mock infected MA-NSP5-EGFP cells (Figure 4.7, A-B) acted as a negative control to be used as a comparison for virally infected cells. Mock infected cells were characterised by healthy cell ultrastructure with intact cellular membranes and normal organelle appearance. There were no observed signs of viral infection or any other anomalous result. Similarly, HD treated MA-NSP5-EGFP mock infected cells were also used as a negative control comparison to confirm that HD treatment alone had no visible effect on cellular ultrastructure (Figure 4.7, C-D). Treated cells were exposed to 4 % (v/v) HD ~30 seconds prior to fixation and TEM sample preparation. HD treated mock infected cells possessed normal cell architecture indistinguishable from the mock infected cells above.

MA-NSP5-EGFP cells infected with rotavirus and imaged at 12 hp_{inf} were markedly healthier than the WT MA104 cells infected with rotavirus. These cells possessed intact cellular membranes and a normal (to the control) cytoplasmic density (Figure 4.8). Numerous viroplasms were observed in the cytoplasm of infected cells, with 55% of the 58 cells imaged having at least one viroplasm and signs of viral infection. Viral features such as capsid clusters and viroplasm positioning was the same as for the HD treated, rotavirus infected WT MA104 cells at 12 hp_{inf} (Figure 4.6). Of note, two different viroplasm morphologies were observed, one electron-dense and the other electron-lucent (Figure 4.8, D). The area of the viroplasms was calculated using ImageJ to establish whether HD treatment altered viroplasm size. The mean

area of the 185 viroplasms imaged in untreated cells at 12 hp_{inf} was 0.180 μm^2 +/- 0.368 μm^2. In summary, the rotavirus life cycle in MA-NSP5-EGFP cells appears to be less virulent than in the WT MA104 cells when imaged at 12 hp_{inf}, allowing for viroplasms to be analysed.

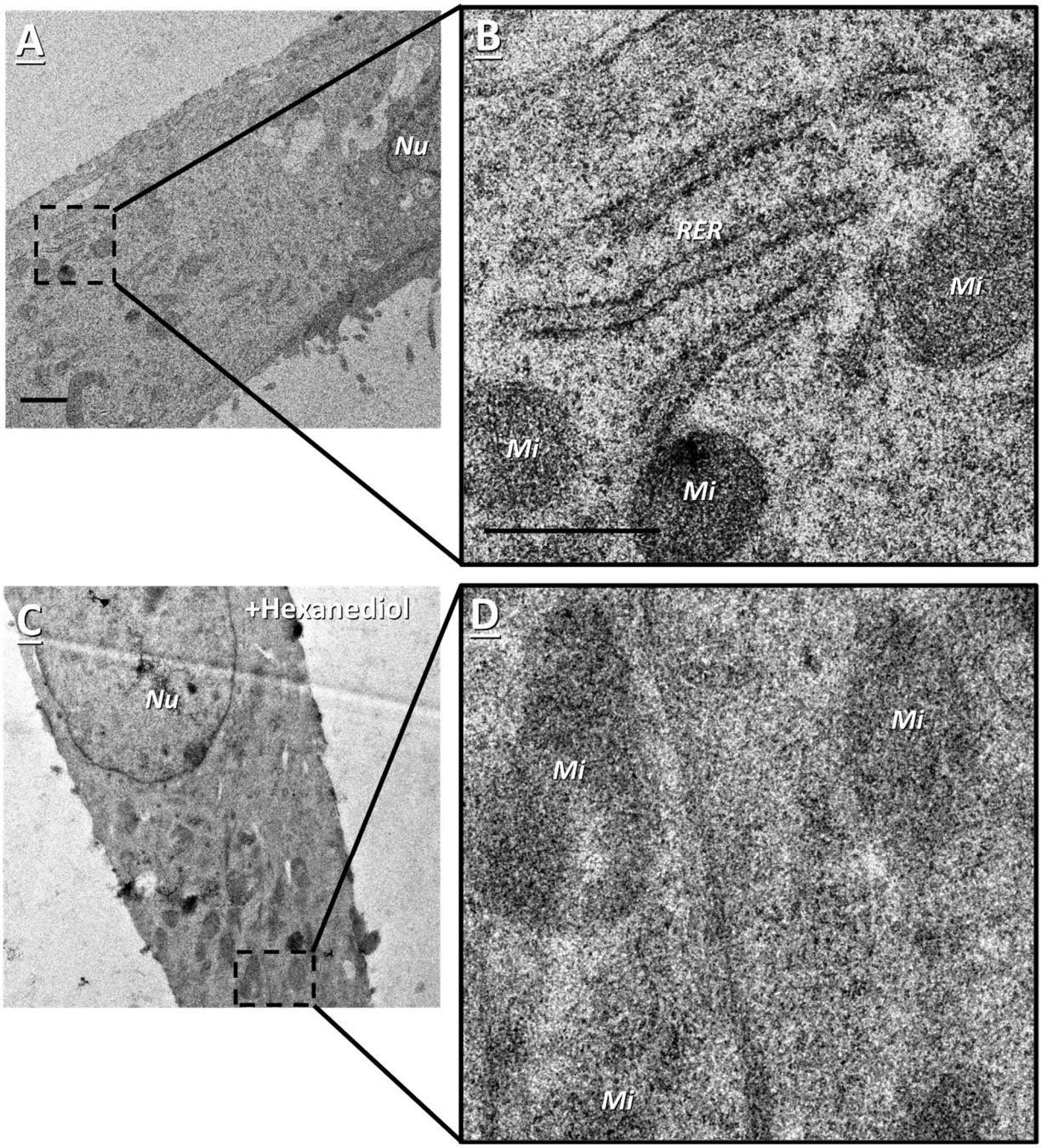

Figure 4.7: Rotavirus mock infected MA-NSP5-EGFP cells and HD treated, mock infected MA-NSP5-EGFP cells.

MA-NSP5-EGFP cells were mock infected with rotavirus and incubated for 12 hp_{inf} (A-B), a separate group of mock infected MA-NSP5-EGFP cells were then treated with 4 % (v/v) hexanediol (HD) for ~ 30 seconds (C-D). Following incubation, cells were processed for TEM. Micrographs A-B and C-D are two different cells, with higher magnification images being shown sequentially on the right. The nucleus (*Nu*), mitochondria (*Mi*), and rough endoplasmic reticulum (*RER*) are labelled accordingly. Scale bars for the two lower magnifications represent 1 µM. The highest magnification scale bar represents 500 nm.

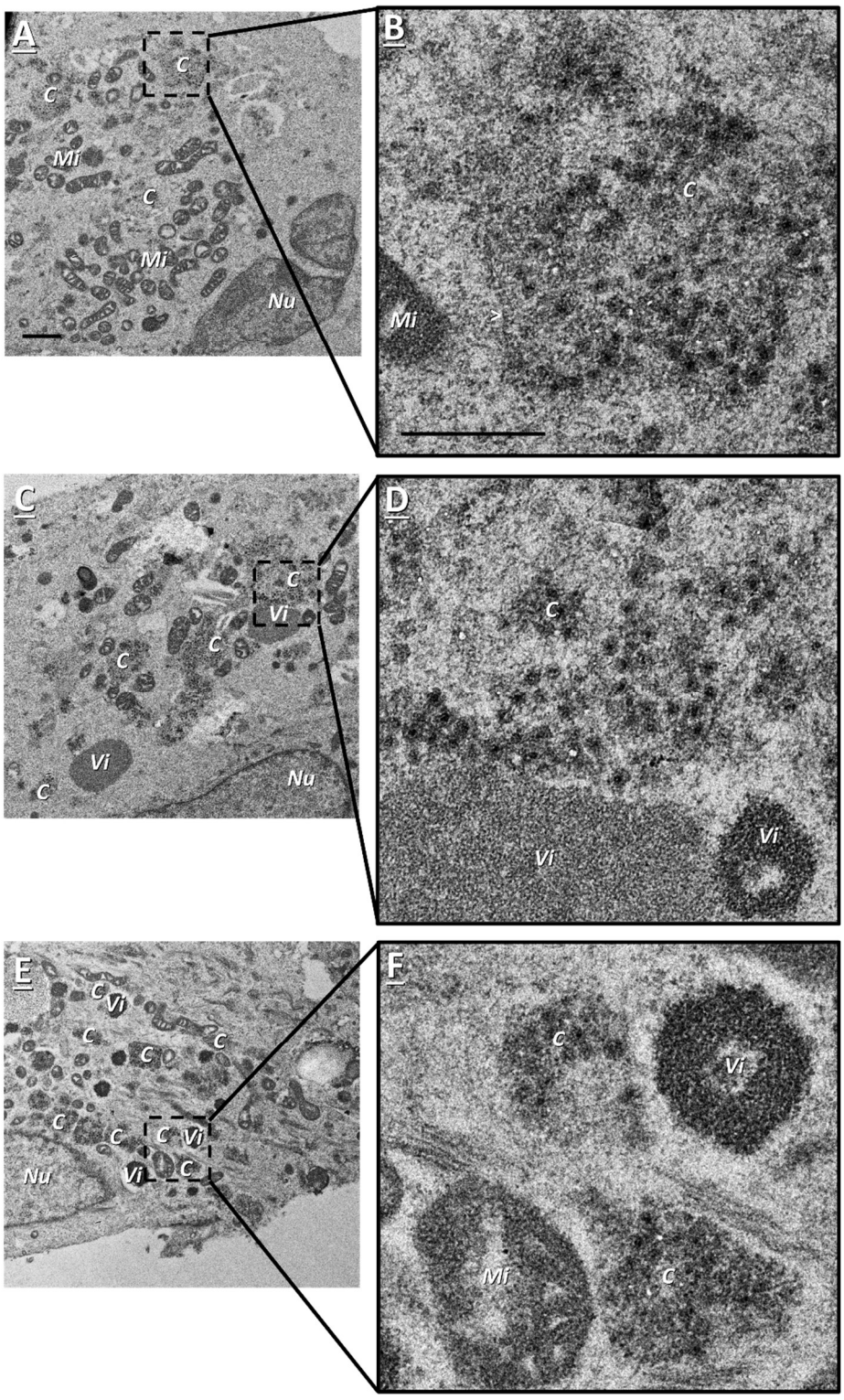

Figure 4.8: 12 hp_{inf} rotavirus infected MA-NSP5-EGFP cells have viroplasms that can be analysed.

MA-NSP5-EGFP cells were infected with rotavirus and incubated for 12 hp_{inf}. Following incubation, cells were processed for TEM. Micrographs A-B, C-D and E-F are three different cells, with higher magnification images being shown sequentially on the right. The nucleus (*Nu*), mitochondria (*Mi*), viroplasms (*Vi*), rotavirus capsids (*C*), and RER membranes (>) are labelled accordingly. Scale bars for the two lower magnifications represent 1 µM. The highest magnification scale bar represents 500 nm.

4.2.4 HD treatment of rotavirus infected MA-NSP5-EGFP cells decreases viroplasm area at 12 hp_{inf}

To establish whether HD has an effect on rotavirus viroplasms, MA-NSP5-EGFP cells infected at 12 hp_{inf} with rotavirus were treated with 4 % (v/v) HD for ~30 seconds and then prepared for TEM (Figure 4.9). Of the 29 cells imaged, 52 % had visible viroplasms and signs of viral infection in the cytoplasm, comparable to non-HD treatment. The imaged HD treated viroplasms had a morphology indistinguishable from viroplasms within untreated, rotavirus infected MA-NSP5-EGFP cells at 12 hp_{inf} (Figure 4.8). However, the mean area of the 53 viroplasms in HD treated cells was 0.0777 μm^2 +/- 0.0595 μm^2 (measured using ImageJ). Therefore the mean viroplasm area in untreated cells at 12 hp_{inf} was larger than in 12 hp_{inf} HD-treated cells. An independent samples t-Test of $log_{(10)}$ transformed data indicated that the viroplasms in 12 hp_{inf} untreated cells were statistically bigger, $t(236) = 1.97$, $p = < 0.001$ (two-tailed). In conclusion, the treatment of rotavirus infected cells with HD may reduce viroplasm area at 12 hp_{inf}. Additionally, as mentioned earlier in section 4.2.3 there were electron-dense and electron-lucent viroplasm morphologies observed (data not shown). In the rotavirus infected cells, 22 % (n = 185) of the viroplasms were electron-lucent. Whereas in the rotavirus infected cells treated with HD, only 4 % (n = 53) of the viroplasms were electron-lucent.

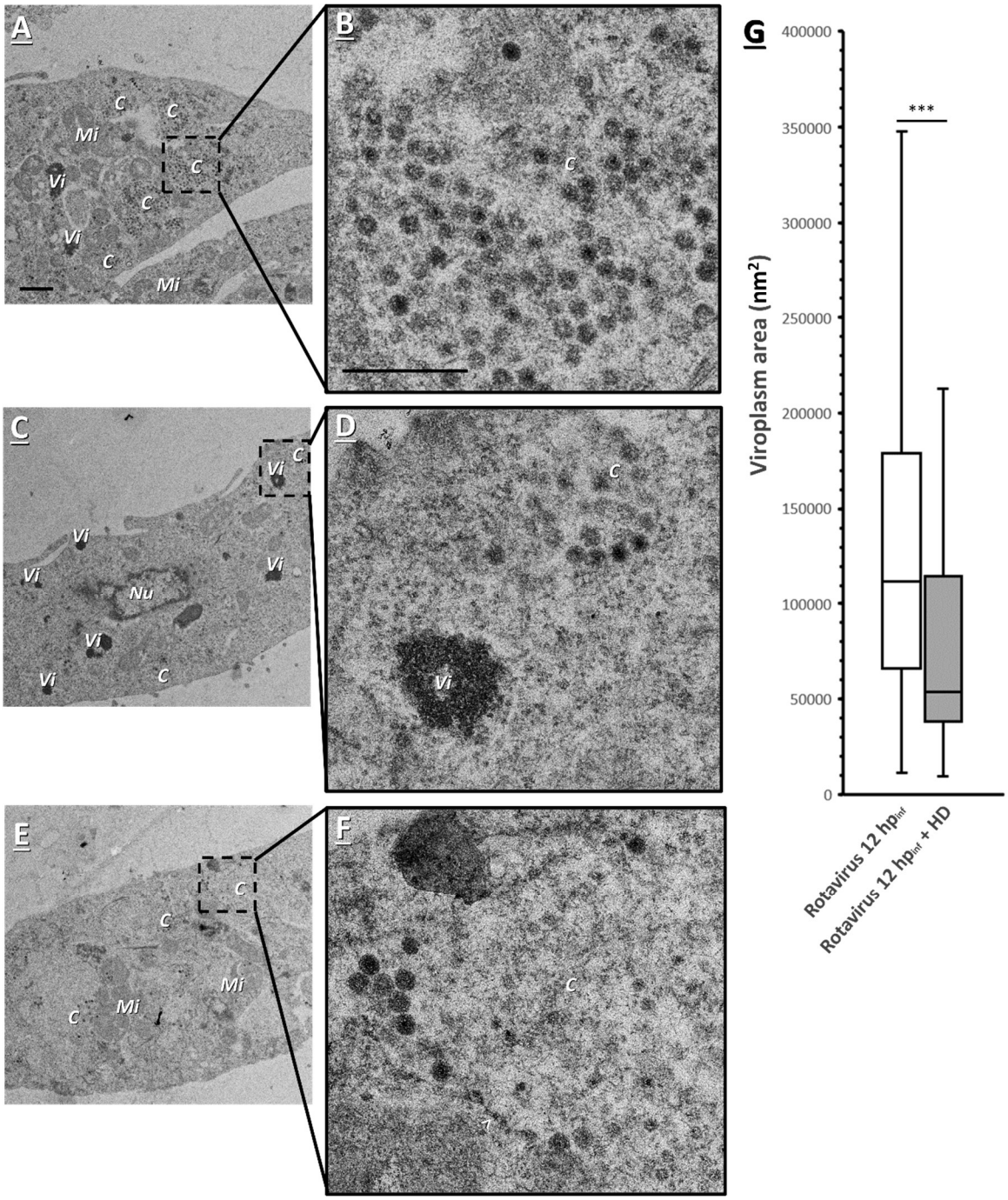

Figure 4.9: HD reduces the size of viroplasms after 12 hp_{inf} in rotavirus infected MA-NSP5-EGFP cells

MA-NSP5-EGFP cells were infected with rotavirus, incubated for 12 hp_{inf} and then treated with 4 % (v/v) hexanediol (HD) for ~30 seconds. Following incubation, cells were processed for TEM. Micrographs A-B, C-D, and E-F are three different cells, with higher magnification images being shown sequentially on the right. The nucleus (*Nu*), mitochondria (*Mi*), viroplasms (*Vi*), rotavirus capsids (*C*), and RER membranes (>) are labelled accordingly. Scale bars for the two lower magnifications represent 1 µM. The highest magnification scale bar represents 500 nm. (G) A comparison of viroplasm area between rotavirus infected MA-NSP5-EGFP cells and rotavirus infected MA-NSP5-EGFP cells treated with HD shown as a boxplot. Error bars represent standard deviation and significance bars represent a p-value of < 0.001.

4.2.5 Bioinformatic analysis of predicted HD target sites

Since HD is predicted to inhibit LLPS through the interruption of hydrophobic bonds (Düster et al., 2021, Ribbeck and Görlich, 2002, Elbaum-Garfinkle, 2019, Alberti et al., 2019), to further explore how HD treatment of infected cells interrupts viroplasms, I carried out a bioinformatic analysis of the of the protein-protein interactions responsible for the phase separation. Similar work from Geiger et al. (2021) found that the protein-protein interactions between NSP2 and NSP5 drive LLPS in rotavirus viroplasms (Geiger et al., 2021). Consequently, I chose to focus the analysis on the hydrophobic-hydrophobic protein interactions between NSP2 and NSP5.

To analyse the hydrophobic regions of both NSP2 and NSP5, the Swiss-Prot ExPASy ProtScale Server (Gasteiger et al., 2005) was used to annotate the hydrophobic regions of both proteins based on amino acid sequence. Three different hydrophobicity tests were used, as recommended by Gasteiger et al. (2005), to ensure that the results were consistent between different tests. The three tests of hydrophobicity used were Kyte and Doolittle (1982) (See Figure 4.10), Abraham and Leo (1987) (data not shown) and Bull and Breese (1974) (data not shown). The Kyte and Doolittle test of hydropathy bases its predictions on experimental data of individual residues and was selected as it is one of the most widely used predictions of hydrophobicity (Huang et al., 2014). A positive result of the Kyte and Doolittle test indicates a hydrophobic region, with the opposite signifying a hydrophilic region. The Kyte and Doolittle scoring is obtained from the interior-exterior distribution of residue side-chains and the water-vapor transfer free energies (Kyte and Doolittle, 1982). A window size of 7 amino acids was used as recommended for identifying surface exposed regions and a score of >1 (e.g. dashed red line on Figure 4.10) was considered as a strong indicator of hydrophobicity (Kyte and Doolittle, 1982). The amino acid sequences were acquired from UniProt, with both proteins sourced from rotavirus A strains (NSP2: A2T3N6 and NSP5: A2T3Q9) (The UniProt, 2021, Kanai et al., 2017, Jiang et al., 2006).

NSP2 has nine hydrophobic regions distributed throughout the protein that pass the threshold value, with peaks 2, 4 and 6 containing $\geq$6 amino acids (Figure 4.10 A). NSP5 has only three hydrophobic regions, with two found on the N-terminus and one found on the C-terminus (Figure 4.10 B). The hydrophobic regions of both NSP2 and NSP5 are summarised below in Table 4.1, which also lists the corresponding amino acid numbers. Most of the hydrophobic regions are relatively short and only span up to 3 amino acids, with hydrophobic region 4 of NSP2 spanning 12 amino acids.

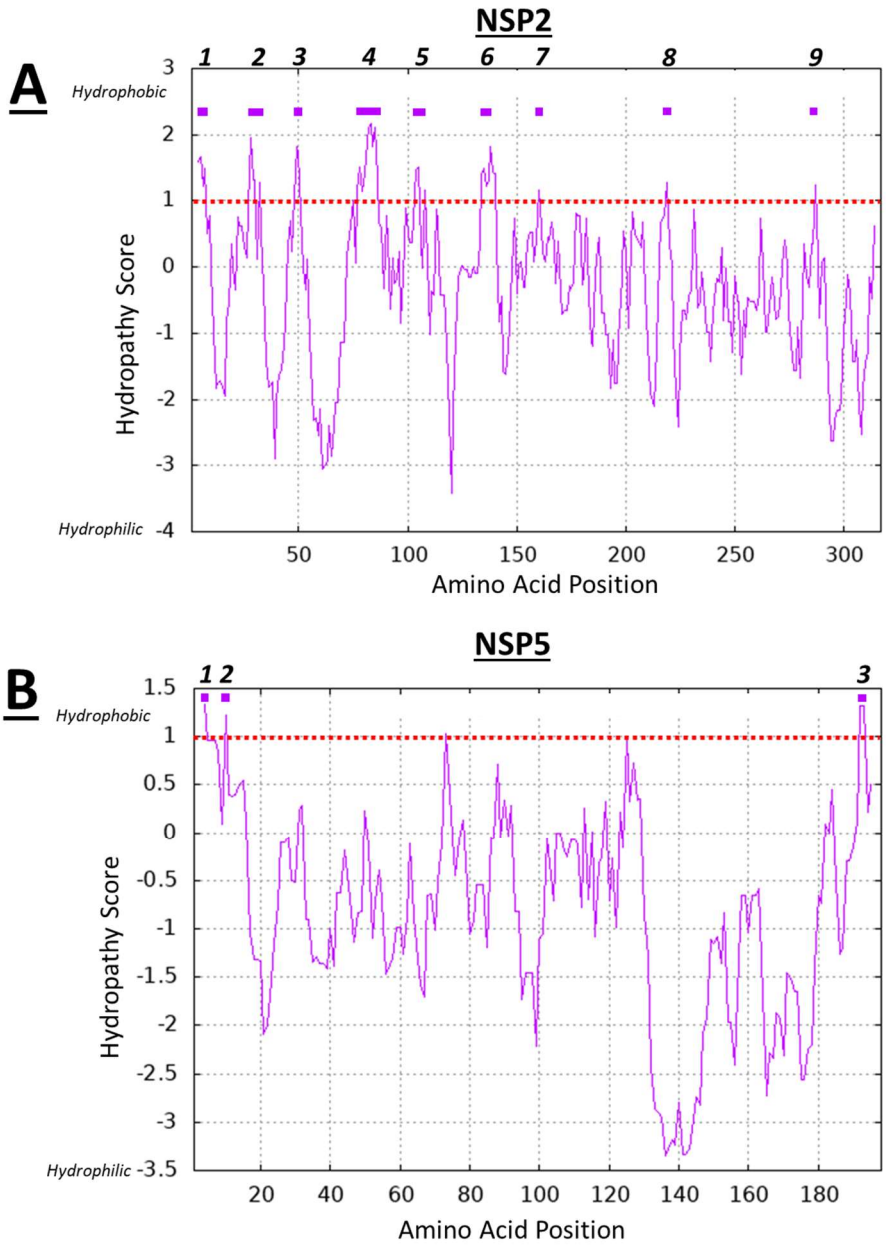

Figure 4.10: Kyte and Doolittle graph predicting the hydrophobic regions of rotavirus A NSP2 and NSP5 proteins.

NSP2 (A) and NSP5 (B) amino acid sequences were acquired from UniProt (NSP2: A2T3N6, and NSP5: A2T3Q9) and were analysed using the Kyte and Doolittle test of hydropathy on the ExPASy ProtScale server (Kanai et al., 2017, Jiang et al., 2006, Kyte and Doolittle, 1982, The UniProt, 2021, Gasteiger et al., 2005). A positive score indicates a hydrophobic region, and a negative score indicates a hydrophilic region. Scores of > 1 were considered to indicate hydrophobic protein regions and were highlighted and numbered.

Table 4.1: Summary of the predicted hydrophobic regions in the rotavirus A proteins NSP2 and NSP5 with their corresponding amino acid numbers.

	Hydrophobic region	*Amino Acid number*
NSP2	1	~4-7
	2	~28-30
	3	~48-51
	4	~77-86
	5	~102-106
	6	~128-141
	7	~159-161
	8	~217-219
	9	~287-289
NSP5	1	~3-5
	2	~9-11
	3	~192-194

To better visualise the hydrophobic regions on NSP2 and NSP5, I mapped the hydrophobic regions on the 3D-protein structure (Figure 4.11, A and B). In addition to mapping the protein hydropathy, I also mapped protein disorder (Figure 4.11, C-E). In LLPS, protein disorder is important as regions of protein-protein interaction occur in organised regions of the protein known as “stickers”, which are separated by relatively disordered regions known as “spacers” (Mehta and Zhang, 2022). As there was no publicly available 3D-structure for the NSP2 used above in figure 4.10 (UniProt code A2T3N6), I used the rotavirus A NSP2 crystallographic structure instead (Protein Data Bank code: 4G0J (Hu et al., 2012a)). To ensure that the two different sequences used for NSP2 A2T3N6 (Figure 4.10) and 4G0J (Figure 4.11) (Hu et al., 2012a, Kanai et al., 2017) were directly comparable. I performed a BLASTP analysis (Gish and States, 1993). This showed that the two proteins have an identical amino acid sequence (data not shown) and therefore NSP2 A2T3N6 and 4G0J are directly comparable.

On the other hand, since there was no crystallographic structure available for NSP5; consequently I used an AlphaFold model generated from the same amino acid

sequence of NSP5 used earlier (A2T3Q9) (Jumper et al., 2021, Varadi et al., 2021, Jiang et al., 2006, The UniProt, 2021).

NSP2 presents a number of hydrophobic and hydrophilic regions scattered around its surface (Figure 4.11 A). However, no surface region of NSP2 is particularly concentrated with either hydrophobic or hydrophilic amino acid residues. Additionally, NSP2 has a disordered region concentrated on the lower lobe of the protein, with more disordered and neutral regions distributed on the upper section (Figure 4.11 B). There are no particularly ordered surface regions of NSP2 according to this structure. The measure of disorder is based on the B-factor or root mean square fluctuations, which are measures of the flexibility of each of the atoms (Sun et al., 2019, Martínez, 2015). Of note, there is no visual correlation between any of the surface hydrophobic or hydrophilic regions and the surface disordered or ordered regions. For NSP5 (Figure 4.11 C to E) the predicted AlphaFold structure shows a small globular region with a looped filament. The AlphaFold model confidence value displays the globular region having a high and very-high degree of confidence, with the looped region having a low and very low degree of confidence (Figure 4.11 C). Like in NSP2, the hydrophobic and hydrophilic surface regions of NSP5 are spread over the surface with no particular region presenting a big patch (Figure 4.11, D). Interestingly, the measure of protein order is the inverse of the measure of model confidence, with the globular region of NSP5 being disordered, and the long filament being relatively more ordered (still only classed as neutral or mildly ordered). This might suggest that at least one of the prediction software's used is unreliable. Similarly to NSP2, there is no correlation between hydrophobic or hydrophilic regions and areas of protein order or disorder.

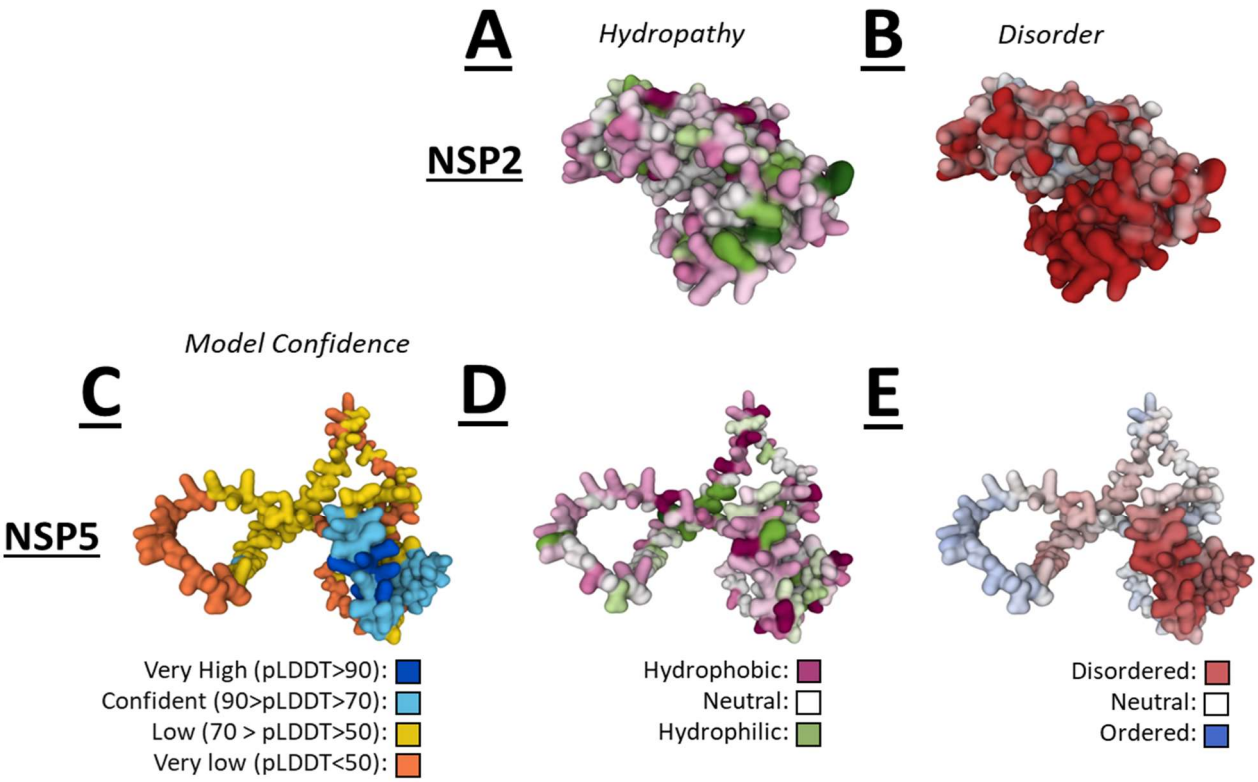

Figure 4.11: Hydrophobicity and disordered predictions mapped onto the 3D-structures of NSP2 and NSP5.

(A and B) The NSP2 3D-structure was based on the Protein Data Bank crystallographic structure 4G0J (Hu et al., 2012a). (C to E) The NSP5 3D-structure was generated using the AlphaFold program using the A2T3Q9 UniProt amino acid sequence (UniProt, 2020, Jumper et al., 2021, Varadi et al., 2021, Jiang et al., 2006).The hydropathy mapping (A and D) shows the hydrophobic (magenta), hydrophilic (green), and neutral (white) amino acid residues on NSP2 and NSP5. The disorder mapping (B and E) shows the disordered (red), neutral (white) and ordered (blue) regions of the protein. Finally, as the NSP5 3D-model is predicted based on the amino acid sequence of the protein by AlphaFold, there is a mapping showing the model confidence (C). The model confidence mapping shows the per-residue confidence measure, which is the predicted local-distance difference test (pLDDT) of the protein, ranging from a higher score having a higher confidence (dark blue), to a lower score having a lower confidence (orange).

Next I compared the hydrophobic regions of NSP2 and NSP5 in different rotavirus species to assess whether there is any conservation that could point towards a specific region being key for LLPS (Figure 4.12). As in Figure 4.10, Kyte and Doolittle's test of hydropathy was used to identify hydrophobic regions of NSP2 and NSP5, using a window size of 7 amino acids (Kyte and Doolittle, 1982, The UniProt, 2021, Gasteiger et al., 2005). For NSP2, rotavirus A (A2T3N6), B (Q86197), C (Q9PY93), D (E2EBU6) and G (U3QY07) were compared (Kanai et al., 2017, Jiang et al., 2005, Taraporewala et al., 2006, Trojnar et al., 2010, Phan et al., 2013).There were no NSP2 submissions on UniProt for rotavirus F, H, I, or J. For NSP5, rotavirus A (A2T3Q9), B (P18571), C (Q00682), D (E2EBV0), F (M4H296) and G (U3R085) were compared (Jiang et al., 2006, Chen et al., 1990, Lambden et al., 1992, Trojnar et al., 2010, Kindler et al., 2013, Phan et al., 2013). There were no NSP5 submissions on UniProt for rotavirus H, I, or J.

The average number of hydrophobic regions in NSP2 across the different rotavirus species is 9 (±1.5) and the average number of hydrophobic regions in NSP5 is 3 (±0.5). NSP2 in rotavirus B (Figure 4.12, C and L) has the least number of hydrophobic regions at 7, with rotavirus C (Figure 4.12, E and L) having the most number of hydrophobic regions at 11. Whereas in NSP5, rotavirus G (Figure 4.12, K and L) has the least number of hydrophobic regions at 2, with rotavirus C, D and F (Figure 4.12, F, H, I and L) having the most number of hydrophobic regions at 4 each. In addition to there being a variance in the frequency of hydrophobic regions within NSP2 and NSP5 across the different rotavirus species, there is also a variance in the positioning of hydrophobic regions. The only regions of either protein which share any homology in the positioning of the hydrophobic region is the N-terminus and C-terminus. In NSP2, 100 % of the rotavirus species have a hydrophobic region within the N-terminus, whereas only 60 % of rotavirus species have a hydrophobic region within the C-terminus. In NSP5 the opposite is true, with 66 % of the rotavirus species having a hydrophobic region within the N-terminus, with 100 % of rotavirus species have a hydrophobic region within the C-terminus.

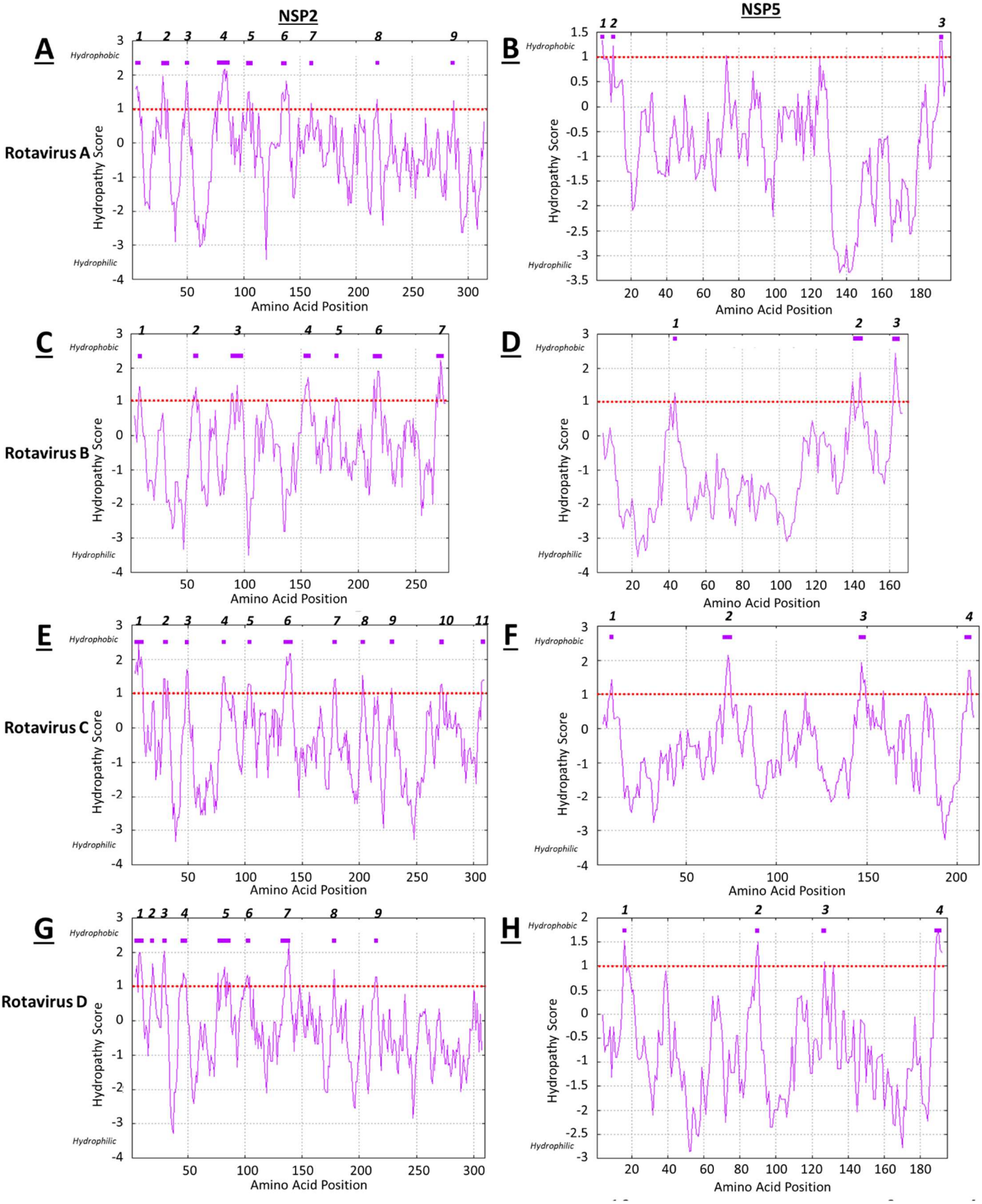
NSP2
NSP5
A
B
C
D
E
F
G
H
Rotavirus A
Rotavirus B
Rotavirus C
Rotavirus D
Hydrophobic
Hydrophilic
Hydropathy Score
Amino Acid Position

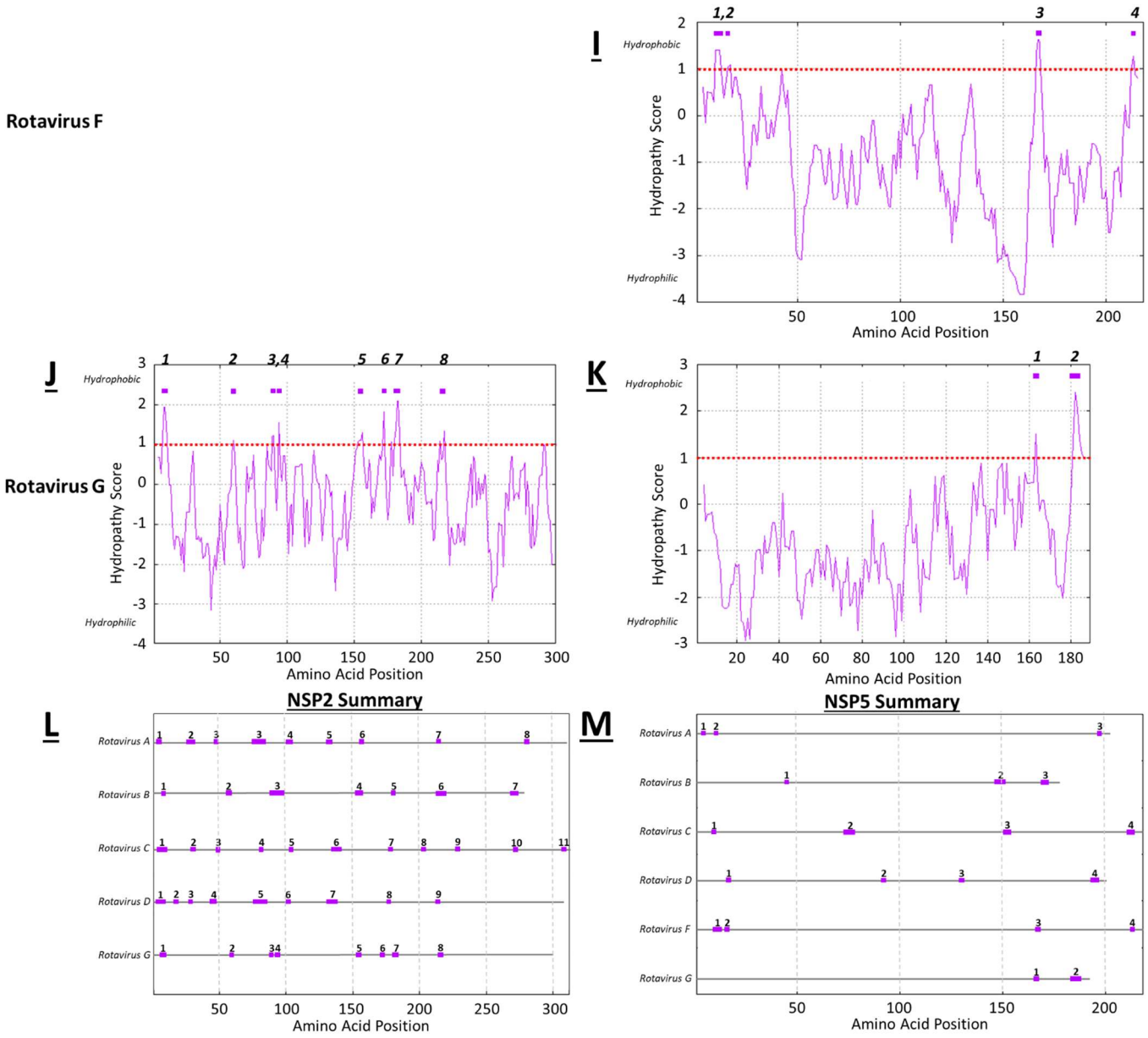

Figure 4.12: A Kyte and Doolittle analysis predicting the hydrophobic regions of NSP2 and NSP5 across different rotavirus species.

NSP2 from different rotavirus species (A2T3N6 (A), Q86197 (C), Q9PY93 (E), E2EBU6 (G) and U3QY07 (J)), alongside with NSP5 from different rotavirus species (A2T3Q9 (B), P18571 (D), Q00682 (F), E2EBV0 (H), M4H296 (I) and U3R085 (K)) amino acid sequences were acquired from UniProt and were analysed using the Kyte and Doolittle test of hydropathy on the ExPASy ProtScale server (Kyte and Doolittle, 1982, The UniProt, 2021, Gasteiger et al., 2005, Kanai et al., 2017, Jiang et al., 2006, Jiang et al., 2005, Taraporewala et al., 2006, Trojnar et al., 2010, Phan et al., 2013, Chen et al., 1990, Lambden et al., 1992, Kindler et al., 2013). A positive score indicates a hydrophobic region and a negative score indicates a hydrophilic region. Scores of > 1 were considered to indicate hydrophobic protein residues and were highlighted and numbered. A schematic summary of the NSP2 (L) and NSP5 (M) hydropathy is shown at the bottom, with hydrophobic regions indicated by purple bars, and the relative length of the proteins indicated by the grey bars.

Finally, to identify whether the hydrophobic regions in NSP2 (A2T3N6) and NSP5 (A2T3Q9) were responsible for driving LLPS, I assessed both proteins with FuzDrop and flDPnn (Figure 4.13) (Kanai et al., 2017, Jiang et al., 2006. Hardenberg et al., 2020, Vendruscolo and Fuxreiter, 2022, Hatos et al., 2022, Hu et al., 2021). This is similar to the work by Geiger et al. (2021), who conducted a catGRANULE (a LLPS predictor equivalent to FuzDrop) and flDPnn analysis of NSP5. FuzDrop (Figure 4.13, E-H) works by using an algorithm to predict the ability of proteins to spontaneously undergo LLPS by analysing the disorder propensity of each residue. The algorithm was trained on 120 proteins which undergo LLPS (Mészáros et al., 2020, Hatos et al., 2022). Each protein residue is given a droplet-promoting probability of residues (P_{DP}) score which is then used to create the probability of the droplet state (P_{LLPS}) score for the entire protein. A P_{LLPS} score of ≥ 0.60 indicates that the protein can undergo spontaneous LLPS.

flDPnn (Figure 4.13, I-L) is a computational tool that similarly predicts protein disorder and so should partially replicate the results from FuzDrop. The flDPnn machine learning model was trained through the use of experimental data of disordered proteins (Hu et al., 2021). flDPnn analyses each protein residue, with a disorder propensity score of ≥ 0.3 being classed as disordered. Additionally, flDPnn highlights regions of the protein which have disorder associated functions such as protein binding (blue), DNA binding (green) and RNA binding (red). The darker the colour highlighting the protein region, the higher the confidence score.

For the predictive modelling, the rotavirus protein VP4 (A0A0D5CDS5) and SARS-CoV-2 nucleocapsid protein N-protein (P0DTC9) were used as negative and positive controls respectively (Delogu et al., 2015, Bessa et al., 2022). VP4 is a rotavirus spike protein that is not documented to undergo LLPS separation in the literature. Whereas the SARS-CoV-2 N-protein is well documented to undergo LLPS (Chen et al., 2020, Wang et al., 2021b, Perdikari et al., 2020, Cascarina and Ross, 2022).

From Figure 4.13 it can be seen that there is a lack of correlation between hydrophobic (Figure 4.13, A-D) and droplet-promoting (Figure 4.13, E-H) regions of either NSP2 or NSP5. Although there are rare occasions where the hydrophobic peaks line up with the droplet promoting regions, the majority do not. For example the hydrophobic regions 1 and 2 of NSP5 (Figure 4.13, A) line up with the droplet promoting region of residues 1-42 (Figure 4.13, E), however this is a rarity. Of note, there are more examples of the hydrophilic areas matching with the droplet promoting regions. An example of this can again be seen in NSP5, where the hydrophilic spike (Figure 4.13, B) around residue 140 matches with the droplet forming region of 121-145 (Figure 4.13, F). However, there are a number of

examples where this is not the case e.g. the hydrophilic spike of NSP2 (Figure 4.13, A) at around residue 120 does not correspond to a droplet region in the FuzDrop analysis (Figure 4.13. E). Consequently, there is no correlation with either hydrophobic or hydrophilic regions and the droplet-promoting regions. Additionally, none of the hydrophobic regions of NSP2, NSP5, VP4, or N-protein are associated with a disordered region from the flDPnn analysis.

Unlike the hydrophobicity, there was a large degree of correlation between the droplet promoting regions of FuzDrop and the measure of disorder from flDPnn. For example, in NSP2 (Figure 4.13, E) the droplet promoting region of 294-317 matches with the disordered region of the C-terminus (Figure 4.13, I). Although there were some discrepancies between the two (e.g. the disordered region of VP4 around residue 120 [figure 4.13, K] which does not correspond to a lipid-droplet promoting region), overall there was a large degree of similarity. Additionally, there is a large degree of similarity between the disordered region predicted by flDPnn, and the disordered regions predicted above, in Figure 4.11 B for NSP2. In NSP2, both analyses predict a large disordered region in the C-terminus. However, there are contradictory findings between flDPnn and Figure 11 E. The disorder analysis in Figure 11 E identifies a large hydrophobic region within the C-terminus of NSP5, whereas flDPnn classifies this area as relatively ordered. In addition to the droplet promoting regions, the FuzDrop analysis provides an a P_{LLPS} score (Hatos et al., 2022). Despite having one droplet forming region, FuzDrop analysis of NSP2 (Figure 4.13, E) suggests it does not undergo spontaneous phase separation (P_{LLPS}= 0.1679 < 0.60). Whereas FuzDrop does suggest that NSP5, with three lipid promoting regions (Figure 4.13, F) does undergo spontaneous phase separation (P_{LLPS}= 0.9846 ≥ 0.60). These results are further supported by the negative control VP4 (Figure 4.13, G) which does not undergo spontaneous phase separation (P_{LLPS}= 0.1161 < 0.60) and the positive control N-protein (Figure 4.13, H) which does undergo spontaneous phase separation (P_{LLPS}= 0.9941 ≥ 0.60). The final element of the protein analysis is the binding region prediction of flDPnn. In NSP2 (figure 4.13, I), there is a strong RNA binding region in the C-terminal. Whereas NSP5 (figure 4.13, J) has several protein, DNA and RNA binding regions predicted.

Overall, the bioinformatic analysis that I have performed suggests that hydrophobicity is not a strong indicator of LLPS propensity. Rather, disorder seems to be the main factor involved. Additionally, my results suggest that rotavirus NSP5 is the key driver of LLPS viral factories and can interact with both protein and nucleic acids, while NSP2 does not have a strong LLPS propensity.

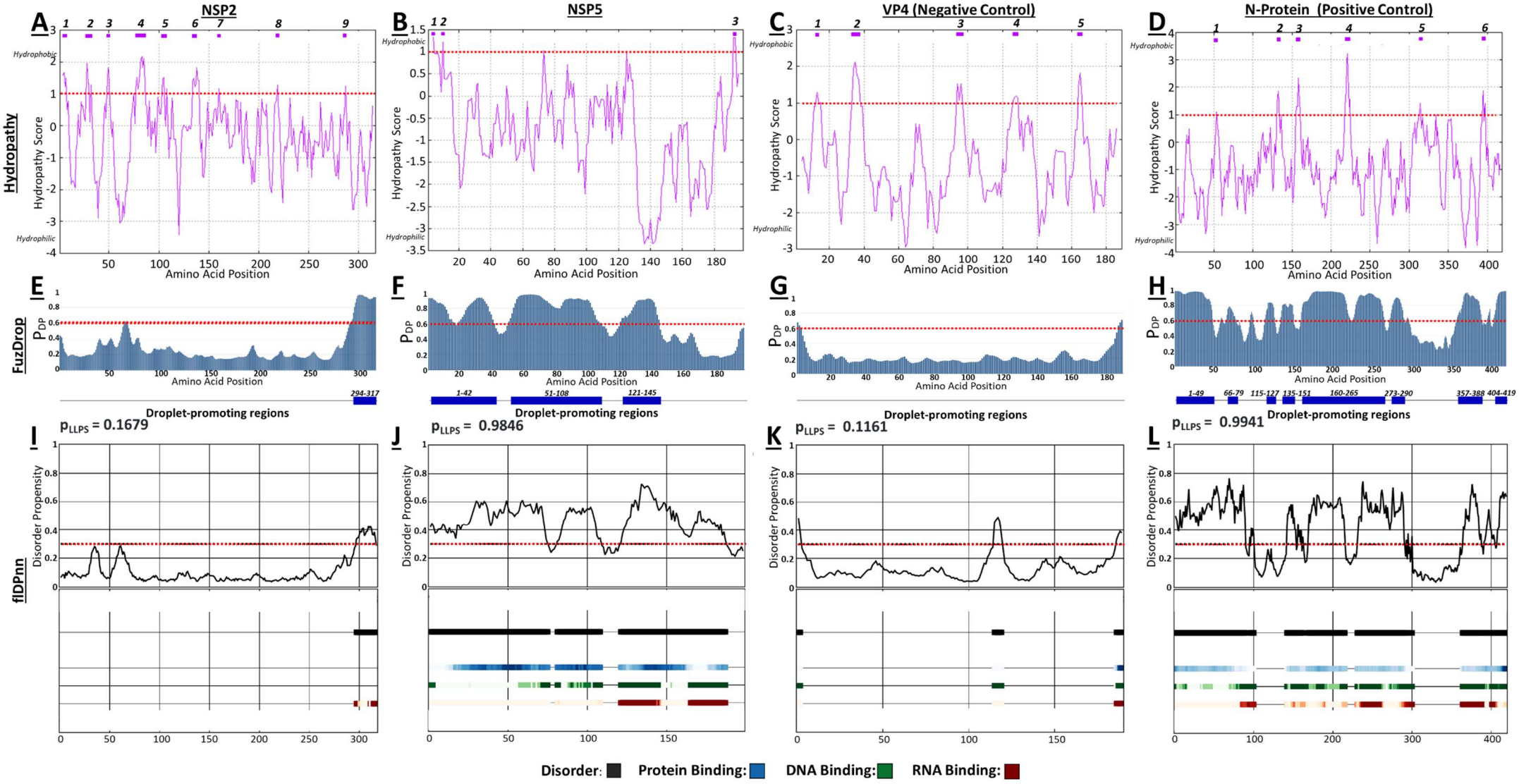
A
NSP2
B
NSP5
C
VP4 (Negative Control)
D
N-Protein (Positive Control)
Hydropathy
Hydrophobic
Hydrophilic
Hydropathy Score
Amino Acid Position
E
F
G
H
FuzDrop
P_{DP}
294-317
1-42
51-108
121-145
1-49
66-79
115-127
135-151
160-265
273-290
357-388
404-419
Droplet-promoting regions
I
J
K
L
flDPnn
Disorder Propensity
p_{LLPS} = 0.1679
p_{LLPS} = 0.9846
p_{LLPS} = 0.1161
p_{LLPS} = 0.9941
Disorder:
Protein Binding:
DNA Binding:
RNA Binding:

Figure 4.13: Comparitive analysis of hydrophobic, droplet forming, and disordered region in rotavirus NSP2 and NSP5.

The amino acid sequences of rotavirus NSP2 (A2T3N6), NSP5 (A2T3Q9), VP4-negative control (A0A0D5CDS5) and SARS-CoV-2 N -protein-positive control (P0DTC9) were used for the analysis (Kanai et al., 2017, Jiang et al., 2006, Delogu et al., 2015, Bessa et al., 2022). (A-D) Firstly, the amino acid sequences were analysed using the Kyte and Doolittle test of hydropathy on the ExPASy ProtScale server (Kyte and Doolittle, 1982, The UniProt, 2021, Gasteiger et al., 2005). (E-H) Next, the proteins were assessed for their ability to undergo liquid-liquid phase separation via FuzDrop (Hardenberg et al., 2020, Vendruscolo and Fuxreiter, 2022, Hatos et al., 2022). A probability of the droplet state (P_{LLPS}) of ≥ 0.60 indicates that the protein undergoes spontaneous liquid-liquid phase separation, with the droplet-promoting probabilities of residues (PDP) scores highlighting the individual residues involved in the process. (I-L) Finally, the protein disorder was assessed via flDPnn, where protein residues with a disorder propensity score of ≥ 0.3 were classed as disordered (Hu et al., 2021). Additionally, flDPnn predicted the regions of the protein which were involved in protein (blue), DNA (green), and RNA binding (Red), with a darker colour indicating a higher prediction confidence level.

4.2.6 Large granular aggregate observed in cells across all conditions

At the start of the rotavirus TEM experiment I had to inspect all cells at high magnification to identify signs of rotavirus infection. Any potential viral identifiers were then matched to other TEM micrographs available in the literature. When imaging both infected and mock infected MA104 cells (and the later MA-NSP5-EGFP cells), large macromolecular structures were observed in the cytoplasm (Figure 4.14). Like the viroplasms that were later identified, these structures were large (> 1 µm diameter), membraneless and had a granular appearance. Unlike the viroplasms, the aggregates were amorphous in shape and had electron dense granules with an electron lucent background. The presence of these unidentified structures in both infected and mock infected conditions raised the possibility of viral contamination of the mock control if the structures were of a viral origin.

One of the main difficulties with EM is distinguishing between relevant structures, irrelevant structures and artifacts (Wisse et al., 2010b). I had to look at a number of references for rotavirus structures, normal cellular organelles and example artifacts to correctly identify the granular aggregates imaged. Eventually I found papers referring to glycogen granules which visually matched the observed structures. Glycogen granules, like the structures observed in figure 4.14, are amorphous cytoplasmic inclusions with electron dense granules surrounded by electron lucent space (Mayeuf-Louchart et al., 2019, Prats et al., 2018, Wu et al., 2008). The

aggregates (also called glycosomes) are the main storage form of glucose, which forms large aggregates within several tissues. There are three types of glycogen structure, with the ones imaged above being classed as α-granules. The glycogen granules are protein-dense and so appear dark when stained with lead and uranyl acetate (Thornell, 1974). Contrast in TEM is created from the scattering of the electron beam as it passes through the sample. The higher the sample molecular weight, the greater the degree of electron scattering, resulting in a darker electron micrograph (Bisht et al., 2016). Samples undergo a post-fixation staining with osmium tetroxide which adds the heavy metal osmium to proteins, increasing contrast (Wigglesworth, 1964). Consequently, the protein-dense glycosomes appear dark. As the structures are likely glycogen granules and not a viral structure, it suggests that the mock infected controls are not virally contaminated.

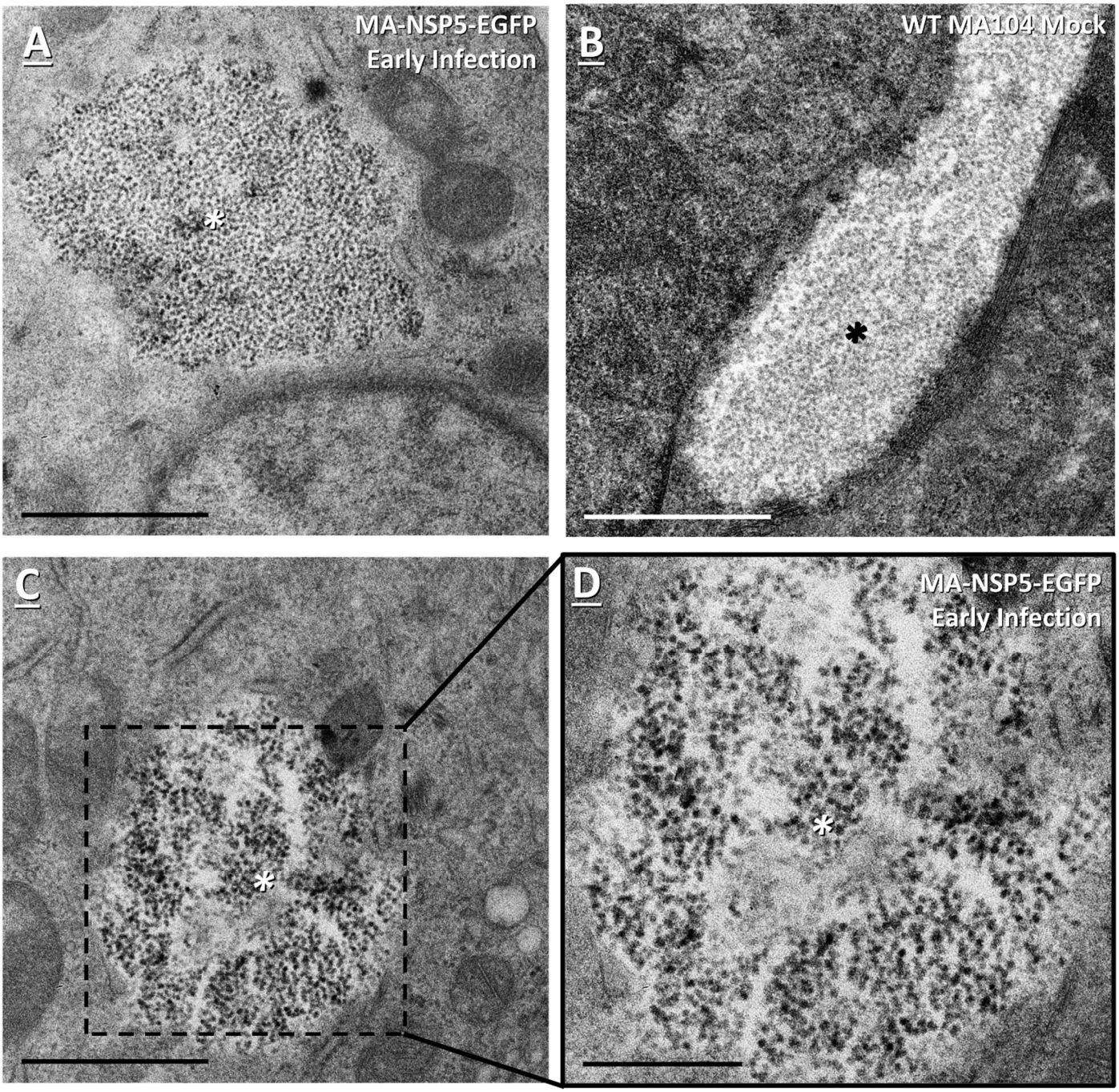

Figure 4.14: Granular aggregates identified in cell cytoplasm.

Cells were either infected with rotavirus and incubated for 4 hp_{inf} (A, C and D), or mock infected and incubated for 12 hp_{inf} (B). Following incubation, cells were processed for TEM. Micrographs A-C are three different cells. The aggregates (*) are labelled accordingly. Scale bars for A to C represent 1 µM, with the scale bar for D representing 500 nm.

4.2.7 Tubule structures observed in HD treated, rotavirus infected MA-NSP5-EGFP cells at 12 hp_{inf}

When examining the MA-NSP5-EGFP cells infected with rotavirus and treated with HD at 12 hp_{inf} an unusual structure was observed in association with rotavirus capsids and viroplasms (Figure 4.15). The structure was large (> 1 µm), membrane bound and had an irregular shape. The interior of the structure consisted of stacks of loosely parallel membrane tubules which were contained within the outer membrane. The tubules counted had an average diameter of 69 nm +/- 12 nm (n=55). Clusters of rotavirus capsids can be identified adjacent to these tubule structures. These capsids also contained within an outer membrane which looks to be a continuation of the same membrane that contains the tubule stacks. Additionally, viroplasms could be identified adjacent to these tubule structures. These tubule structures were only identified in one of the HD treated cell lines, indicating that it is either a result of the treatment, or potentially a rare intermediary step in rotavirus assembly.

As was mentioned earlier in the introduction, rotavirus do enter the ER as a DLP after leaving the viroplasm (Trask et al., 2012, Crawford et al., 2019). However, I was unable to find any papers in the literature that documented similar ER remodelling in rotavirus infected cells. Restructuring of the ER is not uncommon in viral infections, with reovirus, coronavirus, parainfluenza and ZIKV all manipulating ER membranes in some way (Tenorio et al., 2019, Deng and Angelova, 2021, Li et al., 2019, Mohd Ropidi et al., 2020, Romero-Brey et al., 2012a). However, ER restructuring was only seen in one infected cell, and so it is likely a rare cell event, or an anomalous result. If this was to be studied further, CLEM can be used to study rare cellular events. By fluorescently tagging the ER and rotavirus capsids, live cells can be studied for a rare event (e.g. ER remodelling) and then prepared for TEM (Sachse et al., 2019).

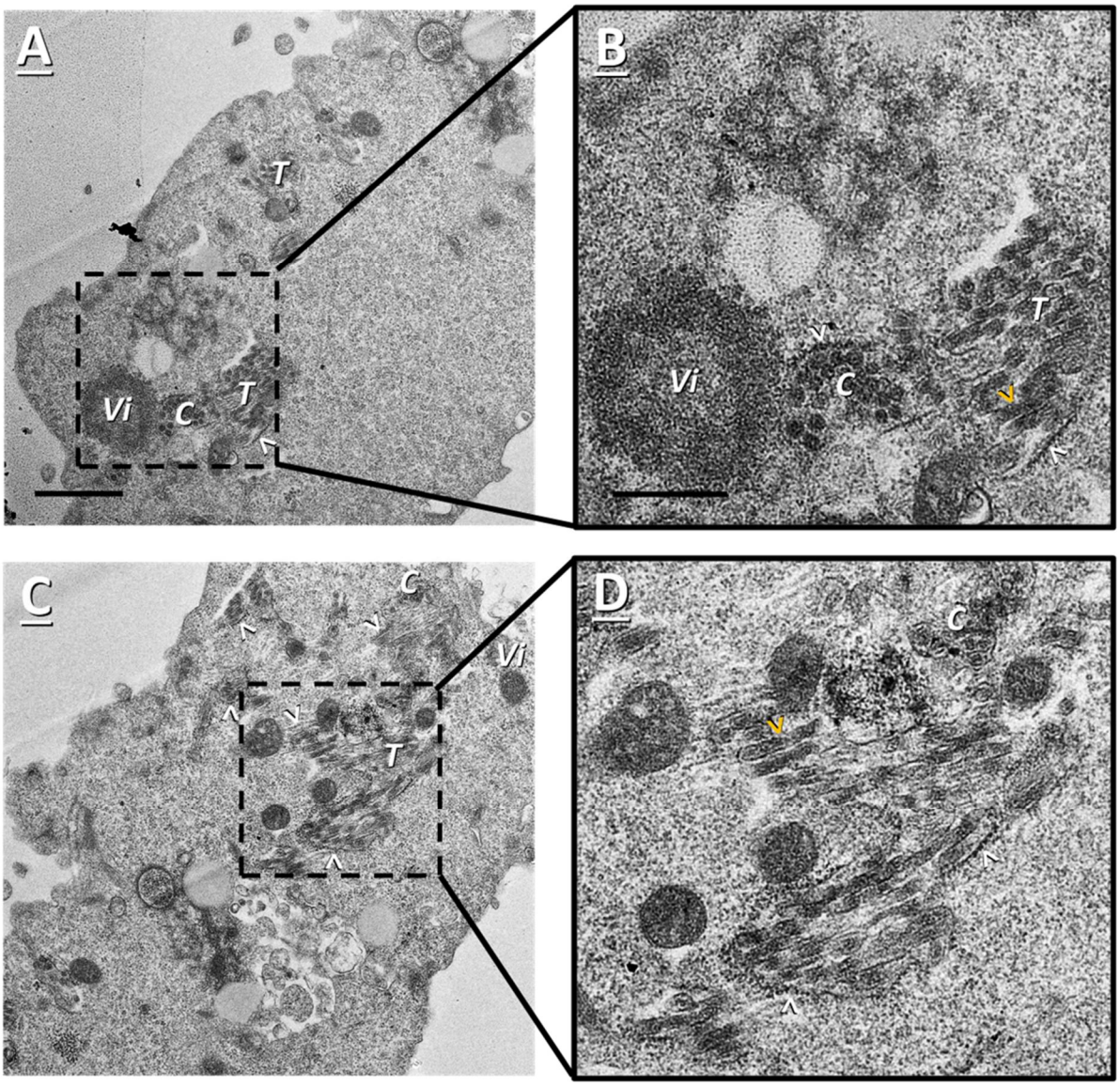

Figure 4.15: Tubular structures identified in rotavirus infected WT cell cytoplasm treated with HD, at 12 hp_{inf}

WT MA104 cells were infected with rotavirus, incubated for 12 hp_{inf} and then treated with 4 % (v/v) hexanediol (HD) for ~30 seconds. Following incubation, cells were processed for TEM. The tubules (*T*), viroplasms (*Vi*), capsids (*C*), outer membrane (white >), Tubule membranes (yellow >) are labelled accordingly. Scale bars for the lower magnifications represent 1 µM. The highest magnification on the right scale bar represents 500 nm.

4.2.8 Rotavirus observed in mitochondrion-like structures in HD treated, GFP-tagged rotavirus infected cells at 12 hp_{inf}

Another unusual observation was made when studying cells infected with GFP-tagged rotavirus and treated with HD at 12 hp_{inf} (Figure 4.16). Rotavirus capsids were found within large cytoplasmic structures. The rotavirus capsids are quite large and so possibly possess RER derived outer capsid shells, however this is difficult to confirm without a smaller neighbouring DLP for a size comparison. These round structures had a greater electron density than the surrounding cytoplasm and also possessed an outer double membrane (Figure 4.16, D). The structures also possessed internal, electron lucent chambers. The electron density, size, internal chambers and outer membrane matches the neighbouring mitochondria (one of which can be seen in figure 4.16, D). Although the architecture is not that of a classic mitochondrion, although mitochondria can have quite varied structures when imaged through TEM. Since rotaviruses have not been described as entering the mitochondria in the literature, this was considered as an anomaly. Fluorescent microscopy or CLEM could be used to fluorescently tag the mitochondria and rotavirus capsids, which could then be inspected for any overlap.

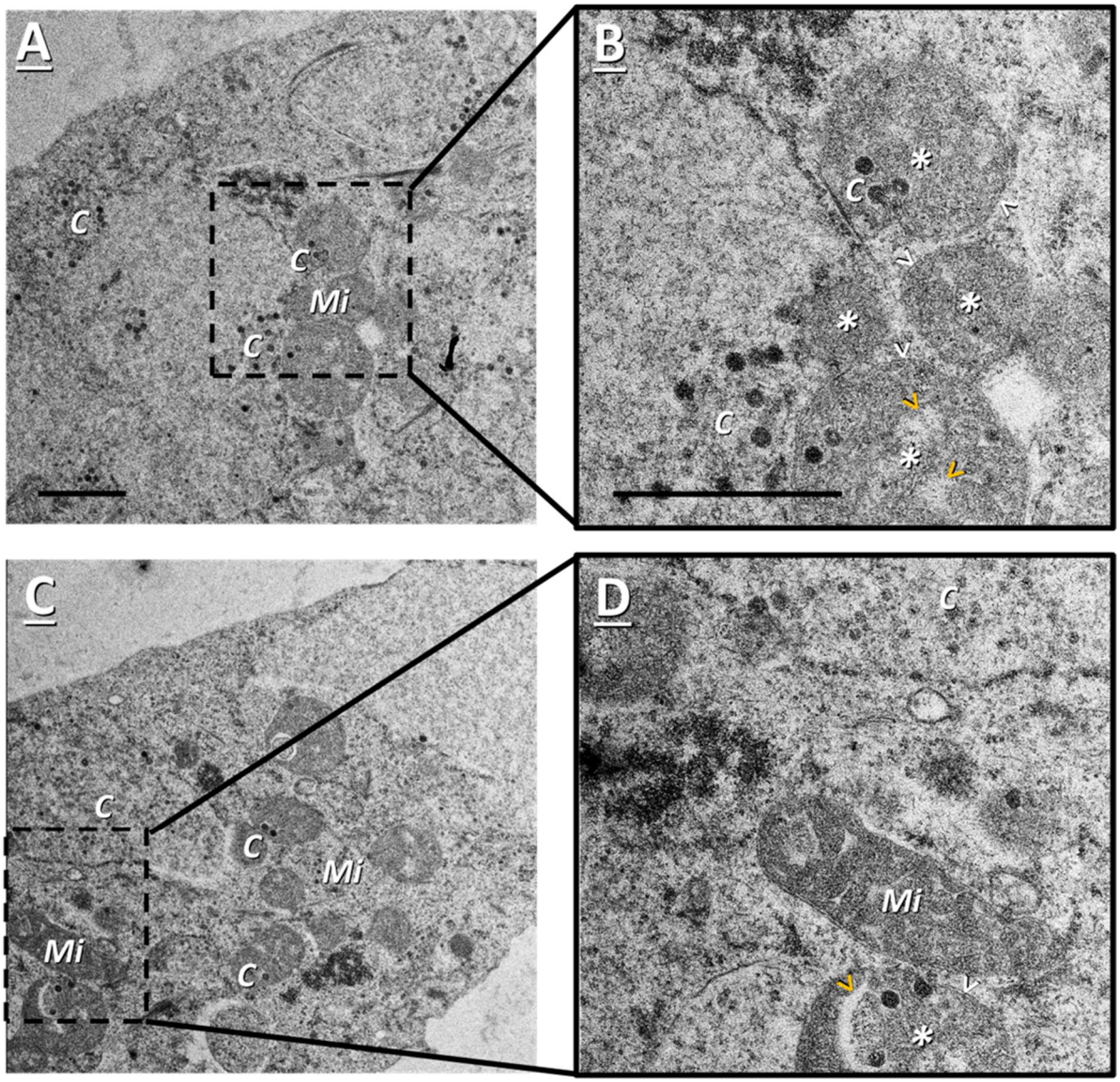

Figure 4.16: Rotavirus capsids identified within mitochondrion-like structures of rotavirus infected MA-NSP5-EGFP cell treated with HD at 12 hp_{inf}

MA-NSP5-EGFP cells were infected with rotavirus, incubated for 12 hp_{inf} and then treated with 4 % (v/v) hexanediol (HD) for ~30 seconds. Following incubation, cells were processed for TEM. The capsids (*C*), mitochondria (*Mi*), mitochondrion-like structure (*), external membrane (white >), and internal chamber (yellow >) are labelled accordingly. Scale bars for the lower magnifications on the left represents 1 µM with the highest magnification scale bar representing 500 nm.

4.2.9 No difference in mitochondria observed in rotavirus infected cells.

Following on from the observation of potential rotavirus particles within mitochondria (Figure 4.16), I decided to compare the morphology of mitochondria across the different experimental conditions (Figure 4.17). As can be seen from the representative mitochondria, there were no obvious morphological differences in mitochondria structure between conditions.

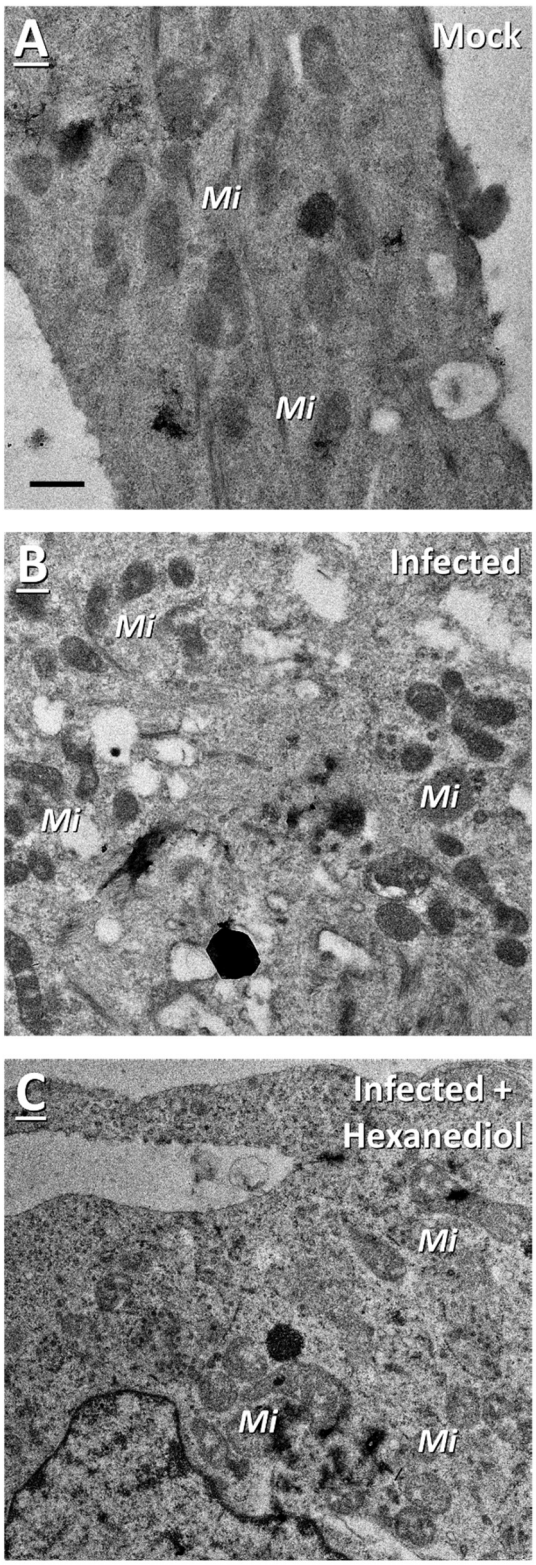

Figure 4.17: Mitochondria imaged across the different conditions in MA-NSP5-EGFP cells at 12 hp_{inf}.

Cells were either mock infected (A), infected with rotavirus (B), or infected with rotavirus and then treated with 4 % (v/v) hexanediol (HD) for 30 seconds (C). All conditions were incubated for 12 hp_{inf}. Following incubation, cells were processed for TEM. Mitochondria (*Mi*) are labelled accordingly. Scale bars represent 500 nm.

4.3 Rotavirus Discussion

The aim of this chapter was to investigate whether rotavirus viroplasms form from LLPS. To test this, rotavirus infected cells were treated with the LLPS interrupter HD during infection(12 hp_{inf}). It was found that HD treatment of rotavirus infected cells significantly reduced viroplasm area at 12 hp_{inf}.

4.3.1 HD treatment of rotavirus viroplasms disrupts LLPS, resulting in smaller viroplasms.

At 12 hp_{inf}, the treatment of rotavirus infected cells with HD resulted in a statistically significant reduction in viroplasm area. Since HD is known to interrupt LLPS, this finding supports the hypothesis that rotavirus viroplasm formation occurs through LLPS.

LLPS describes the spontaneous de-mixing of a mixed solution into two or more separate phases (Mehta and Zhang, 2022). It is formed due to the weak multivalent bonds that form between proteins and nucleic acids causing the macromolecules to drop out of solution and into a separate aggregate (Lafontaine, 2019). Multivalency in proteins and nucleic acids occurs due to tandem binding modules and repetitive motifs (both known as stickers) found throughout the protein which frequently contain charged and aromatic residues (Mehta and Zhang, 2022). These bonds can include electrostatic, hydrophobic, pi-pi and pi-cation interactions (Alberti et al., 2019, Qamar et al., 2018). Stickers are dispersed along a protein, separated by unfolded and relatively disordered regions known as spacers (Mehta and Zhang, 2022). The overall process is similar to the separation that occurs between oil droplets in water, with proteins and nucleic acids forming distinct droplets within the cytoplasm (Lafontaine, 2019). Therefore, it can be said that LLPS is the process in which macromolecule-water interactions are switched for macromolecule- macromolecule and water-water interactions (Alberti et al., 2019). The droplet structures that form from LLPS are highly dynamic and so can rapidly form or breakdown, be deformed, or merge together. Additionally, liquid-like condensates can further mature into solid-like or gel-like structures as the concentration of stickers increases. By increasing or decreasing the concentration of stickers, the characteristics of the condensate can be altered (Mehta and Zhang, 2022, Banani et al., 2017). Recent evidence has pinned LLPS as the mechanism behind the development of membrane-less

structures within cells (e.g. nucleoli, stress granules) (Carey and Guo, 2022, Lafontaine, 2019).

HD is an aliphatic alcohol which is able to interrupt weak hydrophobic bonds, which allows it to disrupt protein-nucleic acid aggregates within cells. This means HD can be used as an indicator of LLPS (Düster et al., 2021, Alberti et al., 2019, Kroschwald et al., 2017, Elbaum-Garfinkle, 2019, Ribbeck and Görlich, 2002). HD is able to interrupt the hydrophobic interactions through its amphiphilic properties (Lin et al., 2021). Consequently, the finding that HD treatment of rotavirus infected cells reduces viroplasm area supports the notion that rotaviruses utilise LLPS. Likely, rotaviruses use LLPS to concentrate the components of their viral replication factory, whilst keeping it separate to the cellular cytoplasm. HD is not the only aliphatic diol that has been used to interrupt LLPS. Propylene glycol has seen some use as an alternative to HD (Geiger et al., 2021). Propylene glycol is used as an alternative as it is less toxic than HD when used at concentrations below 5 % (Mochida and Gomyoda, 1987).

My findings are supported by the work from Geiger et al. (2021), who also found evidence of rotavirus viroplasm formation through LLPS, which they also confirmed through the use of HD. Interestingly, they found that during late infection (12 hp_{inf}), larger rotavirus viroplasms were resistant to HD treatment. HD is only effective at interrupting liquid-like assemblies and cannot disrupt solid-like aggregates (Kroschwald et al., 2017). As infection progresses, rotavirus viroplasms fuse together to form larger structures (Eichwald et al., 2012). The finding from Geiger et al. (2021) that HD does not interrupt larger viroplasms during late infection implies that these larger viral aggregates have transitioned from a liquid-like to a solid-like arrangement. Their use of immunofluorescent imaging allowed them to view the effects of HD treatment on viroplasms in real time, highlighting the resistance of the larger viroplasm against HD post-treatment. Imaging the viroplasms through TEM only gave me a snapshot at 12 hp_{inf} and so I could not see the same characteristic trait. Regardless, both our findings support the notion that rotavirus viroplasms form due to LLPS (Geiger et al., 2021).

The next observation from the HD experiments was the presence of both electron-dense and electron lucent viroplasms at 12 hp_{inf}. Treatment of the rotavirus infected cells reduced the percentage of electron lucent viroplasms from 12 % in non-treated cells, down to 4 % in HD treated cells. The decrease in percentage of electron-lucent viroplasms in HD treated cells indicates that electron-dense viroplasms might be resistant to HD. Similar findings were observed from Geiger et al. (2021) who found via live-cell confocal imaging that during late infection, solid-like viroplasms were

resistant to treatment from propylene glycol (another aliphatic diol with similar properties to HD) (Geiger et al., 2021). When liquid-like condensates transition to solid-like condensates the weak hydrophobic interactions are strengthened, resulting in resistance to the aliphatic alcohols that interrupt the weak interactions (Geiger et al., 2021).

Liquid-like condensates are highly dynamic and over the progress of infection will transition into a more solid, gel-like structure as the concentration of protein and RNA increases within the viroplasm (Knowles et al., 2014). Additionally the conversion to a gel-like structure can be influenced by the post-translational modification of the proteins involved in the phase-separation (Li et al., 2012). In rotavirus infected cells this has been pinpointed to the hyperphosphorylation of NSP5 in late infection, causing the formation of more solid-like viroplasms (Papa et al., 2019b, Geiger et al., 2021). This suggests that the electron-lucent viroplasms imaged at 12 hp_{inf} correspond to liquid-like viroplasms as they were susceptible to HD treatment. Whereas, the electron-dense viroplasms correspond to sold-like condensates as they were resistant to HD treatment.

To confirm this, I would need to establish earlier infection time points to ascertain whether there is higher percentage of electron-lucent, liquid like viroplasms early in infection when imaged through TEM. Additionally, chemical-crosslinking with paraformaldehyde prior to HD treatment would trigger the condensates to transition from liquid to solid-like and therefore should now be resistant to HD. Finally, these experiments could be imaged through live-cell confocal microscopy, allowing for the highly dynamic process of viroplasm disruption to be captured live. This would be particularly viable as the MA-NSP5-EGFP cell line already has a GFP-tagged NSP5 present.

4.3.2 NSP5 drives LLPS in rotavirus viroplasms

Rotavirus is one of the many viruses that utilise LLPS for the formation of viral factories, with viruses such as SARS-CoV-2, respiratory syncytial virus (RSV) and HSV1 also taking advantage of this mechanism (Wei et al., 2022). SARS-CoV-2 is a (+) ssRNA, enveloped virus that replicates within membrane compartments co-opted from the host ER (Artika et al., 2020). In coronaviruses, LLPS has been well established, with the disordered N-protein possessing multivalent RNA binding sites which allow it to drive LLPS (McBride et al., 2014, Chang et al., 2009). This has also been found to be the case in SARS-CoV-2, where viral RNA is compacted by a

dimerised N-protein via LLPS to form RNA-protein complexes, initiating viral assembly. It has further been hypothesised that the compaction of RNA was involved in the packaging of the viral RNA genome into progeny virions, with the disruption of LLPS resulting in replication inhibition (Perdikari et al., 2020, Zhao et al., 2021). Additionally, it was identified that the LLPS of N-protein with viral RNA is able to subvert the innate antiviral immune response via the inhibition of Lys63-linked poly-ubiquitination (Wang et al., 2021b).

RSV is a (-) ssRNA virus that is responsible for causing infections of the respiratory tract (Battles and McLellan, 2019). In fact, it is the most common cause of respiratory hospitalisations in children and can cause pneumonia in the immunocompromised and elderly (Coultas et al., 2019). RSV replicates within the cytoplasm of infected cells where it forms viral inclusion bodies which concentrate the proteins involved in the RNA polymerase complex and mRNA translation (Fearns and Deval, 2016, Strzyz, 2021, Rincheval et al., 2017). Interestingly, the RSV inclusion bodies are not homogenous and have sub-compartments where newly synthesised viral mRNA is sorted (Rincheval et al., 2017). RSV inclusion bodies are liquid-like droplets that form from the interactions between the viral nucleoprotein (N) and phosphoprotein polymerase cofactor (P) which form the N-P complex (Rincheval et al., 2017). The N-P ring complex forms due to the interaction between the C-terminus of P and the N-terminus of N. The ring structure of N-P is then completed by the C-terminus of N binding to the N-terminus of P. Truncation studies revealed that the C-terminus of P contains a disordered region which is essential for the formation of RSV inclusion bodies. Furthermore, the interactions between N and RNA are essential for inclusion body morphogenesis (Galloux et al., 2020).

The final example of a virus that is involved in LLPS is HSV1. HSV1 is a double stranded DNA virus that replicates its genome and assembles progeny virions within the nucleus of infected cells (Kobiler and Weitzman, 2019). Specifically, herpesviruses form distinct inclusions within the nucleus that act as sites of viral replication (Charman and Weitzman, 2020). The HSV1 replication compartments are spherical in structure during early infection and can fuse together upon contact, indicating that they form via LLPS (Chang et al., 2011, Taylor et al., 2003, Tomer et al., 2019). Moreover, the HSV1 transcription factor ICP4 has been found to have intrinsically disordered regions that allow it to act as a driver of LLPS (Seyffert et al., 2021). ICP4 allows for the formation of membraneless replication compartments which are distinct from the surrounding nuclear material. Like in other cases of LLPS, the formation of the liquid-like inclusions is dependent upon the concentration of ICP4, with an increase in ICP4 leading to larger inclusions. It has been hypothesised that viral DNA and the host cellular RNA polymerase II could be involved in the

process, with the former acting as a scaffold for LLPS (Seyffert et al., 2021). However, further studies are needed to identify the other host and viral factors involved in HSV1 LLPS.

Following on from the finding that HD disrupts viroplasms indicating the role of LLPS in viroplasm formation, I decided to carry out a bioinformatic analysis of the sticker domains interrupted by HD. As mentioned above, HD is known to interrupt weak hydrophobic interactions. Furthermore, the involvement of hydrophobic interactions in LLPS has been well documented, with the hydrophobic bonds being facilitated by non-polar, aromatic, or even charged residues on the proteins involved (Dyson et al., 2006). These hydrophobic residues encourage the formation of protein-protein interactions over that of protein-water, resulting in the formation of phase-separated droplets (Lin et al., 2021). An example of a LLPS protein with a large number of hydrophobic residues is elastin, which can phase separate and form filaments due to its numerous hydrophobic residues (Yeo et al., 2011). I identified the hydrophobic regions on both NSP2 and NSP5 performing a Kyte and Doolittle analysis. There were 9 hydrophobic regions identified throughout NSP2 and 3 on NSP5 distributed on either end of the protein.

The importance of the hydrophobic interactions between NSP2 and NSP5 in LLPS could be further studied through the use of NaCl (Lin et al. (2021). NaCl screens out other electrostatic interactions, without affecting hydrophobic bonds. Additionally, it sequesters water away from proteins, promoting LLPS. NaCl could be added to recombinantly-expressed and purified NSP2, NSP5 and a mixture both NSP2 and NSP5 to assess whether droplet formation can still occur. Droplet formation could be imaged through confocal microscopy. If the droplets form, it would demonstrate that the hydrophobic interactions alone are capable of inducing LLPS in NSP2 and NSP5. Successful droplets can then be treated with 4 % HD to disrupt the droplets, confirming the process. The opposite experiment could occur with the use of guanidinium hydrochloride, which weakens the stability hydrophobic protein interactions (Sołtys et al., 2021). Therefore, guanidinium chloride could be used to assess if there are any other type of interactions involved in the LLPS of NSP2 and NSP5. If droplets still form when in the presence of guanidinium hydrochloride, then there must be other interactions involved in the LLPS of NSP2 and NSP5.

When comparing the positioning of the hydrophobic residues between NSP5 and NSP2, both proteins had a hydrophobic N-terminus. In the literature, I found examples of N-terminal hydrophobic regions being involved in protein interactions with lipid droplets. For example, the ER membrane protein AAM-B has a hydrophobic N-terminal that allows it to target lipid droplets. This is similarly the case

for the mitochondrial and ER protein cytochrome b5 reductase 3 (Zehmer et al., 2008). This is of note as rotavirus viroplasms are associated with lipid droplet biogenesis, which is needed for virus production. However, it is currently unknown whether NSP2 or NSP5 directly interact with the lipid droplets (Criglar et al., 2022). Whether the hydrophobic N-terminus of NSP2 and NSP5 are involved in rotavirus lipid biogenesis could be further studied through the use of a protein lipid overlay assay. Protein lipid overlay assays involve spotting lipid droplet serial dilutions onto a nitrocellulose membrane. The proteins in question are then added and the membrane is washed. If the protein binds to the lipid droplet through a lipid-binding region, then it will remain bound to the membrane and can be visualised via immunoblotting (Dowler et al., 2002). Not only could this be used to identify whether NSP2 or NSP5 have lipid binding domains, but it could be also be used to identify whether the hydrophobic N-terminals are involved. N-terminal truncation mutants of both NSP2 and NSP5 could be generated, which would lack the N-terminal hydrophobic residues. The protein lipid overlay assay mentioned above could then be repeated with these truncated mutants to assess whether NSP2 and NSP5 are still able to bind to the lipids without their N-terminal hydrophobicity.

Next, I created 3D-models of both NSP2 and NSP5 with hydrophilic, hydrophobic, ordered and disordered regions highlighted. Of note, there were a number of surface hydrophobic regions in both NSP2 and NSP5. Surface hydrophobic regions on proteins are typically associated with protein-protein interfaces (Young et al., 1994, Keskin et al., 2008, Rego et al., 2021, Hagemans et al., 2015). Consequently, these surface hydrophobic regions could be involved in protein-protein interactions that drive the LLPS. NSP2 and NSP5 are documented to interact with several viral and cellular proteins. For example, NSP2 can bind to NSP5, NSP6, VP1, VP2, Beta-tubulin, HSP90 and Hsc70 to name a few (Viskovska et al., 2014, Buttafuoco et al., 2020, Dhillon et al., 2018). Whereas NSP5 is known to interact with NSP2, NSP6, VP1, VP2, COPII, HSPA5 and casein kinase 1 alpha to name a few (Viskovska et al., 2014, Torres-Vega et al., 2000b, Arnoldi et al., 2007, Buttafuoco et al., 2020, Dhillon et al., 2018, Criglar et al., 2018). Consequently, these surface hydrophobic regions on NSP2 and NSP5 could be involved in any of these protein-protein interactions. In addition to mapping out the surface hydropathy, I also highlighted the disordered regions of the protein. In proteins, a disordered region refers to a section of the protein which lacks a fixed structure (Dunker et al., 2001). As mentioned above, proteins involved in LLPS often have disordered regions of protein (spacers) that separate the binding (stickers) regions of the protein which are responsible for the protein-protein interactions responsible for LLPS (Mehta and Zhang, 2022).

Consequently knowing the location of the disordered regions aids in identifying where the protein-protein contacts could potentially occur.

Following on from this, I decided to identify whether the hydrophobic regions were conserved across NSP2 and NSP5 in different rotavirus species. The formation of cytoplasmic viroplasms is conserved amongst all rotavirus species studied so far (Buttafuoco et al., 2020). Consequently, if the hydrophobic regions in NSP2 and NSP5 are a key aspect of LLPS in viroplasm formation, then they might be conserved between the different rotavirus species. Despite there being variance in the number of hydrophobic regions, there was consistency identified within the N-terminal of NSP2 and the C-terminal of NSP5. Interestingly, the C-terminal region of NSP5 has been implicated in several protein-protein interactions in rotavirus A (e.g. NSP2, NSP6, VP1 and VP2) (Eichwald et al., 2004, Viskovska et al., 2014, Torres-Vega et al., 2000a, Arnoldi et al., 2007, Buttafuoco et al., 2020). These protein-protein interactions could potentially be due to the hydrophobic region present in the C-terminal. To investigate whether the C-terminal hydrophobic region of NSP5 is essential for protein binding, a protein binding assay could be used with or without the presence of guanidinium hydrochloride. As mentioned above, guanidinium hydrochloride weakens hydrophobic interactions. Consequently, if NSP5 cannot bind other viral proteins (e.g. VP1) in the presence of guanidinium hydrochloride, it implies that the protein-protein interactions are dependent upon the hydrophobic bonds. This experiment could similarly be repeated on NSP5 from other rotavirus species to confirm whether this aspect is conserved across the rotavirus genus.

Finally, I compared the hydrophobic regions of NSP2 and NSP5 against the FuzDrop phase separation and flDPnn disorder analysers. Of note, there was no correlation with the hydrophobic and hydrophilic regions of either protein with the P_{DP} spikes of the FuzDrop analysis. As the HD experiments revealed the importance of the hydrophobic bonds to LLPS in rotavirus viroplasm formation, I was expecting there to be more of a correlation. Especially as FuzDrop measures hydrophobicity within droplet promoting regions (Hatos et al., 2022). However, the FuzDrop method is multifactorial and takes into account the residue disorder and how this changes during binding (Hardenberg et al., 2020). Consequently, as hydrophobicity is not the only factor affecting the prediction of droplet promoting regions, it could explain why they do not line up. The other observation was that none of the hydrophobic residues lined up with the disordered regions shown by the flDPnn analysis. Intrinsically disordered protein regions are described as areas of a protein which lack a fixed tertiary structure. One of the reasons for this is that the intrinsically disordered regions lack hydrophobic residues, preventing the formation of a fixed tertiary structure due to the lack of long-range hydrophobic interactions between different

areas of the protein (Babu, 2016). Consequently, it makes sense that there is a lack of hydrophobic regions within the disordered areas of NSP2 and NSP5. Finally, there was a considerable degree of overlap between the droplet promoting regions of FuzDrop and the disordered regions of flDPnn. As FuzDrop factors disordered regions into its phase separation prediction, it makes sense that there is a considerable degree of overlap between the two analyses (Hatos et al., 2022).

One of the biggest findings was the confirmation that NSP5 (with a P_{LLPS} score of >0.60) is suggested to undergo spontaneous LLPS. As a consequence, NSP5 could act as a droplet driver- instigating other proteins to undergo phase separation (Hatos et al., 2022). On the other hand, NSP2 was identified as being unable to undergo spontaneous LLPS (with a PLLPS score of <0.60). This might suggest that NSP2 acts as a droplet-client protein, rather than undergoing LLPS by itself (Hatos et al., 2022). Droplet-client proteins only undergoing LLPS when undergoing specific interactions with another protein (e.g. NSP5). This finding is further supported by the large number of hydrophobic regions identified within NSP2. Hardenberg et al. (2020) found that when analysing the amino acid compositions of over 300 droplet-client and droplet driving proteins from three public databases that droplet-client proteins were enriched in hydrophobic residues when compared to droplet driving proteins (Hardenberg et al., 2020). These findings are supported by the analysis by Geiger et al. (2021) which had the same results, leading them to suggest that NSP5 acts as a 'scaffold' for LLPS in rotavirus infected cells (Geiger et al., 2021). This is further supported by experimental data from the literature that documents the fundamental role that NSP5 plays in viroplasm formation (Poncet et al., 1997, Fabbretti et al., 1999, Mohan et al., 2003, Papa et al., 2019b, Eichwald et al., 2004, Eichwald et al., 2002, Sen et al., 2007).

Finally, the bioinformatic analysis was also predicted the binding regions of NSP2 and NSP5 by flDPnn. NSP2 was predicted to have a RNA binding region on its C-terminus, with no DNA or protein binding regions identified. Experimental data from Hu et al. (2012a) found that NSP2 was able to bind RNA in a sequence specific manner through its residues 104, 105, 107, 221, 223, 236, 243, 244, 239, 240 and 248. However, they also found that the deletion of the NSP2 C-terminal dramatically reduced its ability to bind RNA in a sequence-independent manner, fitting with the flDPnn analysis. Of note, the flDPnn analysis identified no protein binding domains on NSP2, despite NSP2 being well documented to bind to several host and viral proteins. As mentioned above, NSP2 can bind to NSP5, NSP6, VP1, VP2, Beta-tubulin, HSP90 and Hsc70 *etc*. (Viskovska et al., 2014, Buttafuoco et al., 2020, Dhillon et al., 2018).

The flDPnn prediction of RNA binding by NSP5 further matches the findings of Vende et al. (2002), who generated recombinant His tagged NSP5 which was exposed to RNA and then UV cross-linked which confirmed that NSP5 has non-specific RNA binding. Additionally, NSP5 is involved in the packaging of viral RNA into newly formed capsids and so it likely binds to RNA during virion assembly (Vende et al., 2002, Papa et al., 2021, Martin et al., 2011). Like NSP2, NSP5 has also been found to bind to several host and viral proteins (e.g. NSP2, NSP6, VP1, VP2, COPII, HSPA5 and casein kinase 1 alpha) (Viskovska et al., 2014, Torres-Vega et al., 2000a, Arnoldi et al., 2007, Buttafuoco et al., 2020, Dhillon et al., 2018, Criglar et al., 2018). Consequently the flDPnn prediction that NSP5 has several protein-binding regions is in accordance with the literature. Ultimately, the flDPnn prediction that NSP5 binds to DNA is highly unlikely. Not only is there no experimental of DNA- NSP5 binding in the literature, but furthermore NSP5 and the rotavirus replication cycle as a whole is restricted to the cytoplasm and so is unlikely to encounter nuclear DNA. To surmise, the bioinformatic analysis identified and mapped the hydrophobic residues that are interrupted by HD onto NSP2 and NSP5. Both NSP2 and NSP5 have a hydrophobic N-terminal which could act as a lipid-binding site. Additionally, there was little evidence of hydrophobic residue conservation in NSP2 and NSP5 amongst the different rotavirus species. Although the hydrophobic C-terminal of NSP 5 was identified in all of the rotavirus species analysed and could have a role in NSP5-protein binding. Of particular interest was the conclusion from the FuzDrop analysis that NSP5 drives LLPS with NSP2, supporting experimental and bioinformatic evidence provided from other researchers. The additional experiments listed above would be useful to further validate the findings of the bioinformatic analysis and highlight some interesting areas of further study into rotavirus LLPS.

Chapter 5 : An investigation into the role of DOCK5 on herpesvirus cellular egress

5.1 Herpesvirus Introduction

The *Herpesviridae* family consists of dsDNA viruses that are associated with a wide range of diseases in several animal species (mammals, reptiles, birds, fish and invertebrates) (McGeoch and Gatherer, 2005). Despite the wide range of animal hosts, herpesviruses are extremely well tailored to target their specific host (Davison, 2002). Eight human herpesviruses infect over half the global population and are distributed all around the world (Mariggiò et al., 2017, James et al., 2020). In the majority of people, infection is asymptomatic or associated with acute and mild illness. However in certain individuals (e.g. the young, old, or immunocompromised), several life threatening illnesses such as cancer and encephalitis can result from infection (Vega et al., 2020, Darji et al., 2017). Transmission is dependent upon the specific herpesvirus, but often involves direct person-to-person transfer through intimate contact, or indirectly through contaminated blood transfusions (Azab et al., 2018). There are no cures for herpesvirus infection but several antivirals can be used to mitigate symptoms. Additionally, various vaccines are in development with one currently being utilised against the alphaherpesvirus varicella zoster (Schwartz, 2004, Chentoufi et al., 2022, Fatahzadeh and Schwartz, 2007). Herpesvirus virions possess glycoprotein studded lipid envelopes that are wrapped around icosahedral protein capsids (Dünn-Kittenplon et al., 2021, Dai and Zhou, 2018). Characteristic to herpesviruses is their biphasic replication cycles which is divided between a dormant latent phase and an active lytic phase (Grinde, 2013).

5.1.1 Herpesvirus Taxonomy

Herpesviruses are found within the *Herpesviridae* family which belongs to the *Herpesvirales* order (Gatherer et al., 2021). The *Herpesviridae* family has three subfamilies that are known to infect humans (Figure 5.1) (Gatherer et al., 2021). The *Alphaherpesvirinae* subfamily contains HSV1, HSV2 and varicella zoster virus (VZV). The subfamily *Betaherpesvirinae* comprises the roseoloviruses (HHV-6 and HHV-7) and HCMV. Finally, the *Gammaherpesvirinae* includes the oncogenic herpesviruses, EBV and Kaposi's sarcoma-associated herpesvirus (KSHV) (Davison, 2002). There are over a hundred different herpesviruses that infect a large number of different organisms (Naqvi et al., 2018). The herpesviruses have coevolved with specific mammalian, avian and reptilian hosts and are consequently highly adapted to them (Gatherer et al., 2021). In this introduction, most of the focus is on alpha and gamma herpesvirus since my work was based on KSHV and HSV1.

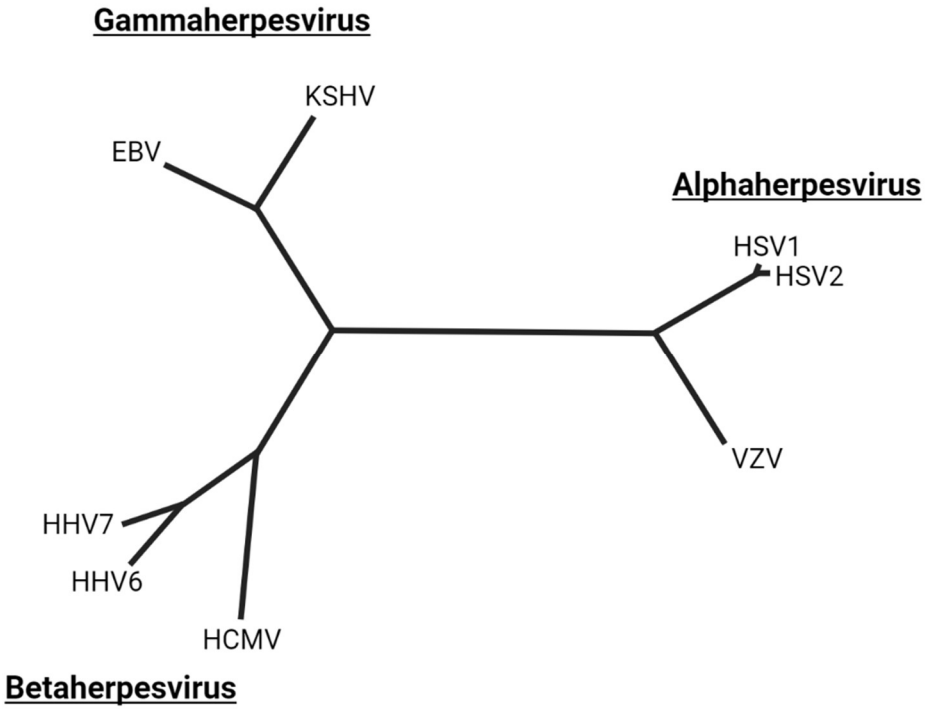

Figure 5.1: A simplified phylogenetic tree of human herpesviruses

Phylogenetic tree is based on a comparison between the amino acid sequences of the major capsid protein from the different human herpesvirus species. The phylogenetic tree includes herpes simplex virus 1 (HSV1) and 2 (HSV2), varicella zoster virus (VZV), human cytomegalovirus (HCMV), human herpesvirus 6 (HHV6) and 7 (HHV7), Epstein-Barr virus (EBV), and Kaposi's sarcoma associated herpesvirus (KSHV). Figure made using BioRender, adapted from figure 2 by Moore et al. (1996).

5.1.2 Herpesvirus Disease

5.1.2.1 Clinical Characteristics

5.1.2.1.1 KSHV clinical characteristics

First discovered in 1994, KSHV is an oncogenic herpesvirus that is responsible for Kaposi's Sarcoma (KS) and is associated with a large variety of B-cell lymphoproliferative illnesses, such as primary effusion lymphoma (PEL) and multicentric Castleman's disease (MCD) (Vega et al., 2020). Disease symptoms occur due to the wide range of cells that KSHV infects, such as lymphocytes, fibroblasts, endothelial and epithelial cells (Bechtel et al., 2003, Garrigues et al., 2017). Whilst in KS the dominant cell is endothelial (spindle cell), MCD and PEL are associated with B-cells (Polizzotto et al., 2012). In KS, cancerous endothelial cells form masses in the skin, mouth, lymph nodes and other organs (Schwartz et al., 2008). Both MCD and PEL are lymphoproliferative illnesses meaning they are associated with the uncontrolled growth of lymphocytes. MCD is associated with severe systemic inflammation and lymph node swelling (Ramaswami et al., 2021). PEL on the other hand is associated with the accumulation of immature B cells within the body cavities. All three of these diseases are commonly associated with HIV co-infection(Fernández-Trujillo et al., 2019).

5.1.2.1.2 HSV1 clinical characteristics

HSV1 infection is frequently asymptomatic, however in those that show symptoms, the classic disease presentation is of blisters around the site of infection (e.g. mouth, tongue *etc.*) known as oral herpes. However other sites can be affected depending upon the site of initial infection (Wei and Coghlin, 2017, Darji et al., 2017). After initial primary infection, recurrent oral herpes is usually less severe (Williams et al., 2015). HSV1 infection of the eye can occur in children and adults, with recurring ocular HSV being a frequent cause blindness in the US (Barker, 2008). More severe illness can occur in the immunocompromised, potentially resulting in herpes encephalitis which has a mortality rate of > 70 % if untreated, or chronic herpes infection (Kennedy and Chaudhuri, 2002, Bradshaw and Venkatesan, 2016). HSV1 infections can also be severe in new-born children, resulting in permanent neurological disability or death (Kimberlin, 2004).

5.1.2.2 Herpesvirus Pathology

In KS, tumours mainly consist of endothelial cells which are primarily latently infected, with smaller subpopulations supporting lytic replication (Bechtel et al., 2003). Currently the cause of this switch from latent to lytic infection *in vivo* is unknown, however in cell culture and in patients it can occur spontaneously (Renne et al., 1996, Casper et al., 2007). Lytic KSHV activation results in the shedding of virions and is sporadic and asymptomatic (Casper et al., 2007, Pauk et al., 2000). It is presumed that the viral shedding caused by lytic infection drives the spread of KSHV, with transmission occurring when infected saliva encounters mucosal regions (Newton et al., 2018). The KSHV lytic cycle can be triggered by viral co-infection, with viral pathogens such as HIV1, HSV1 and 2, HCMV and human papilloma virus all identified as viral co-factors (Purushothaman et al., 2015). For example, HIV1 has been found to directly activate KSHV lytic protein Rta, resulting in lytic replication (Varthakavi et al., 2002).

In KS there are three simultaneous processes occurring: spindle cell proliferation, inflammation and angiogenesis (Ganem, 2010). The three processes are co-dependent, with spindle cells (infected endothelial cells with altered morphology) producing proangiogenic and proinflammatory factors that recruit inflammatory cells which in turn stimulate the growth of spindle cells (Ensoli et al., 2001). KSHV is able to stimulate inflammation through a number of different mechanisms, such as inducing the secretion of IL-6, the activation of the NF-κB signalling pathways and through the stimulation of pro-inflammatory cytokines (Dai et al., 2012, Matta and Chaudhary, 2004, Guo et al., 2017). By using several mechanisms to encourage an inflammatory response, KSHV creates an environment that encourages cell proliferation whilst inhibiting apoptosis (He et al., 2019).

In HSV1, pathogenesis is similarly affected by the lytic and latent replication cycles. Infection with HSV1 can result in an asymptomatic, mild, or even life-threatening illness depending upon the individual. Interactions between the host (e.g. immune system) and virus determine disease outcome (Zhu and Viejo-Borbolla, 2021). HSV1 infects epithelial cells during primary infection and then establishes latency within the neurones (especially neurones of the peripheral nervous system) (D'Aiuto et al., 2019). Once HSV1 has infected epithelial cells via damage or breakage, it can facilitate cell-to-cell transmission in the skin. HSV1 infection has even been found to trigger the polarised migration of skin cells to infection sites, augmenting HSV1 cell-to-cell transmission (Abaitua et al., 2013).

The lytic replication of HSV1 in epithelial cells causes inflammation and tissue damage, resulting in the characteristic herpes blisters (Zhu and Viejo-Borbolla, 2021). Once HSV1 has replicated within the epithelial cells, it transitions to the peripheral nerve endings and travels to neuronal cell body via retrograde transport (Tessier-Lavigne and Goodman, 1996). Once within the neuronal cell body, HSV1 enters latent dormancy which is associated with limited gene expression and no virion production (Bloom, 2016). The reason why HSV1 establishes latency in neuronal cells, whilst undergoing lytic replication in epithelial cells is not currently known, although VP16 has been predicted to play a role in the difference. VP16 is a HSV1 tegument protein that plays a role in lytic activation. Upon entry into the target epithelial cell, VP16 travels to the nucleus where it activates the expression of HSV1 lytic genes (Fan et al., 2020). However, in neuronal cells the distance from cell entry at the nerve endings to the cell body for gene activation is predicted to prevent lytic activation. This is due to VP16 being unable to reach the concentrations needed to activate cell lysis within the neuronal cell bodies (Thompson and Sawtell, 2019, Zhu and Viejo-Borbolla, 2021). Nevertheless the process needs further research.

5.1.2.3 Diagnosis, Treatment and Prevention

5.1.2.3.1 Diagnosis

In KSHV clinical diagnosis can be limited and so histopathological tests can be used as a gold standard for diagnosis (Amerson et al., 2016). However, histopathological testing can be difficult if the pathologist is not familiar with the signs of KSHV-related illnesses. Therefore the immunohistochemical staining of the KSHV latency-associated nuclear antigen (LANA) with antibodies can be combined with the identification of spindle shaped cells (in KS) for a positive diagnosis (Schneider and Dittmer, 2017). For HSV1 infections, the gold standard of diagnosis is serological testing, which is performed after the identification of herpes-related symptoms e.g. blisters. Like in other viral infections, a PCR test provides the most sensitive diagnosis (Fatahzadeh and Schwartz, 2007).

5.1.2.3.2 Treatment and Prevention

Treatment for KSHV is dependent upon the disease in question. In AIDS-associated KS, highly active antiretroviral therapy is used to control HIV viraemia which results

in the restoration of the immune system, leading to KS remission (Vanni et al., 2006). Classical cancer treatments such as surgery, radiotherapy and chemotherapy can also be used for non-AIDS-associated KS (with chemotherapy also working on PEL and MCD) (Coen et al., 2014). Finally, anti-herpetic antivirals such as ganciclovir can be used against KS, MCD and PEL (Schwartz, 2004). HSV1 treatment is usually simpler, with anti-herpetic agents such as acyclovir, valacyclovir and famciclovir being administered (Fatahzadeh and Schwartz, 2007). Currently, there is only one herpesvirus vaccine available and that is against VZV (Mbinta et al., 2021). Development is currently ongoing on a multi-epitope KSHV vaccine that targets several viral glycoproteins (gB, gH, gL, gM and gN) (Chauhan et al., 2019). There is currently no vaccine for HSV, although there are several different vaccines in development (Belshe et al., 2012, Chentoufi et al., 2022).

5.1.3 Herpesvirus Epidemiology

5.1.3.1 Transmission

For KSHV, transmission can occur through both sexual and non-sexual means (Minhas and Wood, 2014). KSHV can be identified within saliva, semen, oropharyngeal mucosa, vaginal secretions and peripheral blood mononuclear cells (Chen and Hudnall, 2006). The primary means of transmission is believed to differ depending on geographical location, subject to the endemicity of the area. In non-endemic regions (e.g. Western Europe, USA, *etc.*) sexual transmission is predicted to be the main route of transfer (Cannon et al., 2001, Mariggiò et al., 2017). However, findings are mixed on the importance of sexual transmission relating to KSHV and it is difficult to separate sexual transmission from transmission through saliva (Minhas and Wood, 2014, Zhang et al., 2014, Malope et al., 2008). An additional transmission pathway for KSHV is through blood transfusion due to the potential presence of KSHV in peripheral blood mononuclear cells (Zavitsanou et al., 2006, Hladik et al., 2006). Another important route of KSHV transmission is vertically from mother to child. In endemic regions there are high rates of KSHV seroprevalence in children, indicating that transmission might occur during or after childbirth, through vaginal secretions, breast milk, or saliva (Lisco et al., 2006, Mantina et al., 2001, Brayfield et al., 2004, Little and Uldrick, 2019).

Transmission in HSV1 is better studied and subsequently clearer than in KSHV. HSV1 transmission occurs primarily through the transfer of infectious bodily fluids

(e.g. saliva) during childhood (Rice, 2021). Like in KSHV, transmission can occur vertically from mother to child (James et al., 2014). Primarily, vertical transmission happens during birth but can also occur *in utero* and after birth (Kimberlin, 2007). Postnatal transmission does not occur through breast milk, but rather follows direct person-to-person transmission (i.e. contact with an oral lesion) (Jones et al., 2014).

5.1.3.2 Geographical Distribution

Unlike other human herpesviruses, KSHV has a very particular global distribution (Mariggiò et al., 2017). It is primarily found in sub-Saharan Africa where there is a prevalence of 50%. Prevalence is also elevated in the Mediterranean basin, where it has a seroprevalence of 3-20% (dependent upon specific location) (Dukers and Rezza, 2003, Enbom et al., 2002, Mariggiò et al., 2017). Compared to Europe as a whole, the seroprevalence rates are 2-3 % in adults (Preiser et al., 2001, Mariggiò et al., 2017). There are also higher levels of seroprevalence amongst specific groups, such as those of Jewish decent, the Uighurs of Xinjiang, indigenous American populations and the men who have sex with men community (Fu et al., 2009, Davidovici et al., 2001, Biggar et al., 2000, Melbye et al., 1998, Labo et al., 2015). For HSV1 (which is one of the most common of human infections), global prevalence in 2016 was at 66.6%, infecting over 3 billion people worldwide (James et al., 2020). Africa in particular is badly affected, having the highest percentage seroprevalence of HSV1 per region (87 %) in 2012 (Looker et al., 2015).

5.1.4 Herpesvirus Structure

Herpesviruses have four morphologically different layers that are characteristic amongst all members (Figure 5.2, A). The innermost layer consists of an icosahedral protein capsid which contains the dsDNA genome, with the capsid surrounded by a glycoprotein studded external lipid bilayer. Between the external membrane and the capsid lies a relatively amorphous collection of proteins known as the tegument, which can be further divided into the inner and outer tegument layers based upon their different roles (Dai et al., 2008, Dai et al., 2014). Despite the viral envelope and nucleocapsid being well defined, the tegument layers remain relatively less understood (Sathish et al., 2012).

Herpesviruses have shared common names for the individual protein capsid components. Consequently, in this following paragraph I will list the common names,

with the species specific protein names being found in (Table 5.1). The icosahedral capsid consists of six viral proteins that combine to form the capsid complex. The capsid outer-shell consists of the major capsid protein (MCP), the small capsid protein (SCP) and two triplex proteins (Figure 5.2, B). The MCP forms all of the hexons and eleven penton subunits (Grzesik et al., 2017, Sathish and Yuan, 2010, Trus et al., 2001, Dai and Zhou, 2018). The twelfth penton consists of a unique portal protein that allows for DNA packaging and expulsion and is filled with last-packaged end of the viral genome (Figure 5.2, C) (Dünn-Kittenplon et al., 2021, Gong et al., 2019, Liu et al., 2019). Despite the tegument layer previously being labelled as an entirely amorphous assembly, more recent studies are suggesting that this is not quite the case. The inner tegument layer is tethered to the capsid and as such remains more structured than the outermost layer (Sathish et al., 2012, Dai et al., 2008). Specifically, the capsid vertex-specific component (CVSC) tegument proteins are found on all of the capsid vertices and are especially enriched at the portal vertex where it interacts with the MCP, SCP, triplex heterotrimer and portal vertex (Gong et al., 2019, Dai et al., 2018). The outer tegument layer consists of a cluster of loosely organised viral and host proteins located between the pleomorphic viral envelope and the more structured inner tegument layer (Sathish et al., 2012, Dai et al., 2008). Outer tegument proteins have a variety of roles that range across most stages of the cell cycle. Finally, the herpesvirus virion is encircled by a lipid bilayer that is spiked with a variety of viral glycoproteins. There are five viral glycoproteins that are conserved amongst herpesviruses (gM, gN and the fusion machinery- gH/gL and gB). Additionally, there are five other unique glycoproteins in the KSHV envelope, which are protein ORF4 (pORF), pORF28, pORF45, pORF68 and K8.1A (Chandran, 2010, Dollery, 2019). Whereas, the HSV1 virions contain the gC, gD, gE, gG, gI, gJ and gK glycoproteins, (Jaggi et al., 2018).

Table 5.1: The nomenclature of orthologous herpesvirus structural proteins

Structural proteins from herpes simplex virus 1 (HSV1) and Kaposi's sarcoma associated herpes virus (KSHV). Adapted from table 1, by Döhner et al. (2021)

Viral Component	HSV1	KSHV
Capsid vertex-specific component (CVSC) 1	pU_L25	pORF19
CVSC 2	pU_L17	pORF32
CVSC 3	pU_L36	pORF64
Major capsid protein (MCP)	pU_L19	pORF25
Portal protein	pU_L6	pORF43
Small capsid protein (SCP)	pU_L35	pORF65
Triplex dimer protein 1	pU_L18	pORF26
Triplex dimer protein 2	pU_L38	pORF62

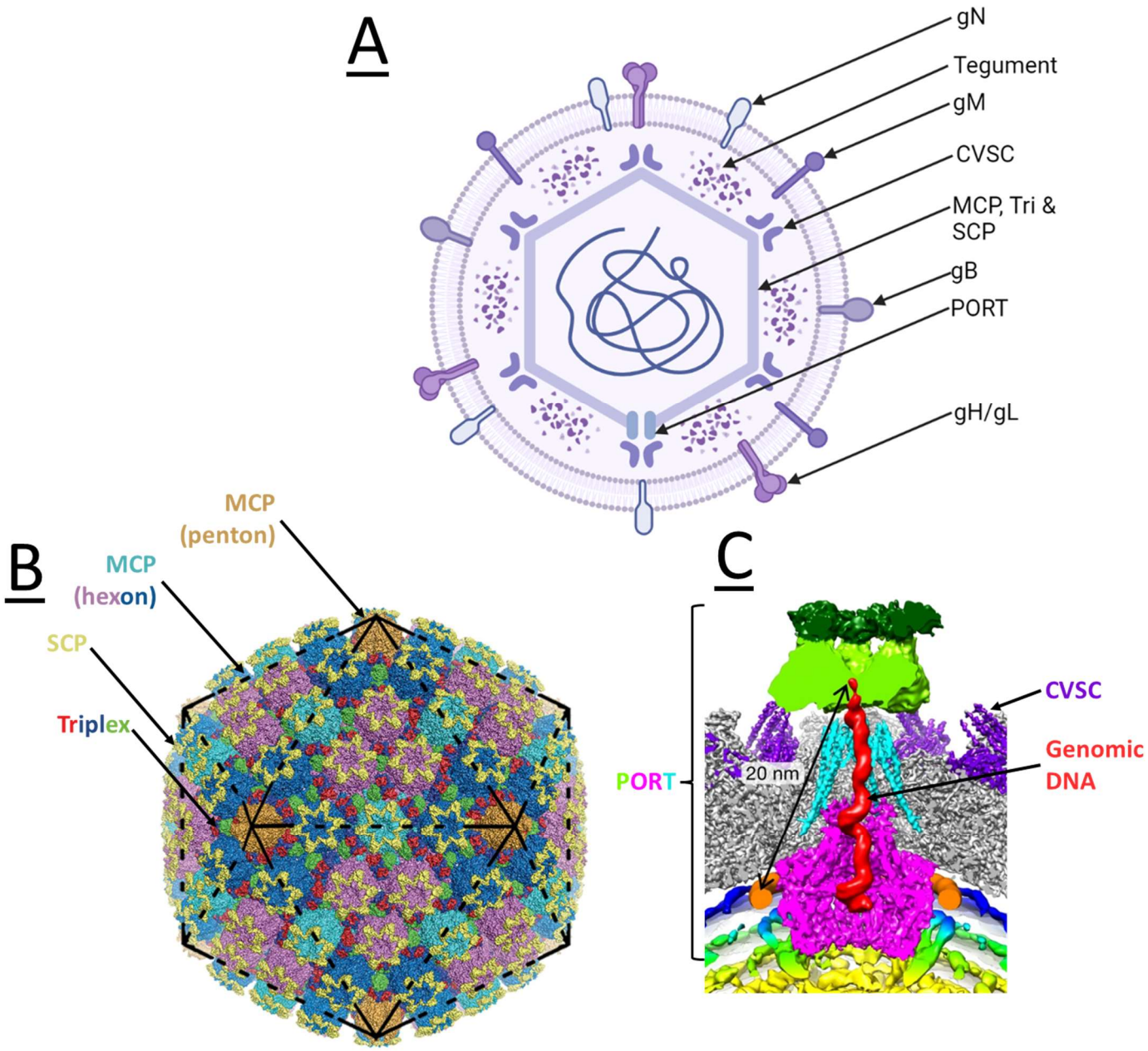

Figure 5.2: An Overview of the herpesvirus virion Structure.

(A) Components of the virion structure from the interior to the exterior: double stranded DNA genome, icosahedral capsid, tegument, lipid envelope, and glycoproteins. The hexons and pentons are formed from the major capsid protein (MCP). The pentons are capped by the small capsid protein (SCP) which cross-link neighbouring MCP subunits in the same hexon. The triplex protein (Tri) is found at the base of the capsid and binds the major capsid subunits. Each herpesvirus capsid has one vertex that is capped by the portal complex (PORT) which acts as a site of entry and exit for viral DNA.Each vertex is capped withcapsid vertex-specific component (CVSC)consisting of inner tegument proteins. Finally, the viral capsid is encircled within a lipid bilayer which is studded with a variety of glycoproteins. There are five glycoproteins that are conserved amongst herpesviruses (gM, gN, gH/gL and gB). This figure was created using BioRender and is based upon figure 1 by Lee et al. (2021). (B) a 3.1 Å cryo-EM structure of the HSV-2 capsid, adapted from figure 1 by Yuan et al. (2018). (C) A 4.3 Å cryo-EM structure of the dodecameric HSV-1 PORT complex, CVSC, and a DNA plug. Adapted from figure 1, D by Liu et al. (2019).

5.1.5 Herpesvirus Genome

Herpesviruses have a large dsDNA genome and possess a characteristic biphasic life cycle consisting of lytic and latent stages that are associated with the expression of distinct groups of genes (Lan et al., 2005).

The KSHV genome is a dsDNA molecule of around 165,000 bp (Arias et al., 2014). The coding region of the genome includes 86 different ORFs which are expressed to produce a number of proteins (pORFs) and microRNAs (miRNAs) (Cornejo-Castro et al., 2020). During latency, the KSHV genome exists in a circular structure known as the episome. There are around 50-100 copies of this episome per latently infected cell (Purushothaman et al., 2016). Despite the KSHV genome sharing gene regions with other herpesviruses, there are also over twenty genes that are unique to KSHV, named K-genes (Figure 5.3) (Veettil et al., 2014). Additionally, there currently exist several distinct KSHV genotypes based upon K-gene variation. The K1 gene has five distinct genotypes (A to E), whereas the K15 gene has been subcategorised into three different genotypes (M, N and P) (Olp et al., 2015). Despite the central genome region being relatively conserved, there are still polymorphisms that have been used to create twelve other KSHV genotypes (Olp et al., 2015).

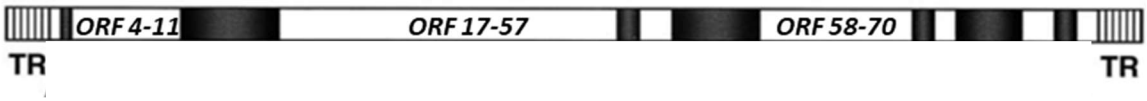

Figure 5.3: A schematic overview of the KSHV genome.

Sections of the genome have been split into regions that are conserved between herpesviruses (white), and regions that are unique to gammaherpesviruses (black). Terminal repeat (TR) regions frame each end. Adapted from figure 2 by Ablashi et al. (2002), and figure 2 by Neipel and Fleckenstein (1999).

The HSV1 genome has around 152,000 bp and is split into long unique (U_L) (82% of the genome) and short unique (U_S) (18% of the genome) sequences (Figure 5.4) (Sandri-Goldin, 2003, Smith et al., 2014). The HSV1 genome encodes over 80 genes, producing proteins (pU_L/pU_S). There are three viral origins of replication, one in the U_L named the OriL and two in the U_S named the OriS (Packard and Dembowski, 2021). The U_L and U_S regions are flanked by the inverted repeat sequences *b* and *c* (respectively), which are in turn flanked by the *a* inverted repeat sequences (Smith et al., 2014). When in the cell, the HSV1 genome exists in linear,

circular, or concatemeric formats depending on the which stage of the viral replication cycle it is in. As the HSV1 genome undergoes replication during lysis it exists as a linear strand, forming head-to-tail and branched concatemers as new genomes are produced. During latency, the HSV1 genome is circularised (Packard and Dembowski, 2021).

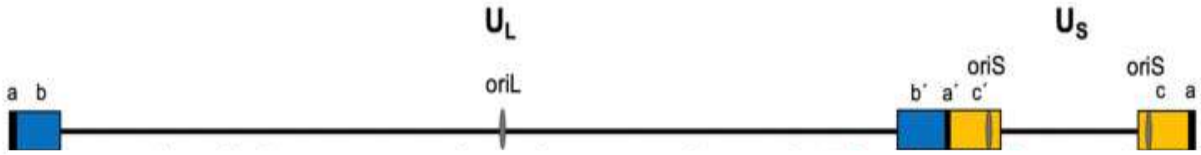

Figure 5.4: A schematic overview of the HSV1 genome

The unique long (U_L) and unique short (U_S) regions encode for over 80 genes and are flanked by the *b* (blue) and *c* (yellow) inverted repeat sequences, respectively. The *b* and *c* inverted sequences are in turn flanked by the *a* inverted repeat sequences. The HSV1 genome has three origins (ori), one in the U_L and two in the U_S. Adapted from figure 1 by Packard and Dembowski (2021).

5.1.5.1 MicroRNAs

miRNAs are found within all metazoan Eukaryotes with humans having more than 200 variations. miRNAs are small (~19-23 nucleotides), non-coding RNAs that act as key regulators of post-transcriptional expression (Kim et al., 2017). Herpesviruses produce miRNAs to silence host genes, augment viral pathogenesis, regulate lytic and latent cycles and supress the host immune system (Grey, 2015). As opposed to proteins, miRNAs offer an attractive solution to combat the innate immunity as miRNAs do not require the large amounts of genetic space that proteins need (Cai et al., 2005, Forte et al., 2015). As viruses are unable to produce their own miRNA, they rely on host cellular machinery (Nanbo et al., 2021). The miRNAs are usually transcribed by RNA polymerase II to produce a pri-miRNA transcript which are then cleaved by the ribonuclease III Drosha to form pre-miRNAs. Next, the pre-miRNAs are exported into the cytoplasm where they are further processed by the RNase III endonuclease Dicer to form the mature miRNA duplex (Pan et al., 2019). These mature miRNAs then bind to the Argonaute family of proteins within the RNA-induced silencing complex (RISC). The mature miRNA then directs the RISC to complimentary mRNA sequences, blocking protein expression through mRNA degradation or translation blocking (O'Brien et al., 2018). If the target mRNA has a

perfect sequence match to the miRNA, it will be cut and degraded by the RISC complex. A less than perfect sequence match leads to multiple RISC binding to the mRNA, preventing translation by blocking ribosomal binding (Cai et al., 2005). Herpesvirus utilise miRNAs to either inhibit protein production, or to reduce protein levels through mRNA destabilisation (Naqvi et al., 2018).

KSHV is known to produce a total of 25 mature viral miRNAs during the latent cycle, which are believed to aid viral replication and pathogenesis (Forte et al., 2015, Mishra et al., 2020). In KSHV, the miRNAs originate from twelve stem-looped pri-miRNA transcripts that are processed to form the mature miRNAs miR-K1 to miR-K12 (Mishra et al., 2020). Like in KSHV, HSV1 encodes 27 of its own miRNAs, which are used during lytic and latent replication to downregulate mRNA translation (Mishra et al., 2020). Different miRNAs are produced depending upon which infection stage HSV1 is in.

5.1.6 Herpesvirus Replication Cycle

The herpesvirus replication cycle begins with the attachment and entry of infectious virions into host cells, which occurs through the interaction of viral glycoproteins with host receptors (Figure 5.5) (Agelidis and Shukla, 2015, Dollery, 2019). Depending upon the specific herpesvirus and cell type, entry is either direct or occurs through endocytosis. Regardless, herpesvirus entry results in the fusion of the viral envelope with the host cell membrane leading to the release of the viral capsid and tegument into the cytoplasm (Kumar and Chandran, 2016, Agelidis and Shukla, 2015). Once within the cytoplasm, the herpesvirus capsid traffics to the nucleus by utilising the microtubule network for retrograde transport to the cell nucleus (Kumar and Chandran, 2016, Striebinger et al., 2016). At the nuclear membrane, the herpesvirus capsid docks at the nuclear pore with the capsid portal through the viral CVSC (Villanueva-Valencia et al., 2021, Dünn-Kittenplon et al., 2021). Once the capsid has docked, the viral dsDNA genome is ejected into the nucleus where it either enters latency related dormancy, or begins lytic replication (Brandariz-Nuñez et al., 2019). Latency is associated with the silencing of viral gene expression and the suppression of host antiviral responses (Broussard and Damania, 2020, Nicoll et al., 2012). Whereas lytic replication sees the expression of immediate-early (IE), early (E) and late genes (LE) culminating in viral genome replication and the production of viral capsids (Broussard and Damania, 2020, Flemington, 2001).

Once the herpesvirus genome has been inserted into the newly produced capsids, progeny nucleocapsids then exit the nucleus. Herpesvirus nucleocapsids exit the nucleus via primary envelopment at the inner nuclear membrane and then de-envelopment at the outer nuclear membrane where they acquire inner tegument proteins (Desai et al., 2012, Arii, 2021). The viral capsid then enters the cytoplasm where it again interacts with the microtubule network to undergo anterograde transport to the site of secondary envelopment (Striebinger et al., 2016, Kumar and Chandran, 2016). The site of secondary envelopment varies per specific herpesvirus, but often includes either Golgi or endocytic derived vesicles (Owen et al., 2015, Krishnan et al., 2005). Nevertheless, secondary envelopment sees the herpesvirus capsid and tegument interact with viral glycoproteins studded within the host membrane. This triggers the budding of the capsid into the membranous vesicle, forming an enveloped virion that is within another host-derived vesicle (Krishnan et al., 2005, Ahmad and Wilson, 2020). This vesicle then traffics to the cell periphery where the vesicular membrane fuses with the outer cell membrane, releasing the newly formed enveloped capsid out of the cell (Krishnan et al., 2005, Ahmad and Wilson, 2020).

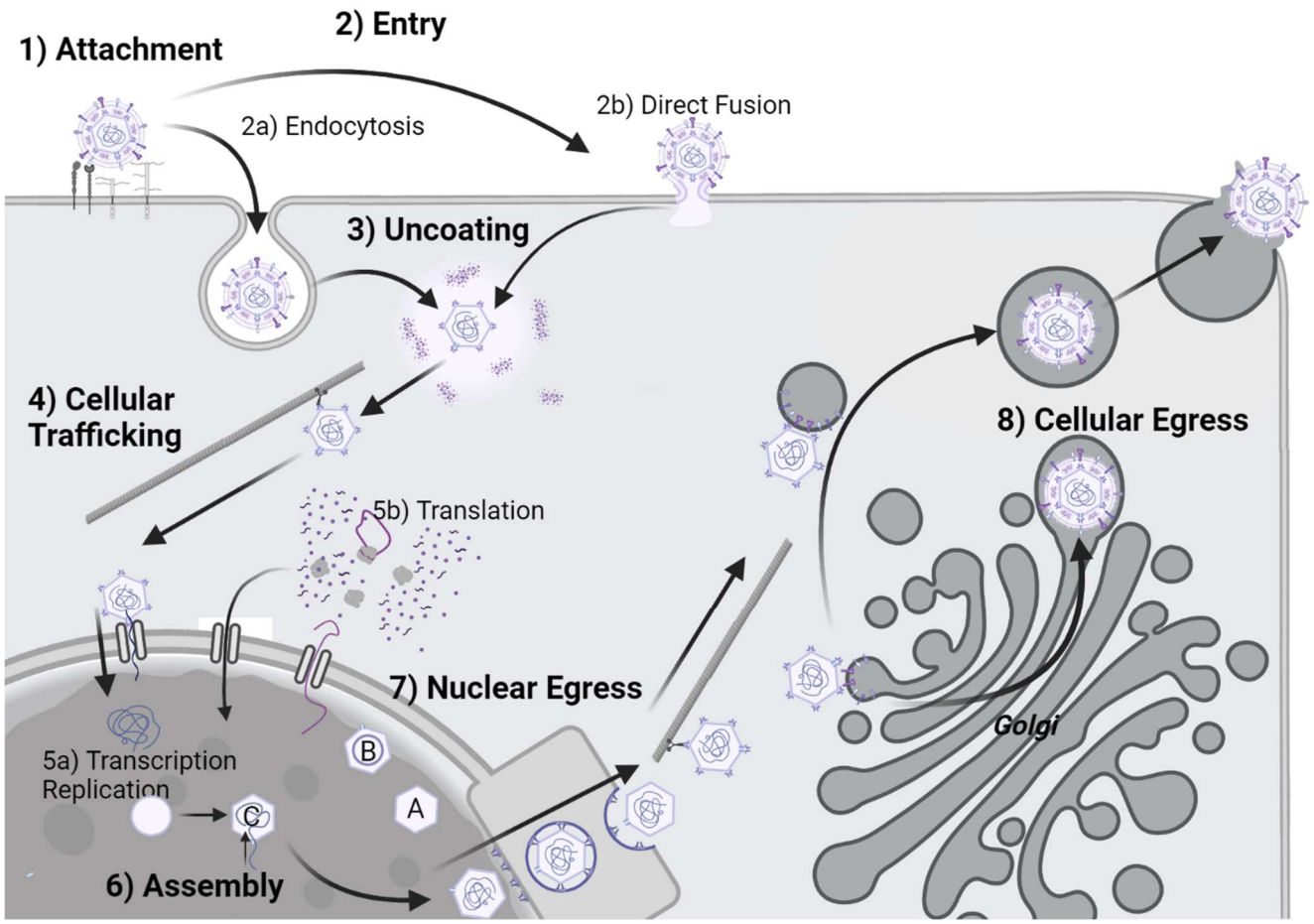

Figure 5.5: A schematic overview of the herpesvirus replication cycle

Herpesviruses use several glycoproteins to facilitate cellular attachment (1) and subsequent entry into the host cell. Upon entry via endocytosis (2a) or direct fusion (2b), the herpesvirus envelope will fuse with cellular membrane (3). This releases the capsid and tegument proteins into the cytoplasm. Inner tegument proteins assist nuclear trafficking via the microtubule dynein system (4). Once the capsid has reached the nucleus, it will inject the viral genome into the nucleus via a nuclear pore. Once the viral genome has entered the nucleus, it will enter latent or lytic replication. Upon lytic activation, viral genome replication and transcription (5a) occur, leading to viral protein production (5b). Viral capsid components are imported into the nucleus to be assembled into procapsids. Once constructed, a viral genome will be inserted into the procapsid, forming the nucleocapsid (6). There are three different types of capsid produced- an empty capsid (A), a capsid containing a ring of viral assembly proteins (B), and a capsid containing the viral genome (C). Nucleocapsids must then leave the nucleus via primary envelopment (7). This envelope is lost as the virus buds into the cytoplasm via the outer nuclear membrane. Next, the cytoplasmic nucleocapsid will bud into a Golgi or endocytic membrane, undergoing secondary envelopment. Afterwards, the capsid will leave the organelle in a host-derived vesicle which will then fuse with the cytoplasmic membrane, allowing for viral egress (8). Figure created using BioRender, based upon figure 2 by Gatherer et al. (2021).

5.1.6.1 Attachment

Once KSHV has come into contact with a susceptible host cell, several viral glycoproteins are responsible for mediating viral binding and entry (Sathish et al., 2012, Dollery, 2019). The main cellular attachment factor for KSHV is the heparan sulphate (HS) proteoglycans, which allows for KSHV concentration upon the cellular surface (Birkmann et al., 2001). The ubiquitous nature of HS explains the broad cellular tropism shown by KSHV when *in vitro* (Kerur et al., 2010). The KSHV glycoproteins gB, gH, gL and K8.1A are responsible for viral attachment as they can bind HS (in a redundant manner) (Subramanian et al., 2010, Dollery, 2019). KSHV is also capable of using the c-type lectin DC-SIGN for attachment onto macrophages, dendritic cells and B-lymphocytes as they lack HS (Jarousse et al., 2008, Rappocciolo et al., 2008). Like in KSHV, HSV1 cell attachment is mediated by the gB glycoprotein which binds to the host HS on the cell surface (Heldwein and Krummenacher, 2008).

5.1.6.2 Entry

The attachment of herpesviruses onto the cell surface allows the virion to interact with the cell-surface receptors needed for entry (Dollery, 2019). KSHV utilises a variety of highly specific entry receptors in different combinations for different cell types (Veettil et al., 2014). The main cellular entry factors for KSHV are integrins. Once KSHV has attached to the target cell through HS, viral glycoprotein conformation changes allowing access to the integrin surface receptors (Veettil et al., 2014). Three integrins, α3β1, αvβ3 and αvβ5, have been implicated with KSHV entry into a number of cell types (Kerur et al., 2010, Akula et al., 2002). Though gB can bind to α3β1, the viral glycoproteins involved in the other integrin binding needs further study (Kerur et al., 2010). Another potential KSHV entry receptor is EphA2, an ephrin receptor. Ephrin receptors make up the principal family of tyrosine kinase receptors and are involved in cell adhesion, actin cytoskeleton assembly, macropinocytosis and clathrin dependent endocytosis (Darling and Lamb, 2019). KSHV glycoproteins gH and gL have been indicated in EphA2 and EphaA4-mediated cellular entry, by binding to each other non-covalently to facilitate binding (Veettil et al., 2014, Hahn et al., 2012, Chen et al., 2019b).

KSHV entry into target cells occurs through endocytosis. There are four different endocytic types: macropinocytosis, phagocytosis, clathrin-mediated and caveolae

mediated endocytosis (Veettil et al., 2014). The mode of entry is dependent upon cell type, with KSHV entering fibroblasts via clathrin-mediated endocytosis. In monocytes, KSHV uses both clathrin and caveolin dependant endocytosis. Macropinocytosis has been linked to the KSHV invasion of endothelial cells (Kerur et al., 2010, Akula et al., 2003, Raghu et al., 2009, Veettil et al., 2014). Once KSHV has been endocytosed, it is still trapped within an endosomal vesicle. A low pH within the endosome is required for membrane fusion and viral release into the cytosol, which is mediated by the herpesvirus core fusion machinery (gH/gL and gB), although the specific glycoprotein interactions are unknown (Kerur et al., 2010, Akula et al., 2003, Raghu et al., 2009, Dollery, 2019). Once membrane fusion has occurred and the KSHV capsid has entered the cell, the different viral tegument layers start to carry out their diverse functions.

In HSV1, entry occurs by one of two mechanisms depending upon the cell type in question (Hilterbrand and Heldwein, 2019). In neuronal cells HSV1 is able to directly fuse with host membranes, whereas in epithelial cells HSV1 utilises the endocytic route (Nicola et al., 2005, Miranda-Saksena et al., 2018). Key to HSV1 entry is its surface glycoproteins. Of its fifteen viral glycoproteins, only four of these are described as essential for cell entry (gD, gH/gL and gB) (Turner et al., 1998). Once gB and gC facilitate cell attachment through HS, gD binds to either 3-O-sulfated-HS, nectin1, or herpes virus entry mediator (Shukla et al., 1999, Krummenacher et al., 2004, Petermann et al., 2015). The attachment of gD to a receptor changes the structure of gD, allowing it to bind to the gH/gL heterodimer, which then triggers gB (Fan et al., 2014). As for all herpesviruses, gB is the fusion protein, which produces the fusion of viral and cell membranes allowing the herpesvirus capsid to enter the cell (Atanasiu et al., 2013, Fontana et al., 2017).

5.1.6.3 Cellular Trafficking

Once the herpesvirus nucleocapsid has entered the cellular cytoplasm, it must transit towards the nucleus. After the nucleocapsid has entered the cytoplasm, the outer tegument layer dissociates from the nucleocapsid and disperses into the surrounding cytoplasm where it interacts with cellular factors (Sathish et al., 2012, Dai et al., 2014). Outer tegument proteins are involved in viral gene activation, immune suppression and virulence (Xu et al., 2016, Full et al., 2014). Whereas the inner tegument layer is responsible for trafficking the nucleocapsid and so remains nearby (Dai et al., 2014). Herpesvirus are known to utilise the host microtubule network as a “rail system”, allowing the nucleocapsids to circumnavigate the cell. When at the

nucleus, the capsid portal connects to a nuclear pore complex (NPC) and inserts the herpesvirus DNA genome into the nucleus (Döhner et al., 2021). In herpesviruses the capsid portal complex and the NPC are aligned through the CVSC (Gong et al., 2019).

KSHV is able to transit to the nucleus via the acetylation of host microtubules through RhoA GTPases which thickens and stabilises the microtubule network (Kumar and Chandran, 2016). In fibroblasts and endothelial cells, KSHV has been found to utilise the microtubule network via dynein motors to reach the nucleus (Naranatt et al., 2005). Upon reaching the nuclear periphery, KSHV is able to insert its DNA into the nucleus through the capsid pore. The capsid pore vertex is comprised of a dodecameric ring of pORF43 and is surrounded by CVSC (Gong et al., 2019). The CVSC and portal complex proteins dock at the host NPC, injecting the viral genome into the nucleus at high pressure (Dünn-Kittenplon et al., 2021, Bauer et al., 2013). Once within the nucleus, viral replication can begin.

Like in KSHV, HSV1 co-opts the host microtubule system and uses dynein and its cofactor dynactin for retrograde transport to the nucleus (Döhner et al., 2002). HSV1 uses the inner tegument protein pU_L36 and pU_L37 to recruit the host motor proteins needed for intracellular transport (Sandbaumhüter et al., 2013). When the HSV1 capsid has arrived at the nucleus, the CVSC proteins interact with the NPC in a similar manner to KSHV. In HSV1, the CVSC protein pU_L25 and pU_L36 are able to interact with the nucleoporins (components of the NPC) and align the capsid portal with the NPC (Pasdeloup et al., 2009, Abaitua et al., 2012, Villanueva-Valencia et al., 2021). When correctly aligned, the HSV1 genome can be forcefully ejected into the nucleus (Sandbaumhüter et al., 2013). Not only is pU_L25 involved in the HSV1 NPC docking, but it has been further implicated in the insertion of the HSV1 genome into the nucleus. When a HSV1 mutant strain with a truncated pU_L25 infected cells, capsids were found to localise at the NPC but were unable to insert their genomes into the nucleus, implicating pU_L25s role in genome insertion (Huffman et al., 2017).

5.1.6.4 Replication, Transcription, and Translation

5.1.6.4.1 Latent Genome Replication

After KSHV has successfully infected a cell, it enters a latent state where the viral genome exists as an episome within the host nucleus. The episome exists separately from host DNA as a minichromosome associated with cellular histones (Toth et al., 2013). The KSHV viral genome needs to be replicated during both lytic

and latent cycles so that a copy of the episome is available for each daughter cell during mitosis (Ballestas et al., 1999). As such, the viral genome is replicated once per cell cycle in latently infected cells. LANA is required for genome maintenance and for the portioning of viral episomes into the two daughter cells (Ye et al., 2004). LANA acts as a tether, binding the KSHV episome to the cellular chromatin. LANA achieves this by binding to the viral episome terminal-repeat region within its C-terminus and by attaching to a linker histone (H1) with its N-terminus (Ballestas and Kaye, 2001). By tethering the episome to host DNA, LANA ensures that each progeny cell carries a copy of the viral episome. Furthermore, LANA recruits several cellular proteins involved in DNA replication to the origin of latent DNA replication (ori-P) at the terminal repeat region of the episome. The ori-P has two LANA binding sites, allowing LANA to attach directly to the ori-P with its terminal repeat binding domain (Grundhoff and Ganem, 2003, Hu et al., 2002). Once bound, LANA recruits the host proteins needed to establish the pre-replication complex, initiating KSHV latent DNA replication alongside host DNA replication. The pre-replication complex includes the host origin replication complex (ORC), cell division cycle 6 (cdc6), Poly(ADP-ribose)polymerase-1 (PARP1) and minichromosome maintenance proteins (MCMs) and other host factors necessary for DNA replication (Ballestas and Kaye, 2011, Verma et al., 2006, Dabral et al., 2019).

HSV1, like other alphaherpesviruses establishes latent infections in nonreplicating neuronal cells. Like in KSHV, the HSV1 genome forms a circular episome within the cell nucleus (Cohen, 2020). Unlike KSHV, HSV1 does not need to replicate its genome as it establishes latency in non-dividing cells (Nicoll et al., 2012).

5.1.6.4.2 Lytic Genome Replication

During lytic infection, the mechanism of viral genome replication is conserved between different herpesviruses, although replication initiation can vary (Weller and Coen, 2012). In herpesviruses, lytic replication is believed to proceed via a rolling circle mechanism, where a continuous genomic concatemer is produced (Mapelli et al., 2005). This concatemer is then split into separate genomes as it is packaged into progeny capsids (Weller and Coen, 2012).

Once the lytic cycle has been activated, the KSHV genome has to be rapidly replicated so that it can be packaged into progeny capsids. Unlike latent DNA replication, lytic DNA replication occurs at the lytic origin (ori-Lyt) (Purushothaman et al., 2015, Lin et al., 2003). Interestingly, the replication of the KSHV genome during the lytic cycle uses a variety of cellular and viral proteins due to the expression of viral proteins associated with lytic replication (Aneja and Yuan, 2017). Lytic genome replication is initiated when Rta binds to the ori-Lyt, which triggers the recruitment of

the pre-replication complex (Wang et al., 2003) The pre-replication complex in lytic infection includes at least eight viral proteins that includes but is not limited to Rta (master regulator), K8, a viral helicase, a viral DNA polymerase and a viral primase (Wang et al., 2006, AuCoin et al., 2004). Viral DNA replication forms a continuous DNA concatemer, which is then cleaved into individual KSHV genomes as it is inserted into progeny capsids (Gardner and Glaunsinger, 2018).

The infection of cells with HSV1 is associated with the formation of large replication complexes within the nucleus which are believed to be sites of viral genome replication, transcription, concatemer cleavage and genome packaging (Weller, 2010). HSV1 encodes a number of viral proteins that are involved in genome replication, with six of these being conserved amongst other herpesviruses. Of these six conserved proteins there is a ssDNA binding protein (pU_L29), a two subunit DNA polymerase (pU_L30-pU_L42) and a three-subunit helicase and primase complex (pU_L5-pU_L8-pU_L52). HSV1 also encodes an extra origin binding protein pU_L9 which is not found in KSHV (or other beta- and gammaherpesviruses) (Weller and Coen, 2012, Packard and Dembowski, 2021). In HSV1, DNA replication begins at one of the three viral origins of replication (OriL, or one of the two OriS's). At one of the origins, the origin binding protein pU_L9 and ssDNA binding protein pU_L29 bind to and unwind the A-T rich region (Makhov et al., 2003, Aslani et al., 2002). The splitting of the dsDNA and subsequent exposure of ssDNA is believed to cause pU_L29 to detach from pU_L9 and bind to the ssDNA, preventing the re-annealing of the strands (Manolaridis et al., 2009, Weller and Coen, 2012). Next, the helicase and primase complex pU_L5-pU_L8-pU_L52 is recruited. The complex binds to the ssDNA made by pU_L29 and pU_L9 and further unwinds the viral DNA whilst producing short RNA primers to allow for polymerase binding (Chen et al., 2011). Finally, the two subunit DNA polymerase pU_L30-pU_L42 is recruited to the replication fork by the active primase and begins leading and lagging DNA synthesis (Carrington-Lawrence and Weller, 2003, Stengel and Kuchta, 2011).

5.1.6.4.3 Transcription

Herpesviruses in general are known for establishing latency in cells. Latency is typically associated with the cessation of viral expression and virion production, with lysis being associated with the opposite (Nicoll et al., 2016). Viral gene expression is limited in the latent stage due to the methylation of the KSHV genome. Methylation causes the viral genome to transition from euchromatin to heterochromatin, preventing gene expression (Toth et al., 2013). In this state, only a small number of the 90 viral ORFs are needed to continue latency (Pearce et al., 2005, Chudasama

et al., 2015). There are four main KSHV proteins that are regularly identified in latently infected cells, kaposin (encoded by ORFK12), v-FLIP (ORF71), v-Cyclin (ORF72) and LANA (ORF73) (Pearce et al., 2005, Garrigues et al., 2017, Talbot et al., 1999). Expression of these genes is believed to lead to host cell proliferation, viral genome maintenance, immune evasion and apoptosis prevention (Pearce et al., 2005).

The lytic cycle in KSHV is associated with the release and propagation of progeny viruses (Talbot et al., 1999). Internal and external stimuli such as hypoxia, oxidative stress and viral-coinfection can induce the KSHV lytic sequence (Purushothaman et al., 2015). Induction of KSHV results in the relaxation of the viral episome, which allows for viral protein expression (Purushothaman et al., 2016). Upon viral induction, the majority of viral genes are expressed in a sequential manner (IE, E and L), leading to production of viral progeny (Verma et al., 2015). The switch from the latent to the lytic cycle is controlled by the viral replication and transcriptional activator known as Rta (Aneja and Yuan, 2017). This IE activator is required for lytic replication and is conserved within all γ2-herpesviruses (Goodwin et al., 2001). Rta is the first gene to be expressed after the stimulation of the lytic cycle and once Rta expression is activated it is able to upregulate itself via a positive feedback loop, resulting in lytic cascade (Purushothaman et al., 2016, Deng et al., 2000). The lytic cascade triggered by Rta results in the expression of the IE, E and L genes allowing for viral genome replication and virion production (Combs et al., 2022).

In HSV1 latency, viral transcription is mainly limited to the latency-associated transcript (LAT). As HSV1 establishes latency within non-dividing neurones, no protein tether is expressed (Cohen, 2020). The LAT is spliced into one minor LAT exon (6.3 kb) and two major LAT introns (1.5 and 2 kb) that are processed into several miRNAs (Nicoll et al., 2016). These miRNAs are used by HSV1 to inhibit the expression of lytic IE genes (e.g. ICP0), dampening the entirety of HSV1 genome expression (Mador et al., 1998, Nicoll et al., 2012). LAT products also have a role in cell apoptosis inhibition which prevents virally-triggered cell death (Thompson and Sawtell, 2001).

In HSV1, lytic gene transcription is orchestrated in a temporal cascade, with IE, E and L genes being transcribed by host RNA polymerase II (Packard and Dembowski, 2021). Of the proteins expressed, HSV1 produces two viral transcription factors that activate the different gene groups. IE transcription is initiated by the tegument protein VP16 which is released into the cytoplasm as the virus enters the cell (Fan et al., 2020). VP16 is transported to the nucleus by binding to the host cell factor 1 in the cytoplasm which has a nuclear localisation sequence (Nicoll et al., 2012). The

transcription of the IE genes results in the expression of the next HSV1 transcription factor, ICP4. ICP4 activates transcription of the E and L genes by recruiting host factors (e.g. the TATA binding protein) (Chaturvedi et al., 2020). Viral genome replication is dependent upon the expression of E genes, which allow for the establishment of replication compartments by expressing viral replication machinery genes (Taylor et al., 2003). Once the HSV1 genome has been replicated, the expression of L genes will be triggered by a currently unknown mechanism. HSV1 structural proteins (e.g. capsid proteins and glycoproteins) are encoded by the L genes, so genome replication triggers the production of progeny virions (Gruffat et al., 2016, Packard and Dembowski, 2021).

5.1.6.4.4 Translation

Most viruses, including herpesviruses, are able to inhibit host protein translation through viral factors.

The main mechanism used by KSHV to inhibit protein expression is the shutoff and exonuclease (SOX) protein (Pardamean and Wu, 2021). The SOX lytic protein is able to prevent the nuclear export of mRNA and also triggers mRNA degradation within the cytoplasm (Glaunsinger and Ganem, 2004). SOX is able to breakdown mRNA by interacting with a host exonuclease. First, SOX cleaves the mRNA internally with its endonuclease activity and then the cleaved fragments are broken down by the cellular exonuclease Xrn1 (Covarrubias et al., 2011). The other aspect of SOX inhibition of host expression is its ability to trap host mRNA within the nucleus. SOX sequesters mRNA within the nucleus through the indirect hyperadenylation of mRNA transcripts, which prevents nuclear export. Furthermore, like in rotavirus, KSHV SOX is able to trap the host PABP within the nucleus, further limiting host expression (Lee and Glaunsinger, 2009). Interestingly, SOX also targets viral mRNA expression, leading to the hypothesis that SOX is also used to fine-tune viral gene expression (Abernathy et al., 2014).

HSV1 has also evolved several ways to subvert host expression and facilitate viral protein production. One example of this is the HSV1 virion host shutoff (VHS) RNase which is able to moderate host translation (Dauber et al., 2011). VHS is a tegument protein that is able to breakdown both viral and host mRNA through associating with the eIF4F translation initiation complex which binds to mRNA 5’ caps (Page and Read, 2010). The activity of VHS is primarily limited to the IE and E lytic stages of HSV1 infection, with VHS activity being reduced by VP16 and VP22 during L stages to allow for viral production (Knez et al., 2003). Not only does VHS shut down host

expression, but it is also essential for the expression of HSV1 L genes as it prevents the accumulation and overwhelming of host translational machinery with host mRNA, or viral mRNA from earlier stages of infection (Dauber et al., 2014). Another way in which HSV1 can augment viral protein expression is through the inhibition of host translation shutdown (Banerjee et al., 2020). Host cells can use cellular kinases to stop translation through the phosphorylation of eIF2α in a bid to halt viral expression (Samuel, 1993). HSV1 is able to prevent this through gB, ICP34.5 and US11 which direct the dephosphorylation of eIF2α (Mulvey et al., 2007, Dauber et al., 2014)

5.1.6.4.5 Herpesviruses and miRNAs

miRNAs are a particularly effective tool for viruses that have a strong emphasis on latent infection (Skalsky and Cullen, 2010). To successfully establish long term latent infections, immune evasion is key. Therefore, the production of miRNAs (which can also directly inhibit the immune system) instead of potentially antigenic viral proteins is evolutionary advantageous (Skalsky and Cullen, 2010). Despite the focus on latent infection, there are also miRNAs involved in lytic replication (Hussein et al., 2019).

One example of a lytic KSHV miRNA is miR-K10. The miRNA miR-K10 shares its mRNA binding sites and sequences with the cellular miR-142-3 and so it is believed to regulate the same gene product (Gottwein et al., 2011). miR-K10 is known to inhibit apoptosis in target cells by preventing TweakR expression, a receptor involved in apoptosis (Chao et al., 2013). Therefore, production of the miR-K10 allows KSHV to prevent planned cell death, circumventing this host defence mechanism. Not only is KSHV capable of producing its own miRNAs, it is also capable of manipulating the expression of host produced miRNAs (Wu et al., 2011; O'Hara et al., 2009). Whereas the production of KSHV encoded miRNAs is associated with latency, manipulation of cellular miRNA is utilised during the lytic cycle. KSHV has been found to downregulate the expression of tumour-suppressing cellular miRNAs miR-221 and miR-222 (Qin et al., 2014). Both miR-221 and miR-222 are involved in angiogenesis and increased endothelial cell migration, which are important factors in tumour development and metastasis (Song et al., 2017).

Similarly, in HSV1 infection miRNAs are utilised for a variety of functions. HSV1 is able to inhibit lytic genes during latency through the viral miRNAs miR-H2-3p and miR-H6 (Mishra et al., 2020). These miRNAs are derived from the LAT and are able to inhibit the HSV1 mRNA transcripts for the IE protein ICP4 (Umbach et al., 2008, Duan et al., 2012). As mentioned earlier, ICP4 is an essential transcription factor that triggers the expression of E and L genes (Chaturvedi et al., 2020). Furthermore, HSV1 is able to induce the expression of the host miR-23a to aid in viral replication (Ru et al., 2014). miR-23a is able to inhibit the IFN pathway which is heavily involved

in the innate antiviral immune response, therefore aiding in HSV1 infection (Yan et al., 2016).

5.1.6.5 Assembly

During the lytic viral cycle, multiple viral proteins are assembled within the nucleus to form the capsid complex. Upon capsid assembly, the viral genome is inserted into the herpesvirus capsid interior (Grzesik et al., 2017). In herpesviruses, the initial, empty capsid is known as the procapsid. The procapsid is spherical and porous, as opposed the final capsid which is angular and sealed (Brown and Newcomb, 2011). The herpesvirus procapsids are packaged with DNA and cleaved by proteases to form one of three capsid types named A to C (Heming et al., 2017). The three different capsids vary on their contents when imaged through EM, with type A-capsids having empty shells that are abortive due to their lack of DNA. The same can be said of type B-capsids, which only contain a ring of SCAF and no DNA. Whereas type C-capsids contain DNA and so are considered to be a precursor to the fully infectious final virion (Heming et al., 2017, Deng et al., 2008, Tandon et al., 2015, Li and Yu, 2020).

In herpesviruses, the capsid capsomere hexons and pentons are formed from the MCPs, which are guided by the SCAF protein (pORF17.5/pU$_L$26.5) (Sathish and Yuan, 2010, Heming et al., 2017). The triplex proteins 1 and 2 connect the capsomeres together along with the SCP which interacts with MCP to decorate the surface. Both the triplex proteins and SCP are essential for capsid shell construction (Perkins et al., 2008). Additionally, in KSHV capsid assembly has been found to be dependent upon the CVSC component pORF19, with its knockdown resulting in the absence of assembled capsids (Naniima et al., 2021). Unlike in KSHV, the CVSC component pU$_L$25 is not required for capsid assembly, it does however play a role in HSV1 DNA encapsidation (McNab et al., 1998). The herpesvirus procapsid is assembled upon the SCAF protein. This scaffolding is later cleaved by the viral protease PRO (pORF17/ pUL26) and removed, leading to the formation of the final capsid (Deng et al., 2008).

Upon capsid assembly, the recently replicated viral genome must be inserted into the capsid, resulting in the formation of the nucleocapsid. In herpesviruses the viral DNA is inserted through the portal-complex (pORF43/ pU$_L$6) (Sathish et al., 2012, Deng et al., 2007, Liu et al., 2019). Additionally, pORF68 has recently been identified as essential for viral genome insertion in KSHV. It is believed that pORF68s DNA

binding and nuclease activity allows for the cleavage of the viral genome during encapsidation (Gardner and Glaunsinger, 2018). For the HSV1 DNA to be inserted into the procapsid, a complex of viral proteins are needed to cleave and package the concatemeric DNA. In HSV1, pU_L15, pU_L28 and pU_L33 form the terminase complex, with the endonuclease activity of pU_L15 cleaving the DNA (Hodge and Stow, 2001, Heming et al., 2017). The terminase complex and bound viral DNA then interact with the pU_L6 portal, where pU_L15 begins to insert the viral DNA into the procapsid (Yang et al., 2009, Wills et al., 2006). The insertion of viral DNA into the procapsid activates the protease pU_L26, resulting in SCAF cleavage and capsid maturation (Heymann et al., 2003, Heming et al., 2017). Once packaged within the capsid, the herpesvirus genome is sealed within by the viral pentameric cap protein pORF19/ pU_L25 (Naniima et al., 2021, Liu et al., 2019).

5.1.6.6 Nuclear Egress

Once the herpesvirus nucleocapsid has been assembled, it gains its primary envelope from the nuclear membrane as it exits the nucleus (Sathish et al., 2012). As the herpesvirus nucleocapsids are too big (~125nm in diameter) to transit through the nuclear pores, they must exit via budding. Firstly, the nucleocapsid must be recruited to the nuclear membrane, where it enters the perinuclear space. This results in the formation of enveloped nucleocapsids contained within the inner nuclear membrane. This membrane allows for the nucleocapsid to fuse with the outer nuclear membrane, resulting in the nucleocapsid entering the cytoplasm (Sherry et al., 2017).

The proteins involved in nuclear egress have been extensively studied in alpha and beta herpesviruses, but less-so in gamma herpesviruses. All herpesviruses possess a heterodimeric complex known as the nuclear egress complex (NEC) which facilitates nuclear egress. In KSHV the NEC is formed from pORF67 and pORF69 (Santarelli et al., 2008, Luitweiler et al., 2013, Lv et al., 2019a). pORF67 alone is capable of inducing host membrane proliferation, resulting in the formation of duplicated nuclear membrane tubules (Luitweiler et al., 2013, Desai et al., 2012). When pORF67 is combined with pORF69 in insect co-expression studies, the tubule structures form virion-sized vesicles that are limited to the nuclear margins (Lv et al., 2019a, Desai et al., 2012). These vesicles are predicted to contain nucleocapsids in actual viral infection, allowing KSHV to exit the nucleus. Upon fusion with the outer nuclear membrane the KSHV nucleocapsid loses its primary envelope and enters the cytoplasm.

In HSV1, the process in better studied. The NEC in HSV1 is composed of pU_L31 and pU_L34 and plays a similar role to the NEC in KSHV, with knockdowns of either protein resulting in failed nuclear egress (Johnson and Baines, 2011, Chang et al., 1997, Roller et al., 2000). The NEC protein pU_L34 is a membrane protein that accumulates on the inner nuclear membrane, whereas pU_L31 is soluble and interacts with pU_L34 to remain nearby (Reynolds et al., 2001, Shiba et al., 2000). Before the HSV1 nucleocapsid can interact with the NEC, it must first disperse the lamina network that coats the inner nuclear membrane (Arii, 2021). The lamina network is composed of lamins which are members of the intermediate filaments and are involved in several nuclear functions in addition to providing structural support (Gruenbaum et al., 2003). HSV1 is able to locally disrupt the lamina network through the activity pU_L34 and viral kinases. pU_L34 recruits the host protein kinase C to the nuclear rim where it phosphorylates lamin B, leading to lamina dissociation (Park and Baines, 2006). Further lamina disruption occurs through the viral kinase pU_S3 which phosphorylates lamin A and lamin C (Bjerke and Roller, 2006, Mou et al., 2007).

Once the lamina has been disrupted, the HSV1 nucleocapsid interacts with the NEC through the CVSC (pU_L25) to bud into the perinuclear space (Yang and Baines, 2011, Yang et al., 2014, Draganova et al., 2020). Primary envelopment is driven by the NEC and results in a vesicle containing a hexagonal lattice of NEC and the HSV1 nucleocapsid (Bigalke and Heldwein, 2015, Bigalke et al., 2014, Thorsen et al., 2021). Interestingly, HSV1 utilises the host ESCRT-III for vesicle scission during primary envelopment (Arii et al., 2018). The final step in nuclear egress is de-envelopment, where the viral nuclear envelope fuses to the outer nuclear membrane releasing a membraneless HSV1 capsid into the cytoplasm. The viral protein kinase pU_S3 is involved in de-envelopment, indicating that phosphorylation may play a role (Klupp et al., 2001). Once within the cytoplasm, the HSV1 nucleocapsid can progress towards the cytoplasmic membrane.

5.1.6.7 Cellular Egress

Upon entry into the cytoplasm, the nucleocapsid incorporates a variety of tegument proteins along with its final site of secondary envelopment (Sathish et al., 2012, Aneja and Yuan, 2017). After the KSHV particle has exited the nucleus, it acquires several tegument proteins. One tegument protein which is hypothesised to play a particularly important role as a tegument hub is pORF64 (Aneja and Yuan, 2017, Rozen et al., 2008). pORF64 is capable of interacting with a number of other

tegument proteins, capsid proteins and also glycoproteins (Rozen et al., 2008). This has led to predications that pORF64 is involved in the localisation of the KSHV nucleocapsids to the Golgi-derived vesicles for secondary envelopment (Aneja and Yuan, 2017). The recruitment of particular tegument proteins can be dependent upon other tegument proteins. For example, the knock-down of pORF33 or pORF38 resulted in the loss of pORF45 (Wu et al., 2016, Gillen and Zhu, 2021). Tegument proteins have been further implicated in KSHV transport around the cell. The pORF45 tegument protein was found to interact with the kinesin-2 motor protein to facilitate anterograde transport along the microtubule network (Sathish et al., 2009). The microtubule system allows KSHV particles to travel from the perinuclear region to either the Golgi-derived vesicles for secondary envelopment, or to the cell periphery for cellular egress, respectively (Sathish et al., 2012, Sathish et al., 2009).

The secondary membrane envelopment event occurs when the KSHV nucleocapsid buds into the endosomal or Golgi membrane. Secondary envelopment in KSHV transpires specifically at membrane-bound lipid rafts, where viral glycoproteins are enriched. The outer tegument protein pORF45 has been found to facilitate KSHV budding and egress by binding to lipid rafts within the endosomal or Golgi membranes (Wang et al., 2015). Once the KSHV virion has undergone secondary envelopment, the enveloped capsid will transit to the cell periphery within a temporary vesicle. The final stage in the herpesvirus life cycle is the exiting of the virion from the infected cell via a membrane-fusion event known as budding (Sathish et al., 2012). In KSHV, relatively less is known about this process when compared to other herpesviruses. However, during egress the KSHV virion loses its outermost vesicle membrane and the fully infectious enveloped KSHV virion is released from the cell (Mettenleiter, 2004).

In HSV-1, the process of secondary envelopment and exocytosis is a complex, multistep process that involves a variety of host and viral proteins. Once in the cytoplasm, the HSV1 nucleocapsid recruits the outer tegument proteins. The inner tegument and CVSC member pU_L36 is responsible for recruiting and binding the outer tegument protein pU_L48 which then interacts with pU_L46, pU_L47 and pU_L49 (Owen et al., 2015, Vittone et al., 2005). Similarly to when the HSV1 nucleocapsid first enters the cell cytoplasm, the progeny virus uses the microtubule network to travel to the cell periphery. This time HSV1 co-opts kinesin rather than dynein for anterograde transport, with herpes infection causing disruption to the microtubule network (Naghavi et al., 2013, Miranda-Saksena et al., 2018, Diefenbach et al., 2002). The inner tegument proteins pU_L36 and pU_L37 are needed for microtubule navigation, as occurs during entry, with pU_L36 and pU_L37 recruiting and binding to kinesin 1 and 2 (Radtke et al., 2010, Sandbaumhüter et al., 2013). Specifically,

pU_L37 interacts with the microtubule network whereas pU_L36 is responsible for recruiting pU_L37 to the cytoplasmic nucleocapsid (Sandbaumhüter et al., 2013). HSV1 nucleocapsids use the microtubules network to travel to the sites of cytoplasmic envelopment, where they gain their viral envelope (Ahmad and Wilson, 2020).

The location of secondary envelopment in HSV1 has been subject to much debate, with locations such as the Golgi, trans-Golgi network and endocytic tubules (to name a few) potentially implicated (Henaff et al., 2012, Turcotte et al., 2005, Hollinshead et al., 2012, Owen et al., 2015). Regardless of which organelle HSV1 undergoes secondary envelopment in, HSV1 uses pU_L37 to bind to gK (pU_L20) within the host membrane (Pasdeloup et al., 2010, Chouljenko et al., 2016, Jambunathan et al., 2014). Once bound, the nucleocapsid buds into the viral glycoprotein studded, membranous organelle, utilising the host ESCRT complex for vesicle curvature, scission and sealing (Barnes and Wilson, 2019). Tegument proteins play an important role in bridging the gap between capsid proteins, other tegument proteins and the cytoplasmic tails of the lipid-bound viral glycoproteins (Owen et al., 2015). Once enveloped, the HSV1 virion traffics to the cell surface within host vesicles, likely utilising the cell secretory pathway (Miranda-Saksena et al., 2009, Hogue et al., 2014). Once at the outer membrane, HSV1 virions exit the cell, losing the outermost vesicle membrane (Ahmad and Wilson, 2020).

5.1.7 Chapter Aims

The herpesvirus life cycle has been well studied, however specific mechanisms that occur during infection remain unknown (Chang et al., 1994, McMahon et al., 2020). Previous work from Christopher Owen and Sophie Schumann (unpublished) from the Whitehouse laboratory found that KSHV upregulates the host miRNA miR-365a-3p (Owen, 2015). miR-365a-3p binds to and inhibits DOCK5 mRNA, downregulating DOCK5 production during KSHV lytic infection (Figure 5.6). When the inhibition of DOCK5 was interrupted through the use of the miRIDIAN microRNA hairpin inhibitor hsa-miR-365a-3p (Figure 5.6), the KSHV capsid protein SCP was found to accumulate within the cytoplasm through immunofluorescence microscopy (Figure 5.7). This indicated that DOCK5 inhibition by KSHV plays an important role in KSHV egress (Owen, 2015).

The DOCK (Dedicator of Cytokinesis) group is one of two families of guanine nucleotide exchange factors (GEFs), which activate the Rho family of GTPases by converting GDP to GTP. Rho GTPases are involved in the regulation of cell motility,

polarity and cytoskeleton reorganisation (Hodge and Ridley, 2016, Laurin and Côté, 2014). There seems to be no clear defined function assigned to DOCK5 as it has been scarcely studied. But research so far suggests that it has a role in microtubule and actin regulation (Ogawa et al., 2014, Vives et al., 2011). Interestingly, this is not the first time that DOCK5 has been implicated in viral replication. Forst et al. (2017) found through a cell-based gene-expression study that influenza A modified the expression of DOCK5 within infected cells. Furthermore, when DOCK5 was knocked down through CRISPR/Cas9, there was a reduction in the production of influenza virus. They additionally identified that DOCK5 is involved in gene regulation that moderates several important cellular processes (e.g. Golgi-vesicle transport, pre-mRNA processing and host defence) that influenza replication is dependent upon (Forst et al., 2017). The conclusion that DOCK5 regulates genes expression was similarly identified by Xu et al. (2017). The researchers suggested that DOCK5 and Rac1 control the expression of various genes through indirect phosphorylation events. When DOCK5 was inhibited, it resulted in multiple signalling cascades that caused rupture of lens cataracts in a mouse model (Xu et al., 2017). Besides influenza and KSHV, there is no other mention of DOCK5 being associated with viral infection. The aim of this chapter is to utilise the higher resolving power of TEM to elucidate further detail about the herpesvirus egress process (e.g. the structure and location of the trapped viral capsids) to identify if DOCK5 plays a role in KSHV and/or HSV1 egress.

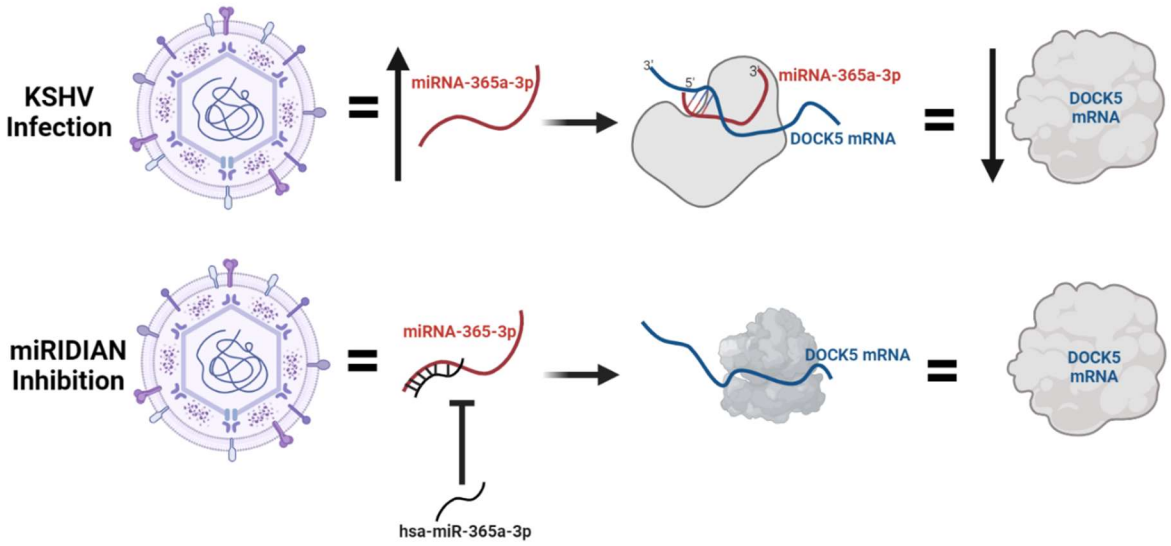

Figure 5.6: The proposed mechanism of KSHV inhibition of Dock5.

A schematic representation demonstrating KSHV upregulating the host microRNA (miRNA) miR-365a-3p, which inhibits DOCK5 mRNA, leading to a decrease in DOCK5 expression. This process can be averted through the use of the miRIDIAN microRNA hairpin inhibitor hsa-miR-365a-3p, which inhibits the complimentary host miRNA miR-365a-3p, preventing it from downregulating DOCK5 expression, resulting in normal DOCK5 levels. Figure made using BioRender.

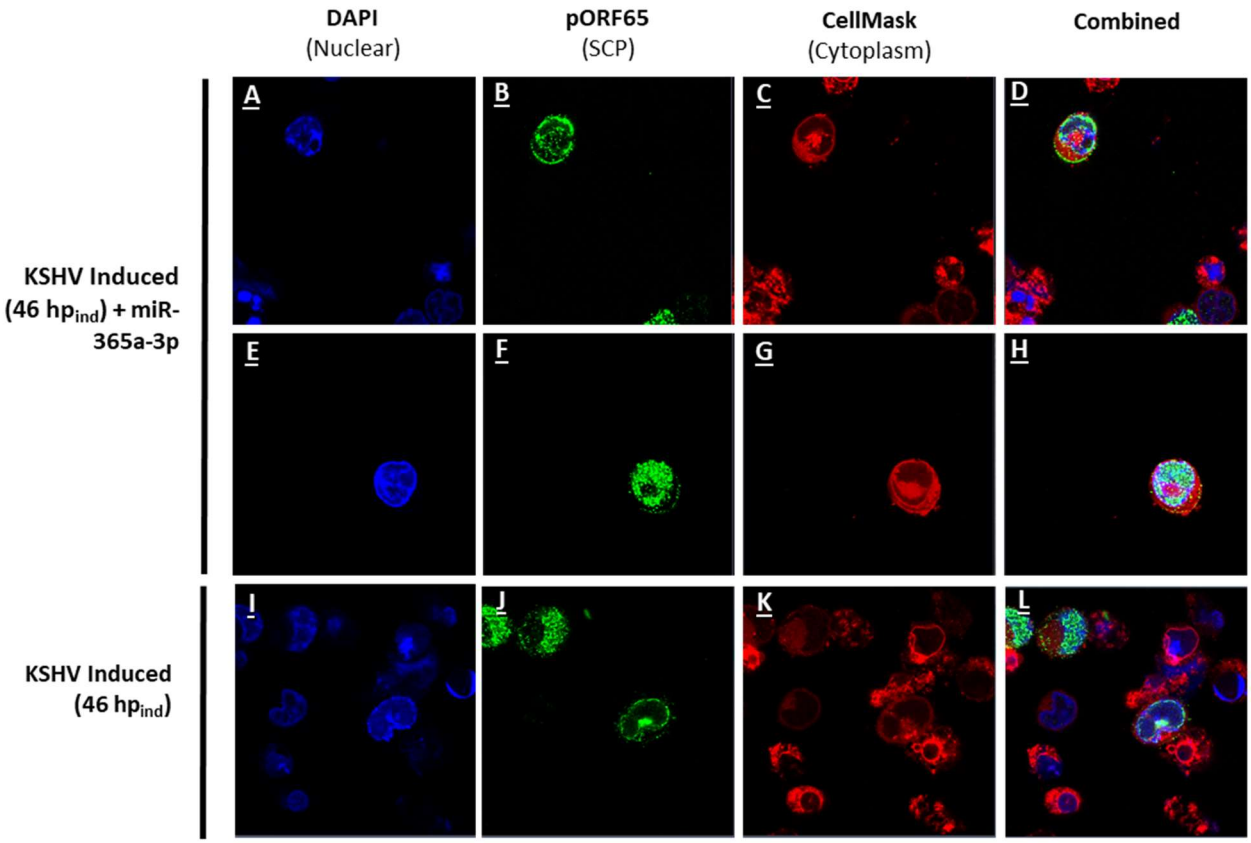

Figure 5.7: miRIDIAN treatment of induced cells at 46 hp_{ind} results in the sequestering of KSHV SCP within the cell cytoplasm periphery

KSHV latently infected TREx BCBL1-Rta cells were transfected with miRIDIAN microRNA hairpin inhibitor hsa-miR-365a-3p via electroporation and were induced with 2.0 µg/ml doxycycline and incubated for 46 hours post induction (A-H). TREx BCBL1-Rta cells were also induced without miRIDIAN treatment (I-L). Following incubation, cells were fixed and immunofluorescence staining performed with appropriate primary and secondary antibodies. Cells were then imaged by confocal immunofluorescence microscopy. The micrographs were taken by Sophie Schumann (unpublished) from the Whitehouse laboratory.

5.2 Herpesvirus Results

5.2.1 Doxycycline induction successfully activates KSHV lytic infection

Due to KSHV being primarily a latent virus, KSHV lytic infection must first be induced through the use of an activator such as doxycycline. To study the effect of DOCK5 on KSHV egress, first I had to optimise lytic viral infection. TREx cells were induced with 2.0 µg/ml doxycycline and incubated for four separate time points representing early, mid and late KSHV infection (Jackson et al., 2011). At the relevant time points the cells were lysed, equalised with a Pierce™ BCA protein assay kit and loaded into an SDS-gel. A western-blot analysis was performed and successful KSHV lytic activation was confirmed through the detection of the essential KSHV protein pORF57 which is frequently used as a lytic indicator (Figure 5.8) (Pilkington et al., 2012). pORF57 expression was present at all of the time points analysed, except the mock which had no expression detected. This indicates that doxycycline successfully activates the KSHV lytic life cycle.

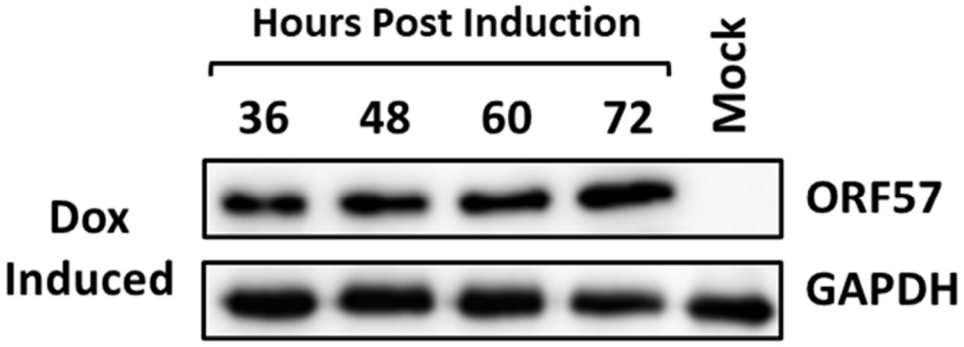

Figure 5.8: Doxycycline induction induces pORF57 production

KSHV latently infected TREx BCBL1-Rta cells were induced with 2.0 µg/ml doxycycline (dox) and incubated for 36, 48, 60, and 72 hours post induction. Whole cells were lysed, and protein levels were equalised using the Pierce™ BCA protein assay kit. Samples were then separated by SDS-PAGE (10% acrylamide gel) and analysed via western blot (n=1). The antibodies used were specific to pORF57, and GAPDH. pORF57 was used as an indicator of successful lytic induction and GAPDH was used as a loading control.

5.2.2 KSHV-induced cells have nuclear capsids at 46 hp_{ind}

Previous work from Christopher Owen and Sophie Schumann found via western blot and immunofluorescence microscopy that preventing KSHV inhibition of DOCK5 resulted in the accumulation of capsids in the cytoplasm (Owen, 2015). EM has a higher resolving power compared to light microscopy due to the shorter wavelengths of electrons compared to light (Smith, 2008). Therefore, TEM could be used to identify more details regarding this phenomenon. For the experiment 46 and 72 hours post induction (hp_{ind}) (representing mid and late infection respectively) were selected based upon Christopher Owen's previous experiments (Owen, 2015). TREx cells were induced with the same induction method as above (Figure 5.8), fixed, embedded in resin, sectioned, stained and finally imaged via TEM.

The mock-induced cells (Figure 5.9) possessed a normal cell architecture of intact cellular membranes with no empty spaces within the cytoplasm or nucleus. This normal cell structure was also present in the 46 hp_{ind} KSHV infected cells (Figure 5.10), however there were signs of viral infection. Numerous KSHV capsids were present within the nucleus of infected cells. Capsids had an icosahedral shape and diameter of ~125 nm which matches the literature (Dünn-Kittenplon et al., 2019). Capsids possessed either an electron dense punctum of KSHV DNA (C-capsid), or were empty (A-capsid) (Gardner and Glaunsinger, 2018). Only four suspected virions were identified within the cytoplasm of KSHV-induced cells. The nucleus also possessed large aggregates which were not present in the mock induced cells and have a similar morphology to viral replication sites identified in the literature. In the cytoplasm of induced cells, RER-like tubules were also observed (Figure 5.10, D). At 46 hp_{ind}, cells had signs of viral infection, but no abundance of cytoplasmic virions.

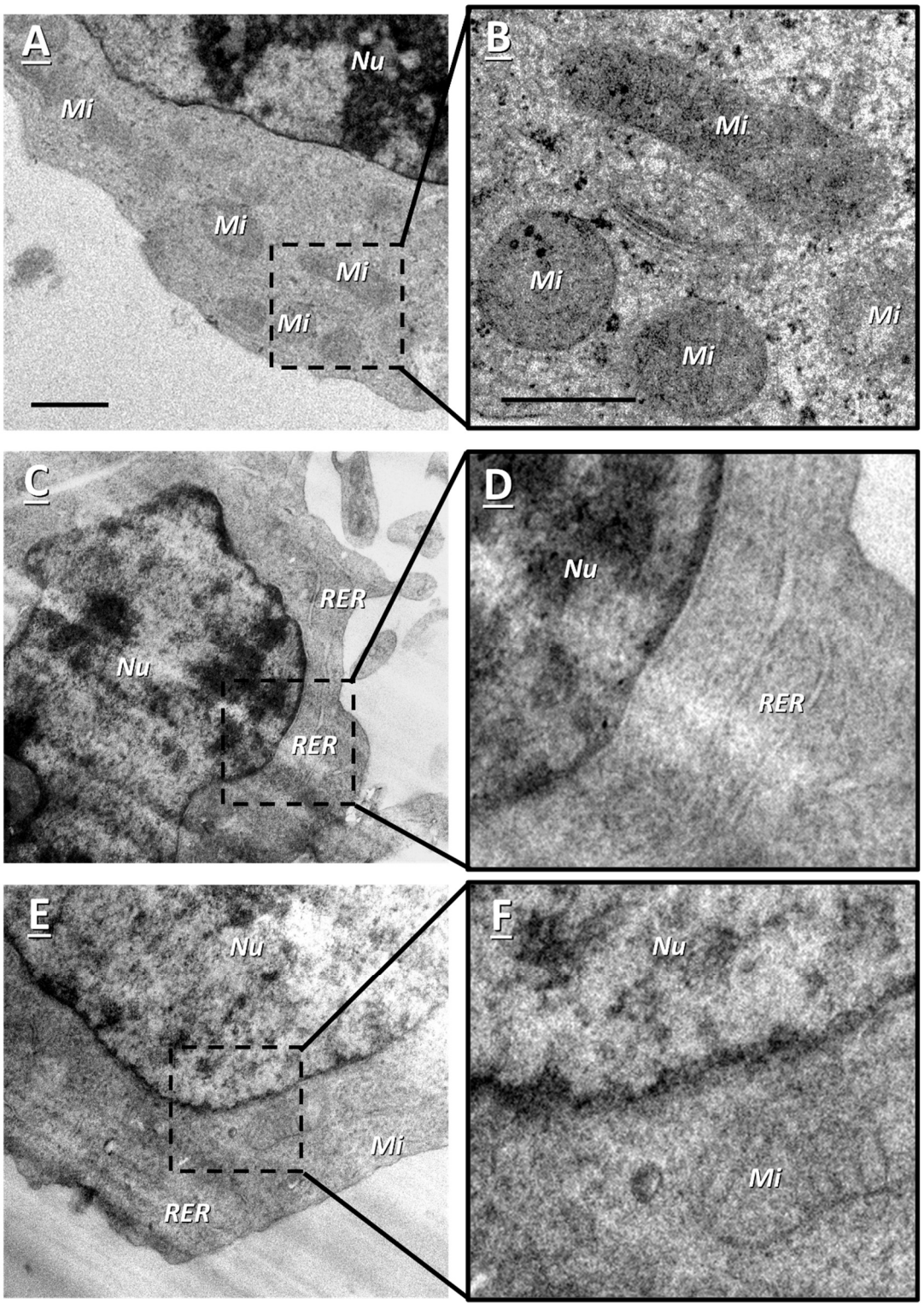

Figure 5.9: 46 hp_{ind} KSHV mock-induced cells

KSHV latently infected TREx BCBL1-Rta cells were mock induced and incubated for 46 hours. Following incubation, cells were processed for TEM. Micrographs A-B, C-D, and E-F are three different cells, with higher magnification images being shown on the right. The nucleus (*Nu*), mitochondria (*Mi*), and rough endoplasmic reticulum (*RER*) are labelled accordingly. Scale bar for the lower magnification represents 1 μM with the highest magnification scale bar represents 500 nm.

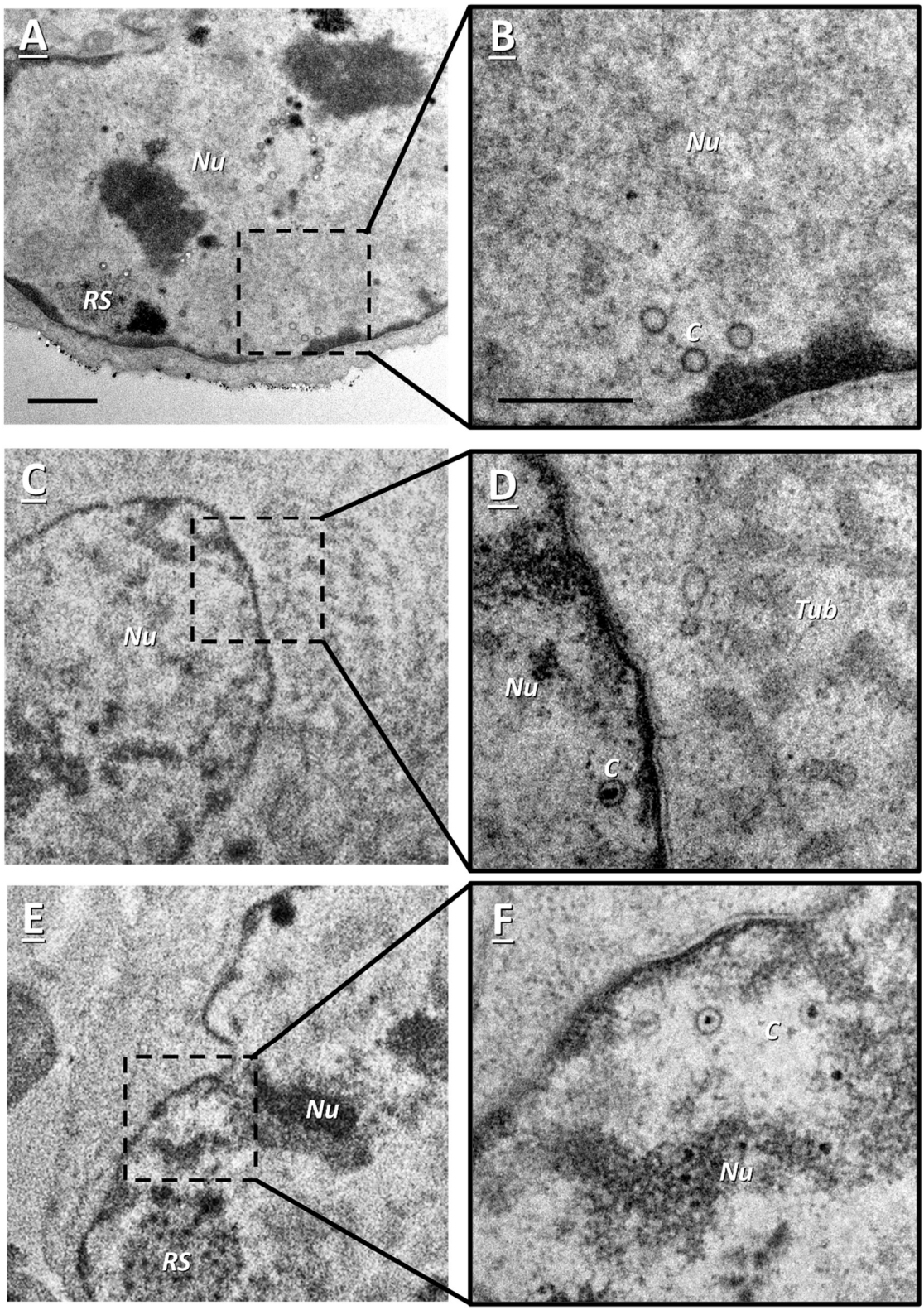

Figure 5.10: 46 hp_{ind} KSHV-induced cells

KSHV latently infected TREx BCBL1-Rta cells were induced with 2.0 µg/ml doxycycline and incubated for 46 hours. Following incubation, cells were processed for TEM. Micrographs A-B, C-D, and E-F are three different cells, with higher magnification images being shown on the right. The nucleus (*Nu*), tubules (*Tub*), capsids (*C*) and replication sites (*RS*) are labelled accordingly. Scale bars for the lower magnification represents 1 µM with the highest magnification scale bar on the right representing 500 nm.

5.2.3 Large KSHV nuclear replication sites used as indicators of viral induction

Inspecting cells for signs of viral infection can be low-throughput due to the small size of viral capsids and the complex nature of cells. This means that each cell imaged must be viewed at a high magnification to confirm viral infection. Large viral structures can be useful as viral signposts, allowing me to focus on imaging cells that have been successfully induced. Large nuclear aggregates were observed in the nucleus of cells that had other signs of viral infection(Figure 5.11). The structures were large and varied, with an average area of 4 μm^2 +/- 7 μm^2 (n = 21) (measured using ImageJ) and matched the KSHV core-like material identified by (Yu et al., 1999) or the capsid assembly sites identified by (Friborg et al., 1999). In this thesis I will refer to these structures as replication sites as it encompasses both of the terms mentioned above. The replication sites characterised by a multitude of dense electron puncta clustered in discrete locations of the nucleus and were flanked by KSHV capsids. The replication sites had a smaller adjacent mass which was extremely electron dense. The large size of the KSHV replication sites means it can be used as a viral indicator at low magnifications.

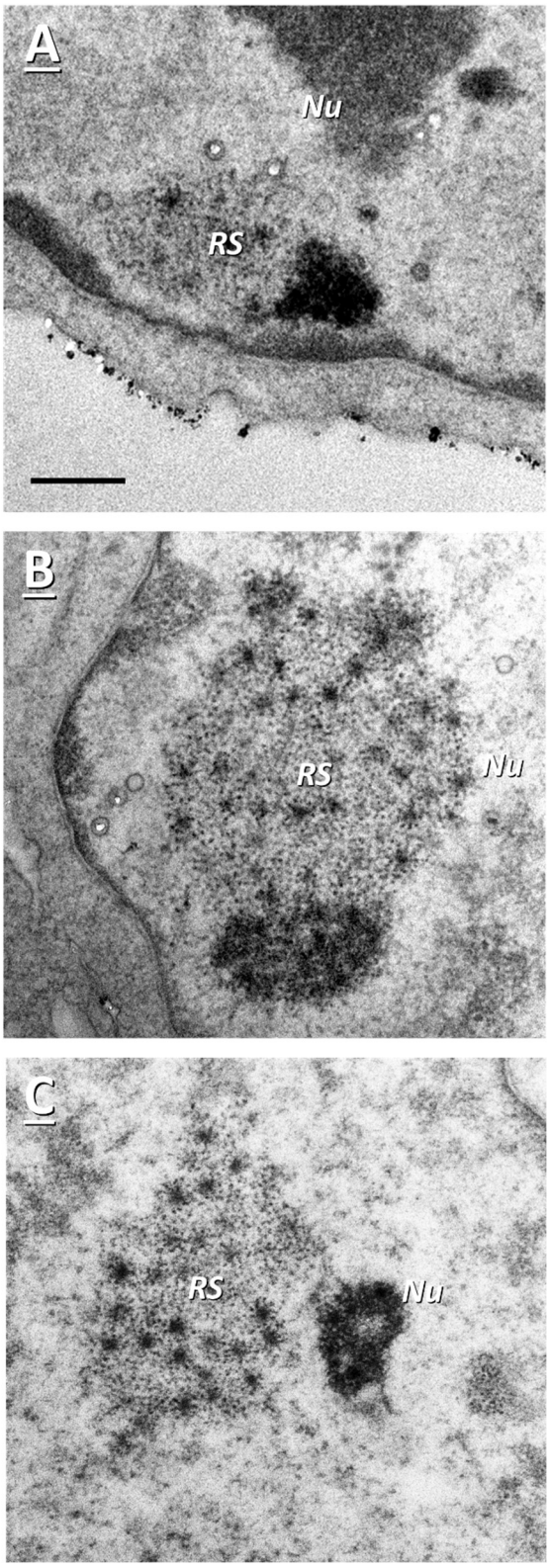

Figure 5.11: A collection of KSHV replication sites in induced cells at 46 hp_{ind}

KSHV latently infected TREx BCBL1-Rta cells were induced with 2.0 µg/ml doxycycline and incubated for 46 hours. Following incubation, cells were processed for TEM. Micrographs A-C are three different cells. The nucleus (Nu) and replication sites (RS) are labelled accordingly. Scale bar represents 500 nm.

5.2.4 No cytoplasmic capsids in miRIDIAN-treated, KSHV-induced cells at 46 hp_{ind}

To confirm whether the inhibition of KSHVs knockdown of DOCK5 resulted in viral accumulation within the cytoplasm, cells were transfected with hsa-miR-365a-3p via electroporation, induced, incubated and then prepared for TEM (Figure 5.12). Cells that were treated with hsa-miR-365a-3p were indistinguishable from untreated cells (Figure 5.10). No signs of CPE were observed and KSHV capsids (type A and C) were found within the nucleus alongside viral replication sites. No capsids were found within the cytoplasm of any cells imaged. There were however modulated RER membranes (Figure 5.12, C) like those seen in figure 5.10, D.

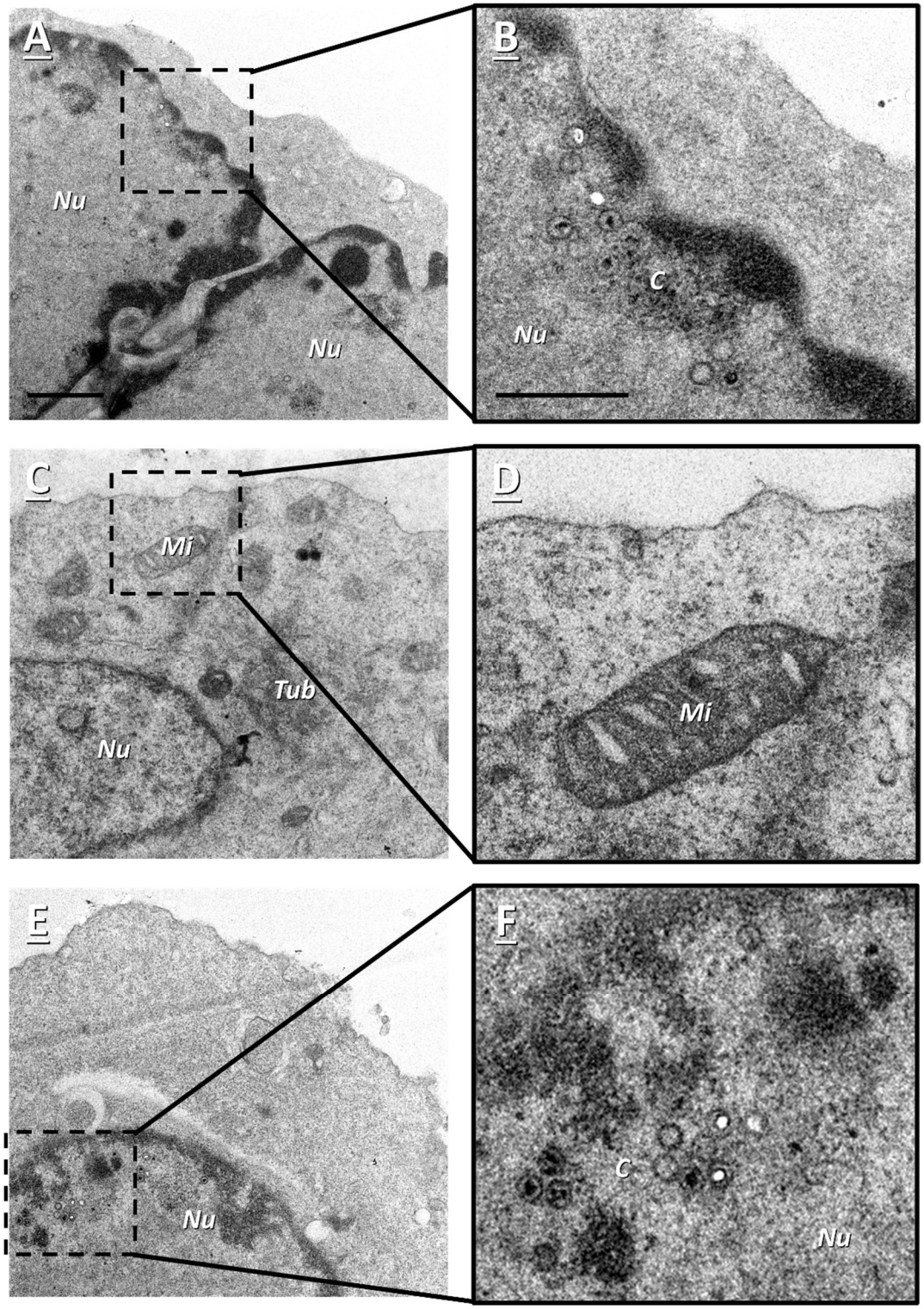

Figure 5.12: 46 hp_{ind} KSHV-induced cells transfected with hsa-miR-365a-3p

KSHV latently infected TREx BCBL1-Rta cells were transfected with miRIDIAN microRNA hairpin inhibitor hsa-miR-365a-3p via electroporation. 24 hours later the cells were induced with 2.0 µg/ml doxycycline and incubated for 46 hours. Following incubation, cells were processed for TEM. Micrographs A-B, C-D, and E-F are three different cells, with higher magnification images being shown on the right. The nucleus (*Nu*), mitochondria (*Mi*), tubules (*Tub*) and capsids (*C*) are labelled accordingly. Scale bars for the lower magnification represents 1 µM with the highest magnification scale bar on the right representing 500 nm.

5.2.5 KSHV lytic infection remodels RER at 46 hp_{ind} in both treated and untreated conditions.

Across both untreated and treated conditions, irregularly shaped tubule structures were observed within the cytoplasm of 46 hp_{ind} cells (Figure 5.10 and Figure 5.12). These structures were morphologically similar to the ER; i.e. tube-like constructs with an outer membrane., and had a granular texture indicating that they were derived from the RER rather than SER. The tubules appeared in dense connected clusters whereas the mock induced RER often appears as long thin tubules which are spread out throughout the cytoplasm (Figure 5.13, A). Furthermore, the inner lumen of the modified RER had a greater electron density than the surrounding cytoplasm. Whereas normal RER is often electron lucent, appearing white compared to the surrounding cytoplasm. Not all the RER in the cell was modified, as can be seen in figure 5.13, D, where normal RER with an electron lucent lumen can be seen connected to the modified RER tubules. Also, only one cluster of modified RER tubules was found per cell. In the 46 hp_{ind} cells, 62 % of the total 82 RER imaged were modified, with 55 % of the 77 total RER imaged in 46 hp_{ind} transfected cells being modified. None of the 62 total imaged RER in mock induced cells had modified RER. In conclusion, KSHV lytic infection may modify the RER, creating a singular mass of interconnected tubules.

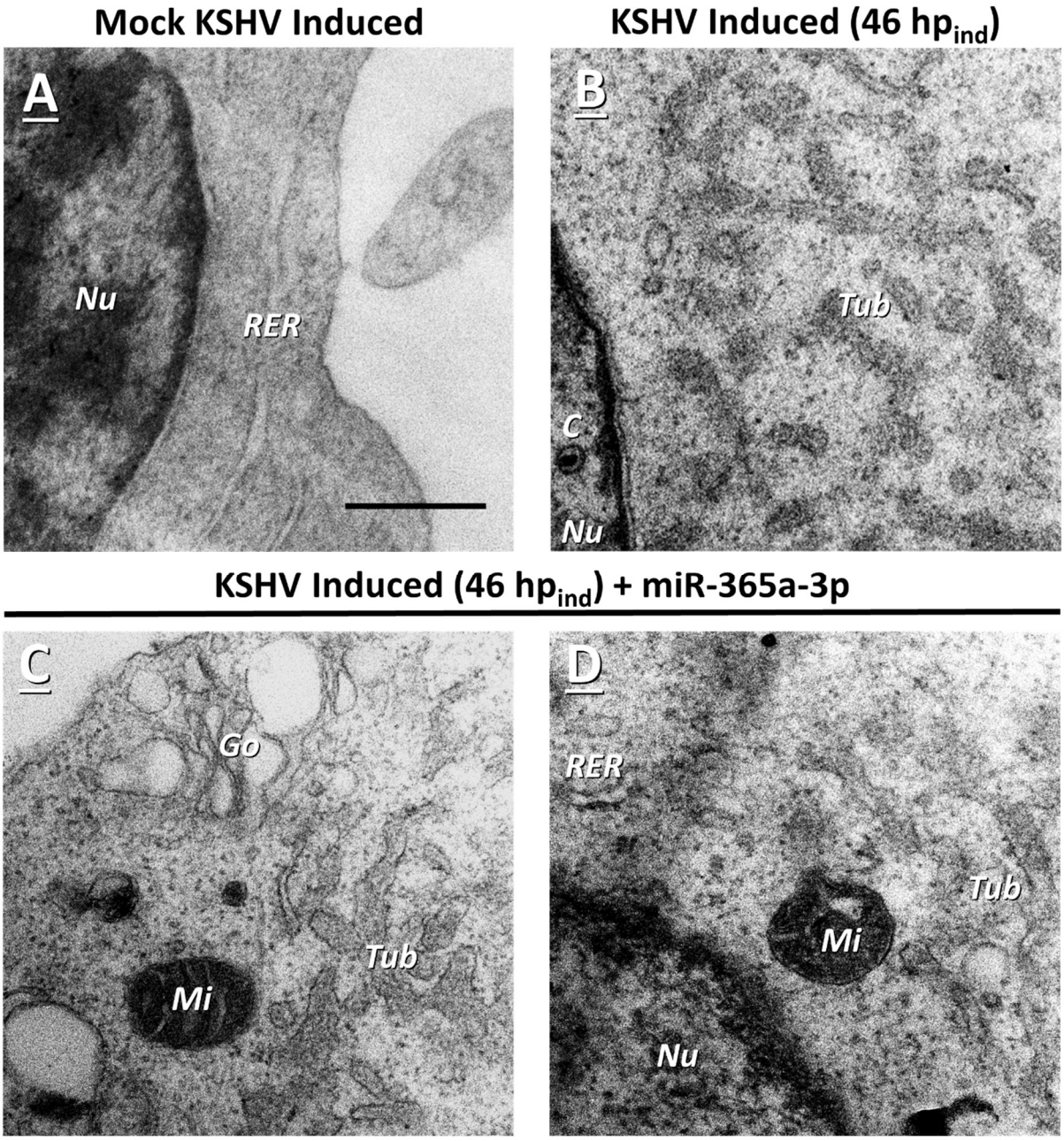

Figure 5.13: A collection of RER tubules across different conditions.

KSHV latently infected TREx BCBL1-Rta cells were either mock induced (A), induced with 2.0 µg/ml doxycycline (B), or transfected hsa-miR-365a-3p and then induced 24-hours later (C-D). Cells were incubated for 46 hours and then processed for TEM. All micrographs are from different cells. The nucleus (*Nu*), mitochondria (*Mi*), rough endoplasmic reticulum (*RER*), Golgi (*Go*), and tubules (*Tub*) are labelled accordingly. Scale bar represents 500 nm.

5.2.6 No accumulation of cytoplasmic capsids in miRIDIAN-treated, KSHV-induced cells at 72 hp_{ind}

There were very few cytoplasmic capsids seen at the mid-infection time point of 46 hp_{ind}. Therefore, 72 hp_{ind} was imaged to assess if cytoplasmic capsids increase in concentration during late infection (Figure 5.14). Due to small difference in time between 46 hp_{ind} and 72 hp_{ind}, only one mock infected control was used (Figure 5.9). The most obvious observation at 72 hp_{ind} was the large number of dead cells. Of the 50 cells imaged, 78 % were dead. Cell were classified as dead by the presence of severe cellular and nuclear membrane damage, low cytoplasmic density and occasional loss of nuclear chromatin. Cytoplasmic virions were identified in low frequency (Figure 5.14, B and F), with nuclear capsids seen more often (Figure 5.14, D). The cytoplasmic virions were enveloped and had another surrounding vesicular membrane. The extra outer membrane indicates that the KSHV nucleocapsid had undergone secondary envelopment (Wang et al., 2015).

Next, the cells that were transfected with hsa-miR-365a-3p and incubated for 72 hp_{ind} were imaged (Figure 5.15). Like the untreated 72 hp_{ind} cells below (Figure 5.14) treated cells had a high death rate, with 85 % of the 20 cells imaged being dead. Furthermore, nuclear capsids and cytoplasmic virions were identified, although none of the cytoplasmic virions were clustered. Like the untreated 72 hp_{ind} cytoplasmic virions, the treated virions were found within suspected Golgi vesicles (Figure 5.15). A collection of all potential cytoplasmic virions across all conditions can be seen below. Differences in virion morphology is due to the production of different capsid types (A-C). Of note, in figure 5.16, W a virion can be seen within an electron dense vesicle. Similarly, electron dense vesicles were present in other transfected cells at 72 hp_{ind}. With only 24 cytoplasmic capsids being imaged by TEM across all conditions, it was concluded that the induction process had to be optimised and other quantification techniques employed to investigate the role of DOCK5 on KHSV egress. As no capsids were found in either condition, a western blot was not used to confirm the successful transfection with hsa-miR-365a-3p as it was unnecessary without visible cytoplasmic capsids. The western blot would probe for DOCK5, if the cells had been successfully transfected then DOCK5 levels in transfected cells would be comparable to the non-infected control.

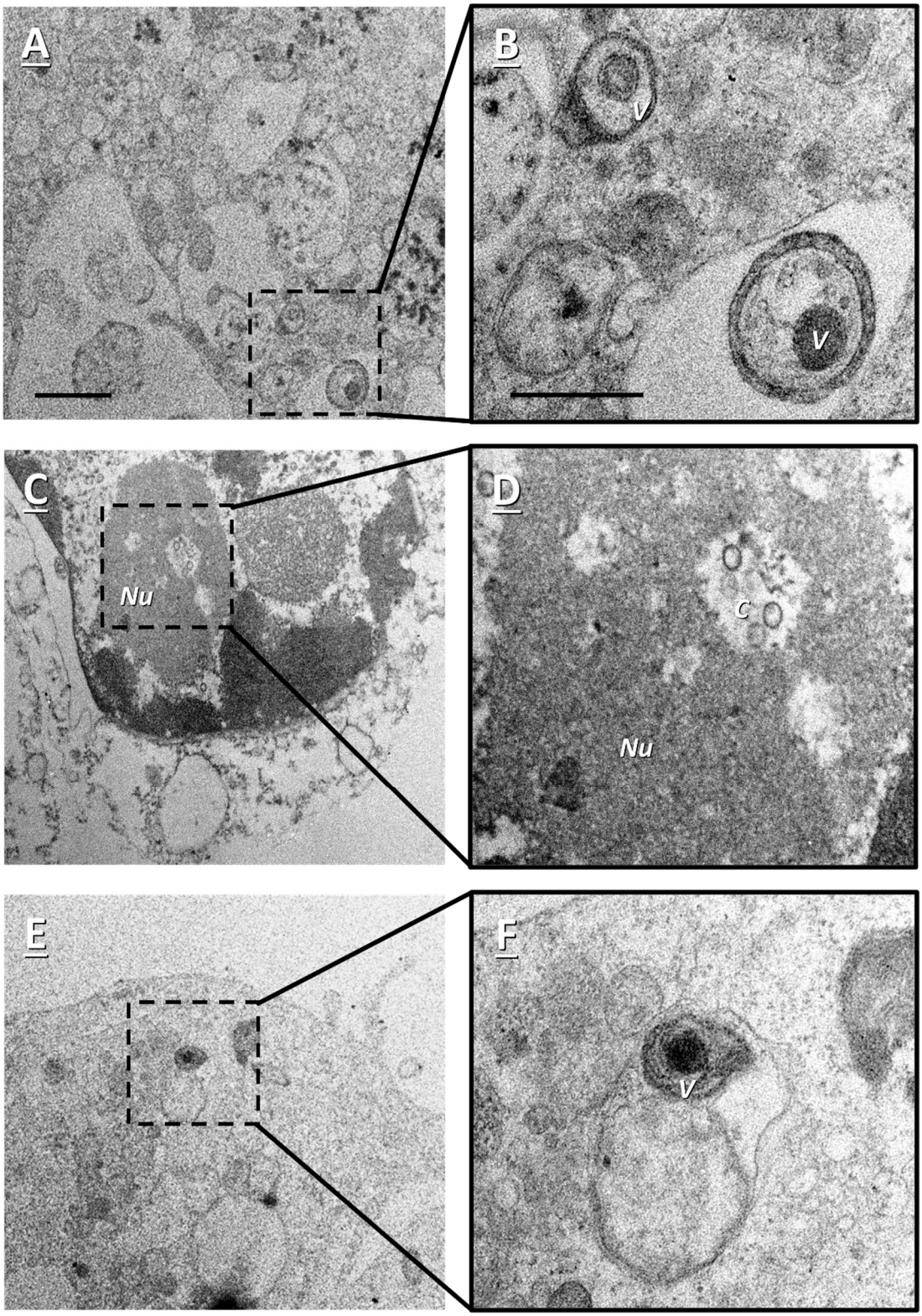

Figure 5.14: 72 hp$_{ind}$ KSHV-induced cells

KSHV latently infected TREx BCBL1-Rta cells were induced with 2.0 μg/ml doxycycline and incubated for 72 hours. Following incubation, cells were processed for TEM. Micrographs A-B, C-D, and E-F are three different cells, with higher magnification images being shown on the right. The nucleus (*Nu*) and virions (*V*) are labelled accordingly. Scale bars for the lower magnification represents 1 μM with the highest magnification scale bar on the right representing 500 nm.

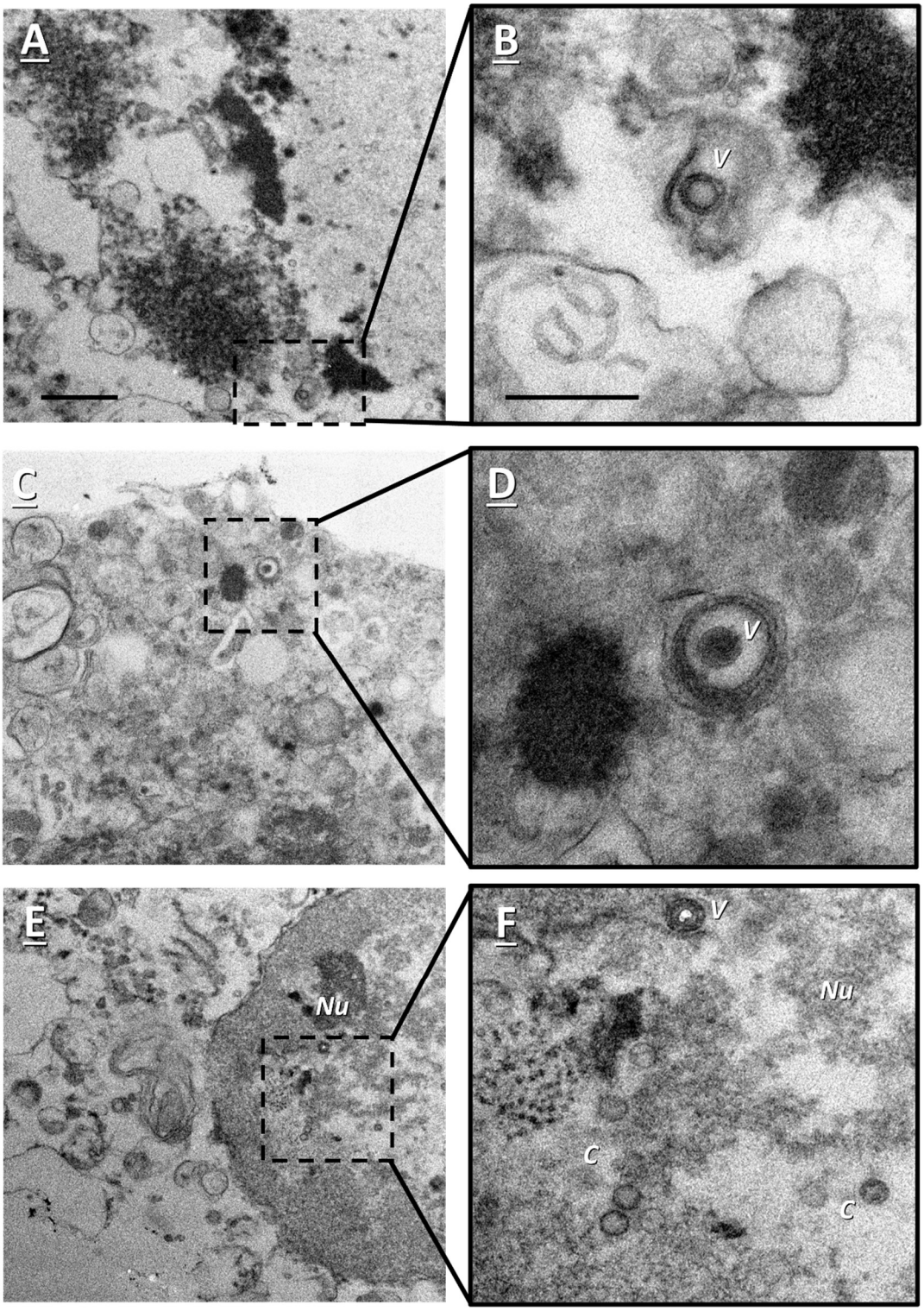

Figure 5.15: 72 hp_{ind} KSHV-induced cells transfected with hsa-miR-365a-3p

KSHV latently infected TREx BCBL1-Rta cells were transfected with miRIDIAN microRNA hairpin inhibitor hsa-miR-365a-3p via electroporation. 24 hours later the cells were induced with 2.0 µg/ml doxycycline and incubated for 72 hours. Following incubation, cells were processed for TEM. Micrographs A-B, C-D, and E-F are three different cells, with higher magnification images being shown on the right. The nucleus (*Nu*), capsids (*C*) and virions (*V*) are labelled accordingly. Scale bars for the lower magnification represents 1 µM with the highest magnification scale bar on the right representing 500 nm.

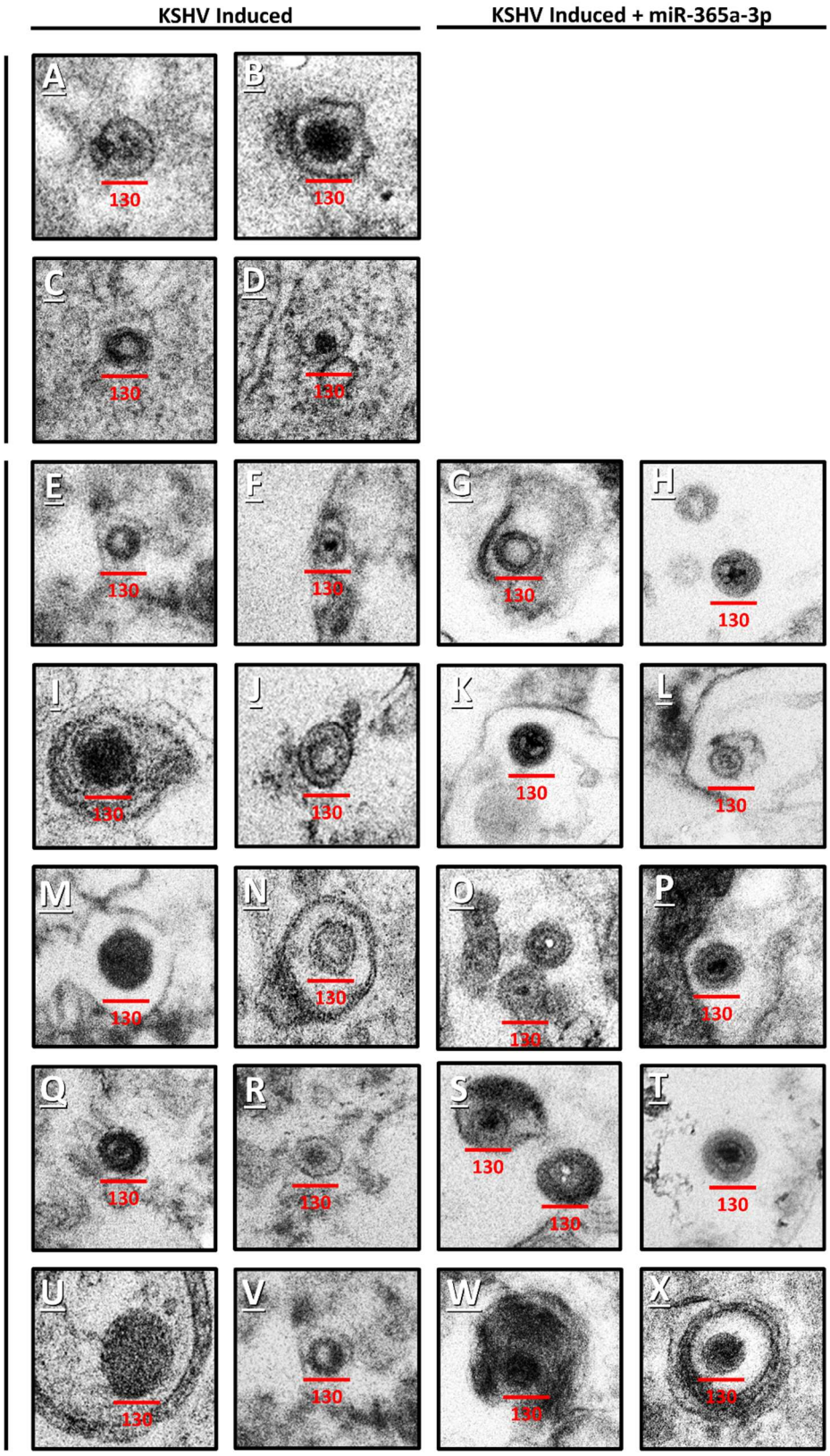

Figure 5.16: A collection of cytoplasmic virions across different KSHV-induced conditions.

KSHV latently infected TREx BCBL1-Rta cells were either mock induced, induced with 2.0 µg/ml doxycycline, or transfected hsa-miR-365a-3p and then induced 24-hours later. Cells were incubated for 46 or 72 hours and then processed for TEM. Scale bar represents 130 nm.

5.2.7 Electron-dense vesicles present at 72 hp_{ind} in miRIDIAN-treated cells

Due to there being no obvious viral accumulation in the hsa-miR-365a-3p treated 72 hp_{ind} cells, I scrutinised the cells for any additional differences. As mentioned earlier, a number of transfected cells had electron dense vesicles. 30 % of the 20 treated cells imaged had cytoplasmic vesicular structures (Figure 5.17), with no comparative vesicles being identified in the mock induced or untreated 72 hp_{ind} cells. These vesicles first drew my attention when a suspected virion was identified within one of the electron dense vesicles (Figure 5.16, W). These vesicles were characterised by being electron dense, spherical and possessing an outer membrane. However, the electron density made it difficult to identify any internal features. The presence of an enveloped KSHV virion being present within a vesicle implies that it could be derived from the Golgi as this is the final stage of the KSHV lifecycle prior to egress (Aneja and Yuan, 2017).

Only one KSHV virion was found within an electron dense vesicle, but it raises the question as to whether the other electron dense vesicles also contained KSHV virions. One technique which could be used to further investigate this could be CLEM. CLEM is a technique that combines the resolving power of EM with the targeting ability of FM (Vijayakrishnan et al., 2020, de Boer et al., 2015, Santarella-Mellwig et al., 2018a, Bykov et al., 2016). CLEM has been used numerous times to study viruses, its ability to highlight features of interest in often overcrowded and complex cell sections is invaluable in understanding viral life cycles. For example, CLEM was used to further understand the structure and creation HCV associated membrane structures. HCV forms membranous webs from clustered vesicles in the cytoplasm of infected cells which act as sites of RNA replication. Through CLEM and other techniques, researchers found that the webs were derived from the ER and possessed RER, mitochondrial and late endosome markers (Romero-Brey et al., 2012b). This technique could be applied to KSHV by fluorescently tagging Golgi and KSHV capsids to seeing if they co-localise, then these locations can be viewed in greater detail via TEM to identify whether these regions correspond to the electron dense vesicles seen in figure 5.17.

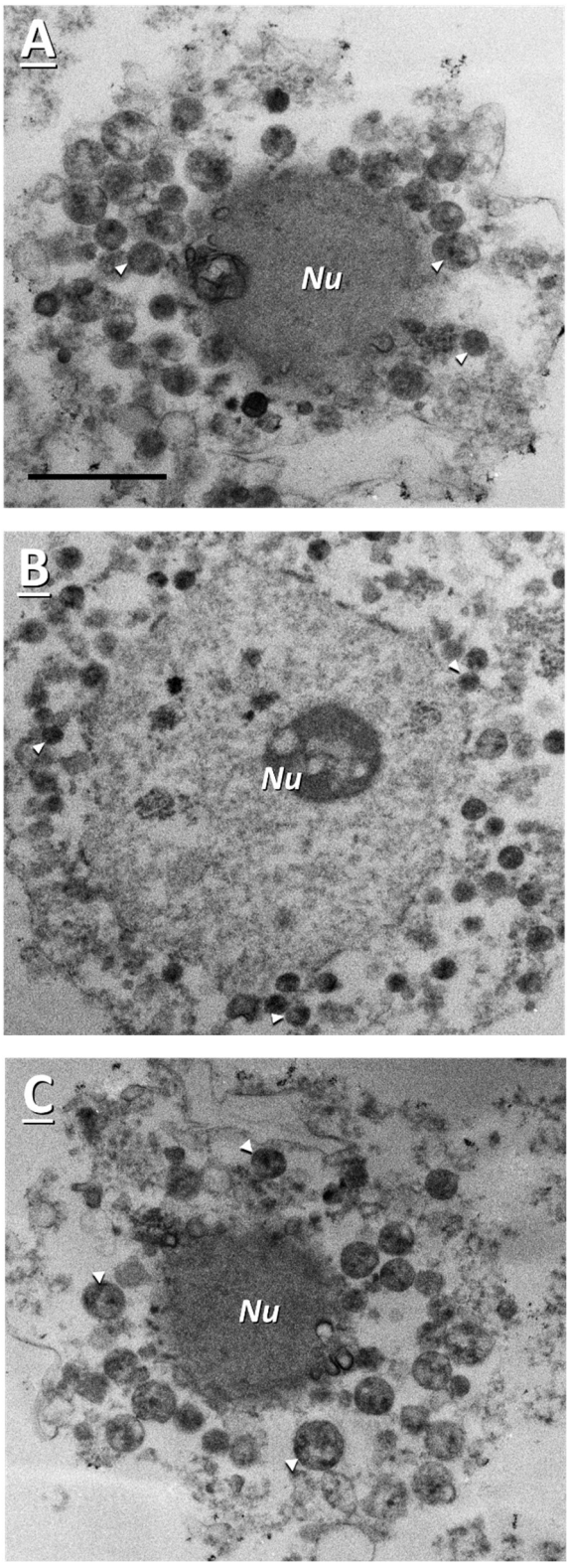

Figure 5.17: A comparison of electron-dense cytoplasmic vesicles across induced and transfected cells at 72 hp_{ind}

KSHV latently infected TREx BCBL1-Rta cells were transfected with hsa-miR-365a-3p and then induced 24-hours later with 2.0 µg/ml doxycycline. Cells were incubated for 72 hours and then processed for TEM. The nucleus (*Nu*) and vesicles (arrowhead) are labelled accordingly. Scale bar represents 1 µM.

5.2.8 None of the three KSHV capsid antibodies tested produced reliable results

Due to the low concentration of KSHV cytoplasmic virions in both hsa-miR-365a-3p treated and untreated cells, it was necessary to optimise KSHV induction. The process of TEM is low throughput, taking a week to embed cells in resin, with sectioning and imaging also being a slow process. A quicker way to quantify cytoplasmic KSHV capsids would be through western blot analysis. An antibody could target KSHV capsids in a cytoplasmic fraction and be resolved via western blot to quantify relative capsid levels.

To start with, I wanted to validate the use of the KSHV capsid antibody. Firstly, I used the KSHV MCP protein pORF25 which was kindly donated by the Whitehouse laboratory. The pORF25 antibody had no bands when incubated with a western blot membrane. The same occurred for the KSHV SCP pORF65 primary antibody which also had no band. Finally, I attempted to use the KSHV pORF62 TRI-1 antibody which produced inconsistent results (Figure 5.18). Initially bands were present in induced cells. However upon repeat, the bands appeared primarily in the mock induced control (Figure 5.18, A). Finally, a western blot was performed with only mock induced cells to confirm whether non-specific binding was occurring (Figure 5.18, B). Mock-induced TREx samples were resolved via western blot analysis in triplicate (biological repeats) alongside HFF1 cells, also in triplicate. The HFF1 cell line was included as TREx cells can have occasional spontaneous lytic activation (Renne et al., 1996). HFF1s have no KSHV genome within the nucleus and therefore there was no possibility of any KSHV capsids being within the cytoplasm. Therefore, no pORF62 band should appear unless there is non-specific binding. The presence of a faint band across all six negative controls confirms that the antibody had non-specific binding. This was confirmed by a comparison between the blot and ponceau stain (Figure 5.18, C) which showed that the pORF62 antibody was binding to most of the protein present on the blot. The inability to find a working KSHV capsid antibody prevented quantifying cytoplasmic KSHV capsids via western blot.

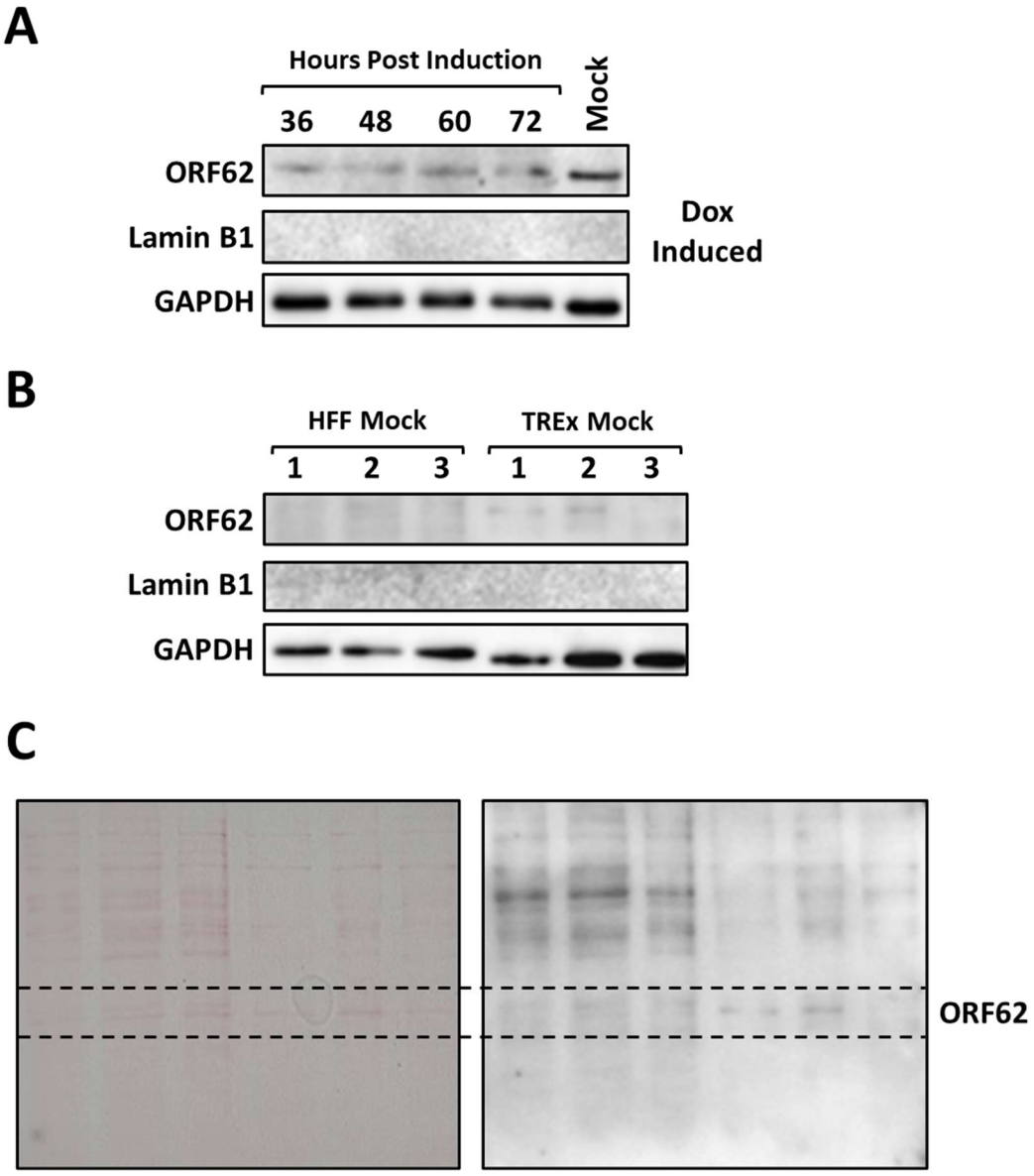

Figure 5.18: Assessing the validity of the KSHV capsid antibody pORF62 for western blot analysis

KSHV latently infected TREx BCBL1-Rta (TREx) cells were induced with 2.0 µg/ml doxycycline and incubated for 36, 48, 60, and 72 hp_{ind} and then cytoplasmic cell lysates were isolated by subcellular. Cytoplasmic fractions were then separated by SDS-PAGE (10 % acrylamide) and analysed via western blot (n=1) (A). TREx and human foreskin fibroblasts (HFF1) cytoplasmic cell lysates were isolated by subcellular fractionation in triplicate (biological repeat). Cytoplasmic fractions were then separated by SDS-PAGE (10 % acrylamide) and analysed via western blot (n=3) (B). The antibodies used were specific to pORF62, lamin B1, and GAPDH. pORF62 was used as a qualitative indicator of KSHV capsid quantity, lamin B1 was used as a nuclear marker to confirm cytoplasmic fraction purity, and GAPDH was used as a loading control. A side-by-side comparison of the full nitrocellulose membrane from B stained with Ponceau S and the same membrane that was later bound with pORF62. A dashed line has been used to indicate the region highlighted in B (C).

5.2.9 A comparison of the effect of different KSHV induction methods on TREx cell viability

Whilst working on selecting a KSHV capsid antibody, I also tried to determine if a different induction technique would increase the lytic KSHV response (Figure 5.19). Before the creation of the doxycycline inducible BCBL1 cell line, non-specific gene activators were used to activate KSHV lytic infection (Nakamura et al., 2003, Myoung and Ganem, 2011). Such pleiotropic inducers included TPA (Naranatt et al., 2003, Yu et al., 1999, Nichols et al., 2011, Chen et al., 2019a), NaB (Yu et al., 1999, Martin et al., 2021, Sharma et al., 2019), TPA-NaB combination (Hughes et al., 2015, Baquero-Pérez and Whitehouse, 2015, Simpson et al., 2018, Long et al., 2021), VPA (Wei et al., 2020, Sharma et al., 2017, Dai et al., 2017, Kook and Ziegelbauer, 2021, Ayers et al., 2018), cobalt chloride (Nichols et al., 2011) and 5-azacytidine (Yan et al., 2019). I opted to select the four most frequently used, NaB, TPA, NaB-TPA combination and VPA. NaB and VPA are short chain fatty acids that act as a histone deacetylase inhibitors, preventing the formation of heterochromatin and allowing for transcription factors to access silenced genes. This results in non-specific gene expression, including the activation of the KSHV genome (Berni Canani et al., 2012, Fan et al., 2005). TPA however, stimulates the mitogen-activated protein kinase /extracellular signal-regulated kinase pathway, resulting in the phosphorylation and activation of Rta, triggering the KSHV lytic cycle (Cohen et al., 2006). In addition to the different inducers, different concentrations of the inducing agents were used. For doxycycline two lower concentrations of 0.2 and 1.0 µg/ml were used alongside the original 2.0 µg/ml. For VPA 0.6- and 1.2-mM concentrations were used as a middle-ground for the wide range of VPA concentration in the literature. The collection of different induced TREx cell growth curves can be seen below in Figure 5.19, A-D, with Figure 5.19, E representing a compilation of the different induction methods. The compilation graph has percentage viable counts normalised against the respective mock-induced negative control.

When carrying out the TREx growth curves, the original plan was to measure the viability via automatic cell counter and then carry out a western blot with the cell lysates to quantify capsid number. The inability to find a working KSHV capsid antibody severely hampered the scope of these findings. However, viability counts are still useful alone. In KSHV 72hp_{ind} untreated and treated conditions (Figure 5.14 and 5.15) the majority of cells were dead (78 % and 85 % respectively). Cell death compromises outer membrane integrity, making it impossible to ascertain whether DOCK5 is involved in herpesvirus egress. Therefore, the induction conditions

selected must have higher viability rates than that seen at 72 hp_{ind} in 2.0 µg/ml doxycycline induction (~40%). Although most induction methods have an equal to or lower viability of 40 % at 72 hp_{ind} (apart from TPA, NaB. and NaB-TPA combined), selecting the earlier time point of 60 hp_{ind} might be more successful. 60 hp_{ind} is still a late infection time point and viability has not dropped as much as at 72 hp_{ind} for most conditions. After 72 hp_{ind}, most controls start to suffer drops in viability (likely due to cell starvation), making time points after 72 hours unsuitable. From Figure 5.19, E, It can be seen that the NaB, TPA and NaB-TPA induction techniques have a higher viability when compared to induction with 2.0 µg/ml doxycycline from 48 to 72 hp_{ind}. Interestingly, TPA alone leads to no cell net loss of viability when compared to the TPA mock induced condition (Figure 5.19, C) indicating that the TPA induction was not successful. This is even more apparent when comparing the NaB and NaB-TPA combination induction techniques which have very similar viability throughout all time points, indicating that potentially only NaB was active. The failure of TPA induction is likely due to either human error when calculating concentration, or expiry of the chemical. Regardless, a western blot targeting the lytic signal pORF57 can be used for confirmation of induction failure. Due to the failure of the TPA inductions, next I would further investigate whether NaB induction alone is capable of producing more KSHV cytoplasmic capsids than induction with 2.0 µg/ml doxycycline.

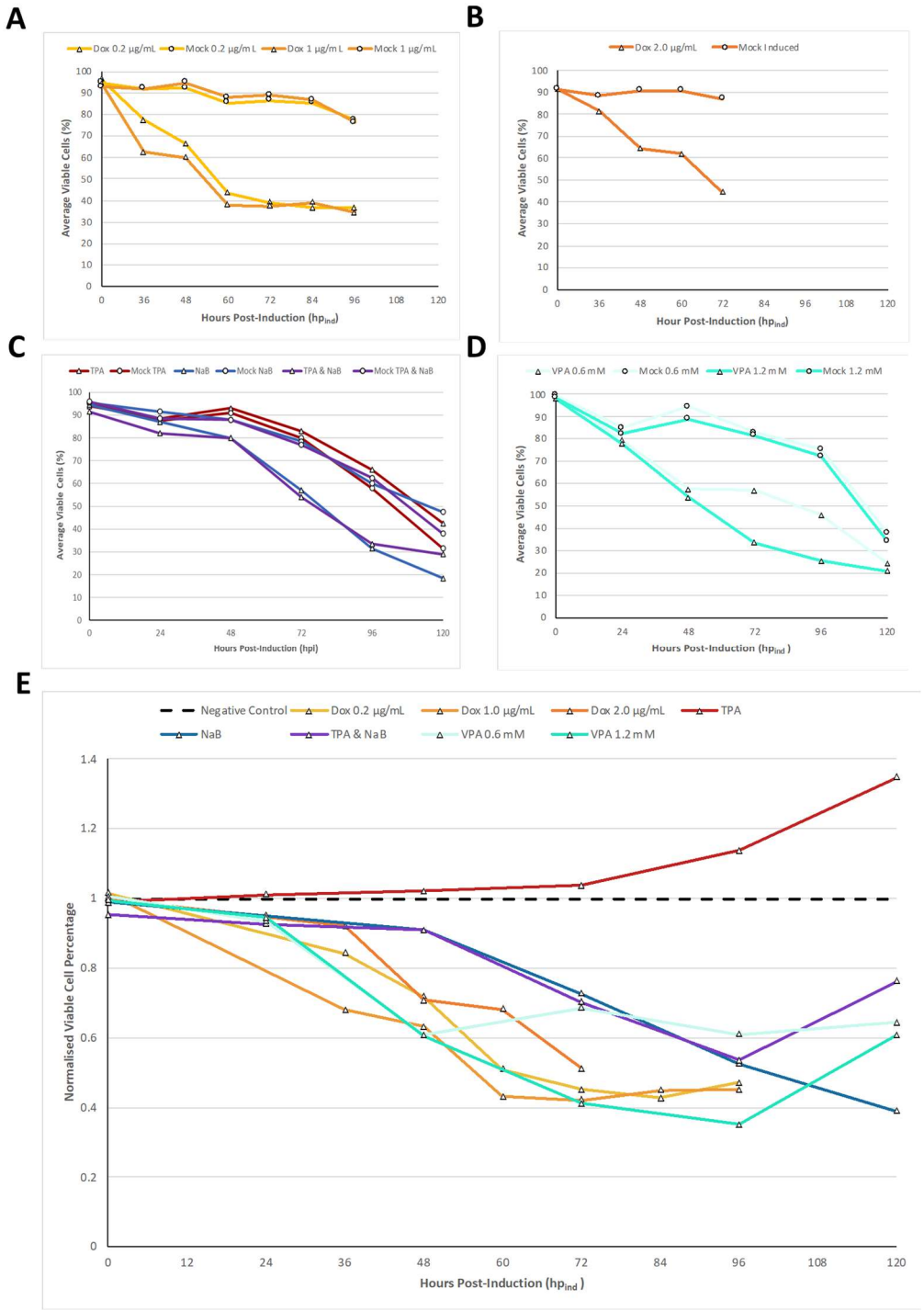

Figure 5.19: TREx cell growth curves for different KSHV lytic induction methods

TREx BCBL1-Rta (TREx) cells were induced with either 0.2 or 1.0 µg/ml doxycycline, with cell viability calculated using an automatic cell counter every 12 hours from 36 to 96 hp_{ind} (A). The same as A, but cells were induced with 2.0 µg/ml doxycycline for up to 72 hp_{ind} (B). TREx cells were induced with 12-O-tetradecanoyl-phorbol-13-acetate (TPA), sodium butyrate (NaB), and both TPA and NaB for up to 120 hp_{ind} (C). TREx cells were induced with 0.6 and 1.2 mM valproic acid (VPA) (D). The viable cell percentages from A-D compiled into a single graph with the percentage viable counts normalised/corrected against their relative mock-induced negative control (E).

5.2.10 Dock5 antibody binds to mid-sized protein

To ascertain whether HSV1 infection knocks down DOCK5 like KSHV, I quantified DOCK5 by western blot analysis (Figure 5.20). Cells infected with HSV1 at 12 hp_{inf} were selected as the time point based on the findings in figure 5.22. DOCK5 is a 215 kDa protein, yet the Thermo Fisher page shows a blot with the Dock5 band at ~250 kDa (ThermoFisher, UniProt, 2022). On the first western blot (Figure 5.20, A) a band appeared in the 75-100 kDa size range, drastically smaller than the 215 kDa size of DOCK5 or the expected 250 kDa band. However, another fainter band can be seen above at the correct size range (~250 kDa) for mock 1. Due to the large size of DOCK5, I decided to optimise the SDS-PAGE by using 8% acrylamide (rather than the original 10%) and by using the high molecular weight protein transfer setting on the BIO-RAD Trans-blot® Turbo™. Both the lower and higher bands increased in intensity, with the faint band at ~250 kDa appearing for all samples (Figure 5.20, B).

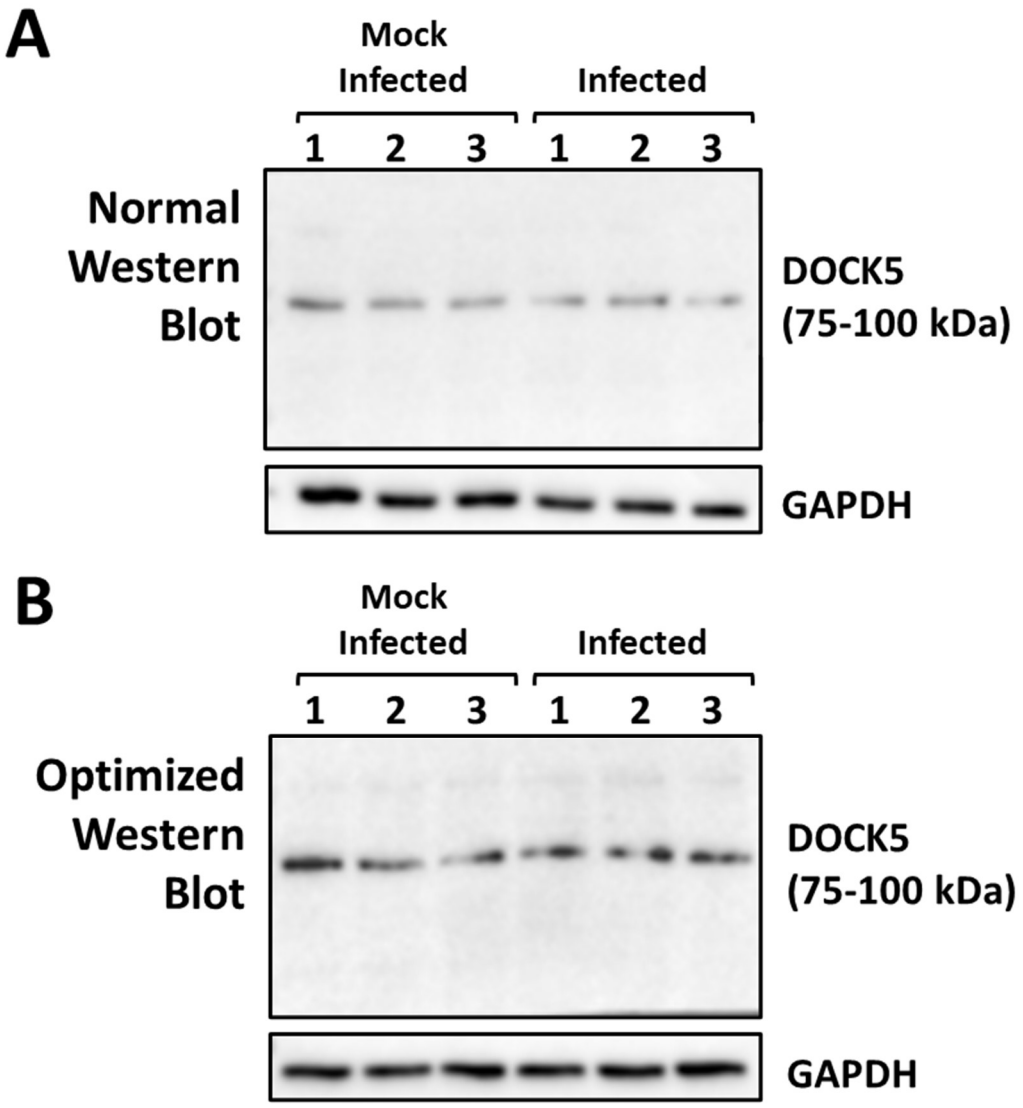

Figure 5.20: Optimization of Dock5 western blots.

(A) Human foreskin fibroblasts (HFF1s) were infected with HSV1 and the cells were lysed at 12 hp_{inf}. The cell lysate protein levels were equalised using the Pierce™ BCA protein assay kit and (then separated by SDS-PAGE (10% acrylamide gel) and analysed via western blot (n=2). The antibodies used were specific to DOCK5 and GAPDH. DOCK5 was used to identify any changes in DOCK5 expression between infected and mock infected cells, and GAPDH was used as a loading control. (B) The same as (A) except an 8% acrylamide gel was used for the SDS-PAGE and the high molecular weight setting was used on the BIO-RAD Trans-blot® Turbo™ Transfer System for the semi-dry protein transfer.

5.2.10.1 Smaller western blot band caused by protein cleavage

One possible cause of the band appearing at a lower size could be due to protein degradation. Protein degradation can occur due to a number of reasons, such as protein extraction and storage. During protein extraction (e.g., cell lysis), proteins can be exposed to cell proteases or peptidases resulting in protein breakdown (Gorr and Vogel, 2015, Bass et al., 2017, Mishra. et al., 2017). Although cells were lysed on ice to slow proteolytic processes, no protease inhibitors were added. Due to the absence of protease inhibitors during cell lysis, it is possible that the smaller DOCK5 fragment originates from unwanted proteolysis. As a result, I decided to prepare fresh cell lysates with protease inhibitors in my following attempts (Figure 5.21).

5.2.11 Dock5 identified in the nuclear fraction of HFF1 and TREx cells

From the previous western blot (Figure 5.20) several issues occurred. Firstly, the absence of a protease inhibitor likely resulted in DOCK5 fragmenting, so new cell lysates were prepared containing protease inhibitors. The cell lysates were created from HFF1 and TREx cell lines in triplicate, with TREx cells being used as it was relevant to optimise the DOCK5 antibody in TREx cells for the KSHV study. Finally, to confirm that the antibody binds to the correct target, a negative control will be included. DOCK5 was identified in intestinal epithelial cells to be located at the cell membrane (Sanders et al., 2009, UniProt-Consortium, 2020). Furthermore, DOCK5 was located within the peripheral ruffles of epithelial cells (Frank et al., 2017). Consequently, as DOCK5 is expressed in most cells and creating a DOCK5 knock-out would take too long, I decided to use the cell nuclear fraction as a negative control (Berglund et al., 2008, Thul et al., 2017, Human-Protein-Atlas).

In the western blot repeat (Figure 5.21) no band was seen at 250 kDa in the cytoplasmic fraction. Also, the previously seen 75-100 kDa band from figure 5.20 was not visible, suggesting that the protease inhibitor was successful. Interestingly, in the nuclear fraction a double band was present across all samples at the ~250 kDa mark. Although all bands were around the 250 kDa mark, the three HFF1 samples were slightly lower. The second repeat of the western blot resulted in a smudged band at the 250 kDa mark in the nuclear fraction (data not shown). I was unable to repeat this again due to time constraints.

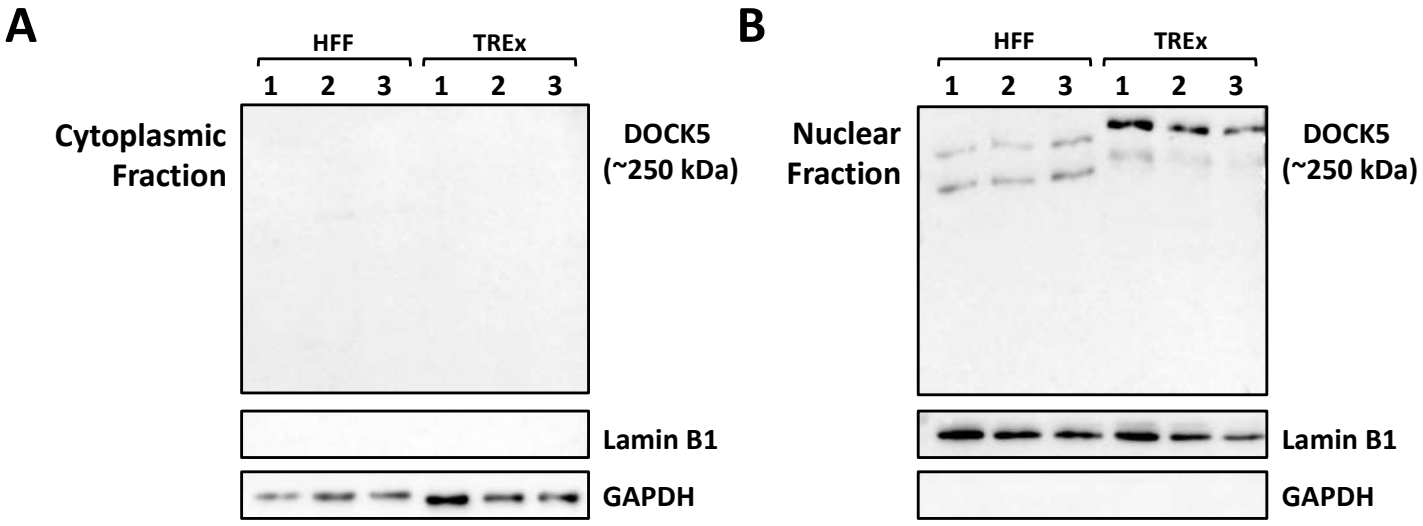

Figure 5.21: DOCK5 western blot of cytoplasmic and nuclear fractions

Human foreskin fibroblasts (HFFs) and TREx BCBL1-Rta (TREx) cytoplasmic (A) and nuclear cell lysates (B) were isolated by subcellular fractionation and then were equalised using the Pierce™ BCA protein assay kit. Samples were then loaded onto a 6% acrylamide gel and analysed via western blot (n=2). The antibodies used were specific to DOCK5, lamin B1 and GAPDH. DOCK5 was used to identify DOCK5 levels with Lamin B1 and GAPDH being used as both loading controls and as nuclear and cytoplasmic markers (respectively) to confirm fraction purity.

5.2.12 Optimisation of HSV1 production and time course

Whilst I was having issues with finding working KSHV capsid antibodies I decided to test if the requirement of DOCK5 previously showed for KSHV egress was also required for other herpesviruses. HSV1 has been studied to a greater extent than KSHV and so there are more commercial antibodies available (e.g., on abcam there are 36 primary antibodies available for HSV1, versus 7 for KSHV). Furthermore, when cells are infected with HSV1 *in vitro*, the virus requires no artificial induction to enter lytic production. This makes it easier to identify cytoplasmic capsids when imaging HSV1 infected cells through TEM. This translates directly into more cellular TEM research into the HSV1 lifecycle (Miranda-Saksena et al., 2002, Zerboni et al., 2012, Wild et al., 2015, Arii et al., 2020, Wild et al., 2017).

In preparation for investigating the role of DOCK5 on HSV1 egress, I decided to optimise HSV1 propagation and also select the optimum time point to image cytoplasmic capsids in the HSV1 infection life cycle. The best time point to image HSV1 egress would be late enough that HSV1 virions are exiting cells, yet not so late that the majority of cells have died. The literature indicates that 24 hours covers the HSV1 life cycle, with the 10-20 hp_{inf} range being optimum for HSV1 virions present within the cytoplasm. A 24-hour infection time course was performed, with HFF1 cells imaged and lysed, and the supernatant collected every 6 hours (6, 12, 18 and 24 hp_{inf}) (Figure 5.22). To ascertain the degree of CPE and cell death at each time point, cells were imaged via phase-contrast light microscopy (Figure 5.22, A). CPE was characterised by cell rounding and loss of cell monolayer (due to lysis) (Anderson et al., 2014). Low levels of CPE were identifiable as early as 6 hp_{inf} when compared to the mock, with cell lysis becoming evident from 18 hp_{inf}. At 24 hp_{inf} the majority of cells showed signs of CPE and ~50% of the monolayer had been lost.

Next, the collected supernatant was used for a plaque assay to ascertain the amount of HSV1 virions being produced at each time point (Figure 5.22, B-C). HSV1 plaques were present at 6 hp_{inf} and by 24 hp_{inf} the entire monolayer had been destroyed (at the 10^{-3} serial dilution), indicating continual infection virion production. The greatest increase in HSV1 viral titre occurred between 0 and 12 $hp_{inf,}$ with the viral titre plateauing afterwards. Finally, the cells at each of the time points were lysed via subcellular fractionation to separate nuclear and cytoplasmic fragments, loaded into an SDS-PAGE gel and then analysed via western blot (Figure 5.22, D). The HSV1 MCP (pU_L19) primary antibody was incubated with the cytoplasmic fraction to comparatively quantify the amount of HSV1 capsids in the cytoplasm at each time point. A faint band can be seen at 6 hp_{inf} which builds in intensity until 18 hp_{inf} where

the band thickness caps. From the results in figure 5.22, 12 hp_{inf} was selected as the optimum time point for imaging HSV1 cytoplasmic capsids. This was based on the low level of CPE and cell death (Figure 5.22, A), the successful egress of infectious virions (Figure 5.22, B-C) and the presence of HSV1 capsids within the cytoplasm of infected cells (Figure 4.2.1, D).

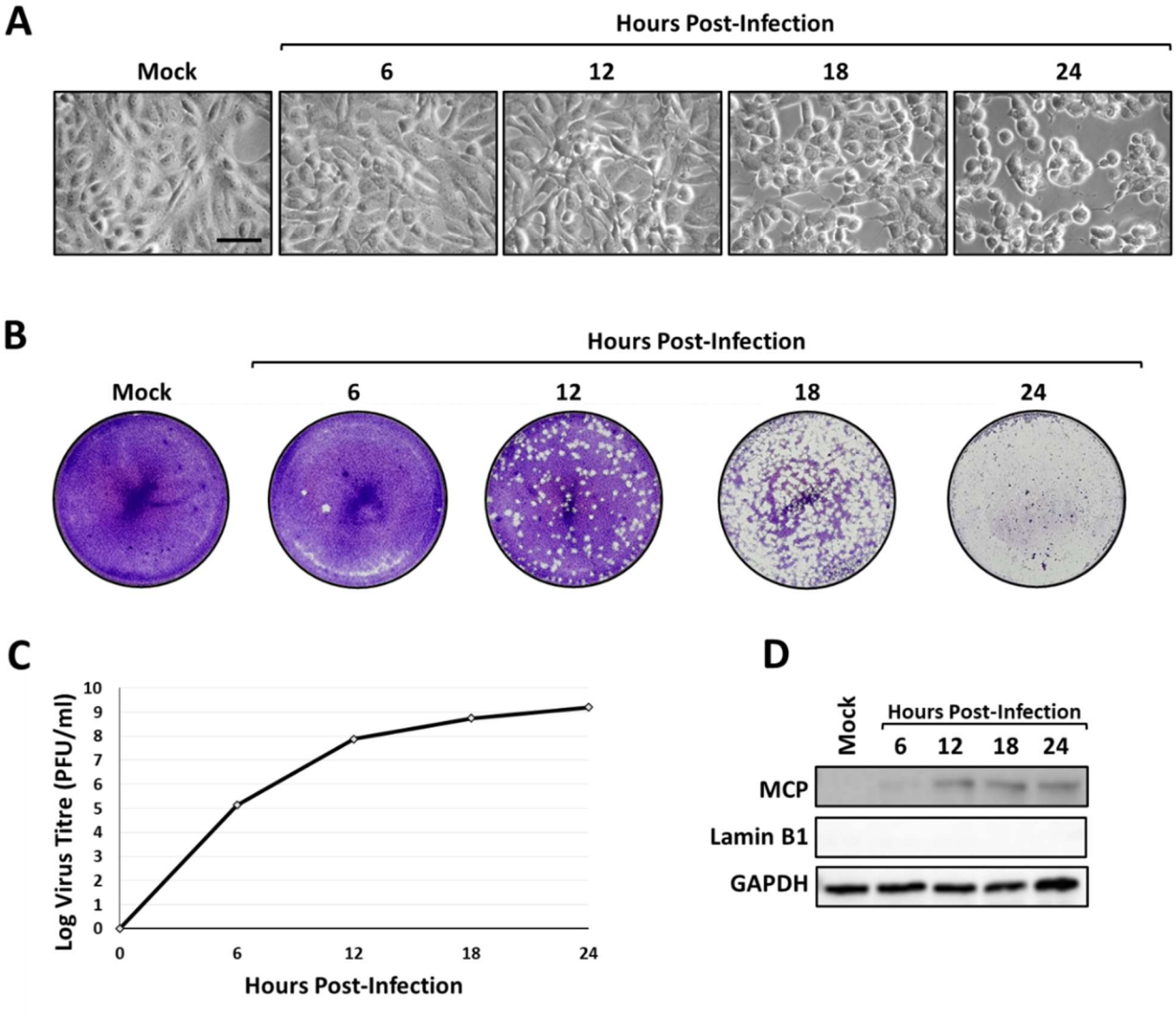

Figure 5.22: Successful propagation of HSV1 and the optimum time point for cytoplasmic capsid concentration.

Confluent human foreskin fibroblasts (HFF1s) were infected with HSV1 (MOI = 4) and then incubated for 6, 12, 18, and 24 hours. The HFF1 cell monolayer was then imaged to document cytopathic effect by phase-contrast light microscopy. Images were taken at 40x magnification and scale bars represent 100 µm. (B-C) The cell supernatants from (A) were collected and a plaque assay was conducted to calculate the viral titre. The images from (B) show the crystal violet-stained cell monolayer and plaques of the 10^{-3} dilution for the different time points and the graph from (C) has the results displayed on a log scale, suitable dilution ranges were selected for each time point. (D) The HFF1s infected with HSV1 from (A) were then harvested, and the cytoplasm was isolated via subcellular fractionation. The cytoplasmic cell lysate protein levels were equalised using the Pierce™ BCA protein assay kit and then then separated by SDS-PAGE (10% acrylamide gel) and analysed via western blot (n=3). The antibodies used were specific to HSV1 major capsid protein (MCP [pU_L19]), lamin B1, and GAPDH. MCP was used as a qualitative indicator of HSV1 capsid quantity, Lamin B1 was used as a nuclear marker to confirm cytoplasmic fraction purity, and GAPDH was used as a loading control.

5.3 Herpesvirus Discussion

The aim of this chapter was to investigate the role of DOCK5 in herpesvirus egress using TEM. To test this, KSHV infected cells were transfected with the microRNA hairpin inhibitor hsa-miR-365a-3p to prevent the downregulation of DOCK5 by herpesviruses, and the cells were then imaged by TEM. Furthermore, the process was investigated in HSV1 through western blot analysis. It was found that the KSHV induction method does not result in the production of enough KSHV cytoplasmic capsids to be imaged by TEM. Additionally, signs of ER restructuring was detected in KSHV induced cells. Finally, DOCK5 was identified within the nucleus of two different cell types by western blot analysis.

5.3.1 KSHV remodels host ER similarly to alpha- and betaherpesviruses

In KSHV infected cells, signs of ER restructuring was identified at 46 hp_{ind} (Figure 5.13). Herpesviruses are known to interact with the ER as part of their life cycle. In the alphaherpesvirus HSV1, viral capsids can travel directly through the ER and then into the Golgi before exiting the cell (Wild et al., 2017). It has also been found that HSV1 infection results in the temporary enlargement of the ER during infection, possibly due to enhanced lipid and protein synthesis (Lv et al., 2019b, Sutter et al., 2012). Furthermore, Maeda et al. (2017) observed that HSV1 compresses the ER around the nuclear periphery using the NEC protein pU_L34. The compression of the ER around the nucleus by HSV1 results in the accumulation of the viral glycoproteins gB and gH within the nuclear membranes, aiding in nuclear egress (Maeda et al., 2017). Other herpesviruses can also remodel host ER membranes e.g. the betaherpesvirus HCMV. HCMV is able to induce the re-organisation of the ER through the ER-resident glycoprotein pU_L148. pU_L148 alone is able to induce a ruffled morphology in the ER by a currently unknown mechanism, which is hypothesised to create an environment more suited for viral protein folding (Nguyen et al., 2020, Zhang et al., 2019). I could find no mention of ER remodelling by the gammaherpesvirus EBV in the literature.

In KSHV the process is slightly different: nucleocapsids do not travel directly through the ER, but rather travel through the cytoplasm where they bud into the viral protein-studded Golgi (Long et al., 2022). KSHV does however fold structural and non-structural viral proteins within the RER which then transit into the Golgi where they join with the KSHV nucleocapsid (Johnston et al., 2019). The presence of viral proteins within the RER could result in the modified RER having the greater electron

density seen in the micrographs (Figure 5.13). Furthermore, KSHV has a precedent of interacting with the ER-remodelling atlastins. Atlastins are host GTPases that control ER membrane structure and have been shown to regulate KSHV lytic infection. It was found that the overexpression of atlastins boosted KSHV lytic activation, with the inhibition of atlastin achieving the opposite (Long et al., 2022). There is no mention of KSHV restructuring the ER in the literature, however the paper by Maeda et al. (2017) suggested that their finding of ER restructuring by HSV1 was the first of its kind for herpesviruses, so the subject has not been well studied.

The restructuring of the ER by herpesviruses is a new topic and so warrants further investigation. The restructuring of the ER by KSHV could be studied structurally through techniques such as cellular tomography or FIB milling which have been mentioned in previous chapters. The study of the ER restructuring by KSHV in 3D could reveal more detailed information regarding the ER morphology than is available by 2D TEM. Additionally in the research above, the viral factors for herpesvirus remodelling have been specified. Although the HCMV protein pU_L148 has no orthologue in KSHV, the HSV1 protein pU_L34 does (Maeda et al., 2017, Zhang et al., 2019). The HSV1 protein pU_L34 is one of the NEC proteins and in KSHV the orthologue is pORF67 (Farina et al., 2013, Desai et al., 2012). It would be interesting to investigate whether pORF67 plays a similar role in ER restructuring that pU_L34 does in HSV1 infected cells. To explore the role of pORF67 in the restructuring of the ER in KSHV infected cells, pORF67 knock-out KSHV mutants can be generated to see if the ER returns to a normal morphology. Furthermore, pORF67 can be transfected into non-infected cells to see if the pORF67 expression alone is enough to induce ER restructuring.

From the observation of remodelled ER in KSHV infected cells, it suggests that KSHV might be capable of restructuring the host ER as has been recently identified in HSV1 and HCMV. From what I could identify in the literature, this is the first time that ER remodelling has been identified in a gammaherpesvirus. Further research will be needed to identify whether host atlastins or pORF67 are involved in the process.

5.3.2 DOCK5 acts as a GEF for the nuclear Rho GTPase Rac1

As mentioned above, according to the literature DOCK5 is a cytoplasmic protein. Despite this, the western blot in figure 5.21 clearly shows a band of the correct size

in the nuclear fraction, with no band observed in the cytoplasmic fraction. The same result was observed in a repeat western blot on the same cell fractions (therefore, a technical repeat). DOCK5 is a member of the DOCK family of GEFs. GEFs regulate Rho GTPases which are involved in cytoskeleton modification (Laurin and Côté, 2014). Rho GTPases were originally linked solely to the cytosol and plasma membrane; however, post-translational modifications allow Rho GTPases to transfer to cellular endomembrane structures (e.g. Golgi, endosomes and nucleus) (Phuyal and Farhan, 2019, Michaelson et al., 2001). For example, Rac1 is a Rho GTPase which has nuclear localisation signals on its C-terminal, enabling its relocation to the nucleus. Rac1 has been shown to modify actin polymerisation in the nucleus allowing Rac1 to moderate nuclear membrane morphology (Navarro-Lérida et al., 2015, Phuyal and Farhan, 2019). The movement of Rac1 in and out of the nucleus is reliant upon the cell cycle, with the G2 phase being associated with higher levels of Rac1 (Michaelson et al., 2008). DOCK5 has been found to activate Rac1 in osteoclast cells, allowing for bone resorption (Vives et al., 2011). Additionally, Kukimoto-Niino et al. (2021) published a 3.8 Å resolution structure of DOCK5 bound to Rac1. This evidence suggests that DOCK5 may have links with to the nucleus through Rac1 and therefore could be located there as seen in Figure 5.21, however it does not explain the total absence of DOCK5 in the cytoplasm in HFF1 and TREx cells. Further experiments will be needed to ascertain whether this result is anomalous or a novel result.

The finding that DOCK5 is exclusively located within the nucleus of both B-cell and fibroblast cell lines requires follow up experiments to confirm its validity. Especially considering that most of the literature points at DOCK5 being primarily a cytoplasmic based protein. If I had the time to continue these experiments, I would start with a biological repeat of Figure 5.21 with new cell lysates to confirm the presence of DOCK5 within the nucleus. This could then be followed up with another commercially bought DOCK5 primary antibody, to rule out atypical antibody binding. Confirmation of successful antibody binding would be aided with improved positive and negative controls. Recombinant DOCK5 can be purchased (or expressed and purified) and used as a positive control in a western blot. For the negative control, DOCK5 could be knocked down through the use of DOCK5 siRNA which would reduce the expression of DOCK5. This would be detectable via western blot and would work as a negative control (Olds and Li, 2016). Following this experiment, a number of cell lines could be selected to represent the main cell types from across the body. A DOCK5 western blot analysis of the representative cell lines (e.g. epithelial [HEK293s] and endothelial [HMVEC]) would establish whether the subcellular location varies between cell types. The findings from the above experiments could

be further supported by immunofluorescence studies of DOCK5, to visualise its subcellular location (Stadler et al., 2013).

5.3.3 Herpesvirus follow-up experiments

I started this project on herpesviruses to identify how DOCK5 was involved in KSHV egress. I initially tried to image the cytoplasmic capsid accumulation (Figure 5.7) that occurred when the KSHV inhibition of DOCK is blocked (identified by the Whitehouse laboratory). However, the inability to find any cytoplasmic capsids via TEM interrupted this plan. Therefore, I tried to use western blot analysis with KSHV capsid antibodies to identify the optimum induction technique for the successful production of KSHV cytoplasmic capsids. This was further impeded by the inability to find a working KSHV capsid antibody. Unfortunately, due to a mixture of failing to find a working KSHV capsid antibody and a significant reduction in laboratory time due to the COVID-19 pandemic, I was unable to follow up these experiments. If I was able to follow up these experiments, I would try to identify a KSHV induction technique that increases cytoplasmic capsids. I would start with the NaB induction method as this was the most promising induction technique identified from the TREx cell growth curves (Figure 5.19). Due to the previously mentioned issues with KSHV capsid antibodies, I would utilise the slower, but more reliable TEM to analyse this.

To investigate the role of DOCK5 in herpesvirus egress, cells would be infected with either KSHV or HSV1 and incubated for the four virus specific time points. Once incubated, cells would be lysed and analysed via western blot analysis using a DOCK5 antibody to assess whether herpesvirus infection alters DOCK5 cellular levels at any of the four time points. To follow up this experiment, TREx and HFF1 cells would then be transfected with the miRIDIAN microRNA hairpin inhibitor hsa-miR-365a-3p. After the relevant time point post induction or infection (dependent upon the first DOCK5 western blot above) cells would then be lysed via subcellular fractionation for later western blot analysis and fixed for TEM. The supernatant of the HSV1 infected HFF1 cells would then be collected for a HSV1 plaque assay. Next, western blot analysis would be used to assess for changes in cytoplasmic HSV1 capsid levels and for changes in DOCK5 levels between transfect and non-transfected KSHV and HSV1 infected cells. This would ascertain whether the transfection of cells with hsa-miR-365a-3p prevents the downregulation of DOCK5 by herpesvirus infection. The cells processed for TEM would be used to ascertain if transfected cells had any visible changes to their viral life cycle, with particular focus on herpesvirus egress. Finally, plaque assays would be used to determine if there

are any changes to infectious HSV1 virion levels between transfected and non-transfected cells. If the prevention of DOCK5 inhibition by herpesviruses did result in an accumulation of cytoplasmic capsids, the experiment could be followed with the DOCK5 inhibitor, C21 (Ferrandez et al., 2017). Blocking the action of DOCK5 would potentially result in a return normal herpesvirus infection (i.e. the downregulation of DOCK5) and therefore the cell phenotype should return to normal viral egress.

Chapter 6 : Concluding remarks

The main aim of my PhD project was to utilise transmission electron microscopy to better understand viral replication cycles. Throughout the three viruses studied here, I have demonstrated how TEM offers a glimpse into the cell, providing structural details regarding viral alterations of cellular architecture. Despite TEM being an old technique that has been used for decades, I was able to use TEM to elucidate novel aspects of viral replication cycles. In TULV infected cells, I utilised TEM alongside Katherine Davies' immunofluorescence to identify filamentous viral structures in an OW Hantavirus for the first time. Additionally, I observed ER enlargement in TULV infected cells, similar to that seen in HTNV infection. In rotavirus infected cells I employed TEM to further support the hypothesis that LLPS drives viroplasm formation. I then combined this with a bioinformatic analysis, which resulted in further evidence that NSP5 acts as a driver of LLPS in rotavirus infected cells. Finally, I employed TEM to image the RER ultrastructure manipulation in KSHV infected cells.

6.1 Limitations of TEM

Despite being a highly useful technique, TEM does have its limitations that I encountered during some of these during this project. One of the first issues I came across with TEM was the subjectivity in identifying cellular and viral structures. Frequently with TEM and most microscopy approaches, features of interest have to be positively identified by the operator. This can be difficult due to the large degree of morphological variation present within samples. Even structures that are easy to identify (e.g. mitochondria) can appear drastically different, even when within the same cell. This is further complicated when looking for rare or novel features which may have little to no reference micrographs in the literature. For example, I came across granular aggregates within the cytoplasm of imaged cells when working on rotavirus (Figure 4.14). It took me around two months to identify the structures as glycogen granules. This issue is mitigated by user experience; the more micrographs one sees, the easier it is for them to identify unknown structures. Furthermore, combining TEM with staining techniques such as immunogold, or fluorescence in CLEM can drastically mitigate subjectivity (Nixon et al., 2009). By tagging molecules or structures of interest with markers, one can objectively identify them later on.

Another issue with TEM can occur when it is used to view rare cellular events. This was particularly evident when imaging cells infected with rotavirus versus KSHV. In

rotavirus, virally infected cells are easy to identify due to the presence of large viroplasms or capsid aggregates. Whereas in KSHV it was extremely difficult to detect cytoplasmic virions due to their scarcity. Therefore it is extremely important to assess the rarity of the subject of interest when designing projects with TEM. Based on my experience, I think that one of the requirements for a successful TEM project is to ensure that the events being imaged are abundant (e.g. in the case of viral replication cycles, this would mean that the virus produces a large number of progeny virions). For example, one of the advantages of identifying viral changes to ER size and shape is the sheer number of ER present in cells. This guarantees a large sample size per number of cell sections imaged, making it easier and quicker to get a representative sample size. Again, the issue of rare cellular events can be mitigated through tagging techniques such as CLEM.

Despite its shortcomings, TEM offers an unparalleled level of structural detail when used to image virally infected cells. With it I was able to elucidate aspects of cytoplasmic replication in three different viruses, which will hopefully contribute to improving our understanding of these viral replication cycles, which could be used to develop new antivirals.

6.2 Viral factories as a common mechanism of viral replication

Viral replication varies greatly depending upon the virus in question. However, a common theme across different viruses is the reorganisation of the infected cell and the formation of a viral factory. Viral factories are discrete, intracellular regions that contain the necessary viral and cellular components to produce progeny virions (Fernandez de Castro et al., 2020). Strikingly, while viral factories can be highly heterogenous across different viruses, they also present some commonalities. This can be seen across the three viruses I studied in this thesis. DNA viruses typically replicate their genomes within the nucleus (e.g. Polyomaviridae), although there are DNA viruses which replicate exclusively within the cytoplasm (e.g. Poxviridae) (Erickson and Garcea, 2019, Kieser et al., 2020). In contrast to this, the majority of RNA viruses form viral factories within the cell cytoplasm (Fernandez de Castro et al., 2020). Within the cytoplasm, there are a number of locations and organelles exploited by viruses which act as sites of replication. For example, invaginations known as spherules can be formed within a number of membranes such as the plasma membrane, ER and endosome by certain viruses (e.g. Togaviridae) (Laurent et al., 2022). Additionally, host membranes can be remodelled to form double-membrane vesicles (e.g. Caliciviridae) and tubules (Hepeviridae) (Snijder et al.,

2020, Bentaleb et al., 2022). Finally, viral factories can be formed without membranes (e.g. Rhabdoviridae) (Nevers et al., 2020).

6.2.1 Comparison of KSHV and other DNA virus replication factories

Regarding DNA viruses, in this thesis I studied the viral factories of the herpesvirus KSHV. These are similar to those generated by polyomaviruses, which are small (40 to 50 nm), non-enveloped DNA viruses which infect mammals and birds (Ahsan and Shah, 2006). Polyomaviruses replicate within the nucleus of infected cells, where they form large replication factories which act as sites of DNA replication and packaging (Erickson and Garcea, 2019). In both John Cunningham (JC) virus and murine polyomavirus (both model polyomaviruses), TEM and ET allowed for the visualisation of the viral replication factories, revealing capsid clusters. This has also been seen for herpesviruses, in which capsid intermediates are frequently observed in large clusters (Myllys et al., 2016). However, in contrast to herpesviruses, polyomaviruses also present tubular intermediate assemblies within the nucleus (Erickson and Garcea, 2019, Erickson et al., 2012). The tubular intermediates are made entirely from the major capsid protein VP1 leading to the conclusion that the tubules act as an intermediate, with capsids budding from the tubes (Erickson et al., 2012, Erickson and Garcea, 2019). Another difference between polyomaviruses and herpesviruses is the way the capsids exit the nucleus. While herpesvirus capsids must undergo a process of envelopment and de-envelopment within the nuclear membrane (as their capsids are too large to pass through the nuclear pores) the process in polyomaviruses is less understood (Panou et al., 2018). Currently, the mechanism by which polyomaviruses undergo nuclear egress is unknown, however the viral agnoprotein has been found to be an essential egress factor. Studies show that when agnoprotein is knocked-down, virions remain trapped within the nucleus (Panou et al., 2018).

Despite being DNA viruses that replicate within the nucleus of infected cells, a key aspect of herpesvirus replication occurs within the cytoplasm, involving tegumentation and envelopment (see section 5.1.6.7) (Owen et al., 2015). My key finding with regards KSHV replication is the RER restructuring I observed by TEM. Of note, similar ER restructuring has been observed in alpha and beta herpesviruses (Maeda et al., 2017, Nguyen et al., 2020), suggesting this is a common theme for herpesviruses.

Another DNA virus family that restructures the ER are poxviruses. Poxviruses are a family of DNA viruses that form a singular viral factory (originally called Guarnieri bodies) within the cytoplasm upon entry into the cell (Kieser et al., 2020). In early

infection, the factories contain viral DNA enclosed within RER-derived membranes, which enlarge over time and form distinct internal regions (Tolonen et al., 2001, Katsafanas and Moss, 2007). These internal factory zones host viral mRNA and translation factors, enabling the expression of viral proteins (Katsafanas and Moss, 2007). In late infection the surrounding RER membranes are reassembled using viral membrane assembly proteins. The RER membranes are reorganised into crescent structures which act as a source of membranes for the newly produced immature virions (Weisberg et al., 2017, Kieser et al., 2020). Immature virions are then processed into mature virions, of which a small number will then obtain additional membranes from the Golgi and then egress via fusion with the plasma membrane (Harrison et al., 2016). As discussed in section 5.31, it will be interesting to see the role of ER restructuring in Herpesviridae viral replication further explored in the future. However, it is tempting to speculate that like in poxviruses, the ER modifications seen in herpesviruses are also related to virus assembly.

6.2.2 Membrane-bound viral factories of RNA viruses

DNA viruses are not the only viruses to produce progeny virions within the cytoplasm of infected cells - RNA viruses are also well established at replicating within the cytoplasm. The majority of RNA viruses replicate their genomes within the cytoplasm as they have no need for the DNA replication machinery within the nucleus. However, replicating RNA within the cytoplasm via RdRp risks triggering the innate immune system. Consequently, RNA viruses have evolved to separate their viral replicons from the cytoplasm via modified cellular membranes or LLPS (Roingeard et al., 2022).

(+) ssRNA viruses represent the best studied examples of cytoplasmic viral factories derived from cellular membranes, forming structures such as double-membrane vesicles and spherules. Many other (+) ssRNA viral factories have been characterised in detail, but their description is outside the scope of this discussion.

Contrary to (+) ssRNA viruses, the viral factories of (-) ssRNA viruses generally do not involve cellular membranes, e.g. rhabdoviruses (see section below). An exception to this are Bunyaviruses (order Bunyavirales), for which the remodelling of host Golgi to form tubular replication factories has been observed for the model bunyavirus BUNV (Salanueva et al., 2003, Novoa et al., 2005, Fontana et al., 2008). These tubes have been found to contain the viral protein NSm, cellular actin and all the elements required for viral replication (including nucleoprotein and polymerase). Additionally, the replication factories contain RNA replication intermediaries such as dsRNA (Elliott, 2014, Fontana et al., 2017). Strikingly, I did not see any of

remodelled Golgi membranes around or within the filamentous structures identified when imaging Tula virus infected cells via TEM, suggesting that the Golgi remodelling for TULV is not as extensive as the one occurring for BUNV. However, Katherine Davies immunofluorescence imaging did identify Golgi proteins amongst the NP filaments. This indicates that the Golgi might be partially involved in the production of progeny virions in Tula virus infected cells. Although I did not observe any morphological changes in Golgi structure via TEM, there was a large degree of ER enlargement and branching as infection progressed. This suggests that TULV might use the ER as a site of viral replication, although this will need further studying (see section 3.3.1.3 and 3.3.2). These results suggest that different families from the Bunyavirales order might differ in their replication strategy. In the future, it will be interesting to follow our understanding on the different types of viral factories formed by this large group of viruses.

6.2.3 Membrane-less viral factories of RNA viruses

In addition to forming viral replication sites within membranous structures, RNA viruses, like Rabies virus, are also capable of forming membrane-less replication compartments, which are similar to the ones formed by rotaviruses (Nevers et al., 2020).

Rabies virus forms membrane-less viral factories within the cytoplasm on infected neurons known as Negri bodies (Kristensson et al., 1996). Rabies virus is a (-) ssRNA, neurotrophic virus of the Rhabdoviridae family that is responsible for causing fatal encephalitis in humans (Fooks et al., 2017). Like the rotavirus viroplasms covered in this thesis, Negri bodies form through LLPS (Nikolic et al., 2017). In rabies virus (and other rhabdoviruses), the inclusion bodies contain the viral nucleoprotein, phosphoprotein, polymerase, matrix protein and RNA (genomic and mRNA) (Nevers et al., 2020). Whilst containing all these components, the formation of the Negri bodies is dependent upon the interaction between the phosphoprotein and nucleoprotein (Nikolic et al., 2017). In fact, the expression of the nucleoprotein and phosphoprotein alone results in the formation of Negri body-like structures. The phosphoprotein contains several disordered regions which enable it to form the multivalent bonds necessary for LLPS, whereas the nucleoprotein is able to bind to RNA (Nikolic et al., 2017). Consequently, it is predicted that the nucleoprotein binds to both viral RNA and the phosphoprotein within the viral inclusions (Mavrakis et al., 2003). Once formed, the Negri bodies act as sites of viral transcription and replication, allowing for the production of progeny virions (Lahaye et al., 2009).

Like in rabies virus and several other viruses which form membrane-less viral factories, my experiments and other research indicates that rotavirus forms its viroplasms via LLPS (Geiger et al., 2021). Additionally, the bioinformatic analysis on NSP2 and NSP5 further support the hypothesis that NSP5 acts as a driver of LLPS viroplasm formation. Interestingly, the role of NSP2 and NSP5 in rotavirus viroplasm formation similarly mirrors the role of the nucleoprotein and phosphoprotein (respectively) in rabies virus inclusion body formation.

6.3 Final conclusion

Overall, this thesis illustrates the great complexity that viral factories can present. Increasing our understanding of their organisation and composition in different viruses will highlight similarities between different viruses, enabling us to tackle the burden caused by viruses.

References

<02-0327.pdf>.
ABAITUA, F., HOLLINSHEAD, M., BOLSTAD, M., CRUMP, C. M. & O'HARE, P. 2012. A Nuclear Localization Signal in Herpesvirus Protein VP1-2 Is Essential for Infection via Capsid Routing to the Nuclear Pore. *Journal of Virology,* 86**,** 8998-9014.
ABAITUA, F., ZIA, F. R., HOLLINSHEAD, M. & O'HARE, P. 2013. Polarized cell migration during cell-to-cell transmission of herpes simplex virus in human skin keratinocytes. *J Virol,* 87**,** 7921-32.
ABERNATHY, E., CLYDE, K., YEASMIN, R., KRUG, L. T., BURLINGAME, A., COSCOY, L. & GLAUNSINGER, B. 2014. Gammaherpesviral gene expression and virion composition are broadly controlled by accelerated mRNA degradation. *PLoS Pathog,* 10**,** e1003882.
ABLASHI, D. V., CHATLYNNE, L. G., WHITMAN, J. J. E. & CESARMAN, E. 2002. Spectrum of Kaposi's Sarcoma-Associated Herpesvirus, or Human Herpesvirus 8, Diseases. *Clinical Microbiology Reviews,* 15**,** 439-464.
ABRAHAM, D. J. & LEO, A. J. 1987. Extension of the fragment method to calculate amino acid zwitterion and side chain partition coefficients. *Proteins: Structure, Function, and Bioinformatics,* 2**,** 130-152.
ABU SIN, M., STARK, K., VAN TREECK, U., DIECKMANN, H., UPHOFF, H., HAUTMANN, W., BORNHOFEN, B., JENSEN, E., PFAFF, G. & KOCH, J. 2007. Risk factors for hantavirus infection in Germany, 2005. *Emerging infectious diseases,* 13**,** 1364-1366.
ABUDUREXITI, A., ADKINS, S., ALIOTO, D., ALKHOVSKY, S. V., AVŠIČ-ŽUPANC, T., BALLINGER, M. J., BENTE, D. A., BEER, M., BERGERON, É., BLAIR, C. D., BRIESE, T., BUCHMEIER, M. J., BURT, F. J., CALISHER, C. H., CHÁNG, C., CHARREL, R. N., CHOI, I. R., CLEGG, J. C. S., DE LA TORRE, J. C., DE LAMBALLERIE, X., DÈNG, F., DI SERIO, F., DIGIARO, M., DREBOT, M. A., DUÀN, X., EBIHARA, H., ELBEAINO, T., ERGÜNAY, K., FULHORST, C. F., GARRISON, A. R., GĀO, G. F., GONZALEZ, J. J., GROSCHUP, M. H., GÜNTHER, S., HAENNI, A. L., HALL, R. A., HEPOJOKI, J., HEWSON, R., HÚ, Z., HUGHES, H. R., JONSON, M. G., JUNGLEN, S., KLEMPA, B., KLINGSTRÖM, J., KÒU, C., LAENEN, L., LAMBERT, A. J., LANGEVIN, S. A., LIU, D., LUKASHEVICH, I. S., LUÒ, T., LǓ, C., MAES, P., DE SOUZA, W. M., MARKLEWITZ, M., MARTELLI, G. P., MATSUNO, K., MIELKE-EHRET, N., MINUTOLO, M., MIRAZIMI, A., MOMING, A., MÜHLBACH, H. P., NAIDU, R., NAVARRO, B., NUNES, M. R. T., PALACIOS, G., PAPA, A., PAUVOLID-CORRÊA, A., PAWĘSKA, J. T., QIÁO, J., RADOSHITZKY, S. R., RESENDE, R. O., ROMANOWSKI, V., SALL, A. A., SALVATO, M. S., SASAYA, T., SHĚN, S., SHÍ, X., SHIRAKO, Y., SIMMONDS, P., SIRONI, M., SONG, J. W., SPENGLER, J. R., STENGLEIN, M. D., SŪ, Z., SŪN, S., TÁNG, S., TURINA, M., WÁNG, B., WÁNG, C., WÁNG, H., WÁNG, J., WÈI, T., WHITFIELD, A. E., ZERBINI, F. M., ZHĀNG, J., ZHĀNG, L., ZHĀNG, Y., ZHANG, Y. Z., ZHĀNG, Y., et al. 2019. Taxonomy of the order Bunyavirales: update 2019. *Arch Virol,* 164**,** 1949-1965.
AGELIDIS, A. M. & SHUKLA, D. 2015. Cell entry mechanisms of HSV: what we have learned in recent years. *Future Virol,* 10**,** 1145-1154.
AHMAD, I. & WILSON, D. W. 2020. HSV-1 Cytoplasmic Envelopment and Egress. *Int J Mol Sci,* 21.
AKTEPE, T. E., LIEBSCHER, S., PRIER, J. E., SIMMONS, C. P. & MACKENZIE, J. M. 2017. The Host Protein Reticulon 3.1A Is Utilized by Flaviviruses to Facilitate Membrane Remodelling. *Cell Rep,* 21**,** 1639-1654.
AKULA, S. M., NARANATT, P. P., WALIA, N. S., WANG, F. Z., FEGLEY, B. & CHANDRAN, B. 2003. Kaposi's sarcoma-associated herpesvirus (Human herpesvirus 8) infection of human fibroblast cells occurs through endocytosis. *Journal of Virology,* 77**,** 7978-7990.

AKULA, S. M., PRAMOD, N. P., WANG, F. Z. & CHANDRAN, B. 2002. Integrin alpha 3 beta 1 (CD 49c/29) is a cellular receptor for Kaposi's sarcoma-associated herpesvirus (KSHV/HHV-8) entry into the target cells. *Cell,* 108**,** 407-419.

ALBERTI, S., GLADFELTER, A. & MITTAG, T. 2019. Considerations and Challenges in Studying Liquid-Liquid Phase Separation and Biomolecular Condensates. *Cell,* 176**,** 419-434.

ALENQUER, M., VALE-COSTA, S., ETIBOR, T. A., FERREIRA, F., SOUSA, A. L. & AMORIM, M. J. 2019. Influenza A virus ribonucleoproteins form liquid organelles at endoplasmic reticulum exit sites. *Nature communications,* 10**,** 1629-1629.

ALIABADI, N., ANTONI, S., MWENDA, J. M., WELDEGEBRIEL, G., BIEY, J. N. M., CHEIKH, D., FAHMY, K., TELEB, N., ASHMONY, H. A., AHMED, H., DANIELS, D. S., VIDEBAEK, D., WASLEY, A., SINGH, S., DE OLIVEIRA, L. H., REY-BENITO, G., SANWOGOU, N. J., WIJESINGHE, P. R., LIYANAGE, J. B. L., NYAMBAT, B., GRABOVAC, V., HEFFELFINGER, J. D., FOX, K., PALADIN, F. J., NAKAMURA, T., AGÓCS, M., MURRAY, J., CHERIAN, T., YEN, C., PARASHAR, U. D., SERHAN, F., TATE, J. E. & COHEN, A. L. 2019. Global impact of rotavirus vaccine introduction on rotavirus hospitalisations among children under 5 years of age, 2008-16: findings from the Global Rotavirus Surveillance Network. *Lancet Glob Health,* 7**,** e893-e903.

ALONSO, D. O., PÉREZ-SAUTU, U., BELLOMO, C. M., PRIETO, K., IGLESIAS, A., COELHO, R., PERIOLO, N., DOMENECH, I., TALMON, G., HANSEN, R., PALACIOS, G. & MARTINEZ, V. P. 2020. Person-to-Person Transmission of Andes Virus in Hantavirus Pulmonary Syndrome, Argentina, 2014. *Emerging infectious diseases,* 26**,** 756-759.

AMERSON, E., WOODRUFF, C. M., FORRESTEL, A., WENGER, M., MCCALMONT, T., LEBOIT, P., MAURER, T., LAKER-OKETTA, M., MUYINDIKE, W., BWANA, M., BUZIBA, N., BUSAKHALA, N., WOOLS-KALOUSTIAN, K. & MARTIN, J. 2016. Accuracy of Clinical Suspicion and Pathologic Diagnosis of Kaposi Sarcoma in East Africa. *J Acquir Immune Defic Syndr,* 71**,** 295-301.

AMIMO, J. O., RAEV, S. A., CHEPNGENO, J., MAINGA, A. O., GUO, Y., SAIF, L. & VLASOVA, A. N. 2021. Rotavirus Interactions With Host Intestinal Epithelial Cells. *Frontiers in Immunology,* 12.

AMROUN, A., PRIET, S., DE LAMBALLERIE, X. & QUÉRAT, G. 2017. Bunyaviridae RdRps: structure, motifs, and RNA synthesis machinery. *Crit Rev Microbiol,* 43**,** 753-778.

ANDERSON, E. J. & WEBER, S. G. 2004. Rotavirus infection in adults. *Lancet Infect Dis,* 4**,** 91-9.

ANDERSON, N. W., BUCHAN, B. W. & LEDEBOER, N. A. 2014. Light microscopy, culture, molecular, and serologic methods for detection of herpes simplex virus. *Journal of clinical microbiology,* 52**,** 2-8.

ANDERSON, P. & KEDERSHA, N. 2008. Stress granules: the Tao of RNA triage. *Trends Biochem Sci,* 33**,** 141-50.

ANEJA, K. K. & YUAN, Y. 2017. Reactivation and Lytic Replication of Kaposi's Sarcoma-Associated Herpesvirus: An Update. *Front Microbiol,* 8**,** 613.

APPENZELLER-HERZOG, C. & HAURI, H. P. 2006. The ER-Golgi intermediate compartment (ERGIC): in search of its identity and function. *J Cell Sci,* 119**,** 2173-83.

ARIAS, C., WEISBURD, B., STERN-GINOSSAR, N., MERCIER, A., MADRID, A. S., BELLARE, P., HOLDORF, M., WEISSMAN, J. S. & GANEM, D. 2014. KSHV 2.0: a comprehensive annotation of the Kaposi's sarcoma-associated herpesvirus genome using next-generation sequencing reveals novel genomic and functional features. *PLoS Pathog,* 10**,** e1003847.

ARIAS, C. F., SILVA-AYALA, D. & LÓPEZ, S. 2015. Rotavirus entry: a deep journey into the cell with several exits. *Journal of virology,* 89**,** 890-893.

ARII 2021. Host and Viral Factors Involved in Nuclear Egress of Herpes Simplex Virus 1. *Viruses,* 13.

ARII, FUKUI, A., SHIMANAKA, Y., KONO, N., ARAI, H., MARUZURU, Y., KOYANAGI, N., KATO, A., MORI, Y., KAWAGUCHI, Y. & SANDRI-GOLDIN, R. M. 2020. Role of Phosphatidylethanolamine Biosynthesis in Herpes Simplex Virus 1-Infected Cells in Progeny Virus Morphogenesis in the Cytoplasm and in Viral Pathogenicity In Vivo. *Journal of Virology,* 94**,** e01572-20.

ARII, WATANABE, M., MAEDA, F., TOKAI-NISHIZUMI, N., CHIHARA, T., MIURA, M., MARUZURU, Y., KOYANAGI, N., KATO, A. & KAWAGUCHI, Y. 2018. ESCRT-III mediates budding across the inner nuclear membrane and regulates its integrity. *Nat Commun,* 9**,** 3379.

ARNOLDI, F., CAMPAGNA, M., EICHWALD, C., DESSELBERGER, U. & BURRONE, O. R. 2007. Interaction of rotavirus polymerase VP1 with nonstructural protein NSP5 is stronger than that with NSP2. *J Virol,* 81**,** 2128-37.

ARRAGAIN, REGUERA, J., DESFOSSES, A., GUTSCHE, I., SCHOEHN, G. & MALET, H. 2019. High resolution cryo-EM structure of the helical RNA-bound Hantaan virus nucleocapsid reveals its assembly mechanisms. *Elife,* 8.

ARTIKA, I. M., DEWANTARI, A. K. & WIYATNO, A. 2020. Molecular biology of coronaviruses: current knowledge. *Heliyon,* 6**,** e04743.

ASLANI, A., OLSSON, M. & ELIAS, P. 2002. ATP-dependent unwinding of a minimal origin of DNA replication by the origin-binding protein and the single-strand DNA-binding protein ICP8 from herpes simplex virus type I. *J Biol Chem,* 277**,** 41204-12.

ATANASIU, D., CAIRNS, T. M., WHITBECK, J. C., SAW, W. T., RAO, S., EISENBERG, R. J., COHEN, G. H. & DERMODY, T. S. 2013. Regulation of Herpes Simplex Virus gB-Induced Cell-Cell Fusion by Mutant Forms of gH/gL in the Absence of gD and Cellular Receptors. *mBio,* 4**,** e00046-13.

AUCOIN, D. P., COLLETTI, K. S., CEI, S. A., PAPOUSKOVÁ, I., TARRANT, M. & PARI, G. S. 2004. Amplification of the Kaposi's sarcoma-associated herpesvirus/human herpesvirus 8 lytic origin of DNA replication is dependent upon a cis-acting AT-rich region and an ORF50 response element and the trans-acting factors ORF50 (K-Rta) and K8 (K-bZIP). *Virology,* 318**,** 542-555.

AVŠIČ-ŽUPANC, T., SAKSIDA, A. & KORVA, M. 2019. Hantavirus infections. *Clin Microbiol Infect,* 21s**,** e6-e16.

AYACHE, J., BEAUNIER, L., BOUMENDIL, J., EHRET, G. & LAUB, D. 2010. Artifacts in Transmission Electron Microscopy. *In:* AYACHE, J., BEAUNIER, L., BOUMENDIL, J., EHRET, G. & LAUB, D. (eds.) *Sample Preparation Handbook for Transmission Electron Microscopy: Methodology.* New York, NY: Springer New York.

AYERS, L. W., BARBACHANO-GUERRERO, A., MCALLISTER, S. C., RITCHIE, J. A., ASIAGO-REDDY, E., BARTLETT, L. C., CESARMAN, E., WANG, D., ROCHFORD, R., MARTIN, J. N. & KING, C. A. 2018. Mast Cell Activation and KSHV Infection in Kaposi Sarcoma. *Clin Cancer Res,* 24**,** 5085-5097.

AZAB, W., DAYARAM, A., GREENWOOD, A. D. & OSTERRIEDER, N. 2018. How Host Specific Are Herpesviruses? Lessons from Herpesviruses Infecting Wild and Endangered Mammals. *Annual Review of Virology,* 5**,** 53-68.

BABU, M. M. 2016. The contribution of intrinsically disordered regions to protein function, cellular complexity, and human disease. *Biochem Soc Trans,* 44**,** 1185-1200.

BADUR, S., ÖZTÜRK, S., PEREIRA, P., ABDELGHANY, M., KHALAF, M., LAGOUBI, Y., OZUDOGRU, O., HANIF, K. & SAHA, D. 2019. Systematic review of the rotavirus infection burden in the WHO-EMRO region. *Human vaccines & immunotherapeutics,* 15**,** 2754-2768.

BALLESTAS, M. E., CHATIS, P. A. & KAYE, K. M. 1999. Efficient persistence of extrachromosomal KSHV DNA mediated by latency-associated nuclear antigen. *Science,* 284**,** 641-4.

BALLESTAS, M. E. & KAYE, K. M. 2001. Kaposi's sarcoma-associated herpesvirus latency-associated nuclear antigen 1 mediates episome persistence through cis-acting terminal repeat (TR) sequence and specifically binds TR DNA. *Journal of Virology,* 75**,** 3250-3258.

BALLESTAS, M. E. & KAYE, K. M. 2011. The latency-associated nuclear antigen, a multifunctional protein central to Kaposi's sarcoma-associated herpesvirus latency. *Future Microbiol,* 6**,** 1399-413.

BANANI, S. F., LEE, H. O., HYMAN, A. A. & ROSEN, M. K. 2017. Biomolecular condensates: organizers of cellular biochemistry. *Nat Rev Mol Cell Biol,* 18**,** 285-298.

BANERJEE, A., KULKARNI, S. & MUKHERJEE, A. 2020. Herpes Simplex Virus: The Hostile Guest That Takes Over Your Home. *Frontiers in Microbiology,* 11.

BAQUERO-PÉREZ, B. & WHITEHOUSE, A. 2015. Hsp70 Isoforms Are Essential for the Formation of Kaposi's Sarcoma-Associated Herpesvirus Replication and Transcription Compartments. *PLoS Pathog,* 11**,** e1005274.

BARKER, N. H. 2008. Ocular herpes simplex. *BMJ Clin Evid,* 2008.

BARNES, J. & WILSON, D. W. 2019. Seeking Closure: How Do Herpesviruses Recruit the Cellular ESCRT Apparatus? *J Virol,* 93.

BASS, J. J., WILKINSON, D. J., RANKIN, D., PHILLIPS, B. E., SZEWCZYK, N. J., SMITH, K. & ATHERTON, P. J. 2017. An overview of technical considerations for Western blotting applications to physiological research. *Scandinavian journal of medicine & science in sports,* 27**,** 4-25.

BATTLES, M. B. & MCLELLAN, J. S. 2019. Respiratory syncytial virus entry and how to block it. *Nature Reviews Microbiology,* 17**,** 233-245.

BAUER, D. W., HUFFMAN, J. B., HOMA, F. L. & EVILEVITCH, A. 2013. Herpes virus genome, the pressure is on. *J Am Chem Soc,* 135**,** 11216-21.

BAUMANN, O. & WALZ, B. 2001. Endoplasmic reticulum of animal cells and its organization into structural and functional domains. *Int Rev Cytol,* 205**,** 149-214.

BECHTEL, J. T., LIANG, Y. Y., HVIDDING, J. & GANEM, D. 2003. Host range of Kaposi's sarcoma-associated herpesvirus in cultured cells. *Journal of Virology,* 77**,** 6474-6481.

BEGEMANN, I. & GALIC, M. 2016. Correlative Light Electron Microscopy: Connecting Synaptic Structure and Function. *Frontiers in Synaptic Neuroscience,* 8.

BELLOMO, C., ALONSO, D. O., RICARDO, T., COELHO, R., KEHL, S., PERIOLO, N., AZOGARAY, V., CASAS, N., OTTONELLI, M., BERGERO, L. C., CUDÓS, M. C., PREVITALI, M. A. & MARTINEZ, V. P. 2021. Emerging hantaviruses in Central Argentina: First case of Hantavirus Pulmonary Syndrome caused by Alto Paraguay virus, and a novel orthohantavirus in Scapteromys aquaticus rodent. *PLoS neglected tropical diseases,* 15**,** e0009842-e0009842.

BELSHE, R. B., LEONE, P. A., BERNSTEIN, D. I., WALD, A., LEVIN, M. J., STAPLETON, J. T., GORFINKEL, I., MORROW, R. L., EWELL, M. G., STOKES-RINER, A., DUBIN, G., HEINEMAN, T. C., SCHULTE, J. M. & DEAL, C. D. 2012. Efficacy results of a trial of a herpes simplex vaccine. *N Engl J Med,* 366**,** 34-43.

BENNETT, E., CLEMENT, J., SANSOM, P., HALL, I., LEACH, S. & MEDLOCK, J. M. 2010. Environmental and ecological potential for enzootic cycles of Puumala hantavirus in Great Britain. *Epidemiology and Infection,* 138**,** 91-98.

BERGLUND, L., BJÖRLING, E., OKSVOLD, P., FAGERBERG, L., ASPLUND, A., SZIGYARTO, C. A., PERSSON, A., OTTOSSON, J., WERNÉRUS, H., NILSSON, P., LUNDBERG, E., SIVERTSSON, A., NAVANI, S., WESTER, K., KAMPF, C., HOBER, S., PONTÉN, F. & UHLÉN, M. 2008. A genecentric Human Protein Atlas for expression profiles based on antibodies. *Mol Cell Proteomics,* 7**,** 2019-27.

BERNI CANANI, R., DI COSTANZO, M. & LEONE, L. 2012. The epigenetic effects of butyrate: potential therapeutic implications for clinical practice. *Clinical Epigenetics,* 4**,** 4.

BESSA, L. M., GUSEVA, S., CAMACHO-ZARCO, A. R., SALVI, N., MAURIN, D., PEREZ, L. M., BOTOVA, M., MALKI, A., NANAO, M., JENSEN, M. R., RUIGROK, R. W. H. & BLACKLEDGE, M. 2022. The intrinsically disordered SARS-CoV-2 nucleoprotein in dynamic complex with its viral partner nsp3a. *Sci Adv,* 8**,** eabm4034.

BIALOWAS, S., HAGBOM, M., NORDGREN, J., KARLSSON, T., SHARMA, S., MAGNUSSON, K. E. & SVENSSON, L. 2016. Rotavirus and Serotonin Cross-Talk in Diarrhoea. *PLoS One,* 11**,** e0159660.

BIGALKE, J. M. & HELDWEIN, E. E. 2015. Structural basis of membrane budding by the nuclear egress complex of herpesviruses. *Embo j,* 34**,** 2921-36.

BIGALKE, J. M., HEUSER, T., NICASTRO, D. & HELDWEIN, E. E. 2014. Membrane deformation and scission by the HSV-1 nuclear egress complex. *Nat Commun,* 5**,** 4131.

BIGGAR, R. J., WHITBY, D., MARSHALL, V., LINHARES, A. C. & BLACK, F. 2000. Human herpesvirus 8 in Brazilian Amerindians: a hyperendemic population with a new subtype. *J Infect Dis,* 181**,** 1562-8.

BIGNON, E. A., ALBORNOZ, A., GUARDADO-CALVO, P., REY, F. A. & TISCHLER, N. D. 2019. Molecular organization and dynamics of the fusion protein Gc at the hantavirus surface. *eLife,* 8**,** e46028.

BIRKMANN, A., MAHR, K., ENSSER, A., YAĞUBOĞLU, S., TITGEMEYER, F., FLECKENSTEIN, B. & NEIPEL, F. 2001. Cell surface heparan sulfate is a receptor for human herpesvirus 8 and interacts with envelope glycoprotein K8.1. *J Virol,* 75**,** 11583-93.

BISHOP, R. F., BARNES, G. L., CIPRIANI, E. & LUND, J. S. 1983. Clinical immunity after neonatal rotavirus infection. A prospective longitudinal study in young children. *N Engl J Med,* 309**,** 72-6.

BISHT, K., SHARMA, K., LACOSTE, B. & TREMBLAY, M. 2016. Dark microglia: Why are they dark? *Commun Integr Biol,* 9**,** e1230575.

BJERKE, S. L. & ROLLER, R. J. 2006. Roles for herpes simplex virus type 1 UL34 and US3 proteins in disrupting the nuclear lamina during herpes simplex virus type 1 egress. *Virology,* 347**,** 261-76.

BLOOM, D. C. 2016. Alphaherpesvirus Latency: A Dynamic State of Transcription and Reactivation. *Adv Virus Res,* 94**,** 53-80.

BLUTT, S. E. & CONNER, M. E. 2007. Rotavirus: to the gut and beyond! *Curr Opin Gastroenterol,* 23**,** 39-43.

BOCK, J. B., KLUMPERMAN, J., DAVANGER, S. & SCHELLER, R. H. 1997. Syntaxin 6 functions in trans-Golgi network vesicle trafficking. *Mol Biol Cell,* 8**,** 1261-71.

BOHNSACK, R. N., SONG, X., OLSON, L. J., KUDO, M., GOTSCHALL, R. R., CANFIELD, W. M., CUMMINGS, R. D., SMITH, D. F. & DAHMS, N. M. 2009. Cation-independent mannose 6-phosphate receptor: a composite of distinct phosphomannosyl binding sites. *The Journal of biological chemistry,* 284**,** 35215-35226.

BOONE, S. A. & GERBA, C. P. 2007. Significance of fomites in the spread of respiratory and enteric viral disease. *Applied and environmental microbiology,* 73**,** 1687-1696.

BORODAVKA, A., DYKEMAN, E. C., SCHRIMPF, W. & LAMB, D. C. 2017. Protein-mediated RNA folding governs sequence-specific interactions between rotavirus genome segments. *Elife,* 6.

BOUDREAUX, C. E., KELLY, D. F. & MCDONALD, S. M. 2015. Electron microscopic analysis of rotavirus assembly-replication intermediates. *Virology,* 477**,** 32-41.

BOUNEDJAH, O., DESFORGES, B., WU, T. D., PIOCHE-DURIEU, C., MARCO, S., HAMON, L., CURMI, P. A., GUERQUIN-KERN, J. L., PIÉTREMENT, O. & PASTRÉ, D. 2014. Free mRNA in excess upon polysome dissociation is a scaffold for protein multimerization to form stress granules. *Nucleic Acids Res,* 42**,** 8678-91.

BOURQUAIN, D., BODENSTEIN, C., SCHÜRER, S. & SCHAADE, L. 2019. Puumala and Tula Virus Differ in Replication Kinetics and Innate Immune Stimulation in Human Endothelial Cells and Macrophages. *Viruses,* 11**,** 855.

BRADSHAW, M. J. & VENKATESAN, A. 2016. Herpes Simplex Virus-1 Encephalitis in Adults: Pathophysiology, Diagnosis, and Management. *Neurotherapeutics,* 13**,** 493-508.

BRANDARIZ-NUÑEZ, A., LIU, T., DU, T. & EVILEVITCH, A. 2019. Pressure-driven release of viral genome into a host nucleus is a mechanism leading to herpes infection. *Elife,* 8.

BRAVO, J. P. K., BARTNIK, K., VENDITTI, L., ACKER, J., GAIL, E. H., COLYER, A., DAVIDOVICH, C., LAMB, D. C., TUMA, R., CALABRESE, A. N. & BORODAVKA, A. 2021. Structural basis of rotavirus RNA chaperone displacement and RNA annealing. *Proceedings of the National Academy of Sciences of the United States of America,* 118**,** e2100198118.

BRAVO, J. P. K., BORODAVKA, A., BARTH, A., CALABRESE, A. N., MOJZES, P., COCKBURN, J. J. B., LAMB, D. C. & TUMA, R. 2018. Stability of local secondary structure determines selectivity of viral RNA chaperones. *Nucleic Acids Res,* 46**,** 7924-7937.

BRAYFIELD, B. P., KANKASA, C., WEST, J. T., MUYANGA, J., BHAT, G., KLASKALA, W., MITCHELL, C. D. & WOOD, C. 2004. Distribution of Kaposi sarcoma-associated herpesvirus/human herpesvirus 8 in maternal saliva and breast milk in Zambia: implications for transmission. *J Infect Dis,* 189**,** 2260-70.

BROUSSARD, G. & DAMANIA, B. 2020. Regulation of KSHV Latency and Lytic Reactivation. *Viruses,* 12.

BROWN, J. C. & NEWCOMB, W. W. 2011. Herpesvirus capsid assembly: insights from structural analysis. *Curr Opin Virol,* 1**,** 142-9.

BULL, H. B. & BREESE, K. 1974. Surface tension of amino acid solutions: a hydrophobicity scale of the amino acid residues. *Arch Biochem Biophys,* 161**,** 665-70.

BURNETT, E., JONESTELLER, C. L., TATE, J. E., YEN, C. & PARASHAR, U. D. 2017. Global Impact of Rotavirus Vaccination on Childhood Hospitalizations and Mortality From Diarrhea. *J Infect Dis,* 215**,** 1666-1672.

BURNETT, E., PARASHAR, U. D. & TATE, J. E. 2020. Real-world effectiveness of rotavirus vaccines, 2006-19: a literature review and meta-analysis. *Lancet Glob Health,* 8**,** e1195-e1202.

BUTTAFUOCO, A., MICHAELSEN, K., TOBLER, K., ACKERMANN, M., FRAEFEL, C. & EICHWALD, C. 2020. Conserved Rotavirus NSP5 and VP2 Domains Interact and Affect Viroplasm. *J Virol,* 94.

BUTZ, A. M., FOSARELLI, P., DICK, J., CUSACK, T. & YOLKEN, R. 1993. Prevalence of rotavirus on high-risk fomites in day-care facilities. *Pediatrics,* 92**,** 202-5.

BYKOV, Y. S., CORTESE, M., BRIGGS, J. A. G. & BARTENSCHLAGER, R. 2016. Correlative light and electron microscopy methods for the study of virus–cell interactions. *FEBS Letters,* 590**,** 1877-1895.

CAI, X. Z., LU, S. H., ZHANG, Z. H., GONZALEZ, C. M., DAMANIA, B. & CULLEN, B. R. 2005. Kaposi's sarcoma-associated herpesvirus expresses an array of viral microRNAs in latently infected cells. *Proceedings of the National Academy of Sciences of the United States of America,* 102**,** 5570-5575.

CAMPOS-MELO, D., HAWLEY, Z. C. E., DROPPELMANN, C. A. & STRONG, M. J. 2021. The Integral Role of RNA in Stress Granule Formation and Function. *Frontiers in Cell and Developmental Biology,* 9.

CANNON, M. J., DOLLARD, S. C., SMITH, D. K., KLEIN, R. S., SCHUMAN, P., RICH, J. D., VLAHOV, D. & PELLETT, P. E. 2001. Blood-borne and sexual transmission of human herpesvirus 8 in women with or at risk for human immunodeficiency virus infection. *N Engl J Med,* 344**,** 637-43.

CAREY, J. L. & GUO, L. 2022. Liquid-Liquid Phase Separation of TDP-43 and FUS in Physiology and Pathology of Neurodegenerative Diseases. *Frontiers in Molecular Biosciences,* 9.

CARLSON, J. A. K., MIDDLETON, P. J., SZYMANSKI, M. T., HUBER, J. & PETRIC, M. 1978. Fatal Rotavirus Gastroenteritis: An Analysis of 21 Cases. *American Journal of Diseases of Children,* 132**,** 477-479.

CARRINGTON-LAWRENCE, S. D. & WELLER, S. K. 2003. Recruitment of polymerase to herpes simplex virus type 1 replication foci in cells expressing mutant primase (UL52) proteins. *J Virol,* 77**,** 4237-47.

CASCARINA, S. M. & ROSS, E. D. 2022. Phase separation by the SARS-CoV-2 nucleocapsid protein: Consensus and open questions. *Journal of Biological Chemistry,* 298**,** 101677.

CASPER, C., KRANTZ, E., SELKE, S., KUNTZ, S. R., WANG, J., HUANG, M. L., PAUK, J. S., COREY, L. & WALD, A. 2007. Frequent and asymptomatic oropharyngeal shedding of human herpesvirus 8 among immunocompetent men. *J Infect Dis,* 195**,** 30-6.

CAVALLERO, S., HUOT, N., FRANCELLE, L., LOMONTE, P., NAAS, T. & LABETOULLE, M. 2014. Biological Features of Herpes Simplex Virus Type 1 Latency in Mice According to Experimental Conditions and Type of Neurones. *Investigative Ophthalmology & Visual Science,* 55**,** 7761-7774.

CDC. 2022. *Reported Cases of Hantavirus Disease* [Online]. Centers for Disease Control and Prevention. Available:

https://www.cdc.gov/hantavirus/surveillance/index.html#:~:text=Reported%20Cases%20of%20Hantavirus%20Pulmonary,and%20non%2Dpulmonary%20hantavirus%20infection. [Accessed 28/05/2022 2022].
CEVALLOS, P. D., LÓPEZ, S., ARIAS, C. F. & ISA, P. 2016. Polarized rotavirus entry and release from differentiated small intestinal cells. *Virology,* 499**,** 65-71.
CHANDRAN, B. 2010. Early Events in Kaposi's Sarcoma-Associated Herpesvirus Infection of Target Cells. *Journal of Virology,* 84**,** 2188-2199.
CHANG-GRAHAM, A. L., PERRY, J. L., STRTAK, A. C., RAMACHANDRAN, N. K., CRIGLAR, J. M., PHILIP, A. A., PATTON, J. T., ESTES, M. K. & HYSER, J. M. 2019. Rotavirus Calcium Dysregulation Manifests as Dynamic Calcium Signaling in the Cytoplasm and Endoplasmic Reticulum. *Scientific Reports,* 9**,** 10822.
CHANG, CESARMAN, E., PESSIN, M. S., LEE, F., CULPEPPER, J., KNOWLES, D. M. & MOORE, P. S. 1994. Identification of herpesvirus-like DNA sequences in AIDS-associated Kaposi's sarcoma. *Science,* 266**,** 1865-9.
CHANG, VAN SANT, C., KRUG, P. W., SEARS, A. E. & ROIZMAN, B. 1997. The null mutant of the U(L)31 gene of herpes simplex virus 1: construction and phenotype in infected cells. *J Virol,* 71**,** 8307-15.
CHANG, C.-K., HSU, Y.-L., CHANG, Y.-H., CHAO, F.-A., WU, M.-C., HUANG, Y.-S., HU, C.-K. & HUANG, T.-H. 2009. Multiple Nucleic Acid Binding Sites and Intrinsic Disorder of Severe Acute Respiratory Syndrome Coronavirus Nucleocapsid Protein: Implications for Ribonucleocapsid Protein Packaging. *Journal of Virology,* 83**,** 2255-2264.
CHANG, L., GODINEZ, W. J., KIM, I. H., TEKTONIDIS, M., DE LANEROLLE, P., EILS, R., ROHR, K. & KNIPE, D. M. 2011. Herpesviral replication compartments move and coalesce at nuclear speckles to enhance export of viral late mRNA. *Proc Natl Acad Sci U S A,* 108**,** E136-44.
CHAO, D. T., SU, M., TANLIMCO, S., SHO, M., CHOI, D., FOX, M., YE, S., HSI, E. D., DURKIN, L., YIN, J., ZHANG, Y., KIM, H., STARLING, G. C. & CULP, P. A. 2013. Expression of TweakR in breast cancer and preclinical activity of enavatuzumab, a humanized anti-TweakR mAb. *Journal of Cancer Research and Clinical Oncology,* 139**,** 315-325.
CHARMAN, M. & WEITZMAN, M. D. 2020. Replication Compartments of DNA Viruses in the Nucleus: Location, Location, Location. *Viruses,* 12.
CHATURVEDI, S., ENGEL, R. & WEINBERGER, L. 2020. The HSV-1 ICP4 Transcriptional Auto-Repression Circuit Functions as a Transcriptional “Accelerator” Circuit. *Frontiers in Cellular and Infection Microbiology,* 10.
CHAUHAN, V., RUNGTA, T., GOYAL, K. & SINGH, M. P. 2019. Designing a multi-epitope based vaccine to combat Kaposi Sarcoma utilizing immunoinformatics approach. *Scientific Reports,* 9**,** 2517.
CHEN, BAI, P., MACKAY, S., KORZA, G., CARSON, J. H., KUCHTA, R. D. & WELLER, S. K. 2011. Herpes simplex virus type 1 helicase-primase: DNA binding and consequent protein oligomerization and primase activation. *J Virol,* 85**,** 968-78.
CHEN, DAI, L., GOLDSTEIN, A., ZHANG, H., TANG, W., FORREST, J. C., POST, S. R., CHEN, X. & QIN, Z. 2019a. Identification of new antiviral agents against Kaposi's sarcoma-associated herpesvirus (KSHV) by high-throughput drug screening reveals the role of histamine-related signaling in promoting viral lytic reactivation. *PLoS pathogens,* 15**,** e1008156-e1008156.
CHEN & HUDNALL, S. D. 2006. Anatomical mapping of human herpesvirus reservoirs of infection. *Mod Pathol,* 19**,** 726-37.
CHEN, ZHANG, X., SCHALLER, S., JARDETZKY, T. S., LONGNECKER, R., SHENK, T., COHEN, G. & ROBERTSON, E. 2019b. Ephrin Receptor A4 is a New Kaposi's Sarcoma-Associated Herpesvirus Virus Entry Receptor. *mBio,* 10**,** e02892-18.
CHEN, G. M., HUNG, T. & MACKOW, E. R. 1990. cDNA cloning of each genomic segment of the group B rotavirus ADRV: molecular characterization of the 11th RNA segment. *Virology,* 175**,** 605-9.

CHEN, H., CUI, Y., HAN, X., HU, W., SUN, M., ZHANG, Y., WANG, P.-H., SONG, G., CHEN, W. & LOU, J. 2020. Liquid–liquid phase separation by SARS-CoV-2 nucleocapsid protein and RNA. *Cell Research,* 30**,** 1143-1145.

CHEN, P., HÜBNER, W., SPINELLI, M. A. & CHEN, B. K. 2007. Predominant mode of human immunodeficiency virus transfer between T cells is mediated by sustained Env-dependent neutralization-resistant virological synapses. *J Virol,* 81**,** 12582-95.

CHENG, CHEN, K., DONG, B., YANG, M., FILBRUN, S. L., MYOUNG, Y., HUANG, T.-X., GU, Y., WANG, G. & FANG, N. 2021. Dynamin-dependent vesicle twist at the final stage of clathrin-mediated endocytosis. *Nature Cell Biology,* 23**,** 859-869.

CHENG, E., WANG, Z. & MIR, M. A. 2014. Interaction between hantavirus nucleocapsid protein (N) and RNA-dependent RNA polymerase (RdRp) mutants reveals the requirement of an N-RdRp interaction for viral RNA synthesis. *J Virol,* 88**,** 8706-12.

CHENG, Y. & WALZ, T. 2009. The advent of near-atomic resolution in single-particle electron microscopy. *Annu Rev Biochem,* 78**,** 723-42.

CHENTOUFI, A. A., DHANUSHKODI, N. R., SRIVASTAVA, R., PRAKASH, S., COULON, P. A., ZAYOU, L., VAHED, H., CHENTOUFI, H. A., HORMI-CARVER, K. K. & BENMOHAMED, L. 2022. Combinatorial Herpes Simplex Vaccine Strategies: From Bedside to Bench and Back. *Front Immunol,* 13**,** 849515.

CHEUNG, W., GILL, M., ESPOSITO, A., KAMINSKI, C. F., COUROUSSE, N., CHWETZOFF, S., TRUGNAN, G., KESHAVAN, N., LEVER, A. & DESSELBERGER, U. 2010. Rotaviruses associate with cellular lipid droplet components to replicate in viroplasms, and compounds disrupting or blocking lipid droplets inhibit viroplasm formation and viral replication. *J Virol,* 84**,** 6782-98.

CHIANG, C.-F., FLINT, M., LIN, J.-M. S. & SPIROPOULOU, C. F. 2016. Endocytic Pathways Used by Andes Virus to Enter Primary Human Lung Endothelial Cells. *PloS one,* 11**,** e0164768-e0164768.

CHOI, Y., KWON, Y. C., KIM, S. I., PARK, J. M., LEE, K. H. & AHN, B. Y. 2008. A hantavirus causing hemorrhagic fever with renal syndrome requires gC1qR/p32 for efficient cell binding and infection. *Virology,* 381**,** 178-83.

CHOULJENKO, D. V., JAMBUNATHAN, N., CHOULJENKO, V. N., NADERI, M., BRYLINSKI, M., CASKEY, J. R. & KOUSOULAS, K. G. 2016. Herpes Simplex Virus 1 UL37 Protein Tyrosine Residues Conserved among All Alphaherpesviruses Are Required for Interactions with Glycoprotein K, Cytoplasmic Virion Envelopment, and Infectious Virus Production. *J Virol,* 90**,** 10351-10361.

CHUDASAMA, P., KONRAD, A., JOCHMANN, R., LAUSEN, B., HOLZ, P., NASCHBERGER, E., NEIPEL, F., BRITZEN-LAURENT, N. & STURZL, M. 2015. Structural proteins of Kaposi's sarcoma-associated herpesvirus antagonize p53-mediated apoptosis. *Oncogene,* 34**,** 639-649.

CIARLET, CRAWFORD, S. E. & ESTES, M. K. 2001. Differential infection of polarized epithelial cell lines by sialic acid-dependent and sialic acid-independent rotavirus strains. *Journal of Virology,* 75**,** 11834-11850.

CIFUENTES-MUÑOZ, N., SALAZAR-QUIROZ, N. & TISCHLER, N. D. 2014. Hantavirus Gn and Gc envelope glycoproteins: key structural units for virus cell entry and virus assembly. *Viruses,* 6**,** 1801-22.

CLARK, A., VAN ZANDVOORT, K., FLASCHE, S., SANDERSON, C., BINES, J., TATE, J., PARASHAR, U. & JIT, M. 2019. Efficacy of live oral rotavirus vaccines by duration of follow-up: a meta-regression of randomised controlled trials. *Lancet Infectious Diseases,* 19**,** 717-727.

CLEMENT, J. & VAN RANST, M. 2016. Three vole species and one (?) novel arvicolid hantavirus pathogen: Tula virus revisited. *Euro Surveill,* 21.

COATES, M., LEE, M. J., NORTON, D. & MACLEOD, A. S. 2019. The Skin and Intestinal Microbiota and Their Specific Innate Immune Systems. *Frontiers in Immunology,* 10.

COEN, N., DURAFFOUR, S., SNOECK, R. & ANDREI, G. 2014. KSHV targeted therapy: an update on inhibitors of viral lytic replication. *Viruses,* 6**,** 4731-59.

COHEN, A., BRODIE, C. & SARID, R. 2006. An essential role of ERK signalling in TPA-induced reactivation of Kaposi's sarcoma-associated herpesvirus. *J Gen Virol,* 87**,** 795-802.
COHEN, J. I. 2020. Herpesvirus latency. *J Clin Invest,* 130**,** 3361-3369.
COLBÈRE-GARAPIN, F., MARTIN-LATIL, S., BLONDEL, B., MOUSSON, L., PELLETIER, I., AUTRET, A., FRANÇOIS, A., NIBORSKI, V., GROMPONE, G., CATONNET, G. & VAN DE MOER, A. 2007. Prevention and treatment of enteric viral infections: possible benefits of probiotic bacteria. *Microbes and Infection,* 9**,** 1623-1631.
COMBS, L. R., SPIRES, L. M., ALONSO, J. D., PAPP, B., TOTH, Z. & GOODRUM, F. 2022. KSHV RTA Induces Degradation of the Host Transcription Repressor ID2 To Promote the Viral Lytic Cycle. *Journal of Virology,* 96**,** e00101-22.
CORNEJO-CASTRO, E. M., MARSHALL, V., LACK, J., LURAIN, K., IMMONEN, T., LABO, N., FISHER, N. C., RAMASWAMI, R., POLIZZOTTO, M. N., KEELE, B. F., YARCHOAN, R., ULDRICK, T. S. & WHITBY, D. 2020. Dual infection and recombination of Kaposi sarcoma herpesvirus revealed by whole-genome sequence analysis of effusion samples. *Virus Evolution,* 6.
CORTESE, K., DIASPRO, A. & TACCHETTI, C. 2009. Advanced correlative light/electron microscopy: current methods and new developments using Tokuyasu cryosections. *J Histochem Cytochem,* 57**,** 1103-12.
CORTESE, M., GOELLNER, S., ACOSTA, E. G., NEUFELDT, C. J., OLEKSIUK, O., LAMPE, M., HASELMANN, U., FUNAYA, C., SCHIEBER, N., RONCHI, P., SCHORB, M., PRUUNSILD, P., SCHWAB, Y., CHATEL-CHAIX, L., RUGGIERI, A. & BARTENSCHLAGER, R. 2017. Ultrastructural Characterization of Zika Virus Replication Factories. *Cell Rep,* 18**,** 2113-2123.
COSTANTINI, L. M. & SNAPP, E. L. 2015. Going Viral with Fluorescent Proteins. *Journal of virology,* 89**,** 9706-9708.
COULTAS, J. A., SMYTH, R. & OPENSHAW, P. J. 2019. Respiratory syncytial virus (RSV): a scourge from infancy to old age. *Thorax,* 74**,** 986.
COVARRUBIAS, S., GAGLIA, M. M., KUMAR, G. R., WONG, W., JACKSON, A. O. & GLAUNSINGER, B. A. 2011. Coordinated destruction of cellular messages in translation complexes by the gammaherpesvirus host shutoff factor and the mammalian exonuclease Xrn1. *PLoS Pathog,* 7**,** e1002339.
CRAWFORD, S. E., CRIGLAR, J. M., LIU, Z., BROUGHMAN, J. R. & ESTES, M. K. 2019. COPII Vesicle Transport Is Required for Rotavirus NSP4 Interaction with the Autophagy Protein LC3 II and Trafficking to Viroplasms. *J Virol,* 94.
CRAWFORD, S. E., RAMANI, S., TATE, J. E., PARASHAR, U. D., SVENSSON, L., HAGBOM, M., FRANCO, M. A., GREENBERG, H. B., O'RYAN, M., KANG, G., DESSELBERGER, U. & ESTES, M. K. 2017. Rotavirus infection. *Nature Reviews Disease Primers,* 3**,** 17083.
CRIGLAR, J. M., ANISH, R., HU, L., CRAWFORD, S. E., SANKARAN, B., PRASAD, B. V. V. & ESTES, M. K. 2018. Phosphorylation cascade regulates the formation and maturation of rotaviral replication factories. *Proc Natl Acad Sci U S A,* 115**,** E12015-e12023.
CRIGLAR, J. M., ESTES, M. K. & CRAWFORD, S. E. 2022. Rotavirus-Induced Lipid Droplet Biogenesis Is Critical for Virus Replication. *Frontiers in Physiology,* 13.
CUPERUS, T., DE VRIES, A., HOORNWEG, T. E., FONVILLE, M., JAARSMA, R. I., OPSTEEGH, M. & MAAS, M. 2021. Seoul Virus in Pet and Feeder Rats in The Netherlands. *Viruses,* 13**,** 443.
D'AIUTO, L., BLOOM, D. C., NACIRI, J. N., SMITH, A., EDWARDS, T. G., MCCLAIN, L., CALLIO, J. A., JESSUP, M., WOOD, J., CHOWDARI, K., DEMERS, M., ABRAHAMSON, E. E., IKONOMOVIC, M. D., VIGGIANO, L., DE ZIO, R., WATKINS, S., KINCHINGTON, P. R. & NIMGAONKAR, V. L. 2019. Modeling Herpes Simplex Virus 1 Infections in Human Central Nervous System Neuronal Cells Using Two- and Three-Dimensional Cultures Derived from Induced Pluripotent Stem Cells. *J Virol,* 93.
D'SOUZA, M. H. & PATEL, T. R. 2020. Biodefense Implications of New-World Hantaviruses. *Frontiers in bioengineering and biotechnology,* 8**,** 925-925.

DABRAL, P., UPPAL, T., ROSSETTO, C. C., VERMA, S. C. & LONGNECKER, R. M. 2019. Minichromosome Maintenance Proteins Cooperate with LANA during the G₁/S Phase of the Cell Cycle To Support Viral DNA Replication. *Journal of Virology,* 93**,** e02256-18.

DAI, BRATOEVA, M., TOOLE, B. P., QIN, Z. & PARSONS, C. 2012. KSHV activation of VEGF secretion and invasion for endothelial cells is mediated through viral upregulation of emmprin-induced signal transduction. *Int J Cancer,* 131**,** 834-43.

DAI, CAO, Y., JIANG, W., ZABALETA, J., LIU, Z., QIAO, J. & QIN, Z. 2017. KSHV co-infection down-regulates HPV16 E6 and E7 from cervical cancer cells. *Oncotarget,* 8**,** 35792-35803.

DAI, GONG, D., LIM, H., JIH, J., WU, T. T., SUN, R. & ZHOU, Z. H. 2018. Structure and mutagenesis reveal essential capsid protein interactions for KSHV replication. *Nature,* 553**,** 521-525.

DAI, GONG, D., WU, T. T., SUN, R. & ZHOU, Z. H. 2014. Organization of capsid-associated tegument components in Kaposi's sarcoma-associated herpesvirus. *J Virol,* 88**,** 12694-702.

DAI, JIA, Q., BORTZ, E., SHAH, S., LIU, J., ATANASOV, I., LI, X., TAYLOR, K. A., SUN, R. & ZHOU, Z. H. 2008. Unique structures in a tumor herpesvirus revealed by cryo-electron tomography and microscopy. *J Struct Biol,* 161**,** 428-38.

DAI & ZHOU, Z. H. 2018. Structure of the herpes simplex virus 1 capsid with associated tegument protein complexes. *Science,* 360**,** eaao7298.

DANYUKOVA, T., SCHÖNECK, K. & POHL, S. 2022. Site-1 and site-2 proteases: A team of two in regulated proteolysis. *Biochimica et Biophysica Acta (BBA) - Molecular Cell Research,* 1869**,** 119138.

DARJI, K., FRISCH, S., ADJEI BOAKYE, E. & SIEGFRIED, E. 2017. Characterization of children with recurrent eczema herpeticum and response to treatment with interferon-gamma. *Pediatr Dermatol,* 34**,** 686-689.

DARLING, T. K. & LAMB, T. J. 2019. Emerging Roles for Eph Receptors and Ephrin Ligands in Immunity. *Frontiers in Immunology,* 10.

DAS, S., JAYARATNE, R. & BARRETT, K. E. 2018. The Role of Ion Transporters in the Pathophysiology of Infectious Diarrhea. *Cellular and molecular gastroenterology and hepatology,* 6**,** 33-45.

DAS, S., RAVI, V. & DESAI, A. 2011. Japanese encephalitis virus interacts with vimentin to facilitate its entry into porcine kidney cell line. *Virus Res,* 160**,** 404-8.

DAUBER, B., PELLETIER, J. & SMILEY, J. R. 2011. The herpes simplex virus 1 vhs protein enhances translation of viral true late mRNAs and virus production in a cell type-dependent manner. *J Virol,* 85**,** 5363-73.

DAUBER, B., SAFFRAN, H. A. & SMILEY, J. R. 2014. The herpes simplex virus 1 virion host shutoff protein enhances translation of viral late mRNAs by preventing mRNA overload. *J Virol,* 88**,** 9624-32.

DAVIDOVICI, B., KARAKIS, I., BOURBOULIA, D., ARIAD, S., ZONG, J., BENHARROCH, D., DUPIN, N., WEISS, R., HAYWARD, G., SAROV, B. & BOSHOFF, C. 2001. Seroepidemiology and molecular epidemiology of Kaposi's sarcoma-associated herpesvirus among Jewish population groups in Israel. *J Natl Cancer Inst,* 93**,** 194-202.

DAVIES, K., AFROUGH, B., MANKOURI, J., HEWSON, R., EDWARDS, T. A. & BARR, J. N. 2019. Tula orthohantavirus nucleocapsid protein is cleaved in infected cells and may sequester activated caspase-3 during persistent infection to suppress apoptosis. *Journal of General Virology,* 100**,** 1208-1221.

DAVIES, K. A., CHADWICK, B., HEWSON, R., FONTANA, J., MANKOURI, J. & BARR, J. N. 2020. The RNA Replication Site of Tula Orthohantavirus Resides within a Remodelled Golgi Network. *Cells,* 9.

DAVISON, A. J. 2002. Evolution of the herpesviruses. *Veterinary Microbiology,* 86**,** 69-88.

DE BOER, P., HOOGENBOOM, J. P. & GIEPMANS, B. N. G. 2015. Correlated light and electron microscopy: ultrastructure lights up! *Nature Methods,* 12**,** 503-513.

DEARING, M. D. & DIZNEY, L. 2010. Ecology of hantavirus in a changing world. *Annals of the New York Academy of Sciences,* 1195**,** 99-112.

DELOGU, R., IANIRO, G., CAMILLONI, B., FIORE, L. & RUGGERI, F. M. 2015. Unexpected spreading of G12P[8] rotavirus strains among young children in a small area of central Italy. *J Med Virol,* 87**,** 1292-302.
DENG, O'CONNOR, C. M., KEDES, D. H. & ZHOU, Z. H. 2007. Direct visualization of the putative portal in the Kaposi's sarcoma-associated herpesvirus capsid by cryoelectron tomography. *J Virol,* 81**,** 3640-4.
DENG, O'CONNOR, C. M., KEDES, D. H. & ZHOU, Z. H. 2008. Cryo-electron tomography of Kaposi's sarcoma-associated herpesvirus capsids reveals dynamic scaffolding structures essential to capsid assembly and maturation. *J Struct Biol,* 161**,** 419-27.
DENG, YOUNG, A. & SUN, R. 2000. Auto-activation of the rta gene of human herpesvirus-8/Kaposi's sarcoma-associated herpesvirus. *J Gen Virol,* 81**,** 3043-3048.
DENG, Y. & ANGELOVA, A. 2021. Coronavirus-Induced Host Cubic Membranes and Lipid-Related Antiviral Therapies: A Focus on Bioactive Plasmalogens. *Frontiers in Cell and Developmental Biology,* 9.
DENK, W. & HORSTMANN, H. 2004. Serial Block-Face Scanning Electron Microscopy to Reconstruct Three-Dimensional Tissue Nanostructure. *PLOS Biology,* 2**,** e329.
DENNEHY, P. H. 2000. Transmission of rotavirus and other enteric pathogens in the home. *Pediatr Infect Dis J,* 19**,** S103-5.
DEO, R. C., GROFT, C. M., RAJASHANKAR, K. R. & BURLEY, S. K. 2002. Recognition of the rotavirus mRNA 3' consensus by an asymmetric NSP3 homodimer. *Cell,* 108**,** 71-81.
DESAI, P. J., PRYCE, E. N., HENSON, B. W., LUITWEILER, E. M. & COTHRAN, J. 2012. Reconstitution of the Kaposi's sarcoma-associated herpesvirus nuclear egress complex and formation of nuclear membrane vesicles by coexpression of ORF67 and ORF69 gene products. *J Virol,* 86**,** 594-8.
DESSELBERGER, U. 2014. Rotaviruses. *Virus Research,* 190**,** 75-96.
DHEERASEKARA, K., SUMATHIPALA, S. & MUTHUGALA, R. 2020. Hantavirus Infections—Treatment and Prevention. *Current Treatment Options in Infectious Diseases,* 12**,** 410-421.
DHILLON, P. & RAO, C. D. 2018. Rotavirus Induces Formation of Remodeled Stress Granules and P Bodies and Their Sequestration in Viroplasms To Promote Progeny Virus Production. *J Virol,* 92.
DHILLON, P., TANDRA, V. N., CHORGHADE, S. G., NAMSA, N. D., SAHOO, L. & RAO, C. D. 2018. Cytoplasmic Relocalization and Colocalization with Viroplasms of Host Cell Proteins, and Their Role in Rotavirus Infection. *J Virol,* 92.
DÍAZ-SALINAS, M. A., SILVA-AYALA, D., LÓPEZ, S. & ARIAS, C. F. 2014. Rotaviruses reach late endosomes and require the cation-dependent mannose-6-phosphate receptor and the activity of cathepsin proteases to enter the cell. *J Virol,* 88**,** 4389-402.
DICKEY, M., JAMISON, L., MICHAUD, L., CARE, M., BERNSTEIN, D. I. & STAAT, M. A. 2009. Rotavirus meningoencephalitis in a previously healthy child and a review of the literature. *Pediatr Infect Dis J,* 28**,** 318-21.
DIEBOLDER, C. A., KOSTER, A. J. & KONING, R. I. 2012. Pushing the resolution limits in cryo electron tomography of biological structures. *Journal of Microscopy,* 248**,** 1-5.
DIEFENBACH, R. J., MIRANDA-SAKSENA, M., DIEFENBACH, E., HOLLAND, D. J., BOADLE, R. A., ARMATI, P. J. & CUNNINGHAM, A. L. 2002. Herpes simplex virus tegument protein US11 interacts with conventional kinesin heavy chain. *J Virol,* 76**,** 3282-91.
DIMITROV, D. S. 2004. Virus entry: molecular mechanisms and biomedical applications. *Nature Reviews Microbiology,* 2**,** 109-122.
DING, K., CELMA, C. C., ZHANG, X., CHANG, T., SHEN, W., ATANASOV, I., ROY, P. & ZHOU, Z. H. 2019. In situ structures of rotavirus polymerase in action and mechanism of mRNA transcription and release. *Nature Communications,* 10**,** 2216.

DITTMAYER, C., MEINHARDT, J., RADBRUCH, H., RADKE, J., HEPPNER, B. I., HEPPNER, F. L., STENZEL, W., HOLLAND, G. & LAUE, M. 2020. Why misinterpretation of electron micrographs in SARS-CoV-2-infected tissue goes viral. *The Lancet,* 396**,** e64-e65.
DÖHNER, K., CORNELIUS, A., SERRERO, M. C. & SODEIK, B. 2021. The journey of herpesvirus capsids and genomes to the host cell nucleus. *Current Opinion in Virology,* 50**,** 147-158.
DÖHNER, K., WOLFSTEIN, A., PRANK, U., ECHEVERRI, C., DUJARDIN, D., VALLEE, R. & SODEIK, B. 2002. Function of Dynein and Dynactin in Herpes Simplex Virus Capsid Transport. *Molecular Biology of the Cell,* 13**,** 2795-2809.
DOLLERY, S. J. 2019. Towards Understanding KSHV Fusion and Entry. *Viruses,* 11.
DOWLER, S., KULAR, G. & ALESSI, D. R. 2002. Protein lipid overlay assay. *Sci STKE,* 2002**,** pl6.
DOYLE, L. M. & WANG, M. Z. 2019. Overview of Extracellular Vesicles, Their Origin, Composition, Purpose, and Methods for Exosome Isolation and Analysis. *Cells,* 8**,** 727.
DRAGANOVA, E. B., ZHANG, J., ZHOU, Z. H. & HELDWEIN, E. E. 2020. Structural basis for capsid recruitment and coat formation during HSV-1 nuclear egress. *eLife,* 9**,** e56627.
DUAN, F., LIAO, J., HUANG, Q., NIE, Y. & WU, K. 2012. HSV-1 miR-H6 inhibits HSV-1 replication and IL-6 expression in human corneal epithelial cells in vitro. *Clin Dev Immunol,* 2012**,** 192791.
DUBOCHET, J., ADRIAN, M., CHANG, J. J., HOMO, J. C., LEPAULT, J., MCDOWALL, A. W. & SCHULTZ, P. 1988. Cryo-electron microscopy of vitrified specimens. *Q Rev Biophys,* 21**,** 129-228.
DUKERS, N. H. & REZZA, G. 2003. Human herpesvirus 8 epidemiology: what we do and do not know. *Aids,* 17**,** 1717-30.
DUNKER, A. K., LAWSON, J. D., BROWN, C. J., WILLIAMS, R. M., ROMERO, P., OH, J. S., OLDFIELD, C. J., CAMPEN, A. M., RATLIFF, C. M., HIPPS, K. W., AUSIO, J., NISSEN, M. S., REEVES, R., KANG, C., KISSINGER, C. R., BAILEY, R. W., GRISWOLD, M. D., CHIU, W., GARNER, E. C. & OBRADOVIC, Z. 2001. Intrinsically disordered protein. *Journal of Molecular Graphics and Modelling,* 19**,** 26-59.
DÜNN-KITTENPLON, D. D., ASHKENAZY-TITELMAN, A., KALT, I., LELLOUCHE, J. P., SHAV-TAL, Y. & SARID, R. 2021. The Portal Vertex of KSHV Promotes Docking of Capsids at the Nuclear Pores. *Viruses,* 13.
DÜNN-KITTENPLON, D. D., KALT, I., LELLOUCHE, J. M. & SARID, R. 2019. The KSHV portal protein ORF43 is essential for the production of infectious viral particles. *Virology,* 529**,** 205-215.
DÜSTER, R., KALTHEUNER, I. H., SCHMITZ, M. & GEYER, M. 2021. 1,6-Hexanediol, commonly used to dissolve liquid-liquid phase separated condensates, directly impairs kinase and phosphatase activities. *J Biol Chem,* 296**,** 100260.
DYSON, H. J., WRIGHT, P. E. & SCHERAGA, H. A. 2006. The role of hydrophobic interactions in initiation and propagation of protein folding. *Proc Natl Acad Sci U S A,* 103**,** 13057-61.
EASTERBROOK, J. D. & KLEIN, S. L. 2008. Immunological mechanisms mediating hantavirus persistence in rodent reservoirs. *PLoS Pathog,* 4**,** e1000172.
ECDC. 2021. *Hantavirus infection Annual Epidemiological Report for 2019* [Online]. European Centre for Disease Prevention and Control. Available: https://www.ecdc.europa.eu/sites/default/files/documents/AER-hantavirus-2019.pdf [Accessed 28/05/2022 2022].
EEA. 2021. *Global and European temperatures* [Online]. European Environment Agency. Available: https://www.eea.europa.eu/ims/global-and-european-temperatures [Accessed 29/05/2022 2022].
EICHWALD, C., ARNOLDI, F., LAIMBACHER, A. S., SCHRANER, E. M., FRAEFEL, C., WILD, P., BURRONE, O. R. & ACKERMANN, M. 2012. Rotavirus viroplasm fusion and perinuclear localization are dynamic processes requiring stabilized microtubules. *PloS one,* 7**,** e47947-e47947.
EICHWALD, C., RODRIGUEZ, J. F. & BURRONE, O. R. 2004. Characterization of rotavirus NSP2/NSP5 interactions and the dynamics of viroplasm formation. *J Gen Virol,* 85**,** 625-634.

EICHWALD, C., VASCOTTO, F., FABBRETTI, E. & BURRONE, O. R. 2002. Rotavirus NSP5: mapping phosphorylation sites and kinase activation and viroplasm localization domains. *J Virol,* 76**,** 3461-70.

ELBAUM-GARFINKLE, S. 2019. Matter over mind: Liquid phase separation and neurodegeneration. *J Biol Chem,* 294**,** 7160-7168.

ELBAZ-ALON, Y., GUO, Y., SEGEV, N., HAREL, M., QUINNELL, D. E., GEIGER, T., AVINOAM, O., LI, D. & NUNNARI, J. 2020. PDZD8 interacts with Protrudin and Rab7 at ER-late endosome membrane contact sites associated with mitochondria. *Nature Communications,* 11**,** 3645.

ENBOM, M., URASSA, W., MASSAMBU, C., THORSTENSSON, R., MHALU, F. & LINDE, A. 2002. Detection of human herpesvirus 8 DNA in serum from blood donors with HHV-8 antibodies indicates possible bloodborne virus transmission. *J Med Virol,* 68**,** 264-7.

ENGDAHL, T. B., KUZMINA, N. A., RONK, A. J., MIRE, C. E., HYDE, M. A., KOSE, N., JOSLEYN, M. D., SUTTON, R. E., MEHTA, A., WOLTERS, R. M., LLOYD, N. M., VALDIVIESO, F. R., KSIAZEK, T. G., HOOPER, J. W., BUKREYEV, A. & CROWE, J. E. 2021. Broad and potently neutralizing monoclonal antibodies isolated from human survivors of New World hantavirus infection. *Cell Reports,* 35**,** 109086.

ENRIA, D. A., BRIGGILER, A. M., PINI, N. & LEVIS, S. 2001. Clinical manifestations of New World hantaviruses. *Curr Top Microbiol Immunol,* 256**,** 117-34.

ENSOLI, B., SGADARI, C., BARILLARI, G., SIRIANNI, M. C., STÜRZL, M. & MONINI, P. 2001. Biology of Kaposi's sarcoma. *Eur J Cancer,* 37**,** 1251-69.

EREN, E., ZAMUDA, K. & PATTON, J. T. 2016. Modeling of the rotavirus group C capsid predicts a surface topology distinct from other rotavirus species. *Virology,* 487**,** 150-162.

ESTROZI, L. F., SETTEMBRE, E. C., GORET, G., MCCLAIN, B., ZHANG, X., CHEN, J. Z., GRIGORIEFF, N. & HARRISON, S. C. 2013. Location of the dsRNA-Dependent Polymerase, VP1, in Rotavirus Particles. *Journal of Molecular Biology,* 425**,** 124-132.

FABBRETTI, E., AFRIKANOVA, I., VASCOTTO, F. & BURRONE, O. R. 1999. Two non-structural rotavirus proteins, NSP2 and NSP5, form viroplasm-like structures in vivo. *J Gen Virol,* 80 (Pt 2)**,** 333-339.

FAJARDO, T., SUNG, P.-Y., CELMA, C. C. & ROY, P. 2017. Rotavirus Genomic RNA Complex Forms via Specific RNA-RNA Interactions: Disruption of RNA Complex Inhibits Virus Infectivity. *Viruses,* 9**,** 167.

FAN, LONGNECKER, R. & CONNOLLY, S. A. 2014. Substitution of herpes simplex virus 1 entry glycoproteins with those of saimiriine herpesvirus 1 reveals a gD-gH/gL functional interaction and a region within the gD profusion domain that is critical for fusion. *J Virol,* 88**,** 6470-82.

FAN, WANG, M., CHENG, A., JIA, R., YANG, Q., WU, Y., ZHU, D., ZHAO, X., CHEN, S., LIU, M., ZHANG, S., OU, X., MAO, S., GAO, Q., SUN, D., WEN, X., LIU, Y., YU, Y., ZHANG, L., TIAN, B., PAN, L. & CHEN, X. 2020. The Role of VP16 in the Life Cycle of Alphaherpesviruses. *Frontiers in Microbiology,* 11.

FAN, S., MAGUIRE, C. A., RAMIREZ, S. H., BRADEL-TRETHEWAY, B., SAPINORO, R., SUI, Z., CHAKRABORTY-SETT, S. & DEWHURST, S. 2005. Valproic acid enhances gene expression from viral gene transfer vectors. *J Virol Methods,* 125**,** 23-33.

FARINA, A., SANTARELLI, R., BLOISE, R., GONNELLA, R., GRANATO, M., BEI, R., MODESTI, A., CIRONE, M., BENGTSSON, L., ANGELONI, A. & FAGGIONI, A. 2013. KSHV ORF67 encoded lytic protein localizes on the nuclear membrane and alters emerin distribution. *Virus Res,* 175**,** 143-50.

FATAHZADEH, M. & SCHWARTZ, R. A. 2007. Human herpes simplex virus infections: Epidemiology, pathogenesis, symptomatology, diagnosis, and management. *Journal of the American Academy of Dermatology,* 57**,** 737-763.

FEARNS, R. & DEVAL, J. 2016. New antiviral approaches for respiratory syncytial virus and other mononegaviruses: Inhibiting the RNA polymerase. *Antiviral Res,* 134**,** 63-76.

FERNÁNDEZ-GARCÍA, Y., REGUERA, J., BUSCH, C., WITTE, G., SÁNCHEZ-RAMOS, O., BETZEL, C., CUSACK, S., GÜNTHER, S. & REINDL, S. 2016. Atomic Structure and Biochemical Characterization of an RNA Endonuclease in the N Terminus of Andes Virus L Protein. *PLoS Pathog,* 12**,** e1005635.

FERNÁNDEZ-TRUJILLO, L., BOLAÑOS, J. E., VELÁSQUEZ, M., GARCÍA, C. & SUA, L. F. 2019. Primary effusion lymphoma in a human immunodeficiency virus-negative patient with unexpected unusual complications: a case report. *Journal of Medical Case Reports,* 13**,** 301.

FERNÁNDEZ DE CASTRO, I., TENORIO, R. & RISCO, C. 2020. Virus Factories. *Reference Module in Life Sciences***,** B978-0-12-814515-9.00001-1.

FERRANDEZ, Y., ZHANG, W., PEUROIS, F., AKENDENGUÉ, L., BLANGY, A., ZEGHOUF, M. & CHERFILS, J. 2017. Allosteric inhibition of the guanine nucleotide exchange factor DOCK5 by a small molecule. *Scientific Reports,* 7**,** 14409.

FIGUEIREDO, MORELI, M. L., BORGES, A. A., FIGUEIREDO, G. G., SOUZA, R. L. & AQUINO, V. H. 2008. Expression of a hantavirus N protein and its efficacy as antigen in immune assays. *Braz J Med Biol Res,* 41**,** 596-9.

FIGUEIREDO, SOUZA, W. M. D., FERRÉS, M. & ENRIA, D. A. 2014. Hantaviruses and cardiopulmonary syndrome in South America. *Virus Research,* 187**,** 43-54.

FLEMINGTON, E. K. 2001. Herpesvirus lytic replication and the cell cycle: arresting new developments. *J Virol,* 75**,** 4475-81.

FONTANA, J., ATANASIU, D., SAW, W. T., GALLAGHER, J. R., COX, R. G., WHITBECK, J. C., BROWN, L. M., EISENBERG, R. J. & COHEN, G. H. 2017. The Fusion Loops of the Initial Prefusion Conformation of Herpes Simplex Virus 1 Fusion Protein Point Toward the Membrane. *mBio,* 8.

FONTANA, J., LÓPEZ-MONTERO, N., ELLIOTT, R. M., FERNÁNDEZ, J. J. & RISCO, C. 2008. The unique architecture of Bunyamwera virus factories around the Golgi complex. *Cell Microbiol,* 10**,** 2012-28.

FORST, C. V., ZHOU, B., WANG, M., CHOU, T.-W., MASON, G., SONG, W.-M., SCHADT, E., GHEDIN, E. & ZHANG, B. 2017. Integrative gene network analysis identifies key signatures, intrinsic networks and host factors for influenza virus A infections. *npj Systems Biology and Applications,* 3**,** 35.

FORTE, E., RAJA, A. N., SHAMULAILATPAM, P., MANZANO, M., SCHIPMA, M. J., CASEY, J. L. & GOTTWEIN, E. 2015. MicroRNA-Mediated Transformation by the Kaposi's Sarcoma-Associated Herpesvirus Kaposin Locus. *Journal of Virology,* 89**,** 2333-2341.

FRANK, S. R., KÖLLMANN, C. P., VAN LIDTH DE JEUDE, J. F., THIAGARAJAH, J. R., ENGELHOLM, L. H., FRÖDIN, M. & HANSEN, S. H. 2017. The focal adhesion-associated proteins DOCK5 and GIT2 comprise a rheostat in control of epithelial invasion. *Oncogene,* 36**,** 1816-1828.

FRANKEN, L. E., GRÜNEWALD, K., BOEKEMA, E. J. & STUART, M. C. A. 2020. A Technical Introduction to Transmission Electron Microscopy for Soft-Matter: Imaging, Possibilities, Choices, and Technical Developments. *Small,* 16**,** 1906198.

FRIBORG, J., KONG, W. P., FLOWERS, C., FLOWERS, S., SUN, Y. N., FOREMAN, K., NICKOLOFF, B. & NABEL, G. 1999. Distinct Biology of Kaposi's Sarcoma-Associated Herpesvirus from Primary Lesions and Body Cavity Lymphomas. *Journal of virology,* 72**,** 10073-82.

FU, B., SUN, F., LI, B., YANG, L., ZENG, Y., SUN, X., XU, F., RAYNER, S., GUADALUPE, M., GAO, S. J. & WANG, L. 2009. Seroprevalence of Kaposi's sarcoma-associated herpesvirus and risk factors in Xinjiang, China. *J Med Virol,* 81**,** 1422-31.

FULL, F., JUNGNICKL, D., REUTER, N., BOGNER, E., BRULOIS, K., SCHOLZ, B., STÜRZL, M., MYOUNG, J., JUNG, J. U., STAMMINGER, T. & ENSSER, A. 2014. Kaposi's Sarcoma Associated Herpesvirus Tegument Protein ORF75 Is Essential for Viral Lytic Replication and Plays a Critical Role in the Antagonization of ND10-Instituted Intrinsic Immunity. *PLOS Pathogens,* 10**,** e1003863.

GALLEGOS, C. O. & PATTON, J. T. 1989. Characterization of rotavirus replication intermediates: a model for the assembly of single-shelled particles. *Virology,* 172**,** 616-27.

GALLOUX, M., RISSO-BALLESTER, J., RICHARD, C. A., FIX, J., RAMEIX-WELTI, M. A. & ELÉOUËT, J. F. 2020. Minimal Elements Required for the Formation of Respiratory Syncytial Virus Cytoplasmic Inclusion Bodies In Vivo and In Vitro. *mBio,* 11.

GANEM, D. 2010. KSHV and the pathogenesis of Kaposi sarcoma: listening to human biology and medicine. *J Clin Invest,* 120**,** 939-49.

GANIME, A. C., LEITE, J. P., FIGUEIREDO, C. E., CARVALHO-COSTA, F. A., MELGAÇO, F. G., MALTA, F. C., FUMIAN, T. M. & MIAGOSTOVICH, M. P. 2016. Dissemination of human adenoviruses and rotavirus species A on fomites of hospital pediatric units. *Am J Infect Control,* 44**,** 1411-1413.

GARCIN, D., LEZZI, M., DOBBS, M., ELLIOTT, R. M., SCHMALJOHN, C., KANG, C. Y. & KOLAKOFSKY, D. 1995. The 5' ends of Hantaan virus (Bunyaviridae) RNAs suggest a prime-and-realign mechanism for the initiation of RNA synthesis. *J Virol,* 69**,** 5754-62.

GARDNER & GLAUNSINGER 2018. Kaposi's sarcoma-associated herpesvirus ORF68 is a DNA binding protein required for viral genome cleavage and packaging. *bioRxiv***,** 322719.

GARG, A. D., ROMANO, E., RUFO, N. & AGOSTINIS, P. 2016. Immunogenic versus tolerogenic phagocytosis during anticancer therapy: mechanisms and clinical translation. *Cell Death Differ,* 23**,** 938-51.

GARRIGUES, H. J., HOWARD, K., BARCY, S., IKOMA, M., MOSES, A. V., DEUTSCH, G. H., WU, D., UEDA, K. & ROSE, T. M. 2017. Full-Length Isoforms of Kaposi's Sarcoma-Associated Herpesvirus Latency-Associated Nuclear Antigen Accumulate in the Cytoplasm of Cells Undergoing the Lytic Cycle of Replication. *Journal of Virology,* 91**,** 27.

GASTEIGER, E., HOOGLAND, C., GATTIKER, A., DUVAUD, S. E., WILKINS, M. R., APPEL, R. D. & BAIROCH, A. 2005. Protein Identification and Analysis Tools on the ExPASy Server. *In:* WALKER, J. M. (ed.) *The Proteomics Protocols Handbook.* Totowa, NJ: Humana Press.

GATHERER, D., DEPLEDGE, D. P., HARTLEY, C. A., SZPARA, M. L., VAZ, P. K., BENKŐ, M., BRANDT, C. R., BRYANT, N. A., DASTJERDI, A., DOSZPOLY, A., GOMPELS, U. A., INOUE, N., JAROSINSKI, K. W., KAUL, R., LACOSTE, V., NORBERG, P., ORIGGI, F. C., ORTON, R. J., PELLETT, P. E., SCHMID, D. S., SPATZ, S. J., STEWART, J. P., TRIMPERT, J., WALTZEK, T. B. & DAVISON, A. J. 2021. ICTV Virus Taxonomy Profile: Herpesviridae 2021. *J Gen Virol,* 102.

GAUNT, E. R., CHEUNG, W., RICHARDS, J. E., LEVER, A. & DESSELBERGER, U. 2013. Inhibition of rotavirus replication by downregulation of fatty acid synthesis. *J Gen Virol,* 94**,** 1310-1317.

GAVRILOVSKAYA, I. N., SHEPLEY, M., SHAW, R., GINSBERG, M. H. & MACKOW, E. R. 1998. beta3 Integrins mediate the cellular entry of hantaviruses that cause respiratory failure. *Proc Natl Acad Sci U S A,* 95**,** 7074-9.

GEIGER, F., ACKER, J., PAPA, G., WANG, X., ARTER, W. E., SAAR, K. L., ERKAMP, N. A., QI, R., BRAVO, J. P., STRAUSS, S., KRAINER, G., BURRONE, O. R., JUNGMANN, R., KNOWLES, T. P., ENGELKE, H. & BORODAVKA, A. 2021. Liquid-liquid phase separation underpins the formation of replication factories in rotaviruses. *Embo j,* 40**,** e107711.

GHOSH, S., AHRENS, W. A., PHATAK, S. U., HWANG, S., SCHRUM, L. W. & BONKOVSKY, H. L. 2011. Association of filamin A and vimentin with hepatitis C virus proteins in infected human hepatocytes. *J Viral Hepat,* 18**,** e568-77.

GILKS, N., KEDERSHA, N., AYODELE, M., SHEN, L., STOECKLIN, G., DEMBER, L. M. & ANDERSON, P. 2004. Stress granule assembly is mediated by prion-like aggregation of TIA-1. *Mol Biol Cell,* 15**,** 5383-98.

GILLEN, J. & ZHU, F. 2021. Disruption of the Interaction between ORF33 and the Conserved Carboxyl-Terminus of ORF45 Abolishes Progeny Virion Production of Kaposi Sarcoma-Associated Herpesvirus. *Viruses,* 13**,** 1828.

GISH, W. & STATES, D. J. 1993. Identification of protein coding regions by database similarity search. *Nat Genet,* 3**,** 266-72.

GLAUNSINGER, B. & GANEM, D. 2004. Lytic KSHV infection inhibits host gene expression by accelerating global mRNA turnover. *Mol Cell,* 13**,** 713-23.

GOLDSMITH, C. S., ELLIOTT, L. H., PETERS, C. J. & ZAKI, S. R. 1995. Ultrastructural characteristics of Sin Nombre virus, causative agent of hantavirus pulmonary syndrome. *Arch Virol,* 140**,** 2107-22.

GONG, D., DAI, X., JIH, J., LIU, Y. T., BI, G. Q., SUN, R. & ZHOU, Z. H. 2019. DNA-Packing Portal and Capsid-Associated Tegument Complexes in the Tumor Herpesvirus KSHV. *Cell,* 178**,** 1329-1343.e12.

GOODWIN, D. J., WALTERS, M. S., SMITH, P. G., THURAU, M., FICKENSCHER, H. & WHITEHOUSE, A. 2001. Herpesvirus Saimiri Open Reading Frame 50 (Rta) Protein Reactivates the Lytic Replication Cycle in a Persistently Infected A549 Cell Line. *Journal of Virology,* 75**,** 4008-4013.

GORR, T. A. & VOGEL, J. 2015. Western blotting revisited: Critical perusal of underappreciated technical issues. *PROTEOMICS – Clinical Applications,* 9**,** 396-405.

GOTTWEIN, E., CORCORAN, D. L., MUKHERJEE, N., SKALSKY, R. L., HAFNER, M., NUSBAUM, J. D., SHAMULAILATPAM, P., LOVE, C. L., DAVE, S. S., TUSCHL, T., OHLER, U. & CULLEN, B. R. 2011. Viral microRNA targetome of KSHV-infected primary effusion lymphoma cell lines. *Cell Host Microbe,* 10**,** 515-26.

GRAHAM, L. & ORENSTEIN, J. M. 2007. Processing tissue and cells for transmission electron microscopy in diagnostic pathology and research. *Nature Protocols,* 2**,** 2439-2450.

GRATIA, M., SAROT, E., VENDE, P., CHARPILIENNE, A., BARON, C. H., DUARTE, M., PYRONNET, S. & PONCET, D. 2015. Rotavirus NSP3 Is a Translational Surrogate of the Poly(A) Binding Protein-Poly(A) Complex. *J Virol,* 89**,** 8773-82.

GREY, F. 2015. Role of microRNAs in herpesvirus latency and persistence. *J Gen Virol,* 96**,** 739-751.

GRIFFITHS, G., SLOT, J. W. & WEBSTER, P. 2015. Kiyoteru Tokuyasu: a pioneer of cryo-ultramicrotomy. *J Microsc,* 260**,** 235-7.

GRINDE, B. 2013. Herpesviruses: latency and reactivation - viral strategies and host response. *J Oral Microbiol,* 5.

GRUENBAUM, Y., GOLDMAN, R. D., MEYUHAS, R., MILLS, E., MARGALIT, A., FRIDKIN, A., DAYANI, Y., PROKOCIMER, M. & ENOSH, A. 2003. The nuclear lamina and its functions in the nucleus. *Int Rev Cytol,* 226**,** 1-62.

GRUFFAT, H., MARCHIONE, R. & MANET, E. 2016. Herpesvirus Late Gene Expression: A Viral-Specific Pre-initiation Complex Is Key. *Front Microbiol,* 7**,** 869.

GRUNDHOFF, A. & GANEM, D. 2003. The latency-associated nuclear antigen of Kaposi's sarcoma-associated herpesvirus permits replication of terminal repeat-containing plasmids. *J Virol,* 77**,** 2779-83.

GRZESIK, P., MACMATH, D., HENSON, B., PRASAD, S., JOSHI, P. & DESAI, P. J. 2017. Incorporation of the Kaposi's sarcoma-associated herpesvirus capsid vertex-specific component (CVSC) into self-assembled capsids. *Virus Research,* 236**,** 9-13.

GUERRERO, C. A., MÉNDEZ, E., ZÁRATE, S., ISA, P., LÓPEZ, S. & ARIAS, C. F. 2000. Integrin alpha(v)beta(3) mediates rotavirus cell entry. *Proc Natl Acad Sci U S A,* 97**,** 14644-9.

GUI, L., EBNER, J. L., MILEANT, A., WILLIAMS, J. A. & LEE, K. K. 2016. Visualization and Sequencing of Membrane Remodeling Leading to Influenza Virus Fusion. *J Virol,* 90**,** 6948-6962.

GUO, Y., LI, W., QIN, J., LU, C. & FAN, W. 2017. Kaposi's sarcoma-associated herpesvirus (KSHV)-encoded microRNAs promote matrix metalloproteinases (MMPs) expression and pro-angiogenic cytokine secretion in endothelial cells. *J Med Virol,* 89**,** 1274-1280.

GUO, Y., WANG, W., SUN, Y., MA, C., WANG, X., WANG, X., LIU, P., SHEN, S., LI, B., LIN, J., DENG, F., WANG, H. & LOU, Z. 2016. Crystal Structure of the Core Region of Hantavirus Nucleocapsid Protein Reveals the Mechanism for Ribonucleoprotein Complex Formation. *J Virol,* 90**,** 1048-61.

GUSEVA, S., MILLES, S., JENSEN, M. R., SALVI, N., KLEMAN, J. P., MAURIN, D., RUIGROK, R. W. H. & BLACKLEDGE, M. 2020. Measles virus nucleo- and phosphoproteins form liquid-like phase-separated compartments that promote nucleocapsid assembly. *Sci Adv,* 6**,** eaaz7095.

GUTIÉRREZ, M., ISA, P., SÁNCHEZ-SAN MARTIN, C., PÉREZ-VARGAS, J., ESPINOSA, R., ARIAS, C. F. & LÓPEZ, S. 2010. Different rotavirus strains enter MA104 cells through different endocytic pathways: the role of clathrin-mediated endocytosis. *Journal of virology,* 84**,** 9161-9169.

HACKER, D., RAJU, R. & KOLAKOFSKY, D. 1989. La Crosse virus nucleocapsid protein controls its own synthesis in mosquito cells by encapsidating its mRNA. *J Virol,* 63**,** 5166-74.

HAFFEJEE, I. E. 1991. Neonatal rotavirus infections. *Rev Infect Dis,* 13**,** 957-62.

HAFFEJEE, I. E., MOOSA, A. & WINDSOR, I. 1990. Circulating and breast-milk anti-rotaviral antibodies and neonatal rotavirus infections: a maternal-neonatal study. *Ann Trop Paediatr,* 10**,** 3-14.

HAGBOM, M., ISTRATE, C., ENGBLOM, D., KARLSSON, T., RODRIGUEZ-DIAZ, J., BUESA, J., TAYLOR, J. A., LOITTO, V.-M., MAGNUSSON, K.-E., AHLMAN, H., LUNDGREN, O. & SVENSSON, L. 2011. Rotavirus stimulates release of serotonin (5-HT) from human enterochromaffin cells and activates brain structures involved in nausea and vomiting. *PLoS pathogens,* 7**,** e1002115-e1002115.

HAGEMANS, D., VAN BELZEN, I. A. E. M., MORÁN LUENGO, T. & RÜDIGER, S. G. D. 2015. A script to highlight hydrophobicity and charge on protein surfaces. *Frontiers in Molecular Biosciences,* 2.

HAHN, A. S., KAUFMANN, J. K., WIES, E., NASCHBERGER, E., PANTELEEV-IVLEV, J., SCHMIDT, K., HOLZER, A., SCHMIDT, M., CHEN, J., KONIG, S., ENSSER, A., MYOUNG, J., BROCKMEYER, N. H., STURZL, M., FLECKENSTEIN, B. & NEIPEL, F. 2012. The ephrin receptor tyrosine kinase A2 is a cellular receptor for Kaposi's sarcoma-associated herpesvirus. *Nature Medicine,* 18**,** 961-+.

HAO, P., YU, J., WARD, R., LIU, Y., HAO, Q., AN, S. & XU, T. 2020. Eukaryotic translation initiation factors as promising targets in cancer therapy. *Cell Communication and Signaling,* 18**,** 175.

HARB, M., BECKER, M. M., VITOUR, D., BARON, C. H., VENDE, P., BROWN, S. C., BOLTE, S., AROLD, S. T. & PONCET, D. 2008. Nuclear localization of cytoplasmic poly(A)-binding protein upon rotavirus infection involves the interaction of NSP3 with eIF4G and RoXaN. *J Virol,* 82**,** 11283-93.

HARDENBERG, M., HORVATH, A., AMBRUS, V., FUXREITER, M. & VENDRUSCOLO, M. 2020. Widespread occurrence of the droplet state of proteins in the human proteome. *Proceedings of the National Academy of Sciences,* 117**,** 33254-33262.

HARDESTAM, J., SIMON, M., HEDLUND, K. O., VAHERI, A., KLINGSTRÖM, J. & LUNDKVIST, Å. 2007. Ex Vivo Stability of the Rodent-Borne Hantaan Virus in Comparison to That of Arthropod-Borne Members of the Bunyaviridae Family. *Applied and Environmental Microbiology,* 73**,** 2547-2551.

HARRIS, K. M., PERRY, E., BOURNE, J., FEINBERG, M., OSTROFF, L. & HURLBURT, J. 2006. Uniform Serial Sectioning for Transmission Electron Microscopy. *The Journal of Neuroscience,* 26**,** 12101-12103.

HATOS, A., TOSATTO, S. C. E., VENDRUSCOLO, M. & FUXREITER, M. 2022. FuzDrop on AlphaFold: visualizing the sequence-dependent propensity of liquid–liquid phase separation and aggregation of proteins. *Nucleic Acids Research,* 50**,** W337-W344.

HAWES, P. C. 2015. Preparation of cultured cells using high-pressure freezing and freeze substitution for subsequent 2D or 3D visualization in the transmission electron microscope. *Methods Mol Biol,* 1282**,** 271-82.

HAZELTON, P. & GELDERBLOM, H. 2003. Electron microscopy for rapid diagnosis of infectious agents in emergent situations. *Emerging infectious diseases,* 9 3**,** 294-303.

HE, M., CHENG, F., DA SILVA, S. R., TAN, B., SOREL, O., GRUFFAZ, M., LI, T. & GAO, S. J. 2019. Molecular Biology of KSHV in Relation to HIV/AIDS-Associated Oncogenesis. *Cancer Treat Res,* 177**,** 23-62.

HE, X., WANG, S., HUANG, X. & WANG, X. 2013. Changes in age distribution of hemorrhagic fever with renal syndrome: an implication of China's expanded program of immunization. *BMC public health,* 13**,** 394-394.

HEINRICH, B. S., MALIGA, Z., STEIN, D. A., HYMAN, A. A. & WHELAN, S. P. J. 2018. Phase Transitions Drive the Formation of Vesicular Stomatitis Virus Replication Compartments. *mBio,* 9.
HELDWEIN, E. E. & KRUMMENACHER, C. 2008. Entry of herpesviruses into mammalian cells. *Cell Mol Life Sci,* 65**,** 1653-68.
HEMING, J. D., CONWAY, J. F. & HOMA, F. L. 2017. Herpesvirus Capsid Assembly and DNA Packaging. *Adv Anat Embryol Cell Biol,* 223**,** 119-142.
HENAFF, D., RADTKE, K. & LIPPÉ, R. 2012. Herpesviruses exploit several host compartments for envelopment. *Traffic,* 13**,** 1443-9.
HEPOJOKI, J., STRANDIN, T., LANKINEN, H. & VAHERI, A. 2012. Hantavirus structure--molecular interactions behind the scene. *J Gen Virol,* 93**,** 1631-1644.
HEPOJOKI, J., STRANDIN, T., WANG, H., VAPALAHTI, O., VAHERI, A. & LANKINEN, H. 2010. Cytoplasmic tails of hantavirus glycoproteins interact with the nucleocapsid protein. *Journal of General Virology,* 91**,** 2341-2350.
HESKETH, E. L., SAUNDERS, K., FISHER, C., POTZE, J., STANLEY, J., LOMONOSSOFF, G. P. & RANSON, N. A. 2018. The 3.3 Å structure of a plant geminivirus using cryo-EM. *Nature Communications,* 9**,** 2369.
HEYMANN, J. B., CHENG, N., NEWCOMB, W. W., TRUS, B. L., BROWN, J. C. & STEVEN, A. C. 2003. Dynamics of herpes simplex virus capsid maturation visualized by time-lapse cryo-electron microscopy. *Nat Struct Biol,* 10**,** 334-41.
HILTERBRAND, A. T. & HELDWEIN, E. E. 2019. Go go gadget glycoprotein!: HSV-1 draws on its sizeable glycoprotein tool kit to customize its diverse entry routes. *PLOS Pathogens,* 15**,** e1007660.
HJELLE, B. & TORRES-PÉREZ, F. 2010. Hantaviruses in the americas and their role as emerging pathogens. *Viruses,* 2**,** 2559-2586.
HLADIK, W., DOLLARD, S. C., MERMIN, J., FOWLKES, A. L., DOWNING, R., AMIN, M. M., BANAGE, F., NZARO, E., KATAAHA, P., DONDERO, T. J., PELLETT, P. E. & LACKRITZ, E. M. 2006. Transmission of human herpesvirus 8 by blood transfusion. *N Engl J Med,* 355**,** 1331-8.
HODGE & RIDLEY 2016. Regulating Rho GTPases and their regulators. *Nature Reviews Molecular Cell Biology,* 17**,** 496-510.
HODGE & STOW, N. D. 2001. Effects of mutations within the herpes simplex virus type 1 DNA encapsidation signal on packaging efficiency. *J Virol,* 75**,** 8977-86.
HOFMANN, J., KRAMER, S., HERRLINGER, K. R., JESKE, K., KUHNS, M., WEISS, S., ULRICH, R. G. & KRÜGER, D. H. 2021. Tula Virus as Causative Agent of Hantavirus Disease in Immunocompetent Person, Germany. *Emerging infectious diseases,* 27**,** 1234-1237.
HOGUE, I. B., BOSSE, J. B., HU, J. R., THIBERGE, S. Y. & ENQUIST, L. W. 2014. Cellular mechanisms of alpha herpesvirus egress: live cell fluorescence microscopy of pseudorabies virus exocytosis. *PLoS Pathog,* 10**,** e1004535.
HOLLINSHEAD, M., JOHNS, H. L., SAYERS, C. L., GONZALEZ-LOPEZ, C., SMITH, G. L. & ELLIOTT, G. 2012. Endocytic tubules regulated by Rab GTPases 5 and 11 are used for envelopment of herpes simplex virus. *Embo j,* 31**,** 4204-20.
HU, G., KATUWAWALA, A., WANG, K., WU, Z., GHADERMARZI, S., GAO, J. & KURGAN, L. 2021. flDPnn: Accurate intrinsic disorder prediction with putative propensities of disorder functions. *Nature Communications,* 12**,** 4438.
HU, J., GARBER, A. C. & RENNE, R. 2002. The latency-associated nuclear antigen of Kaposi's sarcoma-associated herpesvirus supports latent DNA replication in dividing cells. *J Virol,* 76**,** 11677-87.
HU, J., SHIBATA, Y., ZHU, P. P., VOSS, C., RISMANCHI, N., PRINZ, W. A., RAPOPORT, T. A. & BLACKSTONE, C. 2009. A class of dynamin-like GTPases involved in the generation of the tubular ER network. *Cell,* 138**,** 549-61.
HU, L., CHOW, D. C., PATTON, J. T., PALZKILL, T., ESTES, M. K. & PRASAD, B. V. 2012a. Crystallographic Analysis of Rotavirus NSP2-RNA Complex Reveals Specific Recognition of 5' GG Sequence for RTPase Activity. *J Virol,* 86**,** 10547-57.

HU, L., CRAWFORD, S. E., HYSER, J. M., ESTES, M. K. & PRASAD, B. V. 2012b. Rotavirus non-structural proteins: structure and function. *Curr Opin Virol,* 2**,** 380-8.
HUANG, F., OLDFIELD, C. J., XUE, B., HSU, W.-L., MENG, J., LIU, X., SHEN, L., ROMERO, P., UVERSKY, V. N. & DUNKER, A. K. 2014. Improving protein order-disorder classification using charge-hydropathy plots. *BMC Bioinformatics,* 15**,** S4.
HUFFMAN, J. B., DANIEL, G. R., FALCK-PEDERSEN, E., HUET, A., SMITH, G. A., CONWAY, J. F., HOMA, F. L. & SANDRI-GOLDIN, R. M. 2017. The C Terminus of the Herpes Simplex Virus UL25 Protein Is Required for Release of Viral Genomes from Capsids Bound to Nuclear Pores. *Journal of Virology,* 91**,** e00641-17.
HUGGINS, J. W., HSIANG, C. M., COSGRIFF, T. M., GUANG, M. Y., SMITH, J. I., WU, Z. O., LEDUC, J. W., ZHENG, Z. M., MEEGAN, J. M., WANG, Q. N. & ET AL. 1991. Prospective, double-blind, concurrent, placebo-controlled clinical trial of intravenous ribavirin therapy of hemorrhagic fever with renal syndrome. *J Infect Dis,* 164**,** 1119-27.
HUGHES, D. J., WOOD, J. J., JACKSON, B. R., BAQUERO-PÉREZ, B. & WHITEHOUSE, A. 2015. NEDDylation Is Essential for Kaposi's Sarcoma-Associated Herpesvirus Latency and Lytic Reactivation and Represents a Novel Anti-KSHV Target. *PLOS Pathogens,* 11**,** e1004771.
HUISKONEN, J. T., HEPOJOKI, J., LAURINMÄKI, P., VAHERI, A., LANKINEN, H., BUTCHER, S. J. & GRÜNEWALD, K. 2010. Electron cryotomography of Tula hantavirus suggests a unique assembly paradigm for enveloped viruses. *J Virol,* 84**,** 4889-97.
HUMAN-PROTEIN-ATLAS. *DOCK5* [Online]. Human-Protein-Atlas. Available: https://www.proteinatlas.org/ENSG00000147459-DOCK5/subcellular#human [Accessed 05.05.2022 2022].
HUSSEIN, H. A. M., ALFHILI, M. A., PAKALA, P., SIMON, S., HUSSAIN, J., MCCUBREY, J. A. & AKULA, S. M. 2019. miRNAs and their roles in KSHV pathogenesis. *Virus Research,* 266**,** 15-24.
HYSER, J. M., COLLINSON-PAUTZ, M. R., UTAMA, B., ESTES, M. K., PATTON, J. & DERMODY, T. S. 2010. Rotavirus Disrupts Calcium Homeostasis by NSP4 Viroporin Activity. *mBio,* 1**,** e00265-10.
ICTV. 2021. *Virus Taxonomy: 2021 Release* [Online]. International Committee on Taxonomy of Viruses. Available: https://talk.ictvonline.org/taxonomy/ [Accessed 23/06/2022 2022].
IŠA, P., PÉREZ-DELGADO, A., QUEVEDO, I. R., LÓPEZ, S. & ARIAS, C. F. 2020. Rotaviruses Associate with Distinct Types of Extracellular Vesicles. *Viruses,* 12**,** 763.
ISHIKAWA, T. 2016. Electron Tomography. *In:* BRADSHAW, R. A. & STAHL, P. D. (eds.) *Encyclopedia of Cell Biology.* Waltham: Academic Press.
JÄÄSKELÄINEN, K. M., KAUKINEN, P., MINSKAYA, E. S., PLYUSNINA, A., VAPALAHTI, O., ELLIOTT, R. M., WEBER, F., VAHERI, A. & PLYUSNIN, A. 2007. Tula and Puumala hantavirus NSs ORFs are functional and the products inhibit activation of the interferon-beta promoter. *J Med Virol,* 79**,** 1527-36.
JÄÄSKELÄINEN, K. M., PLYUSNINA, A., LUNDKVIST, A., VAHERI, A. & PLYUSNIN, A. 2008. Tula hantavirus isolate with the full-length ORF for nonstructural protein NSs survives for more consequent passages in interferon-competent cells than the isolate having truncated NSs ORF. *Virol J,* 5**,** 3.
JACKSON, B. R., BOYNE, J. R., NOERENBERG, M., TAYLOR, A., HAUTBERGUE, G. M., WALSH, M. J., WHEAT, R., BLACKBOURN, D. J., WILSON, S. A. & WHITEHOUSE, A. 2011. An Interaction between KSHV ORF57 and UIF Provides mRNA-Adaptor Redundancy in Herpesvirus Intronless mRNA Export. *PLOS Pathogens,* 7**,** e1002138.
JAGGI, U., WANG, S., TORMANEN, K., MATUNDAN, H., LJUBIMOV, A. V. & GHIASI, H. 2018. Role of Herpes Simplex Virus Type 1 (HSV-1) Glycoprotein K (gK) Pathogenic CD8+ T Cells in Exacerbation of Eye Disease. *Frontiers in Immunology,* 9.
JAMBUNATHAN, N., CHOULJENKO, D., DESAI, P., CHARLES, A. S., SUBRAMANIAN, R., CHOULJENKO, V. N. & KOUSOULAS, K. G. 2014. Herpes simplex virus 1 protein UL37 interacts with viral

glycoprotein gK and membrane protein UL20 and functions in cytoplasmic virion envelopment. *J Virol,* 88**,** 5927-35.
JAMES, HARFOUCHE, M., WELTON, N. J., TURNER, K. M., ABU-RADDAD, L. J., GOTTLIEB, S. L. & LOOKER, K. J. 2020. Herpes simplex virus: global infection prevalence and incidence estimates, 2016. *Bull World Health Organ,* 98**,** 315-329.
JAMES, SHEFFIELD, J. S. & KIMBERLIN, D. W. 2014. Mother-to-Child Transmission of Herpes Simplex Virus. *J Pediatric Infect Dis Soc,* 3 Suppl 1**,** S19-23.
JAMESON, L. J., TAORI, S. K., ATKINSON, B., LEVICK, P., FEATHERSTONE, C. A., VAN DER BURGT, G., MCCARTHY, N., HART, J., OSBORNE, J. C., WALSH, A. L., BROOKS, T. J. & HEWSON, R. 2013. Pet rats as a source of hantavirus in England and Wales, 2013. *Euro Surveill,* 18.
JANGRA, R. K., HERBERT, A. S., LI, R., JAE, L. T., KLEINFELTER, L. M., SLOUGH, M. M., BARKER, S. L., GUARDADO-CALVO, P., ROMÁN-SOSA, G., DIETERLE, M. E., KUEHNE, A. I., MUENA, N. A., WIRCHNIANSKI, A. S., NYAKATURA, E. K., FELS, J. M., NG, M., MITTLER, E., PAN, J., BHARRHAN, S., WEC, A. Z., LAI, J. R., SIDHU, S. S., TISCHLER, N. D., REY, F. A., MOFFAT, J., BRUMMELKAMP, T. R., WANG, Z., DYE, J. M. & CHANDRAN, K. 2018. Protocadherin-1 is essential for cell entry by New World hantaviruses. *Nature,* 563**,** 559-563.
JÄNTTI, J., HILDÉN, P., RÖNKÄ, H., MÄKIRANTA, V., KERÄNEN, S. & KUISMANEN, E. 1997. Immunocytochemical analysis of Uukuniemi virus budding compartments: role of the intermediate compartment and the Golgi stack in virus maturation. *J Virol,* 71**,** 1162-72.
JAROUSSE, N., CHANDRAN, B. & COSCOY, L. 2008. Lack of heparan sulfate expression in B-cell lines: implications for Kaposi's sarcoma-associated herpesvirus and murine gammaherpesvirus 68 infections. *J Virol,* 82**,** 12591-7.
JHENG, J.-R., HO, J.-Y. & HORNG, J.-T. 2014. ER stress, autophagy, and RNA viruses. *Frontiers in Microbiology,* 5.
JIANG, B., WANG, Y., GLASS, R. I. & FANG, Z. Y. 2005. The evolution of human group B rotaviruses: correction and an update. *J Clin Virol,* 34**,** 158-9.
JIANG, X., JAYARAM, H., KUMAR, M., LUDTKE, S. J., ESTES, M. K. & PRASAD, B. V. 2006. Cryoelectron microscopy structures of rotavirus NSP2-NSP5 and NSP2-RNA complexes: implications for genome replication. *J Virol,* 80**,** 10829-35.
JIMÉNEZ-ZARAGOZA, M., YUBERO, M. P., MARTÍN-FORERO, E., CASTÓN, J. R., REGUERA, D., LUQUE, D., DE PABLO, P. J. & RODRÍGUEZ, J. M. 2018. Biophysical properties of single rotavirus particles account for the functions of protein shells in a multilayered virus. *eLife,* 7**,** e37295.
JIN, M., PARK, J., LEE, S., PARK, B., SHIN, J., SONG, K. J., AHN, T. I., HWANG, S. Y., AHN, B. Y. & AHN, K. 2002. Hantaan virus enters cells by clathrin-dependent receptor-mediated endocytosis. *Virology,* 294**,** 60-9.
JIN, X., CAO, X., WANG, X., JIANG, J., WAN, J., LALIBERTÉ, J.-F. & ZHANG, Y. 2018. Three-Dimensional Architecture and Biogenesis of Membrane Structures Associated with Plant Virus Replication. *Frontiers in Plant Science,* 9.
JOHNE, SCHILLING-LOEFFLER, K., ULRICH, R. G. & TAUSCH, S. H. 2022. Whole Genome Sequence Analysis of a Prototype Strain of the Novel Putative Rotavirus Species L. *Viruses,* 14.
JOHNE, TAUSCH, S. H., GRÜTZKE, J., FALKENHAGEN, A., PATZINA-MEHLING, C., BEER, M., HÖPER, D. & ULRICH, R. G. 2019. Distantly Related Rotaviruses in Common Shrews, Germany, 2004-2014. *Emerging infectious diseases,* 25**,** 2310-2314.
JOHNSON, D. C. & BAINES, J. D. 2011. Herpesviruses remodel host membranes for virus egress. *Nat Rev Microbiol,* 9**,** 382-94.
JOHNSTON, B. P., PRINGLE, E. S. & MCCORMICK, C. 2019. KSHV activates unfolded protein response sensors but suppresses downstream transcriptional responses to support lytic replication. *PLoS pathogens,* 15**,** e1008185-e1008185.
JONES, C. A., RAYNES-GREENOW, C. & ISAACS, D. 2014. Population-based surveillance of neonatal herpes simplex virus infection in Australia, 1997-2011. *Clin Infect Dis,* 59**,** 525-31.

JONES, J. E., LE SAGE, V. & LAKDAWALA, S. S. 2020. Viral and host heterogeneity and their effects on the viral life cycle. *Nature Reviews Microbiology*.

JONSSON & SCHMALJOHN, C. S. 2001. Replication of Hantaviruses. *In:* SCHMALJOHN, C. S. & NICHOL, S. T. (eds.) *Hantaviruses.* Berlin, Heidelberg: Springer Berlin Heidelberg.

JONSSON, C. B., FIGUEIREDO, L. T. M. & VAPALAHTI, O. 2010. A global perspective on hantavirus ecology, epidemiology, and disease. *Clinical microbiology reviews,* 23**,** 412-441.

JUMPER, J., EVANS, R., PRITZEL, A., GREEN, T., FIGURNOV, M., RONNEBERGER, O., TUNYASUVUNAKOOL, K., BATES, R., ŽÍDEK, A., POTAPENKO, A., BRIDGLAND, A., MEYER, C., KOHL, S. A. A., BALLARD, A. J., COWIE, A., ROMERA-PAREDES, B., NIKOLOV, S., JAIN, R., ADLER, J., BACK, T., PETERSEN, S., REIMAN, D., CLANCY, E., ZIELINSKI, M., STEINEGGER, M., PACHOLSKA, M., BERGHAMMER, T., BODENSTEIN, S., SILVER, D., VINYALS, O., SENIOR, A. W., KAVUKCUOGLU, K., KOHLI, P. & HASSABIS, D. 2021. Highly accurate protein structure prediction with AlphaFold. *Nature,* 596**,** 583-589.

KALLIO, E. R., KLINGSTRÖM, J., GUSTAFSSON, E., MANNI, T., VAHERI, A., HENTTONEN, H., VAPALAHTI, O. & LUNDKVIST, Å. 2006. Prolonged survival of Puumala hantavirus outside the host: evidence for indirect transmission via the environment. *J Gen Virol,* 87**,** 2127-2134.

KALLIO, E. R., VOUTILAINEN, L., VAPALAHTI, O., VAHERI, A., HENTTONEN, H., KOSKELA, E. & MAPPES, T. 2007. Endemic hantavirus infection impairs the winter survival of its rodent host. *Ecology,* 88**,** 1911-6.

KANAI, Y., KOMOTO, S., KAWAGISHI, T., NOUDA, R., NAGASAWA, N., ONISHI, M., MATSUURA, Y., TANIGUCHI, K. & KOBAYASHI, T. 2017. Entirely plasmid-based reverse genetics system for rotaviruses. *Proc Natl Acad Sci U S A,* 114**,** 2349-2354.

KANG, G., ITURRIZA-GOMARA, M., WHEELER, J. G., CRYSTAL, P., MONICA, B., RAMANI, S., PRIMROSE, B., MOSES, P. D., GALLIMORE, C. I., BROWN, D. W. & GRAY, J. 2004. Quantitation of group A rotavirus by real-time reverse-transcription-polymerase chain reaction: Correlation with clinical severity in children in South India. *Journal of Medical Virology,* 73**,** 118-122.

KEARSE, M. G. & WILUSZ, J. E. 2017. Non-AUG translation: a new start for protein synthesis in eukaryotes. *Genes Dev,* 31**,** 1717-1731.

KENNEDY, P. G. E. & CHAUDHURI, A. 2002. Herpes simplex encephalitis. *Journal of Neurology, Neurosurgery & Psychiatry,* 73**,** 237.

KERINS, J. L., KOSKE, S. E., KAZMIERCZAK, J., AUSTIN, C., GOWDY, K. & DIBERNARDO, A. 2018. Outbreak of Seoul virus among rats and rat owners - United States and Canada, 2017. *Can Commun Dis Rep,* 44**,** 71-74.

KERUR, N., VEETTIL, M. V., SHARMA-WALIA, N., SADAGOPAN, S., BOTTERO, V., PAUL, A. G. & CHANDRAN, B. 2010. Characterization of entry and infection of monocytic THP-1 cells by Kaposi's sarcoma associated herpesvirus (KSHV): Role of heparan sulfate, DC-SIGN, integrins and signaling. *Virology,* 406**,** 103-116.

KESKIN, O., GURSOY, A., MA, B. & NUSSINOV, R. 2008. Principles of protein-protein interactions: what are the preferred ways for proteins to interact? *Chem Rev,* 108**,** 1225-44.

KHOURY, H., OGILVIE, I., EL KHOURY, A. C., DUAN, Y. & GOETGHEBEUR, M. M. 2011. Burden of rotavirus gastroenteritis in the Middle Eastern and North African pediatric population. *BMC Infect Dis,* 11**,** 9.

KIELIAN, M. & REY, F. A. 2006. Virus membrane-fusion proteins: more than one way to make a hairpin. *Nature Reviews Microbiology,* 4**,** 67-76.

KILLINGSWORTH, M. C. & BOBRYSHEV, Y. V. 2016. Correlative Light- and Electron Microscopy Using Quantum Dot Nanoparticles. *J Vis Exp*.

KILPATRICK, E. D., TERAJIMA, M., KOSTER, F. T., CATALINA, M. D., CRUZ, J. & ENNIS, F. A. 2004. Role of specific CD8+ T cells in the severity of a fulminant zoonotic viral hemorrhagic fever, hantavirus pulmonary syndrome. *J Immunol,* 172**,** 3297-304.

KIM, H., IIZASA, H., KANEHIRO, Y., FEKADU, S. & YOSHIYAMA, H. 2017. Herpesviral microRNAs in Cellular Metabolism and Immune Responses. *Frontiers in Microbiology,* 8.

KIM, J. M., CHUNG, Y. S., JO, H. J., LEE, N. J., KIM, M. S., WOO, S. H., PARK, S., KIM, J. W., KIM, H. M. & HAN, M. G. 2020. Identification of Coronavirus Isolated from a Patient in Korea with COVID-19. *Osong Public Health Res Perspect,* 11**,** 3-7.

KIMBERLIN, D. W. 2004. Neonatal herpes simplex infection. *Clin Microbiol Rev,* 17**,** 1-13.

KIMBERLIN, D. W. 2007. Herpes simplex virus infections of the newborn. *Semin Perinatol,* 31**,** 19-25.

KINDLER, E., TROJNAR, E., HECKEL, G., OTTO, P. H. & JOHNE, R. 2013. Analysis of rotavirus species diversity and evolution including the newly determined full-length genome sequences of rotavirus F and G. *Infection, Genetics and Evolution,* 14**,** 58-67.

KING, C. K., GLASS, R., BRESEE, J. S. & DUGGAN, C. 2003. Managing acute gastroenteritis among children: oral rehydration, maintenance, and nutritional therapy. *MMWR Recomm Rep,* 52**,** 1-16.

KLEINFELTER, L. M., JANGRA, R. K., JAE, L. T., HERBERT, A. S., MITTLER, E., STILES, K. M., WIRCHNIANSKI, A. S., KIELIAN, M., BRUMMELKAMP, T. R., DYE, J. M. & CHANDRAN, K. 2015. Haploid Genetic Screen Reveals a Profound and Direct Dependence on Cholesterol for Hantavirus Membrane Fusion. *mBio,* 6**,** e00801.

KLEMPA, B., WITKOWSKI, P. T., POPUGAEVA, E., AUSTE, B., KOIVOGUI, L., FICHET-CALVET, E., STRECKER, T., TER MEULEN, J. & KRÜGER, D. H. 2012. Sangassou virus, the first hantavirus isolate from Africa, displays genetic and functional properties distinct from those of other murinae-associated hantaviruses. *Journal of virology,* 86**,** 3819-3827.

KLUPP, B. G., GRANZOW, H. & METTENLEITER, T. C. 2001. Effect of the pseudorabies virus US3 protein on nuclear membrane localization of the UL34 protein and virus egress from the nucleus. *J Gen Virol,* 82**,** 2363-2371.

KNEZ, J., BILAN, P. T. & CAPONE, J. P. 2003. A single amino acid substitution in herpes simplex virus type 1 VP16 inhibits binding to the virion host shutoff protein and is incompatible with virus growth. *J Virol,* 77**,** 2892-902.

KNOWLES, T. P., VENDRUSCOLO, M. & DOBSON, C. M. 2014. The amyloid state and its association with protein misfolding diseases. *Nat Rev Mol Cell Biol,* 15**,** 384-96.

KOBILER, O. & WEITZMAN, M. D. 2019. Herpes simplex virus replication compartments: From naked release to recombining together. *PLOS Pathogens,* 15**,** e1007714.

KOMANDURI, K. V., LUCE, J. A., MCGRATH, M. S., HERNDIER, B. G. & NG, V. L. 1996. The natural history and molecular heterogeneity of HIV-associated primary malignant lymphomatous effusions. *J Acquir Immune Defic Syndr Hum Retrovirol,* 13**,** 215-26.

KONING, R. I., KOSTER, A. J. & SHARP, T. H. 2018. Advances in cryo-electron tomography for biology and medicine. *Annals of Anatomy - Anatomischer Anzeiger,* 217**,** 82-96.

KOOK, I. & ZIEGELBAUER, J. M. 2021. Monocyte chemoattractant protein-induced protein 1 directly degrades viral miRNAs with a specific motif and inhibits KSHV infection. *Nucleic Acids Research,* 49**,** 4456-4471.

KOONIN, E. V., DOLJA, V. V. & KRUPOVIC, M. 2015. Origins and evolution of viruses of eukaryotes: The ultimate modularity. *Virology,* 479-480**,** 2-25.

KRAAY, A. N. M., BROUWER, A. F., LIN, N., COLLENDER, P. A., REMAIS, J. V. & EISENBERG, J. N. S. 2018. Modeling environmentally mediated rotavirus transmission: The role of temperature and hydrologic factors. *Proceedings of the National Academy of Sciences,* 115**,** E2782-E2790.

KRAUTKRÄMER, E. & ZEIER, M. 2008. Hantavirus causing hemorrhagic fever with renal syndrome enters from the apical surface and requires decay-accelerating factor (DAF/CD55). *J Virol,* 82**,** 4257-64.

KRISHNAN, H. H., SHARMA-WALIA, N., ZENG, L., GAO, S. J. & CHANDRAN, B. 2005. Envelope glycoprotein gB of Kaposi's sarcoma-associated herpesvirus is essential for egress from infected cells. *J Virol,* 79**,** 10952-67.

KROSCHWALD, S., MAHARANA, S. & ALBERTI, S. 2017. Hexanediol: a chemical probe to investigate the material properties of membrane-less compartments. *Matters*.

KRÜGER, SCHÖNRICH, G. & KLEMPA, B. 2011. Human pathogenic hantaviruses and prevention of infection. *Hum Vaccin,* 7**,** 685-93.
KRÜGER, ULRICH, R. G. & HOFMANN, J. 2013. Hantaviruses as zoonotic pathogens in Germany. *Deutsches Arzteblatt international,* 110**,** 461-467.
KRUGER, D. H., FIGUEIREDO, L. T., SONG, J. W. & KLEMPA, B. 2015. Hantaviruses--globally emerging pathogens. *J Clin Virol,* 64**,** 128-36.
KRUMMENACHER, C., BARIBAUD, F., PONCE DE LEON, M., BARIBAUD, I., WHITBECK, J. C., XU, R., COHEN, G. H. & EISENBERG, R. J. 2004. Comparative usage of herpesvirus entry mediator A and nectin-1 by laboratory strains and clinical isolates of herpes simplex virus. *Virology,* 322**,** 286-99.
KUKIMOTO-NIINO, M., KATSURA, K., KAUSHIK, R., EHARA, H., YOKOYAMA, T., UCHIKUBO-KAMO, T., NAKAGAWA, R., MISHIMA-TSUMAGARI, C., YONEMOCHI, M., IKEDA, M., HANADA, K., ZHANG, K. Y. J. & SHIROUZU, M. 2021. Cryo-EM structure of the human ELMO1-DOCK5-Rac1 complex. *Sci Adv,* 7.
KUMAR, B. & CHANDRAN, B. 2016. KSHV Entry and Trafficking in Target Cells-Hijacking of Cell Signal Pathways, Actin and Membrane Dynamics. *Viruses,* 8.
KYTE, J. & DOOLITTLE, R. F. 1982. A simple method for displaying the hydropathic character of a protein. *J Mol Biol,* 157**,** 105-32.
LABO, N., MILEY, W., BENSON, C. A., CAMPBELL, T. B. & WHITBY, D. 2015. Epidemiology of Kaposi's sarcoma-associated herpesvirus in HIV-1-infected US persons in the era of combination antiretroviral therapy. *Aids,* 29**,** 1217-25.
LAENEN, L., VERGOTE, V., CALISHER, C. H., KLEMPA, B., KLINGSTRÖM, J., KUHN, J. H. & MAES, P. 2019. Hantaviridae: Current Classification and Future Perspectives. *Viruses,* 11**,** 788.
LAFONTAINE, D. L. J. 2019. Birth of Nucleolar Compartments: Phase Separation-Driven Ribosomal RNA Sorting and Processing. *Molecular Cell,* 76**,** 694-696.
LAMBDEN, P. R., COOKE, S. J., CAUL, E. O. & CLARKE, I. N. 1992. Cloning of noncultivatable human rotavirus by single primer amplification. *J Virol,* 66**,** 1817-22.
LAN, K., KUPPERS, D. A., VERMA, S. C., SHARMA, N., MURAKAMI, M. & ROBERTSON, E. S. 2005. Induction of Kaposi's sarcoma-associated herpesvirus latency-associated nuclear antigen by the lytic transactivator RTA: A novel mechanism for establishment of latency. *Journal of Virology,* 79**,** 7453-7465.
LAURIN & CÔTÉ 2014. Insights into the biological functions of Dock family guanine nucleotide exchange factors. *Genes & development,* 28**,** 533-547.
LAWTON, J. A., ESTES, M. K. & PRASAD, B. V. 1997. Three-dimensional visualization of mRNA release from actively transcribing rotavirus particles. *Nat Struct Biol,* 4**,** 118-21.
LAWTON, J. A., ESTES, M. K. & PRASAD, B. V. 2000. Mechanism of genome transcription in segmented dsRNA viruses. *Adv Virus Res,* 55**,** 185-229.
LEE, SHIM, J. & KIM, S. J. 2021. Stunning symmetries involved in the self-assembly of the HSV-1 capsid. *Journal of the Korean Physical Society,* 78**,** 357-364.
LEE, Y. J. & GLAUNSINGER, B. A. 2009. Aberrant herpesvirus-induced polyadenylation correlates with cellular messenger RNA destruction. *PLoS Biol,* 7**,** e1000107.
LI, DING, S., FENG, N., MOONEY, N., OOI, Y. S., REN, L., DIEP, J., KELLY, M. R., YASUKAWA, L. L., PATTON, J. T., YAMAZAKI, H., SHIRAO, T., JACKSON, P. K. & GREENBERG, H. B. 2017. Drebrin restricts rotavirus entry by inhibiting dynamin-mediated endocytosis. *Proc Natl Acad Sci U S A,* 114**,** E3642-e3651.
LI, GUO, D., QIN, Y. & CHEN, M. 2019. PI4KB on Inclusion Bodies Formed by ER Membrane Remodeling Facilitates Replication of Human Parainfluenza Virus Type 3. *Cell Reports,* 29**,** 2229-2242.e4.
LI, LANKINEN, H., PUTKURI, N., VAPALAHTI, O. & VAHERI, A. 2005. Tula hantavirus triggers pro-apoptotic signals of ER stress in Vero E6 cells. *Virology,* 333**,** 180-189.

LI, SHEN, Y., SONG, Y., ZHANG, Y., ZHANG, C., MA, Y., ZHANG, F. & CHEN, L. 2021. ER stress-related molecules induced by Hantaan virus infection in differentiated THP-1 cells. *Cell stress & chaperones,* 26**,** 41-50.

LI, P., BANJADE, S., CHENG, H. C., KIM, S., CHEN, B., GUO, L., LLAGUNO, M., HOLLINGSWORTH, J. V., KING, D. S., BANANI, S. F., RUSSO, P. S., JIANG, Q. X., NIXON, B. T. & ROSEN, M. K. 2012. Phase transitions in the assembly of multivalent signalling proteins. *Nature,* 483**,** 336-40.

LI, Z., BAKER, M. L., JIANG, W., ESTES, M. K. & PRASAD, B. V. 2009. Rotavirus architecture at subnanometer resolution. *J Virol,* 83**,** 1754-66.

LI, Z. & YU, X. 2020. Progress towards revealing the mechanism of herpesvirus capsid maturation and genome packaging. *Protein & Cell,* 11**,** 316-317.

LIN, C. L., LI, H., WANG, Y., ZHU, F. X., KUDCHODKAR, S. & YUAN, Y. 2003. Kaposi's sarcoma-associated herpesvirus lytic origin (ori-Lyt)-dependent DNA replication: identification of the ori-Lyt and association of K8 bZip protein with the origin. *J Virol,* 77**,** 5578-88.

LIN, J. H., WALTER, P. & YEN, T. S. B. 2008. Endoplasmic reticulum stress in disease pathogenesis. *Annual review of pathology,* 3**,** 399-425.

LIN, Y., FICHOU, Y., LONGHINI, A. P., LLANES, L. C., YIN, P., BAZAN, G. C., KOSIK, K. S. & HAN, S. 2021. Liquid-Liquid Phase Separation of Tau Driven by Hydrophobic Interaction Facilitates Fibrillization of Tau. *J Mol Biol,* 433**,** 166731.

LISCO, A., BARBIERATO, M., FIORE, J. R., GASPERINI, P., FAVIA, A., VOLPE, A., CHIRONNA, M., PASTORE, G., CHIECO-BIANCHI, L. & CALABRÒ, M. L. 2006. Pregnancy and human herpesvirus 8 reactivation in human immunodeficiency virus type 1-infected women. *J Clin Microbiol,* 44**,** 3863-71.

LITTLE, R. F. & ULDRICK, T. S. 2019. Are There Clues to Oral Kaposi Sarcoma–Associated Herpesvirus Shedding and Kaposi Sarcoma Oncogenesis in the Oral Microbiome? *The Journal of Infectious Diseases,* 221**,** 1226-1228.

LIU, R., MA, H., SHU, J., ZHANG, Q., HAN, M., LIU, Z., JIN, X., ZHANG, F. & WU, X. 2020. Vaccines and Therapeutics Against Hantaviruses. *Frontiers in microbiology,* 10**,** 2989-2989.

LIU, Y. T., JIH, J., DAI, X., BI, G. Q. & ZHOU, Z. H. 2019. Cryo-EM structures of herpes simplex virus type 1 portal vertex and packaged genome. *Nature,* 570**,** 257-261.

LÖBER, C., ANHEIER, B., LINDOW, S., KLENK, H. D. & FELDMANN, H. 2001. The Hantaan virus glycoprotein precursor is cleaved at the conserved pentapeptide WAASA. *Virology,* 289**,** 224-9.

LONG, C. P. & MCDONALD, S. M. 2017. Rotavirus genome replication: Some assembly required. *PLoS pathogens,* 13**,** e1006242-e1006242.

LONG, W.-Y., ZHAO, G.-H. & WU, Y. 2022. Endoplasmic Reticulum-Shaping Atlastin Proteins Facilitate KSHV Replication. *Frontiers in Cellular and Infection Microbiology,* 11.

LONG, W.-Y., ZHAO, G.-H., WU, Y. & LIU, Y. 2021. Gallic acid inhibits Kaposi's Sarcoma-associated herpesvirus lytic reactivation by suppressing RTA transcriptional activities. *Food Science & Nutrition,* 9**,** 847-854.

LOOKER, K. J., MAGARET, A. S., MAY, M. T., TURNER, K. M., VICKERMAN, P., GOTTLIEB, S. L. & NEWMAN, L. M. 2015. Global and Regional Estimates of Prevalent and Incident Herpes Simplex Virus Type 1 Infections in 2012. *PLoS One,* 10**,** e0140765.

LÓPEZ, OCEGUERA, A. & SANDOVAL-JAIME, C. 2016. Stress Response and Translation Control in Rotavirus Infection. *Viruses,* 8**,** 162.

LÓPEZ, SILVA-AYALA, D., LÓPEZ, S. & ARIAS, C. 2011. Methods suitable for high-throughput screening of siRNAs and other chemical compounds with the potential to inhibit rotavirus replication. *Journal of virological methods,* 179**,** 242-9.

LOPEZ, S. & ARIAS, C. F. 2006. Early steps in rotavirus cell entry. *Curr Top Microbiol Immunol,* 309**,** 39-66.

LOW, W. K., DANG, Y., SCHNEIDER-POETSCH, T., SHI, Z., CHOI, N. S., MERRICK, W. C., ROMO, D. & LIU, J. O. 2005. Inhibition of eukaryotic translation initiation by the marine natural product pateamine A. *Mol Cell,* 20**,** 709-22.

LUIS, A. D., DOUGLASS, R. J., HUDSON, P. J., MILLS, J. N. & BJØRNSTAD, O. N. 2012. Sin Nombre hantavirus decreases survival of male deer mice. *Oecologia,* 169**,** 431-9.

LUITWEILER, E. M., HENSON, B. W., PRYCE, E. N., PATEL, V., COOMBS, G., MCCAFFERY, J. M. & DESAI, P. J. 2013. Interactions of the Kaposi's Sarcoma-Associated Herpesvirus Nuclear Egress Complex: ORF69 Is a Potent Factor for Remodeling Cellular Membranes. *Journal of Virology,* 87**,** 3915-3929.

LUNDGREN, O. & SVENSSON, L. 2001. Pathogenesis of rotavirus diarrhea. *Microbes and infection,* 3**,** 1145-1156.

LV, SHEN, S., XIANG, L., JIA, X., HOU, Y., WANG, D., DENG, H. & LONGNECKER, R. M. 2019a. Functional Identification and Characterization of the Nuclear Egress Complex of a Gammaherpesvirus. *Journal of Virology,* 93**,** e01422-19.

LV, ZHOU, S., GAO, S. & DENG, H. 2019b. Remodeling of host membranes during herpesvirus assembly and egress. *Protein Cell,* 10**,** 315-326.

MACKOW, E. R. & GAVRILOVSKAYA, I. N. 2009. Hantavirus regulation of endothelial cell functions. *Thromb Haemost,* 102**,** 1030-41.

MADOR, N., GOLDENBERG, D., COHEN, O., PANET, A. & STEINER, I. 1998. Herpes simplex virus type 1 latency-associated transcripts suppress viral replication and reduce immediate-early gene mRNA levels in a neuronal cell line. *J Virol,* 72**,** 5067-75.

MAEDA, F., ARII, J., HIROHATA, Y., MARUZURU, Y., KOYANAGI, N., KATO, A. & KAWAGUCHI, Y. 2017. Herpes Simplex Virus 1 UL34 Protein Regulates the Global Architecture of the Endoplasmic Reticulum in Infected Cells. *J Virol,* 91.

MAES, P., KEYAERTS, E., CLEMENT, J., BONNET, V., ROBERT, A. & VAN RANST, M. 2004. Detection of Puumala hantavirus antibody with ELISA using a recombinant truncated nucleocapsid protein expressed in Escherichia coli. *Viral Immunol,* 17**,** 315-21.

MAKHOV, A. M., LEE, S. S., LEHMAN, I. R. & GRIFFITH, J. D. 2003. Origin-specific unwinding of herpes simplex virus 1 DNA by the viral UL9 and ICP8 proteins: visualization of a specific preunwinding complex. *Proc Natl Acad Sci U S A,* 100**,** 898-903.

MALOPE, B. I., MACPHAIL, P., MBISA, G., MACPHAIL, C., STEIN, L., RATSHIKHOPHA, E. M., NDHLOVU, L., SITAS, F. & WHITBY, D. 2008. No evidence of sexual transmission of Kaposi's sarcoma herpes virus in a heterosexual South African population. *Aids,* 22**,** 519-26.

MANOLARIDIS, I., MUMTSIDU, E., KONAREV, P., MAKHOV, A. M., FULLERTON, S. W., SINZ, A., KALKHOF, S., MCGEEHAN, J. E., CARY, P. D., GRIFFITH, J. D., SVERGUN, D., KNEALE, G. G. & TUCKER, P. A. 2009. Structural and biophysical characterization of the proteins interacting with the herpes simplex virus 1 origin of replication. *J Biol Chem,* 284**,** 16343-16353.

MANTINA, H., KANKASA, C., KLASKALA, W., BRAYFIELD, B., CAMPBELL, J., DU, Q., BHAT, G., KASOLO, F., MITCHELL, C. & WOOD, C. 2001. Vertical transmission of Kaposi's sarcoma-associated herpesvirus. *Int J Cancer,* 94**,** 749-52.

MAPELLI, M., PANJIKAR, S. & TUCKER, P. A. 2005. The Crystal Structure of the Herpes Simplex Virus 1 ssDNA-binding Protein Suggests the Structural Basis for Flexible, Cooperative Single-stranded DNA Binding *. *Journal of Biological Chemistry,* 280**,** 2990-2997.

MARIGGIÒ, G., KOCH, S. & SCHULZ, T. F. 2017. Kaposi sarcoma herpesvirus pathogenesis. *Philos Trans R Soc Lond B Biol Sci,* 372.

MARTELLA, V., BÁNYAI, K., MATTHIJNSSENS, J., BUONAVOGLIA, C. & CIARLET, M. 2010. Zoonotic aspects of rotaviruses. *Veterinary Microbiology,* 140**,** 246-255.

MARTIN, D., DUARTE, M., LEPAULT, J. & PONCET, D. 2010. Sequestration of free tubulin molecules by the viral protein NSP2 induces microtubule depolymerization during rotavirus infection. *J Virol,* 84**,** 2522-32.

MARTIN, D., OULDALI, M., MÉNÉTREY, J. & PONCET, D. 2011. Structural Organisation of the Rotavirus Nonstructural Protein NSP5. *Journal of Molecular Biology,* 413**,** 209-221.
MARTIN, S. E., GAN, H., TOOMER, G., SRIDHAR, N. & SZTUBA-SOLINSKA, J. 2021. The m6A landscape of polyadenylated nuclear (PAN) RNA and its related methylome in the context of KSHV replication. *bioRxiv*.
MARTÍNEZ, EICHWALD, C., SCHRANER, E. M., LÓPEZ, S. & ARIAS, C. F. 2022. Lipid metabolism is involved in the association of rotavirus viroplasms with endoplasmic reticulum membranes. *Virology,* 569**,** 29-36.
MARTÍNEZ, LÓPEZ, S., ARIAS, C. F. & ISA, P. 2013. Gangliosides have a functional role during rotavirus cell entry. *J Virol,* 87**,** 1115-22.
MARTÍNEZ, L. 2015. Automatic identification of mobile and rigid substructures in molecular dynamics simulations and fractional structural fluctuation analysis. *PLoS One,* 10**,** e0119264.
MARTINEZ, V. P., BELLOMO, C., SAN JUAN, J., PINNA, D., FORLENZA, R., ELDER, M. & PADULA, P. J. 2005. Person-to-person transmission of Andes virus. *Emerg Infect Dis,* 11**,** 1848-53.
MARTÍNEZ, V. P., DI PAOLA, N., ALONSO, D. O., PÉREZ-SAUTU, U., BELLOMO, C. M., IGLESIAS, A. A., COELHO, R. M., LÓPEZ, B., PERIOLO, N., LARSON, P. A., NAGLE, E. R., CHITTY, J. A., PRATT, C. B., DÍAZ, J., CISTERNA, D., CAMPOS, J., SHARMA, H., DIGHERO-KEMP, B., BIONDO, E., LEWIS, L., ANSELMO, C., OLIVERA, C. P., PONTORIERO, F., LAVARRA, E., KUHN, J. H., STRELLA, T., EDELSTEIN, A., BURGOS, M. I., KALER, M., RUBINSTEIN, A., KUGELMAN, J. R., SANCHEZ-LOCKHART, M., PERANDONES, C. & PALACIOS, G. 2020. "Super-Spreaders" and Person-to-Person Transmission of Andes Virus in Argentina. *N Engl J Med,* 383**,** 2230-2241.
MASTRONARDE, D. N. & HELD, S. R. 2017. Automated tilt series alignment and tomographic reconstruction in IMOD. *Journal of structural biology,* 197**,** 102-113.
MATEUS, D., MARINI, E. S., PROGIDA, C. & BAKKE, O. 2018. Rab7a modulates ER stress and ER morphology. *Biochimica et Biophysica Acta (BBA) - Molecular Cell Research,* 1865**,** 781-793.
MATHEUS, S., MEYNARD, J. B., ROLLIN, P., MAUBERT, B. & MORVAN, J. 2006. New World hantavirus in humans, French Guiana. *Emerging infectious diseases,* 12**,** 1294-1295.
MATTA, H. & CHAUDHARY, P. M. 2004. Activation of alternative NF-kappa B pathway by human herpes virus 8-encoded Fas-associated death domain-like IL-1 beta-converting enzyme inhibitory protein (vFLIP). *Proc Natl Acad Sci U S A,* 101**,** 9399-404.
MATTAR, S., GUZMÁN, C. & FIGUEIREDO, L. T. 2015. Diagnosis of hantavirus infection in humans. *Expert Review of Anti-infective Therapy,* 13**,** 939-946.
MATTHIJNSSENS, J., HEYLEN, E., ZELLER, M., RAHMAN, M., LEMEY, P. & VAN RANST, M. 2010. Phylodynamic Analyses of Rotavirus Genotypes G9 and G12 Underscore Their Potential for Swift Global Spread. *Molecular Biology and Evolution,* 27**,** 2431-2436.
MATTHIJNSSENS, J., OTTO, P. H., CIARLET, M., DESSELBERGER, U., VAN RANST, M. & JOHNE, R. 2012. VP6-sequence-based cutoff values as a criterion for rotavirus species demarcation. *Archives of Virology,* 157**,** 1177-1182.
MATTHYS, V., GORBUNOVA, E. E., GAVRILOVSKAYA, I. N., PEPINI, T. & MACKOW, E. R. 2011. The C-terminal 42 residues of the Tula virus Gn protein regulate interferon induction. *Journal of virology,* 85**,** 4752-4760.
MAYEUF-LOUCHART, A., LANCEL, S., SEBTI, Y., POURCET, B., LOYENS, A., DELHAYE, S., DUHEM, C., BEAUCHAMP, J., FERRI, L., THOREL, Q., BOULINGUIEZ, A., ZECCHIN, M., DUBOIS-CHEVALIER, J., EECKHOUTE, J., VAUGHN, L. T., ROACH, P. J., DANI, C., PEDERSON, B. A., VINCENT, S. D., STAELS, B. & DUEZ, H. 2019. Glycogen Dynamics Drives Lipid Droplet Biogenesis during Brown Adipocyte Differentiation. *Cell Reports,* 29**,** 1410-1418.e6.
MAZROUI, R., SUKARIEH, R., BORDELEAU, M. E., KAUFMAN, R. J., NORTHCOTE, P., TANAKA, J., GALLOUZI, I. & PELLETIER, J. 2006. Inhibition of ribosome recruitment induces stress granule formation independently of eukaryotic initiation factor 2alpha phosphorylation. *Mol Biol Cell,* 17**,** 4212-9.

MBINTA, J. F., NGUYEN, B. P., AWUNI, P. M. A., EME, P. E. & SIMPSON, C. R. 2021. Postlicensure herpes zoster vaccine effectiveness: systematic review protocol. *BMJ Open,* 11**,** e040964.
MCBRIDE, R., VAN ZYL, M. & FIELDING, B. C. 2014. The coronavirus nucleocapsid is a multifunctional protein. *Viruses,* 6**,** 2991-3018.
MCDONALD, S. M., NELSON, M. I., TURNER, P. E. & PATTON, J. T. 2016. Reassortment in segmented RNA viruses: mechanisms and outcomes. *Nat Rev Microbiol,* 14**,** 448-60.
MCGEOCH, D. J. & GATHERER, D. 2005. Integrating reptilian herpesviruses into the family Herpesviridae. *Journal of Virology,* 79**,** 725-731.
MCINTOSH, R., NICASTRO, D. & MASTRONARDE, D. 2005. New views of cells in 3D: an introduction to electron tomography. *Trends Cell Biol,* 15**,** 43-51.
MCMAHON, D. E., MAURER, T. & FREEMAN, E. E. 2020. 25 Years of Kaposi Sarcoma Herpesvirus: Discoveries, Disparities, and Diagnostics. *JCO Global Oncology***,** 505-507.
MCNAB, A. R., DESAI, P., PERSON, S., ROOF, L. L., THOMSEN, D. R., NEWCOMB, W. W., BROWN, J. C. & HOMA, F. L. 1998. The product of the herpes simplex virus type 1 UL25 gene is required for encapsidation but not for cleavage of replicated viral DNA. *J Virol,* 72**,** 1060-70.
MECKES, D. G., JR., MENAKER, N. F. & RAAB-TRAUB, N. 2013. Epstein-Barr virus LMP1 modulates lipid raft microdomains and the vimentin cytoskeleton for signal transduction and transformation. *J Virol,* 87**,** 1301-11.
MEDICI, M. C., ABELLI, L. A., GUERRA, P., DODI, I., DETTORI, G. & CHEZZI, C. 2011. Case report: detection of rotavirus RNA in the cerebrospinal fluid of a child with rotavirus gastroenteritis and meningism. *J Med Virol,* 83**,** 1637-40.
MEHTA, S. & ZHANG, J. 2022. Liquid–liquid phase separation drives cellular function and dysfunction in cancer. *Nature Reviews Cancer,* 22**,** 239-252.
MEIER, K., THORKELSSON, S. R., QUEMIN, E. R. J. & ROSENTHAL, M. 2021. Hantavirus Replication Cycle-An Updated Structural Virology Perspective. *Viruses,* 13**,** 1561.
MELBYE, M., COOK, P. M., HJALGRIM, H., BEGTRUP, K., SIMPSON, G. R., BIGGAR, R. J., EBBESEN, P. & SCHULZ, T. F. 1998. Risk factors for Kaposi's-sarcoma-associated herpesvirus (KSHV/HHV-8) seropositivity in a cohort of homosexual men, 1981-1996. *Int J Cancer,* 77**,** 543-8.
MERTENS, M., HOFMANN, J., PETRAITYTE-BURNEIKIENE, R., ZILLER, M., SASNAUSKAS, K., FRIEDRICH, R., NIEDERSTRASSER, O., KRÜGER, D. H., GROSCHUP, M. H., PETRI, E., WERDERMANN, S. & ULRICH, R. G. 2011. Seroprevalence study in forestry workers of a non-endemic region in eastern Germany reveals infections by Tula and Dobrava-Belgrade hantaviruses. *Med Microbiol Immunol,* 200**,** 263-8.
MÉSZÁROS, B., ERDŐS, G., SZABÓ, B., SCHÁD, É., TANTOS, Á., ABUKHAIRAN, R., HORVÁTH, T., MURVAI, N., KOVÁCS, O. P., KOVÁCS, M., TOSATTO, S. C. E., TOMPA, P., DOSZTÁNYI, Z. & PANCSA, R. 2020. PhaSePro: the database of proteins driving liquid-liquid phase separation. *Nucleic Acids Res,* 48**,** D360-d367.
METTENLEITER, T. C. 2004. Budding events in herpesvirus morphogenesis. *Virus Research,* 106**,** 167-180.
MEYER, B. J. & SCHMALJOHN, C. S. 2000. Persistent hantavirus infections: characteristics and mechanisms. *Trends Microbiol,* 8**,** 61-7.
MICHAELSON, ABIDI, W., GUARDAVACCARO, D., ZHOU, M., AHEARN, I., PAGANO, M. & PHILIPS, M. R. 2008. Rac1 accumulates in the nucleus during the G2 phase of the cell cycle and promotes cell division. *The Journal of cell biology,* 181**,** 485-496.
MICHAELSON, SILLETTI, J., MURPHY, G., D'EUSTACHIO, P., RUSH, M. & PHILIPS, M. R. 2001. Differential localization of Rho GTPases in live cells: regulation by hypervariable regions and RhoGDI binding. *The Journal of cell biology,* 152**,** 111-126.
MIDGLEY, S. E., HJULSAGER, C. K., LARSEN, L. E., FALKENHORST, G. & BÖTTIGER, B. 2012. Suspected zoonotic transmission of rotavirus group A in Danish adults. *Epidemiology and Infection,* 140**,** 1013-1017.

MINHAS, V. & WOOD, C. 2014. Epidemiology and transmission of Kaposi's sarcoma-associated herpesvirus. *Viruses,* 6**,** 4178-94.
MIR, M. A., DURAN, W. A., HJELLE, B. L., YE, C. & PANGANIBAN, A. T. 2008. Storage of cellular 5' mRNA caps in P bodies for viral cap-snatching. *Proc Natl Acad Sci U S A,* 105**,** 19294-9.
MIR, M. A. & PANGANIBAN, A. T. 2004. Trimeric hantavirus nucleocapsid protein binds specifically to the viral RNA panhandle. *J Virol,* 78**,** 8281-8.
MIR, M. A. & PANGANIBAN, A. T. 2008. A protein that replaces the entire cellular eIF4F complex. *Embo j,* 27**,** 3129-39.
MIRANDA-SAKSENA, BOADLE, R., ARMATI, P. & CUNNINGHAM, A. 2002. In Rat Dorsal Root Ganglion Neurons, Herpes Simplex Virus Type 1 Tegument Forms in the Cytoplasm of the Cell Body. *Journal of virology,* 76**,** 9934-51.
MIRANDA-SAKSENA, BOADLE, R. A., AGGARWAL, A., TIJONO, B., RIXON, F. J., DIEFENBACH, R. J. & CUNNINGHAM, A. L. 2009. Herpes simplex virus utilizes the large secretory vesicle pathway for anterograde transport of tegument and envelope proteins and for viral exocytosis from growth cones of human fetal axons. *J Virol,* 83**,** 3187-99.
MIRANDA-SAKSENA, DENES, C. E., DIEFENBACH, R. J. & CUNNINGHAM, A. L. 2018. Infection and Transport of Herpes Simplex Virus Type 1 in Neurons: Role of the Cytoskeleton. *Viruses,* 10**,** 92.
MISHRA, KUMAR, A., INGLE, H. & KUMAR, H. 2020. The Interplay Between Viral-Derived miRNAs and Host Immunity During Infection. *Frontiers in Immunology,* 10.
MISHRA., TIWARI, S. & GOMES, A. V. 2017. Protein purification and analysis: next generation Western blotting techniques. *Expert review of proteomics,* 14**,** 1037-1053.
MITTLER, E., DIETERLE, M. E., KLEINFELTER, L. M., SLOUGH, M. M., CHANDRAN, K. & JANGRA, R. K. 2019. Hantavirus entry: Perspectives and recent advances. *Advances in virus research,* 104**,** 185-224.
MOCHIDA, K. & GOMYODA, M. 1987. Toxicity of ethylene glycol, diethylene glycol, and propylene glycol to human cells in culture. *Bull Environ Contam Toxicol,* 38**,** 151-3.
MOHAN, K. V., MULLER, J., SOM, I. & ATREYA, C. D. 2003. The N- and C-terminal regions of rotavirus NSP5 are the critical determinants for the formation of viroplasm-like structures independent of NSP2. *J Virol,* 77**,** 12184-92.
MOHD, M. I., KHAZALI, A. S., NOR RASHID, N. & YUSOF, R. 2020. Endoplasmic reticulum: a focal point of Zika virus infection. *Journal of Biomedical Science,* 27**,** 27.
MOHD ROPIDI, M. I., KHAZALI, A. S., NOR RASHID, N. & YUSOF, R. 2020. Endoplasmic reticulum: a focal point of Zika virus infection. *Journal of Biomedical Science,* 27**,** 27.
MONKS, J., ROSNER, D., JON GESKE, F., LEHMAN, L., HANSON, L., NEVILLE, M. C. & FADOK, V. A. 2005. Epithelial cells as phagocytes: apoptotic epithelial cells are engulfed by mammary alveolar epithelial cells and repress inflammatory mediator release. *Cell Death & Differentiation,* 12**,** 107-114.
MOORE, P. S., GAO, S. J., DOMINGUEZ, G., CESARMAN, E., LUNGU, O., KNOWLES, D. M., GARBER, R., PELLETT, P. E., MCGEOCH, D. J. & CHANG, Y. 1996. Primary characterization of a herpesvirus agent associated with Kaposi's sarcomae. *J Virol,* 70**,** 549-58.
MORELI, M. L., MARQUES-SILVA, A. C., PIMENTEL, V. A. & DA COSTA, V. G. 2014. Effectiveness of the ribavirin in treatment of hantavirus infections in the Americas and Eurasia: a meta-analysis. *Virusdisease,* 25**,** 385-389.
MORELI, M. L., SOUSA, R. L. & FIGUEIREDO, L. T. 2004. Detection of Brazilian hantavirus by reverse transcription polymerase chain reaction amplification of N gene in patients with hantavirus cardiopulmonary syndrome. *Mem Inst Oswaldo Cruz,* 99**,** 633-8.
MOU, D. L., WANG, Y. P., HUANG, C. X., LI, G. Y., PAN, L., YANG, W. S. & BAI, X. F. 2006. Cellular entry of Hantaan virus A9 strain: specific interactions with beta3 integrins and a novel 70kDa protein. *Biochem Biophys Res Commun,* 339**,** 611-7.

MOU, F., FOREST, T. & BAINES, J. D. 2007. US3 of herpes simplex virus type 1 encodes a promiscuous protein kinase that phosphorylates and alters localization of lamin A/C in infected cells. *J Virol,* 81**,** 6459-70.

MOUGARI, S., SAHMI-BOUNSIAR, D., LEVASSEUR, A., COLSON, P. & LA SCOLA, B. 2019. Virophages of Giant Viruses: An Update at Eleven. *Viruses,* 11**,** 733.

MULL, N., JACKSON, R., SIRONEN, T. & FORBES, K. M. 2020. Ecology of Neglected Rodent-Borne American Orthohantaviruses. *Pathogens (Basel, Switzerland),* 9**,** 325.

MULVEY, M., ARIAS, C. & MOHR, I. 2007. Maintenance of endoplasmic reticulum (ER) homeostasis in herpes simplex virus type 1-infected cells through the association of a viral glycoprotein with PERK, a cellular ER stress sensor. *J Virol,* 81**,** 3377-90.

MUNIR, N., JAHANGEER, M., HUSSAIN, S., MAHMOOD, Z., ASHIQ, M., EHSAN, F., AKRAM, M., ALI SHAH, S. M., RIAZ, M. & SANA, A. 2021. Hantavirus diseases pathophysiology, their diagnostic strategies and therapeutic approaches: A review. *Clinical and Experimental Pharmacology and Physiology,* 48**,** 20-34.

MUSALEM, C. & ESPEJO, R. T. 1985. Release of progeny virus from cells infected with simian rotavirus SA11. *J Gen Virol,* 66 (Pt 12)**,** 2715-24.

MUSTONEN, J., MÄKELÄ, S., OUTINEN, T., LAINE, O., JYLHÄVÄ, J., ARSTILA, P. T., HURME, M. & VAHERI, A. 2013. The pathogenesis of nephropathia epidemica: New knowledge and unanswered questions. *Antiviral Research,* 100**,** 589-604.

MUYANGWA, M., MARTYNOVA, E. V., KHAIBOULLINA, S. F., MORZUNOV, S. P. & RIZVANOV, A. A. 2015. Hantaviral Proteins: Structure, Functions, and Role in Hantavirus Infection. *Frontiers in Microbiology,* 6.

MYOUNG, J. & GANEM, D. 2011. Generation of a doxycycline-inducible KSHV producer cell line of endothelial origin: maintenance of tight latency with efficient reactivation upon induction. *Journal of virological methods,* 174**,** 12-21.

NAGHAVI, M. H., GUNDERSEN, G. G. & WALSH, D. 2013. Plus-end tracking proteins, CLASPs, and a viral Akt mimic regulate herpesvirus-induced stable microtubule formation and virus spread. *Proc Natl Acad Sci U S A,* 110**,** 18268-73.

NAKAMURA, H., LU, M., GWACK, Y., SOUVLIS, J., ZEICHNER, S. L. & JUNG, J. U. 2003. Global changes in Kaposi's sarcoma-associated virus gene expression patterns following expression of a tetracycline-inducible Rta transactivator. *Journal of Virology,* 77**,** 4205-4220.

NANBO, A., FURUYAMA, W. & LIN, Z. 2021. RNA Virus-Encoded miRNAs: Current Insights and Future Challenges. *Frontiers in Microbiology,* 12.

NANIIMA, P., NAIMO, E., KOCH, S., CURTH, U., ALKHARSAH, K. R., STRÖH, L. J., BINZ, A., BENEKE, J.-M., VOLLMER, B., BÖNING, H., BORST, E. M., DESAI, P., BOHNE, J., MESSERLE, M., BAUERFEIND, R., LEGRAND, P., SODEIK, B., SCHULZ, T. F. & KREY, T. 2021. Assembly of infectious Kaposi's sarcoma-associated herpesvirus progeny requires formation of a pORF19 pentamer. *PLOS Biology,* 19**,** e3001423.

NAQVI, A. R., SHANGO, J., SEAL, A., SHUKLA, D. & NARES, S. 2018. Herpesviruses and MicroRNAs: New Pathogenesis Factors in Oral Infection and Disease? *Front Immunol,* 9**,** 2099.

NARANATT, P. P., AKULA, S. M., ZIEN, C. A., KRISHNAN, H. H. & CHANDRAN, B. 2003. Kaposi's sarcoma-associated herpesvirus induces the phosphatidylinositol 3-kinase-PKC-zeta-MEK-ERK signaling pathway in target cells early during infection: implications for infectivity. *Journal of virology,* 77**,** 1524-1539.

NARANATT, P. P., KRISHNAN, H. H., SMITH, M. S. & CHANDRAN, B. 2005. Kaposi's sarcoma-associated herpesvirus modulates microtubule dynamics via RhoA-GTP-diaphanous 2 signaling and utilizes the dynein motors to deliver its DNA to the nucleus. *J Virol,* 79**,** 1191-206.

NAVARRO-LÉRIDA, I., PELLINEN, T., SANCHEZ, S. A., GUADAMILLAS, M. C., WANG, Y., MIRTTI, T., CALVO, E. & DEL POZO, M. A. 2015. Rac1 nucleocytoplasmic shuttling drives nuclear shape changes and tumor invasion. *Dev Cell,* 32**,** 318-34.

NEIPEL, F. & FLECKENSTEIN, B. 1999. The role of HHV-8 in Kaposi's sarcoma. *Semin Cancer Biol,* 9**,** 151-64.

NEWTON, R., LABO, N., WAKEHAM, K., MARSHALL, V., ROSHAN, R., NALWOGA, A., SEBINA, I., MUHANGI, L., WEBB, E. L., MILEY, W., ROCHFORD, R., ELLIOTT, A. M. & WHITBY, D. 2018. Determinants of Gammaherpesvirus Shedding in Saliva Among Ugandan Children and Their Mothers. *J Infect Dis,* 218**,** 892-900.

NGUYEN, C. C., DOMMA, A. J., ZHANG, H., KAMIL, J. P. & LONGNECKER, R. M. 2020. Endoplasmic Reticulum (ER) Reorganization and Intracellular Retention of CD58 Are Functionally Independent Properties of the Human Cytomegalovirus ER-Resident Glycoprotein UL148. *Journal of Virology,* 94**,** e01435-19.

NICHOLS, L. A., ADANG, L. A. & KEDES, D. H. 2011. Rapamycin Blocks Production of KSHV/HHV8: Insights into the Anti-Tumor Activity of an Immunosuppressant Drug. *PLOS ONE,* 6**,** e14535.

NICOLA, A. V., HOU, J., MAJOR, E. O. & STRAUS, S. E. 2005. Herpes simplex virus type 1 enters human epidermal keratinocytes, but not neurons, via a pH-dependent endocytic pathway. *J Virol,* 79**,** 7609-16.

NICOLL, M. P., HANN, W., SHIVKUMAR, M., HARMAN, L. E., CONNOR, V., COLEMAN, H. M., PROENÇA, J. T. & EFSTATHIOU, S. 2016. The HSV-1 Latency-Associated Transcript Functions to Repress Latent Phase Lytic Gene Expression and Suppress Virus Reactivation from Latently Infected Neurons. *PLoS Pathog,* 12**,** e1005539.

NICOLL, M. P., PROENÇA, J. T. & EFSTATHIOU, S. 2012. The molecular basis of herpes simplex virus latency. *FEMS Microbiol Rev,* 36**,** 684-705.

NIELSON, A. J. & GRIFFITH, W. P. 1979. Tissue fixation by osmium tetroxide. A possible role for proteins. *J Histochem Cytochem,* 27**,** 997-9.

NIXON-ABELL, J., OBARA, C. J., WEIGEL, A. V., LI, D., LEGANT, W. R., XU, C. S., PASOLLI, H. A., HARVEY, K., HESS, H. F., BETZIG, E., BLACKSTONE, C. & LIPPINCOTT-SCHWARTZ, J. 2016. Increased spatiotemporal resolution reveals highly dynamic dense tubular matrices in the peripheral ER. *Science,* 354**,** aaf3928.

NOTTINGHAM, R. M., PUSAPATI, G. V., GANLEY, I. G., BARR, F. A., LAMBRIGHT, D. G. & PFEFFER, S. R. 2012. RUTBC2 protein, a Rab9A effector and GTPase-activating protein for Rab36. *The Journal of biological chemistry,* 287**,** 22740-22748.

O'BRIEN, J., HAYDER, H., ZAYED, Y. & PENG, C. 2018. Overview of MicroRNA Biogenesis, Mechanisms of Actions, and Circulation. *Frontiers in Endocrinology,* 9.

OGAWA, K., TANAKA, Y., URUNO, T., DUAN, X. F., HARADA, Y., SANEMATSU, F., YAMAMURA, K., TERASAWA, M., NISHIKIMI, A., COTE, J. F. & FUKUI, Y. 2014. DOCK5 functions as a key signaling adaptor that links Fc epsilon RI signals to microtubule dynamics during mast cell degranulation. *Journal of Experimental Medicine,* 211**,** 1401-1413.

OLAL, D. & DAUMKE, O. 2016. Structure of the Hantavirus Nucleoprotein Provides Insights into the Mechanism of RNA Encapsidation. *Cell Rep,* 14**,** 2092-2099.

OLDS, W. & LI, J. 2016. siRNA knockdown validation 101: Incorporating negative controls in antibody research. *F1000Research,* 5**,** 308-308.

OLP, L. N., JEANNIARD, A., MARIMO, C., WEST, J. T. & WOOD, C. 2015. Whole-Genome Sequencing of Kaposi's Sarcoma-Associated Herpesvirus from Zambian Kaposi's Sarcoma Biopsy Specimens Reveals Unique Viral Diversity. *Journal of Virology,* 89**,** 12299-12308.

OLSCHEWSKI, S., CUSACK, S. & ROSENTHAL, M. 2020. The Cap-Snatching Mechanism of Bunyaviruses. *Trends Microbiol,* 28**,** 293-303.

OLZMANN, J. A. & CARVALHO, P. 2019. Dynamics and functions of lipid droplets. *Nature Reviews Molecular Cell Biology,* 20**,** 137-155.

OMATOLA, C. A. & OLANIRAN, A. O. 2022. Rotaviruses: From Pathogenesis to Disease Control-A Critical Review. *Viruses,* 14**,** 875.

OORSCHOT, V., LINDSEY, B. W., KASLIN, J. & RAMM, G. 2021. TEM, SEM, and STEM-based immuno-CLEM workflows offer complementary advantages. *Scientific Reports,* 11**,** 899.

OWEN. 2015. *Utilising Omics Approaches to Understand Kaposi's Sarcoma-associated Herpesvirus.* PhD PhD, University of Leeds
OWEN, CRUMP, C. M. & GRAHAM, S. C. 2015. Tegument Assembly and Secondary Envelopment of Alphaherpesviruses. *Viruses,* 7**,** 5084-114.
PACKARD, J. E. & DEMBOWSKI, J. A. 2021. HSV-1 DNA Replication-Coordinated Regulation by Viral and Cellular Factors. *Viruses,* 13.
PAGE, H. G. & READ, G. S. 2010. The virion host shutoff endonuclease (UL41) of herpes simplex virus interacts with the cellular cap-binding complex eIF4F. *J Virol,* 84**,** 6886-90.
PAN, D., LI, G., MORRIS-LOVE, J., QI, S., FENG, L., MERTENS, M. E., JURAK, I., KNIPE, D. M., COEN, D. M., MENG, X.-J., SANDRI-GOLDIN, R. & RAAB-TRAUB, N. 2019. Herpes Simplex Virus 1 Lytic Infection Blocks MicroRNA (miRNA) Biogenesis at the Stage of Nuclear Export of Pre-miRNAs. *mBio,* 10**,** e02856-18.
PAPA, G., BORODAVKA, A. & DESSELBERGER, U. 2021. Viroplasms: Assembly and Functions of Rotavirus Replication Factories. *Viruses,* 13**,** 1349.
PAPA, G., VENDITTI, L., ARNOLDI, F., SCHRANER, E. M., POTGIETER, C., BORODAVKA, A., EICHWALD, C. & BURRONE, O. R. 2019a. Recombinant Rotaviruses Rescued by Reverse Genetics Reveal the Role of NSP5 Hyperphosphorylation in the Assembly of Viral Factories. *Journal of virology,* 94**,** e01110-19.
PAPA, G., VENDITTI, L., ARNOLDI, F., SCHRANER, E. M., POTGIETER, C., BORODAVKA, A., EICHWALD, C. & BURRONE, O. R. 2019b. Recombinant Rotaviruses Rescued by Reverse Genetics Reveal the Role of NSP5 Hyperphosphorylation in the Assembly of Viral Factories. *J Virol,* 94.
PARASHAR, U. D., NELSON, E. A. S. & KANG, G. 2013. Diagnosis, management, and prevention of rotavirus gastroenteritis in children. *BMJ : British Medical Journal,* 347**,** f7204.
PARDAMEAN, C. I. & WU, T.-T. 2021. Inhibition of Host Gene Expression by KSHV: Sabotaging mRNA Stability and Nuclear Export. *Frontiers in Cellular and Infection Microbiology,* 11.
PARK, R. & BAINES, J. D. 2006. Herpes simplex virus type 1 infection induces activation and recruitment of protein kinase C to the nuclear membrane and increased phosphorylation of lamin B. *J Virol,* 80**,** 494-504.
PARVATE, A., SENGUPTA, R., WILLIAMS, E. P., XUE, Y., CHU, Y.-K., STAHELIN, R. V. & JONSSON, C. B. 2020. Cryofixation of Inactivated Hantavirus-Infected Cells as a Method for Obtaining High-Quality Ultrastructural Preservation for Electron Microscopic Studies. *Frontiers in cellular and infection microbiology,* 10**,** 580339-580339.
PARVATE, A., WILLIAMS, E. P., TAYLOR, M. K., CHU, Y. K., LANMAN, J., SAPHIRE, E. O. & JONSSON, C. B. 2019. Diverse Morphology and Structural Features of Old and New World Hantaviruses. *Viruses,* 11.
PASDELOUP, BEILSTEIN, F., ROBERTS, A. P., MCELWEE, M., MCNAB, D. & RIXON, F. J. 2010. Inner tegument protein pUL37 of herpes simplex virus type 1 is involved in directing capsids to the trans-Golgi network for envelopment. *J Gen Virol,* 91**,** 2145-51.
PASDELOUP, BLONDEL, D., ISIDRO, A. L. & RIXON, F. J. 2009. Herpesvirus Capsid Association with the Nuclear Pore Complex and Viral DNA Release Involve the Nucleoporin CAN/Nup214 and the Capsid Protein pUL25. *Journal of Virology,* 83**,** 6610-6623.
PATRA, U., MUKHOPADHYAY, U., MUKHERJEE, A., DUTTA, S. & CHAWLA-SARKAR, M. 2021. Treading a HOSTile path: Mapping the dynamic landscape of host cell-rotavirus interactions to explore novel host-directed curative dimensions. *Virulence,* 12**,** 1022-1062.
PATTABIRAMAN, S., AZAD, G. K., AMEN, T., BRIELLE, S., PARK, J. E., SZE, S. K., MESHORER, E. & KAGANOVICH, D. 2020. Vimentin protects differentiating stem cells from stress. *Scientific Reports,* 10**,** 19525.
PAUK, J., HUANG, M. L., BRODIE, S. J., WALD, A., KOELLE, D. M., SCHACKER, T., CELUM, C., SELKE, S. & COREY, L. 2000. Mucosal shedding of human herpesvirus 8 in men. *N Engl J Med,* 343**,** 1369-77.

PEARCE, M., MATSUMURA, S. & WILSON, A. C. 2005. Transcripts encoding K12, v-FLIP, v-Cyclin, and the MicroRNA cluster of Kaposi's sarcoma-associated herpesvirus originate from a common promoter. *Journal of Virology,* 79**,** 14457-14464.

PERDIKARI, T. M., MURTHY, A. C., RYAN, V. H., WATTERS, S., NAIK, M. T. & FAWZI, N. L. 2020. SARS-CoV-2 nucleocapsid protein phase-separates with RNA and with human hnRNPs. *Embo j,* 39**,** e106478.

PERKINS, E. M., ANACKER, D., DAVIS, A., SANKAR, V., AMBINDER, R. F. & DESAI, P. 2008. Small capsid protein pORF65 is essential for assembly of Kaposi's sarcoma-associated herpesvirus capsids. *J Virol,* 82**,** 7201-11.

PETERMANN, P., RAHN, E., THIER, K., HSU, M. J., RIXON, F. J., KOPP, S. J. & KNEBEL-MÖRSDORF, D. 2015. Role of Nectin-1 and Herpesvirus Entry Mediator as Cellular Receptors for Herpes Simplex Virus 1 on Primary Murine Dermal Fibroblasts. *J Virol,* 89**,** 9407-16.

PHAN, T. G., VO, N. P., BOROS, Á., PANKOVICS, P., REUTER, G., LI, O. T., WANG, C., DENG, X., POON, L. L. & DELWART, E. 2013. The viruses of wild pigeon droppings. *PLoS One,* 8**,** e72787.

PHUYAL, S. & FARHAN, H. 2019. Multifaceted Rho GTPase Signaling at the Endomembranes. *Frontiers in Cell and Developmental Biology,* 7.

PILKINGTON, G. R., MAJERCIAK, V., BEAR, J., URANISHI, H., ZHENG, Z.-M. & FELBER, B. K. 2012. Kaposi's sarcoma-associated herpesvirus ORF57 is not a bona fide export factor. *Journal of virology,* 86**,** 13089-13094.

PIZARRO, E., NAVARRETE, M., MENDEZ, C., ZAROR, L., MANSILLA, C., TAPIA, M., CARRASCO, C., SALAZAR, P., MURUA, R., PADULA, P., OTTH, C. & RODRÍGUEZ, E. M. 2019. Immunocytochemical and Ultrastructural Evidence Supporting That Andes Hantavirus (ANDV) Is Transmitted Person-to-Person Through the Respiratory and/or Salivary Pathways. *Front Microbiol,* 10**,** 2992.

PLUMMER, E. M., THOMAS, D., DESTITO, G., SHRIVER, L. P. & MANCHESTER, M. 2012. Interaction of cowpea mosaic virus nanoparticles with surface vimentin and inflammatory cells in atherosclerotic lesions. *Nanomedicine (Lond),* 7**,** 877-88.

POLIZZOTTO, M. N., ULDRICK, T. S., HU, D. & YARCHOAN, R. 2012. Clinical Manifestations of Kaposi Sarcoma Herpesvirus Lytic Activation: Multicentric Castleman Disease (KSHV-MCD) and the KSHV Inflammatory Cytokine Syndrome. *Front Microbiol,* 3**,** 73.

PONCET, D., LAURENT, S. & COHEN, J. 1994. Four nucleotides are the minimal requirement for RNA recognition by rotavirus non-structural protein NSP3. *Embo j,* 13**,** 4165-73.

PONCET, D., LINDENBAUM, P., L'HARIDON, R. & COHEN, J. 1997. In vivo and in vitro phosphorylation of rotavirus NSP5 correlates with its localization in viroplasms. *J Virol,* 71**,** 34-41.

PRASAD, B. V., ROTHNAGEL, R., ZENG, C. Q., JAKANA, J., LAWTON, J. A., CHIU, W. & ESTES, M. K. 1996. Visualization of ordered genomic RNA and localization of transcriptional complexes in rotavirus. *Nature,* 382**,** 471-3.

PRASAD, B. V. & SCHMID, M. 2012. Principles of Virus Structural Organization. *Viral Molecular Machines,* 726**,** 17 - 47.

PRATS, C., GRAHAM, T. E. & SHEARER, J. 2018. The dynamic life of the glycogen granule. *J Biol Chem,* 293**,** 7089-7098.

PREISER, W., SZÉP, N. I., LANG, D., DOERR, H. W. & RABENAU, H. F. 2001. Kaposi's sarcoma-associated herpesvirus seroprevalence in selected german patients: evaluation by different test systems. *Med Microbiol Immunol,* 190**,** 121-7.

PROTTER, D. S. W. & PARKER, R. 2016. Principles and Properties of Stress Granules. *Trends Cell Biol,* 26**,** 668-679.

PUNCH, E. K., HOVER, S., BLEST, H. T. W., FULLER, J., HEWSON, R., FONTANA, J., MANKOURI, J. & BARR, J. N. 2018. Potassium is a trigger for conformational change in the fusion spike of an enveloped RNA virus. *J Biol Chem,* 293**,** 9937-9944.

PURUSHOTHAMAN, P., DABRAL, P., GUPTA, N., SARKAR, R. & VERMA, S. C. 2016. KSHV Genome Replication and Maintenance. *Frontiers in Microbiology,* 7**,** 14.

PURUSHOTHAMAN, P., UPPAL, T. & VERMA, S. C. 2015. Molecular biology of KSHV lytic reactivation. *Viruses,* 7**,** 116-53.

QAMAR, S., WANG, G., RANDLE, S. J., RUGGERI, F. S., VARELA, J. A., LIN, J. Q., PHILLIPS, E. C., MIYASHITA, A., WILLIAMS, D., STRÖHL, F., MEADOWS, W., FERRY, R., DARDOV, V. J., TARTAGLIA, G. G., FARRER, L. A., KAMINSKI SCHIERLE, G. S., KAMINSKI, C. F., HOLT, C. E., FRASER, P. E., SCHMITT-ULMS, G., KLENERMAN, D., KNOWLES, T., VENDRUSCOLO, M. & ST GEORGE-HYSLOP, P. 2018. FUS Phase Separation Is Modulated by a Molecular Chaperone and Methylation of Arginine Cation-π Interactions. *Cell,* 173**,** 720-734.e15.

QIN, Z., PERUZZI, F., REISS, K. & DAI, L. 2014. Role of host microRNAs in Kaposi's sarcoma-associated herpesvirus pathogenesis. *Viruses,* 6**,** 4571-80.

RADTKE, K., KIENEKE, D., WOLFSTEIN, A., MICHAEL, K., STEFFEN, W., SCHOLZ, T., KARGER, A. & SODEIK, B. 2010. Plus- and minus-end directed microtubule motors bind simultaneously to herpes simplex virus capsids using different inner tegument structures. *PLoS Pathog,* 6**,** e1000991.

RAGHU, H., SHARMA-WALIA, N., VEETTIL, M. V., SADAGOPAN, S. & CHANDRAN, B. 2009. Kaposi's Sarcoma-Associated Herpesvirus Utilizes an Actin Polymerization-Dependent Macropinocytic Pathway To Enter Human Dermal Microvascular Endothelial and Human Umbilical Vein Endothelial Cells. *Journal of Virology,* 83**,** 4895-4911.

RAMANATHAN, CHUNG, PLANE, SZTUL, CHU, GUTTIERI, MCDOWELL, ALI & JONSSON 2007. Dynein-dependent transport of the hantaan virus nucleocapsid protein to the endoplasmic reticulum-Golgi intermediate compartment. *J Virol,* 81**,** 8634-47.

RAMANATHAN, HARISH, JONSSON & COLLEEN. 2008. New and Old World hantaviruses differentially utilize host cytoskeletal components during their life cycles. *Virology,* 374**,** 138-150.

RAMASWAMI, R., LURAIN, K., POLIZZOTTO, M. N., EKWEDE, I., WALDON, K., STEINBERG, S. M., MANGUSAN, R., WIDELL, A., RUPERT, A., GEORGE, J., GONÇALVES, P. H., MARSHALL, V. A., WHITBY, D., WANG, H. W., PITTALUGA, S., JAFFE, E. S., LITTLE, R. F., ULDRICK, T. S. & YARCHOAN, R. 2021. Characteristics and outcomes of KSHV-associated multicentric Castleman disease with or without other KSHV diseases. *Blood Adv,* 5**,** 1660-1670.

RAPPOCCIOLO, G., HENSLER, H. R., JAIS, M., REINHART, T. A., PEGU, A., JENKINS, F. J. & RINALDO, C. R. 2008. Human herpesvirus 8 infects and replicates in primary cultures of activated B lymphocytes through DC-SIGN. *J Virol,* 82**,** 4793-806.

RAÚL VELÁZQUEZ, F., CALVA, J. J., LOURDES GUERRERO, M., MASS, D., GLASS, R. I., PICKERING, L. K. & RUIZ-PALACIOS, G. M. 1993. Cohort study of rotavirus serotype patterns in symptomatic and asymptomatic infections in Mexican children. *The Pediatric infectious disease journal,* 12**,** 54-61.

RAVKOV, E. V., NICHOL, S. T. & COMPANS, R. W. 1997. Polarized entry and release in epithelial cells of Black Creek Canal virus, a New World hantavirus. *J Virol,* 71**,** 1147-54.

RAYMOND, T., GORBUNOVA, E., GAVRILOVSKAYA, I. N. & MACKOW, E. R. 2005. Pathogenic hantaviruses bind plexin-semaphorin-integrin domains present at the apex of inactive, bent alphavbeta3 integrin conformers. *Proc Natl Acad Sci U S A,* 102**,** 1163-8.

REGO, N. B., XI, E. & PATEL, A. J. 2021. Identifying hydrophobic protein patches to inform protein interaction interfaces. *Proceedings of the National Academy of Sciences,* 118**,** e2018234118.

RENNE, R., ZHONG, W., HERNDIER, B., MCGRATH, M., ABBEY, N., KEDES, D. & GANEM, D. 1996. Lytic growth of Kaposi's sarcoma-associated herpesvirus (human herpesvirus 8) in culture. *Nat Med,* 2**,** 342-6.

REUSKEN, C. & HEYMAN, P. 2013. Factors driving hantavirus emergence in Europe. *Current Opinion in Virology,* 3**,** 92-99.

REYNES, J. M., CARLI, D., BOUKEZIA, N., DEBRUYNE, M. & HERTI, S. 2015. Tula hantavirus infection in a hospitalised patient, France, June 2015. *Euro Surveill,* 20.

REYNES, J. M., CARLI, D., BOUR, J. B., BOUDJELTIA, S., DEWILDE, A., GERBIER, G., NUSSBAUMER, T., JACOMO, V., RAPT, M. P., ROLLIN, P. E. & SEPTFONS, A. 2017. Seoul Virus Infection in Humans, France, 2014-2016. *Emerg Infect Dis,* 23**,** 973-977.

REYNOLDS, A. E., RYCKMAN, B. J., BAINES, J. D., ZHOU, Y., LIANG, L. & ROLLER, R. J. 2001. U(L)31 and U(L)34 proteins of herpes simplex virus type 1 form a complex that accumulates at the nuclear rim and is required for envelopment of nucleocapsids. *J Virol,* 75**,** 8803-17.

REYNOLDS, E. S. 1963. The use of lead citrate at high pH as an electron-opaque stain in electron microscopy. *J Cell Biol,* 17**,** 208-12.

REYNOLDS, E. S. 1981. CITATION CLASSIC - THE USE OF LEAD CITRATE AT HIGH PH AS AN ELECTRON-OPAQUE STAIN IN ELECTRON-MICROSCOPY. *Current Contents/Life Sciences***,** 16-16.

RIBBECK, K. & GÖRLICH, D. 2002. The permeability barrier of nuclear pore complexes appears to operate via hydrophobic exclusion. *Embo j,* 21**,** 2664-71.

RICE, S. A. 2021. Release of HSV-1 Cell-Free Virions: Mechanisms, Regulation, and Likely Role in Human-Human Transmission. *Viruses,* 13.

RINCHEVAL, V., LELEK, M., GAULT, E., BOUILLIER, C., SITTERLIN, D., BLOUQUIT-LAYE, S., GALLOUX, M., ZIMMER, C., ELEOUET, J. F. & RAMEIX-WELTI, M. A. 2017. Functional organization of cytoplasmic inclusion bodies in cells infected by respiratory syncytial virus. *Nat Commun,* 8**,** 563.

RISCO, C., RODRÍGUEZ, J. R., LÓPEZ-IGLESIAS, C., CARRASCOSA, J. L., ESTEBAN, M. & RODRÍGUEZ, D. 2002. Endoplasmic reticulum-Golgi intermediate compartment membranes and vimentin filaments participate in vaccinia virus assembly. *Journal of virology,* 76**,** 1839-1855.

ROINGEARD, P., HOURIOUX, C., BLANCHARD, E. & PRENSIER, G. 2008. Hepatitis C virus budding at lipid droplet-associated ER membrane visualized by 3D electron microscopy. *Histochem Cell Biol,* 130**,** 561-6.

ROLLER, R. J., ZHOU, Y., SCHNETZER, R., FERGUSON, J. & DESALVO, D. 2000. Herpes simplex virus type 1 U(L)34 gene product is required for viral envelopment. *J Virol,* 74**,** 117-29.

ROMERO-BREY, I. & BARTENSCHLAGER, R. 2015. Viral Infection at High Magnification: 3D Electron Microscopy Methods to Analyze the Architecture of Infected Cells. *Viruses,* 7**,** 6316-45.

ROMERO-BREY, I., MERZ, A., CHIRAMEL, A., LEE, J.-Y., CHLANDA, P., HASELMAN, U., SANTARELLA-MELLWIG, R., HABERMANN, A., HOPPE, S., KALLIS, S., WALTHER, P., ANTONY, C., KRIJNSE-LOCKER, J. & BARTENSCHLAGER, R. 2012a. Three-Dimensional Architecture and Biogenesis of Membrane Structures Associated with Hepatitis C Virus Replication. *PLOS Pathogens,* 8**,** e1003056.

ROMERO-BREY, I., MERZ, A., CHIRAMEL, A., LEE, J.-Y., CHLANDA, P., HASELMAN, U., SANTARELLA-MELLWIG, R., HABERMANN, A., HOPPE, S., KALLIS, S., WALTHER, P., ANTONY, C., LOCKER, J. & BARTENSCHLAGER, R. 2012b. Three-Dimensional Architecture and Biogenesis of Membrane Structures Associated with Hepatitis C Virus Replication. *PLoS pathogens,* 8**,** e1003056.

ROMERO-BREY, I., MERZ, A., CHIRAMEL, A., LEE, J. Y., CHLANDA, P., HASELMAN, U., SANTARELLA-MELLWIG, R., HABERMANN, A., HOPPE, S., KALLIS, S., WALTHER, P., ANTONY, C., KRIJNSE-LOCKER, J. & BARTENSCHLAGER, R. 2012c. Three-dimensional architecture and biogenesis of membrane structures associated with hepatitis C virus replication. *PLoS Pathog,* 8**,** e1003056.

ROSSIGNOL, E. D., PETERS, K. N., CONNOR, J. H. & BULLITT, E. 2017. Zika virus induced cellular remodelling. *Cellular Microbiology,* 19**,** e12740.

ROTHENBERGER, S., TORRIANI, G., JOHANSSON, M. U., KUNZ, S. & ENGLER, O. 2016. Conserved Endonuclease Function of Hantavirus L Polymerase. *Viruses,* 8.

ROZEN, R., SATHISH, N., LI, Y. & YUAN, Y. 2008. Virion-Wide Protein Interactions of Kaposi's Sarcoma-Associated Herpesvirus. *Journal of Virology,* 82**,** 4742-4750.

RU, J., SUN, H., FAN, H., WANG, C., LI, Y., LIU, M. & TANG, H. 2014. MiR-23a facilitates the replication of HSV-1 through the suppression of interferon regulatory factor 1. *PLoS One,* 9**,** e114021.

RUSNAK, J. M., BYRNE, W. R., CHUNG, K. N., GIBBS, P. H., KIM, T. T., BOUDREAU, E. F., COSGRIFF, T., PITTMAN, P., KIM, K. Y., ERLICHMAN, M. S., REZVANI, D. F. & HUGGINS, J. W. 2009. Experience with intravenous ribavirin in the treatment of hemorrhagic fever with renal syndrome in Korea. *Antiviral Res,* 81**,** 68-76.

SACHET, M., LIANG, Y. Y. & OEHLER, R. 2017. The immune response to secondary necrotic cells. *Apoptosis : an international journal on programmed cell death,* 22**,** 1189-1204.

SACHSE, M., FERNÁNDEZ DE CASTRO, I., TENORIO, R. & RISCO, C. 2019. The viral replication organelles within cells studied by electron microscopy. *Advances in virus research,* 105**,** 1-33.

SAKSIDA, A., WRABER, B. & AVŠIČ-ŽUPANC, T. 2011. Serum levels of inflammatory and regulatory cytokines in patients with hemorrhagic fever with renal syndrome. *BMC Infect Dis,* 11**,** 142.

SALGADO, E. N., UPADHYAYULA, S. & HARRISON, S. C. 2017. Single-Particle Detection of Transcription following Rotavirus Entry. *Journal of virology,* 91**,** e00651-17.

SAMUEL, C. E. 1993. The eIF-2 alpha protein kinases, regulators of translation in eukaryotes from yeasts to humans. *J Biol Chem,* 268**,** 7603-6.

SANDBAUMHÜTER, M., DÖHNER, K., SCHIPKE, J., BINZ, A., POHLMANN, A., SODEIK, B. & BAUERFEIND, R. 2013. Cytosolic herpes simplex virus capsids not only require binding inner tegument protein pUL36 but also pUL37 for active transport prior to secondary envelopment. *Cellular Microbiology,* 15**,** 248-269.

SANDERS, M. A., AMPASALA, D. & BASSON, M. D. 2009. DOCK5 and DOCK1 regulate Caco-2 intestinal epithelial cell spreading and migration on collagen IV. *The Journal of biological chemistry,* 284**,** 27-35.

SANDRI-GOLDIN, R. M. 2003. Replication of the herpes simplex virus genome: Does it really go around in circles? *Proceedings of the National Academy of Sciences,* 100**,** 7428-7429.

SANTAOLALLA, R., FUKATA, M. & ABREU, M. T. 2011. Innate immunity in the small intestine. *Current opinion in gastroenterology,* 27**,** 125-131.

SANTARELLA-MELLWIG, R., HASELMANN, U., SCHIEBER, N. L., WALTHER, P., SCHWAB, Y., ANTONY, C., BARTENSCHLAGER, R. & ROMERO-BREY, I. 2018a. Correlative Light Electron Microscopy (CLEM) for Tracking and Imaging Viral Protein Associated Structures in Cryo-immobilized Cells. *Journal of visualized experiments : JoVE***,** 58154.

SANTARELLA-MELLWIG, R., HASELMANN, U., SCHIEBER, N. L., WALTHER, P., SCHWAB, Y., ANTONY, C., BARTENSCHLAGER, R. & ROMERO-BREY, I. 2018b. Correlative Light Electron Microscopy (CLEM) for Tracking and Imaging Viral Protein Associated Structures in Cryo-immobilized Cells. *J Vis Exp*.

SANTARELLI, R., FARINA, A., GRANATO, M., GONNELLA, R., RAFFA, S., LEONE, L., BEI, R., MODESTI, A., FRATI, L., TORRISI, M. R. & FAGGIONI, A. 2008. Identification and characterization of the product encoded by ORF69 of Kaposi's sarcoma-associated herpesvirus. *Journal of Virology,* 82**,** 4562-4572.

SANTIANA, M., GHOSH, S., HO, B. A., RAJASEKARAN, V., DU, W. L., MUTSAFI, Y., DE JÉSUS-DIAZ, D. A., SOSNOVTSEV, S. V., LEVENSON, E. A., PARRA, G. I., TAKVORIAN, P. M., CALI, A., BLECK, C., VLASOVA, A. N., SAIF, L. J., PATTON, J. T., LOPALCO, P., CORCELLI, A., GREEN, K. Y. & ALTAN-BONNET, N. 2018. Vesicle-Cloaked Virus Clusters Are Optimal Units for Inter-organismal Viral Transmission. *Cell Host Microbe,* 24**,** 208-220.e8.

SANZ-SÁNCHEZ, L. & RISCO, C. 2013. Multilamellar Structures and Filament Bundles Are Found on the Cell Surface during Bunyavirus Egress. *PLOS ONE,* 8**,** e65526.

SATHISH, N., WANG, X. & YUAN, Y. 2012. Tegument proteins of Kaposi's sarcoma-associated herpesvirus and related gamma-herpesviruses. *Frontiers in Microbiology,* 3**,** 13.

SATHISH, N. & YUAN, Y. 2010. Functional characterization of Kaposi's sarcoma-associated herpesvirus small capsid protein by bacterial artificial chromosome-based mutagenesis. *Virology,* 407**,** 306-318.

SATHISH, N., ZHU, F. X. & YUAN, Y. 2009. Kaposi's sarcoma-associated herpesvirus ORF45 interacts with kinesin-2 transporting viral capsid-tegument complexes along microtubules. *PLoS Pathog,* 5**,** e1000332.
SCARFF, C. A., FULLER, M. J. G., THOMPSON, R. F. & IADANZA, M. G. 2018. Variations on Negative Stain Electron Microscopy Methods: Tools for Tackling Challenging Systems. *J Vis Exp*.
SCHAUFLINGER, M., VILLINGER, C., MERTENS, T., WALTHER, P. & VON EINEM, J. 2013a. Analysis of human cytomegalovirus secondary envelopment by advanced electron microscopy. *Cellular Microbiology,* 15**,** 305-314.
SCHAUFLINGER, M., VILLINGER, C. & WALTHER, P. 2013b. Three-dimensional visualization of virus-infected cells by serial sectioning: an electron microscopic study using resin embedded cells. *Methods Mol Biol,* 1064**,** 227-37.
SCHELHAAS, M., JANSEN, M., HAASE, I. & KNEBEL-MÖRSDORF, D. 2003. Herpes simplex virus type 1 exhibits a tropism for basal entry in polarized epithelial cells. *J Gen Virol,* 84**,** 2473-2484.
SCHILLING, S., EMMERICH, P., KLEMPA, B., AUSTE, B., SCHNAITH, E., SCHMITZ, H., KRÜGER, D. H., GÜNTHER, S. & MEISEL, H. 2007. Hantavirus disease outbreak in Germany: limitations of routine serological diagnostics and clustering of virus sequences of human and rodent origin. *J Clin Microbiol,* 45**,** 3008-14.
SCHNEIDER, C. A., RASBAND, W. S. & ELICEIRI, K. W. 2012. NIH Image to ImageJ: 25 years of image analysis. *Nature Methods,* 9**,** 671-675.
SCHNEIDER, J. W. & DITTMER, D. P. 2017. Diagnosis and Treatment of Kaposi Sarcoma. *Am J Clin Dermatol,* 18**,** 529-539.
SCHÖNRICH, G. & RAFTERY, M. J. 2019. Dendritic Cells (DCs) as "Fire Accelerants" of Hantaviral Pathogenesis. *Viruses,* 11.
SCHUCK, S., PRINZ, W. A., THORN, K. S., VOSS, C. & WALTER, P. 2009. Membrane expansion alleviates endoplasmic reticulum stress independently of the unfolded protein response. *The Journal of cell biology,* 187**,** 525-536.
SCHWARTZ 2004. Kaposi's sarcoma: an update. *J Surg Oncol,* 87**,** 146-51.
SCHWARTZ, MICALI, G., NASCA, M. R. & SCUDERI, L. 2008. Kaposi sarcoma: A continuing conundrum. *Journal of the American Academy of Dermatology,* 59**,** 179-206.
SCHWARZ, D. S. & BLOWER, M. D. 2016. The endoplasmic reticulum: structure, function and response to cellular signaling. *Cellular and molecular life sciences : CMLS,* 73**,** 79-94.
SCOTT, M. C., CHEN, C. C., MECKLENBURG, M., ZHU, C., XU, R., ERCIUS, P., DAHMEN, U., REGAN, B. C. & MIAO, J. 2012. Electron tomography at 2.4-angstrom resolution. *Nature,* 483**,** 444-7.
SEN, A., SEN, N. & MACKOW ERICH, R. 2007. The Formation of Viroplasm-Like Structures by the Rotavirus NSP5 Protein Is Calcium Regulated and Directed by a C-Terminal Helical Domain. *Journal of Virology,* 81**,** 11758-11767.
SERRIS, STASS, R., BIGNON, E. A., MUENA, N. A., MANUGUERRA, J.-C., JANGRA, R. K., LI, S., CHANDRAN, K., TISCHLER, N. D., HUISKONEN, J. T., REY, F. A. & GUARDADO-CALVO, P. 2020. The Hantavirus Surface Glycoprotein Lattice and Its Fusion Control Mechanism. *Cell,* 183**,** 442-456.e16.
SETTEMBRE, E. C., CHEN, J. Z., DORMITZER, P. R., GRIGORIEFF, N. & HARRISON, S. C. 2011. Atomic model of an infectious rotavirus particle. *The EMBO journal,* 30**,** 408-416.
SEVERSON, W. E., XU, X. & JONSSON, C. B. 2001. cis-Acting signals in encapsidation of Hantaan virus S-segment viral genomic RNA by its N protein. *J Virol,* 75**,** 2646-52.
SEYFFERT, M., GEORGI, F., TOBLER, K., BOURQUI, L., ANFOSSI, M., MICHAELSEN, K., VOGT, B., GREBER, U. F. & FRAEFEL, C. 2021. The HSV-1 Transcription Factor ICP4 Confers Liquid-Like Properties to Viral Replication Compartments. *Int J Mol Sci,* 22.
SHARMA, MAJERCIAK, V., KRUHLAK, M. J., YU, L., KANG, J. G., YANG, A., GU, S., FRITZLER, M. J. & ZHENG, Z. M. 2019. KSHV RNA-binding protein ORF57 inhibits P-body formation to promote viral multiplication by interaction with Ago2 and GW182. *Nucleic Acids Res,* 47**,** 9368-9385.

SHARMA, MAJERCIAK, V., KRUHLAK, M. J. & ZHENG, Z.-M. 2017. KSHV inhibits stress granule formation by viral ORF57 blocking PKR activation. *PLOS Pathogens,* 13**,** e1006677.

SHERMAN, M. B., TRUJILLO, J., LEAHY, I., RAZMUS, D., DEHATE, R., LORCHEIM, P., CZARNESKI, M. A., ZIMMERMAN, D., NEWTON, J. T., HADDOW, A. D. & WEAVER, S. C. 2013. Construction and organization of a BSL-3 cryo-electron microscopy laboratory at UTMB. *J Struct Biol,* 181**,** 223-33.

SHERRY, M. R., HAY, T. J. M., GULAK, M. A., NASSIRI, A., FINNEN, R. L. & BANFIELD, B. W. 2017. The Herpesvirus Nuclear Egress Complex Component, UL31, Can Be Recruited to Sites of DNA Damage Through Poly-ADP Ribose Binding. *Sci Rep,* 7**,** 1882.

SHI, X. & ELLIOTT, R. M. 2004. Analysis of N-linked glycosylation of hantaan virus glycoproteins and the role of oligosaccharide side chains in protein folding and intracellular trafficking. *J Virol,* 78**,** 5414-22.

SHIBA, C., DAIKOKU, T., GOSHIMA, F., TAKAKUWA, H., YAMAUCHI, Y., KOIWAI, O. & NISHIYAMA, Y. 2000. The UL34 gene product of herpes simplex virus type 2 is a tail-anchored type II membrane protein that is significant for virus envelopment. *J Gen Virol,* 81**,** 2397-2405.

SHORT, B. 2009. Sizing up the ER stress response. *The Journal of Cell Biology,* 187**,** 444-444.

SHUKLA, D., LIU, J., BLAIKLOCK, P., SHWORAK, N. W., BAI, X., ESKO, J. D., COHEN, G. H., EISENBERG, R. J., ROSENBERG, R. D. & SPEAR, P. G. 1999. A novel role for 3-O-sulfated heparan sulfate in herpes simplex virus 1 entry. *Cell,* 99**,** 13-22.

SILVA-AYALA, D., LÓPEZ, T., GUTIÉRREZ, M., PERRIMON, N., LÓPEZ, S. & ARIAS, C. F. 2013. Genome-wide RNAi screen reveals a role for the ESCRT complex in rotavirus cell entry. *Proc Natl Acad Sci U S A,* 110**,** 10270-5.

SILVA, M. T. 2010. Secondary necrosis: The natural outcome of the complete apoptotic program. *FEBS Letters,* 584**,** 4491-4499.

SIMPSON, S., FICHES, G., JEAN, M. J., DIERINGER, M., MCGUINNESS, J., JOHN, S. P., SHAMAY, M., DESAI, P., ZHU, J. & SANTOSO, N. G. 2018. Inhibition of Tip60 Reduces Lytic and Latent Gene Expression of Kaposi's Sarcoma-Associated Herpes Virus (KSHV) and Proliferation of KSHV-Infected Tumor Cells. *Front Microbiol,* 9**,** 788.

SMITH, REUVEN, N., MOHNI, K. N., SCHUMACHER, A. J. & WELLER, S. K. 2014. Structure of the herpes simplex virus 1 genome: manipulation of nicks and gaps can abrogate infectivity and alter the cellular DNA damage response. *J Virol,* 88**,** 10146-56.

SMITH, D. J. 2008. Ultimate resolution in the electron microscope? *Materials Today,* 11**,** 30-38.

SMITH, J. L. 2003. The role of gastric acid in preventing foodborne disease and how bacteria overcome acid conditions. *J Food Prot,* 66**,** 1292-303.

SOŁTYS, K., WYCISK, K. & OŻYHAR, A. 2021. Liquid-liquid phase separation of the intrinsically disordered AB region of hRXRγ is driven by hydrophobic interactions. *International Journal of Biological Macromolecules,* 183**,** 936-949.

SONG, OUYANG, Y., CHE, J., LI, X., ZHAO, Y., YANG, K., ZHAO, X., CHEN, Y., FAN, C. & YUAN, W. 2017. Potential Value of miR-221/222 as Diagnostic, Prognostic, and Therapeutic Biomarkers for Diseases. *Frontiers in Immunology,* 8.

SOSINSKY, G. E., CRUM, J., JONES, Y. Z., LANMAN, J., SMARR, B., TERADA, M., MARTONE, M. E., DEERINCK, T. J., JOHNSON, J. E. & ELLISMAN, M. H. 2008. The combination of chemical fixation procedures with high pressure freezing and freeze substitution preserves highly labile tissue ultrastructure for electron tomography applications. *J Struct Biol,* 161**,** 359-71.

SPERBER, H. S., WELKE, R.-W., PETAZZI, R. A., BERGMANN, R., SCHADE, M., SHAI, Y., CHIANTIA, S., HERRMANN, A. & SCHWARZER, R. 2019. Self-association and subcellular localization of Puumala hantavirus envelope proteins. *Scientific reports,* 9**,** 707-707.

STADLER, C., REXHEPAJ, E., SINGAN, V. R., MURPHY, R. F., PEPPERKOK, R., UHLÉN, M., SIMPSON, J. C. & LUNDBERG, E. 2013. Immunofluorescence and fluorescent-protein tagging show high correlation for protein localization in mammalian cells. *Nature Methods,* 10**,** 315-323.

STADTLÄNDER, C. 2005. Dehydration and Rehydration Issues in Biological Tissue Processing for Electron Microscopy. *Microscopy Today,* 13**,** 32-35.
STEFANOVIC, S., WINDSOR, M., NAGATA, K. I., INAGAKI, M. & WILEMAN, T. 2005. Vimentin rearrangement during African swine fever virus infection involves retrograde transport along microtubules and phosphorylation of vimentin by calcium calmodulin kinase II. *J Virol,* 79**,** 11766-75.
STENGEL, G. & KUCHTA, R. D. 2011. Coordinated leading and lagging strand DNA synthesis by using the herpes simplex virus 1 replication complex and minicircle DNA templates. *J Virol,* 85**,** 957-67.
STOECKENIUS, W. & MAHR, S. C. 1965. STUDIES ON THE REACTION OF OSMIUM TETROXIDE WITH LIPIDS AND RELATED COMPOUNDS. *Lab Invest,* 14**,** 1196-207.
STRANDIN, T., HEPOJOKI, J., WANG, H., VAHERI, A. & LANKINEN, H. 2011. The cytoplasmic tail of hantavirus Gn glycoprotein interacts with RNA. *Virology,* 418**,** 12-20.
STRIEBINGER, H., FUNK, C., RASCHBICHLER, V. & BAILER, S. M. 2016. Subcellular Trafficking and Functional Relationship of the HSV-1 Glycoproteins N and M. *Viruses,* 8**,** 83.
STROUHALOVA, K., PŘECHOVÁ, M., GANDALOVIČOVÁ, A., BRÁBEK, J., GREGOR, M. & ROSEL, D. 2020. Vimentin Intermediate Filaments as Potential Target for Cancer Treatment. *Cancers (Basel),* 12.
STRZYZ, P. 2021. Targeting viruses in their phase. *Nat Rev Mol Cell Biol,* 22**,** 585.
STUDER, D., HUMBEL, B. M. & CHIQUET, M. 2008. Electron microscopy of high pressure frozen samples: bridging the gap between cellular ultrastructure and atomic resolution. *Histochemistry and Cell Biology,* 130**,** 877-889.
SUBRAMANIAN, R., SEHGAL, I., D'AUVERGNE, O. & KOUSOULAS, K. G. 2010. Kaposi's Sarcoma-Associated Herpesvirus Glycoproteins B and K8.1 Regulate Virion Egress and Synthesis of Vascular Endothelial Growth Factor and Viral Interleukin-6 in BCBL-1 Cells. *Journal of Virology,* 84**,** 1704-1714.
SUN, X., LI, D. & DUAN, Z. 2021. Structural Basis of Glycan Recognition of Rotavirus. *Frontiers in Molecular Biosciences,* 8.
SUN, Z., LIU, Q., QU, G., FENG, Y. & REETZ, M. T. 2019. Utility of B-Factors in Protein Science: Interpreting Rigidity, Flexibility, and Internal Motion and Engineering Thermostability. *Chem Rev,* 119**,** 1626-1665.
SUTTER, E., DE OLIVEIRA, A. P., TOBLER, K., SCHRANER, E. M., SONDA, S., KAECH, A., LUCAS, M. S., ACKERMANN, M. & WILD, P. 2012. Herpes simplex virus 1 induces de novo phospholipid synthesis. *Virology,* 429**,** 124-35.
SWANINK, C., REIMERINK, J., GISOLF, J., DE VRIES, A., CLAASSEN, M., MARTENS, L., WAEGEMAEKERS, T., ROZENDAAL, H., VALKENBURGH, S., HOORNWEG, T. & MAAS, M. 2018. Autochthonous Human Case of Seoul Virus Infection, the Netherlands. *Emerg Infect Dis,* 24**,** 2158-2163.
TAKADA, Y., YE, X. & SIMON, S. 2007. The integrins. *Genome Biology,* 8**,** 215.
TALBOT, S. J., WEISS, R. A., KELLAM, P. & BOSHOFF, C. 1999. Transcriptional analysis of human herpesvirus-8 open reading frames 71, 72, 73, K14, and 74 in a primary effusion lymphoma cell line. *Virology,* 257**,** 84-94.
TANDON, R., MOCARSKI, E. S. & CONWAY, J. F. 2015. The A, B, Cs of herpesvirus capsids. *Viruses,* 7**,** 899-914.
TARAPOREWALA, Z. F., JIANG, X., VASQUEZ-DEL CARPIO, R., JAYARAM, H., PRASAD, B. V. & PATTON, J. T. 2006. Structure-function analysis of rotavirus NSP2 octamer by using a novel complementation system. *J Virol,* 80**,** 7984-94.
TARAPOREWALA, Z. F. & PATTON, J. T. 2001. Identification and characterization of the helix-destabilizing activity of rotavirus nonstructural protein NSP2. *Journal of virology,* 75**,** 4519-4527.
TATE, J. E., BURTON, A. H., BOSCHI-PINTO, C., PARASHAR, U. D., NETWORK, F. T. W. H. O. C. G. R. S., AGOCS, M., SERHAN, F., DE OLIVEIRA, L., MWENDA, J. M., MIHIGO, R., RANJAN WIJESINGHE,

P., ABEYSINGHE, N., FOX, K., PALADIN, F. & NETWORK, F. T. W. H. O. C. G. R. S. 2016. Global, Regional, and National Estimates of Rotavirus Mortality in Children <5 Years of Age, 2000–2013. *Clinical Infectious Diseases,* 62**,** S96-S105.

TATE, J. E., BURTON, A. H., BOSCHI-PINTO, C., STEELE, A. D., DUQUE, J. & PARASHAR, U. D. 2012. 2008 estimate of worldwide rotavirus-associated mortality in children younger than 5 years before the introduction of universal rotavirus vaccination programmes: a systematic review and meta-analysis. *Lancet Infect Dis,* 12**,** 136-41.

TAYLOR, J. A., O'BRIEN, J. A. & YEAGER, M. 1996. The cytoplasmic tail of NSP4, the endoplasmic reticulum-localized non-structural glycoprotein of rotavirus, contains distinct virus binding and coiled coil domains. *Embo j,* 15**,** 4469-76.

TAYLOR, T. J., MCNAMEE, E. E., DAY, C. & KNIPE, D. M. 2003. Herpes simplex virus replication compartments can form by coalescence of smaller compartments. *Virology,* 309**,** 232-47.

TEASDALE, R. D., D'AGOSTARO, G. & GLEESON, P. A. 1992. The signal for Golgi retention of bovine beta 1,4-galactosyltransferase is in the transmembrane domain. *Journal of Biological Chemistry,* 267**,** 4084-4096.

TENORIO, R., FERNÁNDEZ DE CASTRO, I., KNOWLTON, J. J., ZAMORA, P. F., SUTHERLAND, D. M., RISCO, C. & DERMODY, T. S. 2019. Function, Architecture, and Biogenesis of Reovirus Replication Neoorganelles. *Viruses,* 11**,** 288.

TESSIER-LAVIGNE, M. & GOODMAN, C. S. 1996. The molecular biology of axon guidance. *Science,* 274**,** 1123-33.

THE UNIPROT, C. 2021. UniProt: the universal protein knowledgebase in 2021. *Nucleic Acids Research,* 49**,** D480-D489.

THERMOFISHER. *DOCK5 Polyclonal Antibody* [Online]. Available: https://www.thermofisher.com/antibody/product/DOCK5-Antibody-Polyclonal/A304-988A-M [Accessed 07/07/2022 2022].

THOMPSON, R. L. & SAWTELL, N. M. 2001. Herpes simplex virus type 1 latency-associated transcript gene promotes neuronal survival. *J Virol,* 75**,** 6660-75.

THOMPSON, R. L. & SAWTELL, N. M. 2019. Targeted Promoter Replacement Reveals That Herpes Simplex Virus Type-1 and 2 Specific VP16 Promoters Direct Distinct Rates of Entry Into the Lytic Program in Sensory Neurons in vivo. *Front Microbiol,* 10**,** 1624.

THORNELL, L. E. 1974. The fine structure of Purkinje fiber glycogen. A comparative study of negatively stained and cytochemically stained particles. *J Ultrastruct Res,* 49**,** 157-66.

THORSEN, M. K., LAI, A., LEE, M. W., HOOGERHEIDE, D. P., WONG, G. C. L., FREED, J. H. & HELDWEIN, E. E. 2021. Highly basic clusters in the HSV-1 nuclear egress complex drive membrane budding by inducing lipid ordering. *bioRxiv***,** 2021.05.18.444627.

THUL, P. J., ÅKESSON, L., WIKING, M., MAHDESSIAN, D., GELADAKI, A., AIT BLAL, H., ALM, T., ASPLUND, A., BJÖRK, L., BRECKELS, L. M., BÄCKSTRÖM, A., DANIELSSON, F., FAGERBERG, L., FALL, J., GATTO, L., GNANN, C., HOBER, S., HJELMARE, M., JOHANSSON, F., LEE, S., LINDSKOG, C., MULDER, J., MULVEY, C. M., NILSSON, P., OKSVOLD, P., ROCKBERG, J., SCHUTTEN, R., SCHWENK, J. M., SIVERTSSON, Å., SJÖSTEDT, E., SKOGS, M., STADLER, C., SULLIVAN, D. P., TEGEL, H., WINSNES, C., ZHANG, C., ZWAHLEN, M., MARDINOGLU, A., PONTÉN, F., VON FEILITZEN, K., LILLEY, K. S., UHLÉN, M. & LUNDBERG, E. 2017. A subcellular map of the human proteome. *Science,* 356.

TIAN, P., ESTES, M. K., HU, Y., BALL, J. M., ZENG, C. Q. & SCHILLING, W. P. 1995. The rotavirus nonstructural glycoprotein NSP4 mobilizes Ca2+ from the endoplasmic reticulum. *J Virol,* 69**,** 5763-72.

TOKUYASU, K. T. 1978. A study of positive staining of ultrathin frozen sections. *Journal of Ultrastructure Research,* 63**,** 287-307.

TOMER, E., COHEN, E. M., DRAYMAN, N., AFRIAT, A., WEITZMAN, M. D., ZARITSKY, A. & KOBILER, O. 2019. Coalescing replication compartments provide the opportunity for recombination between coinfecting herpesviruses. *Faseb j,* 33**,** 9388-9403.

TORRES-FLORES, J. M., SILVA-AYALA, D., ESPINOZA, M. A., LÓPEZ, S. & ARIAS, C. F. 2015. The tight junction protein JAM-A functions as coreceptor for rotavirus entry into MA104 cells. *Virology,* 475**,** 172-178.

TORRES-VEGA, M. A., GONZÁLEZ, R. A., DUARTE, M., PONCET, D., LÓPEZ, S. & ARIAS, C. F. 2000a. The C-terminal domain of rotavirus NSP5 is essential for its multimerization, hyperphosphorylation and interaction with NSP6. *J Gen Virol,* 81**,** 821-30.

TORRES-VEGA, M. A., GONZÁLEZ, R. A., DUARTE, M., PONCET, D., LÓPEZ, S. & ARIAS, C. F. 2000b. The C-terminal domain of rotavirus NSP5 is essential for its multimerization, hyperphosphorylation and interaction with NSP6. *Journal of General Virology,* 81**,** 821-830.

TORRIANI, G., MAYOR, J., ZIMMER, G., KUNZ, S., ROTHENBERGER, S. & ENGLER, O. 2019. Macropinocytosis contributes to hantavirus entry into human airway epithelial cells. *Virology,* 531**,** 57-68.

TOTH, Z., BRULOIS, K., LEE, H. R., IZUMIYA, Y., TEPPER, C., KUNG, H. J. & JUNG, J. U. 2013. Biphasic euchromatin-to-heterochromatin transition on the KSHV genome following de novo infection. *PLoS Pathog,* 9**,** e1003813.

TRASK, S. D., MCDONALD, S. M. & PATTON, J. T. 2012. Structural insights into the coupling of virion assembly and rotavirus replication. *Nature Reviews Microbiology,* 10**,** 165-177.

TROEGER, C., KHALIL, I. A., RAO, P. C., CAO, S., BLACKER, B. F., AHMED, T., ARMAH, G., BINES, J. E., BREWER, T. G., COLOMBARA, D. V., KANG, G., KIRKPATRICK, B. D., KIRKWOOD, C. D., MWENDA, J. M., PARASHAR, U. D., PETRI, W. A., JR, RIDDLE, M. S., STEELE, A. D., THOMPSON, R. L., WALSON, J. L., SANDERS, J. W., MOKDAD, A. H., MURRAY, C. J. L., HAY, S. I. & REINER, R. C., JR 2018. Rotavirus Vaccination and the Global Burden of Rotavirus Diarrhea Among Children Younger Than 5 Years. *JAMA Pediatrics,* 172**,** 958-965.

TROJNAR, E., OTTO, P., ROTH, B., REETZ, J. & JOHNE, R. 2010. The genome segments of a group D rotavirus possess group A-like conserved termini but encode group-specific proteins. *Journal of virology,* 84**,** 10254-10265.

TRUS, B. L., HEYMANN, J. B., NEALON, K., CHENG, N. Q., NEWCOMB, W. W., BROWN, J. C., KEDES, D. H. & STEVEN, A. C. 2001. Capsid structure of Kaposi's sarcoma-associated herpesvirus, a gammaherpesvirus, compared to those of an alphaherpesvirus, herpes simplex virus type 1, and a betaherpesvirus, cytomegalovirus. *Journal of Virology,* 75**,** 2879-2890.

TURCOTTE, S., LETELLIER, J. & LIPPÉ, R. 2005. Herpes simplex virus type 1 capsids transit by the trans-Golgi network, where viral glycoproteins accumulate independently of capsid egress. *J Virol,* 79**,** 8847-60.

TURK, V., STOKA, V., VASILJEVA, O., RENKO, M., SUN, T., TURK, B. & TURK, D. 2012. Cysteine cathepsins: From structure, function and regulation to new frontiers. *Biochimica et Biophysica Acta (BBA) - Proteins and Proteomics,* 1824**,** 68-88.

TURKKI, P., LAAJALA, M., FLODSTRÖM-TULLBERG, M., MARJOMÄKI, V. & LÓPEZ, S. 2020. Human Enterovirus Group B Viruses Rely on Vimentin Dynamics for Efficient Processing of Viral Nonstructural Proteins. *Journal of Virology,* 94**,** e01393-19.

UDUGAMA, B., KADHIRESAN, P., KOZLOWSKI, H. N., MALEKJAHANI, A., OSBORNE, M., LI, V. Y. C., CHEN, H., MUBAREKA, S., GUBBAY, J. B. & CHAN, W. C. W. 2020. Diagnosing COVID-19: The Disease and Tools for Detection. *ACS Nano,* 14**,** 3822-3835.

ULRICH, R., MEISEL, H., SCHÜTT, M., SCHMIDT, J., KUNZ, A., KLEMPA, B., NIEDRIG, M., PAULI, G., KRÜGER, D. H. & KOCH, J. 2004. [Prevalence of hantavirus infections in Germany]. *Bundesgesundheitsblatt Gesundheitsforschung Gesundheitsschutz,* 47**,** 661-70.

UMBACH, J. L., KRAMER, M. F., JURAK, I., KARNOWSKI, H. W., COEN, D. M. & CULLEN, B. R. 2008. MicroRNAs expressed by herpes simplex virus 1 during latent infection regulate viral mRNAs. *Nature,* 454**,** 780-783.

UNIPROT-CONSORTIUM, T. 2020. UniProt: the universal protein knowledgebase in 2021. *Nucleic Acids Research,* 49**,** D480-D489.

UNIPROT 2020. UniProt: the universal protein knowledgebase in 2021. *Nucleic Acids Research,* 49**,** D480-D489.
UNIPROT. 2022. *Q9H7D0 · DOCK5_HUMAN* [Online]. Available: https://www.uniprot.org/uniprotkb/Q9H7D0/entry [Accessed 07/07/2022 2022].
VAHERI, HENTTONEN, H. & MUSTONEN, J. 2021. Hantavirus Research in Finland: Highlights and Perspectives. *Viruses,* 13**,** 1452.
VAHERI, STRANDIN, T., HEPOJOKI, J., SIRONEN, T., HENTTONEN, H., MÄKELÄ, S. & MUSTONEN, J. 2013. Uncovering the mysteries of hantavirus infections. *Nature Reviews Microbiology,* 11**,** 539-550.
VAN KNIPPENBERG, I., FRAGKOUDIS, R. & ELLIOTT, R. M. 2013. The transient nature of Bunyamwera orthobunyavirus NSs protein expression: effects of increased stability of NSs protein on virus replication. *PLoS One,* 8**,** e64137.
VAN LOOCK, F., THOMAS, I., CLEMENT, J., GHOOS, S. & COLSON, P. 1999. A case-control study after a hantavirus infection outbreak in the south of Belgium: who is at risk? *Clin Infect Dis,* 28**,** 834-9.
VANHECKE, D., GRABER, W. & STUDER, D. 2008. Close-to-native ultrastructural preservation by high pressure freezing. *Methods Cell Biol,* 88**,** 151-64.
VANNI, T., SPRINZ, E., MACHADO, M. W., SANTANA RDE, C., FONSECA, B. A. & SCHWARTSMANN, G. 2006. Systemic treatment of AIDS-related Kaposi sarcoma: current status and perspectives. *Cancer Treat Rev,* 32**,** 445-55.
VAPALAHTI, O., LUNDKVIST, A., KUKKONEN, S. K., CHENG, Y., GILLJAM, M., KANERVA, M., MANNI, T., PEJCOCH, M., NIEMIMAA, J., KAIKUSALO, A., HENTTONEN, H., VAHERI, A. & PLYUSNIN, A. 1996. Isolation and characterization of Tula virus, a distinct serotype in the genus Hantavirus, family Bunyaviridae. *J Gen Virol,* 77 (Pt 12)**,** 3063-7.
VAPALAHTI, O., MUSTONEN, J., LUNDKVIST, A., HENTTONEN, H., PLYUSNIN, A. & VAHERI, A. 2003. Hantavirus infections in Europe. *Lancet Infect Dis,* 3**,** 653-61.
VARADI, M., ANYANGO, S., DESHPANDE, M., NAIR, S., NATASSIA, C., YORDANOVA, G., YUAN, D., STROE, O., WOOD, G., LAYDON, A., ŽÍDEK, A., GREEN, T., TUNYASUVUNAKOOL, K., PETERSEN, S., JUMPER, J., CLANCY, E., GREEN, R., VORA, A., LUTFI, M., FIGURNOV, M., COWIE, A., HOBBS, N., KOHLI, P., KLEYWEGT, G., BIRNEY, E., HASSABIS, D. & VELANKAR, S. 2021. AlphaFold Protein Structure Database: massively expanding the structural coverage of protein-sequence space with high-accuracy models. *Nucleic Acids Research,* 50**,** D439-D444.
VARGA, I., GHALLAB, A. & DANIŠOVIČ, Ľ. 2020. Artifacts in Electron Microscopic Research Corresponding author. *Physiological research / Academia Scientiarum Bohemoslovaca,* 69**,** 405-413.
VARTHAKAVI, V., SMITH, R. M., DENG, H., SUN, R. & SPEARMAN, P. 2002. Human immunodeficiency virus type-1 activates lytic cycle replication of Kaposi's sarcoma-associated herpesvirus through induction of KSHV Rta. *Virology,* 297**,** 270-80.
VEETTIL, M. V., BANDYOPADHYAY, C., DUTTA, D. & CHANDRAN, B. 2014. Interaction of KSHV with Host Cell Surface Receptors and Cell Entry. *Viruses-Basel,* 6**,** 4024-4046.
VEGA, F., MIRANDA, R. N. & MEDEIROS, L. J. 2020. KSHV/HHV8-positive large B-cell lymphomas and associated diseases: a heterogeneous group of lymphoproliferative processes with significant clinicopathological overlap. *Modern Pathology,* 33**,** 18-28.
VELASQUEZ, D. E., PARASHAR, U. & JIANG, B. 2018. Decreased performance of live attenuated, oral rotavirus vaccines in low-income settings: causes and contributing factors. *Expert review of vaccines,* 17**,** 145-161.
VENDE, P., TARAPOREWALA, Z. F. & PATTON, J. T. 2002. RNA-binding activity of the rotavirus phosphoprotein NSP5 includes affinity for double-stranded RNA. *J Virol,* 76**,** 5291-9.
VENDRUSCOLO, M. & FUXREITER, M. 2022. Sequence Determinants of the Aggregation of Proteins Within Condensates Generated by Liquid-liquid Phase Separation. *Journal of Molecular Biology,* 434**,** 167201.

VENKATARAM, P., B. V., SHANKER, S., HU, L., CHOI, J.-M., CRAWFORD, S. E., RAMANI, S., CZAKO, R., ATMAR, R. L. & ESTES, M. K. 2014. Structural basis of glycan interaction in gastroenteric viral pathogens. *Current opinion in virology,* 7**,** 119-127.

VERA-OTAROLA, J., SOLIS, L., LOWY, F., OLGUÍN, V., ANGULO, J., PINO, K., TISCHLER, N. D., OTTH, C., PADULA, P. & LÓPEZ-LASTRA, M. 2020. The Andes Orthohantavirus NSs Protein Antagonizes the Type I Interferon Response by Inhibiting MAVS Signaling. *Journal of virology,* 94**,** e00454-20.

VERGOTE, V., LAENEN, L., VANMECHELEN, B., VAN RANST, M., VERBEKEN, E., HOOPER, J. W. & MAES, P. 2017. A lethal disease model for New World hantaviruses using immunosuppressed Syrian hamsters. *PLoS neglected tropical diseases,* 11**,** e0006042-e0006042.

VERMA, CHOUDHURI, T., KAUL, R. & ROBERTSON, E. S. 2006. Latency-associated nuclear antigen (LANA) of Kaposi's sarcoma-associated herpesvirus interacts with origin recognition complexes at the LANA binding sequence within the terminal repeats. *J Virol,* 80**,** 2243-56.

VERMA, LI, D. J., KRUEGER, B., RENNE, R. & SWAMINATHAN, S. 2015. Identification of the physiological gene targets of the essential lytic replicative Kaposi's sarcoma-associated herpesvirus ORF57 protein. *J Virol,* 89**,** 1688-702.

VERNER-CARLSSON, J., LÕHMUS, M., SUNDSTRÖM, K., STRAND, T. M., VERKERK, M., REUSKEN, C., YOSHIMATSU, K., ARIKAWA, J., VAN DE GOOT, F. & LUNDKVIST, Å. 2015. First evidence of Seoul hantavirus in the wild rat population in the Netherlands. *Infect Ecol Epidemiol,* 5**,** 27215.

VIJAYAKRISHNAN, S., MCELWEE, M., LONEY, C., RIXON, F. & BHELLA, D. 2020. In situ structure of virus capsids within cell nuclei by correlative light and cryo-electron tomography. *Scientific Reports,* 10**,** 17596.

VILLANUEVA-VALENCIA, J. R., TSIMTSIRAKIS, E. & EVILEVITCH, A. 2021. Role of HSV-1 Capsid Vertex-Specific Component (CVSC) and Viral Terminal DNA in Capsid Docking at the Nuclear Pore. *Viruses,* 13.

VILLINGER, C., NEUSSER, G., KRANZ, C., WALTHER, P. & MERTENS, T. 2015. 3D Analysis of HCMV Induced-Nuclear Membrane Structures by FIB/SEM Tomography: Insight into an Unprecedented Membrane Morphology. *Viruses,* 7**,** 5686-5704.

VISKOVSKA, M., ANISH, R., HU, L., CHOW, D. C., HURWITZ, A. M., BROWN, N. G., PALZKILL, T., ESTES, M. K. & PRASAD, B. V. 2014. Probing the sites of interactions of rotaviral proteins involved in replication. *J Virol,* 88**,** 12866-81.

VITTONE, V., DIEFENBACH, E., TRIFFETT, D., DOUGLAS, M. W., CUNNINGHAM, A. L. & DIEFENBACH, R. J. 2005. Determination of interactions between tegument proteins of herpes simplex virus type 1. *J Virol,* 79**,** 9566-71.

VIVES, V., LAURIN, M., CRES, G., LARROUSSE, P., MORICHAUD, Z., NOEL, D., CÔTÉ, J.-F. & BLANGY, A. 2011. The Rac1 exchange factor Dock5 is essential for bone resorption by osteoclasts. *Journal of bone and mineral research : the official journal of the American Society for Bone and Mineral Research,* 26**,** 1099-1110.

VOELTZ, G. K., PRINZ, W. A., SHIBATA, Y., RIST, J. M. & RAPOPORT, T. A. 2006. A class of membrane proteins shaping the tubular endoplasmic reticulum. *Cell,* 124**,** 573-86.

WANG, TANG, Q., MAUL, G. G. & YUAN, Y. 2006. Kaposi's sarcoma-associated herpesvirus ori-Lyt-dependent DNA replication: dual role of replication and transcription activator. *J Virol,* 80**,** 12171-86.

WANG, TAO, L., LU, S.-Y., ZHU, C.-Q., AI, L.-L., LUO, Y., YU, R.-B., LV, H., ZHANG, Y., WANG, C.-C. & TAN, W.-L. 2022. Genetic and hosts characterization of hantaviruses in port areas in Hainan Province, P. R. China. *PLOS ONE,* 17**,** e0264859.

WANG, WU, F. Y., FUJIMURO, M., ZONG, J., HAYWARD, S. D. & HAYWARD, G. S. 2003. Role of CCAAT/Enhancer-Binding Protein Alpha (C/EBPα) in Activation of the Kaposi's Sarcoma-Associated Herpesvirus (KSHV) Lytic-Cycle Replication-Associated Protein (RAP)

Promoter in Cooperation with the KSHV Replication and Transcription Activator (RTA) and RAP. *Journal of Virology,* 77**,** 600-623.
WANG, YUE, M., YAO, P., ZHU, C., AI, L., HU, D., ZHANG, B., YANG, Z., YANG, X., LUO, F., WANG, C., HOU, W. & TAN, W. 2021a. Epidemic Trend and Molecular Evolution of HV Family in the Main Hantavirus Epidemic Areas From 2004 to 2016, in P.R. China. *Frontiers in Cellular and Infection Microbiology,* 10.
WANG, ZHANG, S., SUN, C., YUAN, Z. G., WU, X., WANG, D., DING, Z. & HU, R. 2011. Proteomic profiles of mouse neuro N2a cells infected with variant virulence of rabies viruses. *J Microbiol Biotechnol,* 21**,** 366-73.
WANG, ZHU, N., LI, W., ZHU, F., WANG, Y. & YUAN, Y. 2015. Mono-ubiquitylated ORF45 Mediates Association of KSHV Particles with Internal Lipid Rafts for Viral Assembly and Egress. *PLOS Pathogens,* 11**,** e1005332.
WANG, L., ENG, E. T., LAW, K., GORDON, R. E., RICE, W. J. & CHEN, B. K. 2017. Visualization of HIV T Cell Virological Synapses and Virus-Containing Compartments by Three-Dimensional Correlative Light and Electron Microscopy. *J Virol,* 91.
WANG, S., DAI, T., QIN, Z., PAN, T., CHU, F., LOU, L., ZHANG, L., YANG, B., HUANG, H., LU, H. & ZHOU, F. 2021b. Targeting liquid–liquid phase separation of SARS-CoV-2 nucleocapsid protein promotes innate antiviral immunity by elevating MAVS activity. *Nature Cell Biology,* 23**,** 718-732.
WARD, R. L., BERNSTEIN, D. I., YOUNG, E. C., SHERWOOD, J. R., KNOWLTON, D. R. & SCHIFF, G. M. 1986. Human rotavirus studies in volunteers: determination of infectious dose and serological response to infection. *J Infect Dis,* 154**,** 871-80.
WATSON, M. L. 1958. Staining of tissue sections for electron microscopy with heavy metals. II. Application of solutions containing lead and barium. *J Biophys Biochem Cytol,* 4**,** 727-30.
WEI & COGHLIN, D. T. 2017. Beyond Folliculitis: Recognizing Herpes Gladiatorum in Adolescent Athletes. *J Pediatr,* 190**,** 283.
WEI, DONG, J., CHENG, C.-C., JI, M., YU, L., LUO, S., WU, S., BAI, L. & LAN, K. 2020. Host RAB11FIP5 protein inhibits the release of Kaposi's sarcoma-associated herpesvirus particles by promoting lysosomal degradation of ORF45. *PLOS Pathogens,* 16**,** e1009099.
WEI, W., BAI, L., YAN, B., MENG, W., WANG, H., ZHAI, J., SI, F. & ZHENG, C. 2022. When liquid-liquid phase separation meets viral infections. *Frontiers in Immunology,* 13.
WELKE, R.-W., SPERBER, H. S., BERGMANN, R., KOIKKARAH, A., MENKE, L., SIEBEN, C., KRÜGER, D. H., CHIANTIA, S., HERRMANN, A. & SCHWARZER, R. 2022. Characterization of Hantavirus N Protein Intracellular Dynamics and Localization. *Viruses,* 14**,** 457.
WELLER, S. K. 2010. Herpes simplex virus reorganizes the cellular DNA repair and protein quality control machinery. *PLoS Pathog,* 6**,** e1001105.
WELLER, S. K. & COEN, D. M. 2012. Herpes simplex viruses: mechanisms of DNA replication. *Cold Spring Harb Perspect Biol,* 4**,** a013011.
WESTERMAN, L. E., JIANG, B., MCCLURE, H. M., SNIPES-MAGALDI, L. J., GRIFFIN, D. D., SHIN, G., GENTSCH, J. R. & GLASS, R. I. 2006. Isolation and characterization of a new simian rotavirus, YK-1. *Virology Journal,* 3**,** 40.
WHEELER, J. R., MATHENY, T., JAIN, S., ABRISCH, R. & PARKER, R. 2016. Distinct stages in stress granule assembly and disassembly. *eLife,* 5**,** e18413.
WHO 2007. Rotavirus vaccines= Vaccins antirotavirus. *Weekly Epidemiological Record= Relevé épidémiologique hebdomadaire,* 82**,** 285-295.
WHO, P. 2017. *Hantavirus* [Online]. World Health Organization, and Pan American Health Organization. Available: https://www3.paho.org/hq/index.php?option=com_content&view=article&id=14911:hantavirus&Itemid=40721&lang=en [Accessed 28/05/2022 2022].
WIGGLESWORTH, V. B. 1964. The Union of Protein and Nucleic Acid in the Living Cell and its Demonstration by Osmium Staining. *Journal of Cell Science,* s3-105**,** 113-122.

WILD, KAECH, A., SCHRANER, E. M., WALSER, L. & ACKERMANN, M. 2017. Endoplasmic reticulum-to-Golgi transitions upon herpes virus infection. *F1000Res,* 6**,** 1804.

WILD, P., LEISINGER, S., DE OLIVEIRA, A. P., SCHRANER, E. M., KAECH, A., ACKERMANN, M. & TOBLER, K. 2015. Herpes Simplex Virus 1 Us3 Deletion Mutant is Infective Despite Impaired Capsid Translocation to the Cytoplasm. *Viruses,* 7**,** 52-71.

WILLIAMS, C., WELLS, J., KLEIN, R., SYLVESTER, T. & SUNENSHINE, R. 2015. Notes from the field: outbreak of skin lesions among high school wrestlers--Arizona, 2014. *MMWR Morb Mortal Wkly Rep,* 64**,** 559-60.

WILLS, E., SCHOLTES, L. & BAINES, J. D. 2006. Herpes simplex virus 1 DNA packaging proteins encoded by UL6, UL15, UL17, UL28, and UL33 are located on the external surface of the viral capsid. *J Virol,* 80**,** 10894-9.

WINEY, M., MEEHL, J. B., O'TOOLE, E. T. & GIDDINGS, T. H., JR. 2014. Conventional transmission electron microscopy. *Mol Biol Cell,* 25**,** 319-23.

WISSE, E., BRAET, F., DUIMEL, H., VREULS, C., KOEK, G., OLDE DAMINK, S. W., VAN DEN BROEK, M. A., DE GEEST, B., DEJONG, C. H., TATENO, C. & FREDERIK, P. 2010a. Fixation methods for electron microscopy of human and other liver. *World J Gastroenterol,* 16**,** 2851-66.

WISSE, E., BRAET, F., DUIMEL, H., VREULS, C., KOEK, G., OLDE DAMINK, S. W. M., VAN DEN BROEK, M. A. J., DE GEEST, B., DEJONG, C. H. C., TATENO, C. & FREDERIK, P. 2010b. Fixation methods for electron microscopy of human and other liver. *World journal of gastroenterology,* 16**,** 2851-2866.

WOLF, M., DEAL, E. M. & GREENBERG, H. B. 2012. Rhesus rotavirus trafficking during entry into MA104 cells is restricted to the early endosome compartment. *Journal of virology,* 86**,** 4009-4013.

WU, G., GAO, X., YE, G., LI, K., HU, C. & CHENG, J.-A. 2008. Ultrastructural alterations in midgut and Malpighian tubules of Boettcherisca peregrina exposure to cadmium and copper. *Ecotoxicology and environmental safety,* 72**,** 1137-47.

WU, J.-J., AVEY, D., LI, W., GILLEN, J., FU, B., MILEY, W., WHITBY, D., ZHU, F. & JUNG, J. U. 2016. ORF33 and ORF38 of Kaposi's Sarcoma-Associated Herpesvirus Interact and Are Required for Optimal Production of Infectious Progeny Viruses. *Journal of Virology,* 90**,** 1741-1756.

WYLLIE, A. H., KERR, J. F. & CURRIE, A. R. 1980. Cell death: the significance of apoptosis. *Int Rev Cytol,* 68**,** 251-306.

XU, X., CHE, Y. & LI, Q. 2016. HSV-1 tegument protein and the development of its genome editing technology. *Virol J,* 13**,** 108.

XU, X., YOSHIZAKI, H., ISHIGAKI, Y., KUBO, E., MINATO, H. & KIYOKAWA, E. 2017. Upregulation of multiple signaling pathways by Dock5 deletion in epithelial cells. *Mol Vis,* 23**,** 1081-1092.

YAN, LIANG, Z., DU, Q., YANG, M. & GELLER, D. A. 2016. MicroRNA-23a downregulates the expression of interferon regulatory factor-1 in hepatocellular carcinoma cells. *Oncol Rep,* 36**,** 633-40.

YAN, MAJERCIAK, V., ZHENG, Z.-M. & LAN, K. 2019. Towards Better Understanding of KSHV Life Cycle: from Transcription and Posttranscriptional Regulations to Pathogenesis. *Virologica Sinica,* 34**,** 135-161.

YANG & BAINES, J. D. 2011. Selection of HSV capsids for envelopment involves interaction between capsid surface components pUL31, pUL17, and pUL25. *Proc Natl Acad Sci U S A,* 108**,** 14276-81.

YANG, WILLS, E. & BAINES, J. D. 2009. The putative leucine zipper of the UL6-encoded portal protein of herpes simplex virus 1 is necessary for interaction with pUL15 and pUL28 and their association with capsids. *J Virol,* 83**,** 4557-64.

YANG, WILLS, E., LIM, H. Y., ZHOU, Z. H. & BAINES, J. D. 2014. Association of herpes simplex virus pUL31 with capsid vertices and components of the capsid vertex-specific complex. *J Virol,* 88**,** 3815-25.

YE, F. C., ZHOU, F. C., YOO, S. M., XIE, J. P., BROWNING, P. J. & GAO, S. J. 2004. Disruption of Kaposi's sarcoma-associated herpesvirus latent nuclear antigen leads to abortive episome persistence. *J Virol,* 78**,** 11121-9.

YEO, G. C., KEELEY, F. W. & WEISS, A. S. 2011. Coacervation of tropoelastin. *Advances in Colloid and Interface Science,* 167**,** 94-103.

YOUNG, L., JERNIGAN, R. L. & COVELL, D. G. 1994. A role for surface hydrophobicity in protein-protein recognition. *Protein Sci,* 3**,** 717-29.

YU, Y., BLACK, J. B., GOLDSMITH, C. S., BROWNING, P. J., BHALLA, K. & OFFERMANN, M. K. 1999. Induction of human herpesvirus-8 DNA replication and transcription by butyrate and TPA in BCBL-1 cells. *J Gen Virol,* 80 (Pt 1)**,** 83-90.

YUAN, S., WANG, J., ZHU, D., WANG, N., GAO, Q., CHEN, W., TANG, H., WANG, J., ZHANG, X., LIU, H., RAO, Z. & WANG, X. 2018. Cryo-EM structure of a herpesvirus capsid at 3.1 Å. *Science,* 360**,** eaao7283.

ZAKI, S. R., GREER, P. W., COFFIELD, L. M., GOLDSMITH, C. S., NOLTE, K. B., FOUCAR, K., FEDDERSEN, R. M., ZUMWALT, R. E., MILLER, G. L., KHAN, A. S. & ET AL. 1995. Hantavirus pulmonary syndrome. Pathogenesis of an emerging infectious disease. *Am J Pathol,* 146**,** 552-79.

ZAVITSANOU, A., SYPSA, V., PETRODASKALAKI, M., PSICHOGIOU, M., KATSOULIDOU, A., BOLETIS, J., HADJICONSTANTINOU, V., KARALIS, D., KALAPOTHAKI, V. & HATZAKIS, A. 2006. Human herpesvirus 8 infection in hemodialysis patients. *Am J Kidney Dis,* 47**,** 167-70.

ZEHMER, J. K., BARTZ, R., LIU, P. & ANDERSON, R. G. 2008. Identification of a novel N-terminal hydrophobic sequence that targets proteins to lipid droplets. *J Cell Sci,* 121**,** 1852-60.

ZELENÁ, H., MRÁZEK, J. & KUHN, T. 2013. Tula hantavirus infection in immunocompromised host, Czech Republic. *Emerg Infect Dis,* 19**,** 1873-5.

ZERBONI, L., CHE, X., REICHELT, M., QIAO, Y., GU, H. & ARVIN, A. 2012. Herpes Simplex Virus 1 Tropism for Human Sensory Ganglion Neurons in the Severe Combined Immunodeficiency Mouse Model of Neuropathogenesis. *Journal of virology,* 87.

ZHANG, READ, C., NGUYEN, C. C., SIDDIQUEY, M. N. A., SHANG, C., HALL, C. M., EINEM, J. V., KAMIL, J. P. & SHENK, T. 2019. The Human Cytomegalovirus Nonstructural Glycoprotein UL148 Reorganizes the Endoplasmic Reticulum. *mBio,* 10**,** e02110-19.

ZHANG, YANG, Y., YU, F., ZHAO, Y., LIN, F., MINHAS, V., WOOD, C. & HE, N. 2014. Kaposi`s sarcoma associated herpesvirus infection among female sex workers and general population women in Shanghai, China: a cross-sectional study. *BMC Infect Dis,* 14**,** 58.

ZHANG, Y., ZHU, J., HONG, X., ZHOU, Y., REN, K., SHU, X. & WANG, Q. 2013. The membrane molecule RCAS1 induces immune cell apoptosis via the RCAS1-RCAS1R pathway. *Int J Mol Med,* 31**,** 1319-26.

ZHAO, M., YU, Y., SUN, L. M., XING, J. Q., LI, T., ZHU, Y., WANG, M., YU, Y., XUE, W., XIA, T., CAI, H., HAN, Q. Y., YIN, X., LI, W. H., LI, A. L., CUI, J., YUAN, Z., ZHANG, R., ZHOU, T., ZHANG, X. M. & LI, T. 2021. GCG inhibits SARS-CoV-2 replication by disrupting the liquid phase condensation of its nucleocapsid protein. *Nat Commun,* 12**,** 2114.

ZHENG, Y. & KIELIAN, M. 2013. Imaging of the alphavirus capsid protein during virus replication. *J Virol,* 87**,** 9579-89.

ZHU, S. & VIEJO-BORBOLLA, A. 2021. Pathogenesis and virulence of herpes simplex virus. *Virulence,* 12**,** 2670-2702.

ZINSZNER, H., KURODA, M., WANG, X., BATCHVAROVA, N., LIGHTFOOT, R. T., REMOTTI, H., STEVENS, J. L. & RON, D. 1998. CHOP is implicated in programmed cell death in response to impaired function of the endoplasmic reticulum. *Genes Dev,* 12**,** 982-95.